

A Study on the Mandra Flash Flood of 2017 using a coupled 1D/2D Model (SWMM/P-DWave)

Master's Thesis
Department of Civil, Geo and Environmental Engineering
Technical University of Munich

Supervisors	Dr. phil. Jorge Eduardo Teixeira Leandro Chair of Hydrology and River Basin Management (Prof. Disse) Department of Civil, Geo and Environmental Engineering Technical University of Munich Prof. Anastasios I. Stamou Department of Water Resources and Environmental Engineering School of Civil Engineering National Technical University of Athens
Author	MEng Nikolaos Zafeirakos (03727792)
Degree Course	M.Sc. Water Resources Science and Technology
Place and Date	Munich, 08.06.2020

Acknowledgements

I would like to extend my deepest appreciation to my academic supervisors Dr. phil. Jorge Eduardo Teixeira Leandro of the Chair of Hydrology and River Basin Management of TUM and Professor Anastasios I. Stamou of the Department of Water Resources and Environmental Engineering of NTUA for their willingness to donate their expertise and valuable experience, for their guidance, their continuous support and their undisputable belief in me and my goals.

I would like to express my warm thanks to all the employees of the European Educational Programmes Offices of TUM and NTUA, in particular to Lucia Celinkovic and Spyros Pitsikalis, for their kind help before and throughout my stay at Munich.

Special thanks are due to Ioanna Zerva and Georgios Mavrogeorgos, civil engineers for the provision of useful data from their own academic theses; to Laura Passiou, technical consultant to the Mayor of the municipality of Mandra and to Basilis Sapoulidis, rural and surveying engineer, for their valuable information and assistance regarding the Mandra flash flood of 2017; to the whole team at TUM, in particular to Daniel Sturm and Lea Sophie Rosenberger, environmental engineers for their cooperation and our interesting meetings. I thank you all for your kindness and help throughout.

My grateful thanks are also extended to Theodora Tsami, for helping me along the way and making the journey all the more enjoyable.

Finally, I would like to express my deepest gratitude to my parents Anna and Alexis Zafeirakos, for always being there for me, for giving me the chance to make my dreams come true. It is to them that I dedicate this thesis.

Abstract

The present thesis uses the 2D parallel diffusive wave model P-DWave coupled with the 1D Stormwater Management Model SWMM to simulate the flash flood of 2017 at the town of Mandra, Greece. The 2D overland model P-DWave uses an explicit finite volume solution for the simplified shallow water equations neglecting the inertial terms. The study area for the surface routing covers a total area (hydraulic simulation area) of 10.823 km². The 1D closed conduit model consists of 51 nodes (26 of them are storages and the other 25 are outfalls) and 26 conduits with a total length of 10,106 meters. The good statistical evaluation (RMSE=0.494, NSE=0.871, MAE=0.362) of the maximum water depths at the checkpoints in conjunction with the very high percentage of 96.0% of the real flood extent compared to the recorded flood extent, validate the coupled 1D/2D model and its setup and indicate that P-DWave is suitable for flash flood simulations. The refined DEM (building-block method (BB), elevation reduction at streets and flooded buildings, additional topographic maps and data) with a mesh resolution of 5 m, as a compromise between precision, accuracy and computational time, is unable to represent small features but is adequate for accurately modelling a flash flood even for narrow riverbed and streets. The model is applied to four rainfall scenarios (T=20, 50, 100 and 1000 years) where it is shown that the return period of the flood is over T=100 years and more precisely between T=235 and T=391 years. The coupled 1D/2D approach is mainly used to apply flood mitigation and protection strategies in areas of weakness (the main residential area and the main industrial area of Mandra) as well. The impact of proper maintenance of the closed conduits is low but not negligible. The implementation of private protection measures (raising fences to protect the flooded basements in the main industrial area) reduces the average maximum water depth by 58.1%, the flood extent by 48.5% and the flooding by 54.3% in the main industrial area. The impact of the extension of the rainfall zone over the flooded area is huge on the flood extent (increase by 255.2%) but moderate on the average maximum water depth (increase by 46.1%). The incorporation of a stream diversion and a retention pond (public works to protect the main residential area) leads to an important flood mitigation reducing all the parameters (average maximum depth, flood extent and flooding) in the main residential area but increasing them in the main industrial area. Finally, the comparison of 3 different scenarios, regarding public protection measures, with the basic Scenario for T=50 years proves that the model results are reliable and the solution to the flood problem requires diversion as well as stream canalisation works.

Abbreviations

1D	One-dimensional
2D	Two-dimensional
AA	Agia Aikaterini
AMWD	Average Maximum Water Depth
ASCII	American Standard Code for Information Interchange
AWMWD	Average Wet Maximum Water Depth
BB	Building-Block
BH	Building-Hole
BR	Building-Resistance
CHI	Computational Hydraulics International
CN	Curve Number
DEM	Digital Elevation Model
DHL	Dalsey Hillblom Lynn
DLL	Dynamic Link Libraries
DTM	Digital Terrain Model
EET	Eastern European Time
ELSTAT	Elliniki Statistiki Arxi (Hellenic Statistical Authority)
Gev	Generalized extreme value
HSG	Hydrological Soil Groups
IDF	Intensity Duration Frequency
MAE	Mean-Average-Error
NB	No-Building
NSE	Nash-Sutcliffe-Efficiency
P-DWave	Parallel Diffusive Wave Model
PEOATH	Palaia Ethniki Odos Athinon-Thivon (Old Athens-Thebes National Highway)
RMSE	Root-Mean-Square-Error
S	Soures
SCS	Soil Conservation Service
SWE	Shallow Water Equations
SWMM	Stormwater Management Model
USEPA	United States Environmental Protection Agency
YPEKA	Ypourgeio Perivallontos & Energeias (Greek Ministry of Environment and Development)

List of figures

Figure 1	Location of the study area in Greece, Attica and town of Mandra.....	3
Figure 2	The town of Mandra with the hydrographic network and technical works ...	5
Figure 3	The catchment areas of the study area (Mavrogeorgos 2019).....	7
Figure 4	Rainfall hyetograph (left) and accumulative rainfall depth (right) from the estimations of X-POL (Kalogiros et al. 2017).....	8
Figure 5	Course of Agia Aikaterini and Soures streams	9
Figure 6	Mapping of the maximum extent of the flood (Mavrogeorgos 2019)	10
Figure 7	Checkpoints mapping.....	11
Figure 8	The parametric synthetic unit hydrograph with its characteristics (Efstratiadis et al. 2014)	15
Figure 9	Model interaction scheme	31
Figure 10	Model input data	32
Figure 11	Spatial distribution of the hydrological simulation area where the circles mark the inflow locations generated by the hydrological simulation	32
Figure 12	Spatial distribution of the coupled 1D/2D model where the circles mark the inflow locations generated by the hydrological simulation.....	33
Figure 13	The simulated rainfall for 95% confidence interval on virtual station X (Mavrogeorgos 2019).....	34
Figure 14	Synthetic unit hydrographs for rainfall duration $d=0.5$ h (Mavrogeorgos 2019).....	36
Figure 15	Inlet hydrographs for the hydraulic model (Mavrogeorgos 2019)	37
Figure 16	Land uses of the hydraulic simulation area.....	38
Figure 17	Rainfall for the hydraulic simulation area.....	39
Figure 18	Rainfall intensity for the hydraulic simulation area	40
Figure 19	Comparison of IDF curves for rainfall duration ($d=12$ h) for the four examined return periods T (Mavrogeorgos 2019).....	41
Figure 20	Inlet storm hydrographs for the hydraulic model for s. Soures (Mavrogeorgos 2019).....	42

Figure 21	Inlet storm hydrographs for the hydraulic model for s. Agia Aikaterini (Mavrogeorgos 2019).....	43
Figure 22	Technical works (Scenario “Real flood”).....	45
Figure 23	Mapping of fences (Scenario “Fences”).....	46
Figure 24	New technical works of diversion and retention pond (Scenario “Diversion and retention pond”).....	47
Figure 25	Plan of the new technical works of diversion and retention pond (Scenario “Diversion and retention pond”).....	47
Figure 26	New technical works of diversion and retention pond (Scenario “Diversion, retention pond and METRO fence”).....	50
Figure 27	New technical works of diversion and retention pond (Scenario “New diversion and retention pond”).....	50
Figure 28	Display of the DEM of the hydraulic simulation area.....	54
Figure 29	Display of the Manning’s roughness value in the hydraulic simulation area (Mavrogeorgos 2019 adjusted).....	56
Figure 30	Mapping of the particular areas	59
Figure 31	Time change of water depths at the checkpoints of Agia Aikaterini stream	61
Figure 32	Time change of water depths at the checkpoints of Soures stream upstream of the confluence with Agia Aikaterini stream	62
Figure 33	Time change of water depths at the checkpoints of Soures stream downstream of the confluence with Agia Aikaterini stream	63
Figure 34	Simulated maximum water depths compared to the maximum observed water depths for Agia Aikaterini stream (Scenario “Real flood”).....	64
Figure 35	Simulated maximum water depths compared to the maximum observed water depths for Soures stream (Scenario “Real flood”)	64
Figure 36	Simulated maximum water depths and the recorded flood extent in a five sections spatial distribution (Scenario “Real flood”).....	65
Figure 37	Simulated maximum water depths and the recorded flood extent – Section 1 (Scenario “Real flood”)	66
Figure 38	Simulated maximum water depths and the recorded flood extent – Section 2 (Scenario “Real flood”)	66

Figure 39	Simulated maximum water depths and the recorded flood extent – Section 3 (Scenario “Real flood”)	67
Figure 40	Simulated maximum water depths and the recorded flood extent – Section 4 (Scenario “Real flood”)	68
Figure 41	Simulated maximum water depths and the recorded flood extent – Section 5 (Scenario “Real flood”)	69
Figure 42	Simulated maximum water depths within the particular areas (Scenario “Real flood”)	69
Figure 43	Comparison of real flood extent with recorded flood extent (Scenario “Real flood”).....	70
Figure 44	Flood extent within the particular areas (Scenario “Real flood”).....	71
Figure 45	Time change of water depths at the checkpoints of Agia Aikaterini stream	72
Figure 46	Time change of water depths at the checkpoints of Soures stream upstream of the confluence with Agia Aikaterini stream	73
Figure 47	Time change of water depths at the checkpoints of Soures stream downstream of the confluence with Agia Aikaterini stream	74
Figure 48	Comparison of maximum water depths for Agia Aikaterini stream (Scenario “Fully operated conduits”).....	75
Figure 49	Comparison of maximum water depths for Soures stream (Scenario “Fully operated conduits”)	75
Figure 50	Maximum water depths within the particular areas (Scenario “Fully operated conduits”)	76
Figure 51	Differences of maximum water depths between Scenario “Fully operated conduits” and Scenario “Real flood”	77
Figure 52	Comparison of the flood extent with the real flood extent (Scenario “Fully operated conduits”)	79
Figure 53	Flood extent within the particular areas (Scenario “Fully operated conduits”)	79
Figure 54	Time change of water depths at the checkpoints of Soures stream upstream of the confluence with Agia Aikaterini stream	82
Figure 55	Time change of water depths at the checkpoints of Soures stream downstream of the confluence with Agia Aikaterini stream	83

Figure 56	Comparison of maximum water depths for Agia Aikaterini stream (Scenario “Fences”).....	84
Figure 57	Comparison of maximum water depths for Soures stream (Scenario “Fences”).....	84
Figure 58	Maximum water depths within the particular areas (Scenario “Fences”)....	85
Figure 59	Differences of maximum water depths between Scenario “Fences” and Scenario “Real flood”.....	86
Figure 60	Comparison of the flood extent with the real flood extent (Scenario “Fences”).....	88
Figure 61	Flood extent within the particular areas (Scenario “Fences”).....	88
Figure 62	Time change of water depths at the checkpoints of Agia Aikaterini stream	91
Figure 63	Time change of water depths at the checkpoints of Soures stream upstream of the confluence with Agia Aikaterini stream	92
Figure 64	Time change of water depths at the checkpoints of Soures stream downstream of the confluence with Agia Aikaterini stream	93
Figure 65	Comparison of maximum water depths for Agia Aikaterini stream (Scenario “Spatially extended rainfall”).....	94
Figure 66	Comparison of maximum water depths for Soures stream (Scenario “Spatially extended rainfall”).....	94
Figure 67	Maximum water depths within the particular areas (Scenario “Spatially extended rainfall”)	95
Figure 68	Differences of maximum water depths between Scenario “Spatially extended rainfall” and Scenario “Real flood”.....	96
Figure 69	Comparison of the flood extent with the real flood extent (Scenario “Spatially extended rainfall”).....	98
Figure 70	Flood extent within the particular areas (Scenario “Spatially extended rainfall”).....	98
Figure 71	Maximum water depths within the particular areas (Scenario “Diversion and retention pond”).....	101
Figure 72	Maximum water depths within the particular areas (Scenario “Diversion and retention pond”).....	101

Figure 73	Time change of water depths at the checkpoints of Agia Aikaterini stream	102
Figure 74	Time change of water depths at the checkpoints of Soures stream upstream of the confluence with Agia Aikaterini stream	103
Figure 75	Time change of water depths at the checkpoints of Soures stream downstream of the confluence with Agia Aikaterini stream	104
Figure 76	Comparison of maximum water depths for Agia Aikaterini stream (Scenario “Diversion and retention pond”)	105
Figure 77	Comparison of maximum water depths for Soures stream (Scenario “Diversion and retention pond”)	105
Figure 78	Maximum water depths within the particular areas (Scenario “Diversion and retention pond”).....	106
Figure 79	Differences of maximum water depths between Scenario “Diversion and retention pond” and Scenario “Real flood”	107
Figure 80	Comparison of the flood extent with the real flood extent (Scenario “Diversion and retention pond”)	109
Figure 81	Flood extent within the particular areas (Scenario “Diversion and retention pond”)	109
Figure 82	Average wet maximum water depth of the different Scenarios for the particular areas	113
Figure 83	Average maximum water depth of the different Scenarios for the particular areas.....	113
Figure 84	Average wet maximum water depth percentage of the different Scenarios for the particular areas	114
Figure 85	Average maximum water depth percentage of the different Scenarios for the particular areas	114
Figure 86	Flood extent of the different Scenarios for the particular areas.....	115
Figure 87	Flood extents percentage of the different Scenarios for the particular areas	115
Figure 88	Flooding of the different Scenarios for the particular areas.....	116
Figure 89	Floodings percentage of the different Scenarios for the particular areas	116

Figure 90	Time change of water depths at the checkpoints of Agia Aikaterini stream	117
Figure 91	Time change of water depths at the checkpoints of Soures stream upstream of the confluence with Agia Aikaterini stream	118
Figure 92	Time change of water depths at the checkpoints of Soures stream downstream of the confluence with Agia Aikaterini stream	119
Figure 93	Maximum water depths within the particular areas (Scenario "Real flood")	120
Figure 94	Maximum water depths within the particular areas (Scenario "Real flood")	121
Figure 95	Maximum water depths within the particular areas (Scenario "Real flood")	121
Figure 96	Maximum water depths within the particular areas (Scenario "Real flood")	122
Figure 97	Average wet maximum water depths for the particular areas (Scenario "Real flood")	122
Figure 98	Average wet maximum water depth percentage between floods with return period T=20, 50, 100 and 1000 years and real flood for the particular areas	123
Figure 99	Average wet maximum water depth percentage between floods with return period T=20, 50, 100 and 1000 years and real flood for the particular areas	124
Figure 100	Average maximum water depths for the particular areas (Scenario "Real flood")	124
Figure 101	Average maximum water depth percentage between floods with return period T=20, 50, 100 and 1000 years and real flood for the particular areas	125
Figure 102	Average maximum water depth percentage between floods with return period T=20, 50, 100 and 1000 years and real flood for the particular areas	125
Figure 103	Comparison of flood extent within the particular areas for T=20, 50, 100 and 1000 years (Scenario "Real flood")	126

Figure 104	Comparison of flood extent within the particular areas for T=100, 1000 years and real flood (Scenario “Real flood”).....	126
Figure 105	Flood extent for the particular areas (Scenario “Real flood”).....	127
Figure 106	Flood extents percentage of floods with return period T=20, 50, 100 and 1000 years and real flood for the particular areas	128
Figure 107	Flooding for the particular areas (Scenario “Real flood”).....	128
Figure 108	Floodings percentage of floods with return period T=20, 50, 100 and 1000 years and real flood for the particular areas.....	129
Figure 109	Maximum water depths within the particular areas (Alternative Scenario “Diversion, retention pond and METRO fence”).....	130
Figure 110	Maximum water depths within the particular areas (Alternative Scenario “New diversion and retention pond”).....	130
Figure 111	Average wet maximum water depth percentage of Scenarios “Diversion and retention pond” and alternative Scenarios for the particular areas	131
Figure 112	Average maximum water depth percentage of Scenarios “Diversion and retention pond” and alternative Scenarios for the particular areas	132
Figure 113	Flood extents percentage of Scenarios “Diversion and retention pond” and alternative Scenarios for the particular areas	132
Figure 114	Floodings percentage of Scenarios “Diversion and retention pond” and alternative Scenarios for the particular areas.....	133
Figure 115	Exemplary P-DWave master file (Scenario “Real flood”).....	150

List of tables

Table 1	Water depths at the checkpoints (Mavrogeorgos 2019)	11
Table 2	The suggested values of initial abstraction percentage α (Efstratiadis et al. 2014)	20
Table 3	Calculation of concentration time according to Giandotti.....	35
Table 4	Calculation of concentration time	35
Table 5	CN _{II} according to Land use and Hydrological Soil Groups (Mavrogeorgos 2019)	37
Table 6	Runoff curve number CN _{II} of the hydraulic simulation area	38
Table 7	Assessment of the characteristics of unit hydrograph of s. Soures examined return periods (Mavrogeorgos 2019).....	42
Table 8	Assessment of the characteristics of unit hydrograph of s. Agia Aikaterini examined return periods (Mavrogeorgos 2019)	42
Table 9	Peak discharges of storm hydrographs (m ³ /s) for the examined return periods (Mavrogeorgos 2019)	43
Table 10	Technical works of Agia Aikaterini and Soures streams (Mavrogeorgos 2019 adjusted)	44
Table 11	Existing and new technical works of Agia Aikaterini and Soures streams ..	47
Table 12	Summary of the simulation scenarios.....	50
Table 13	Summary of the simulations concerning the influence of the return period	51
Table 14	Summary of the simulations concerning the alternatives and the validation of the design of the new technical works	51
Table 15	Selected Manning's n coefficient according to the land uses (1) (Mavrogeorgos 2019 adjusted).....	55
Table 16	Selected Manning's n coefficient according to the land uses (2) (Mavrogeorgos 2019)	56
Table 17	Comparison of average wet maximum water depths for the particular areas (Scenario "Fully operated conduits" vs. Scenario "Real flood")	76
Table 18	Comparison of average maximum water depths for the particular areas (Scenario "Fully operated conduits" vs. Scenario "Real flood")	78

Table 19	Comparison of flood extent for the particular areas (Scenario “Fully operated conduits” vs. Scenario “Real flood”).....	80
Table 20	Comparison of flooding for the particular areas (Scenario “Fully operated conduits” vs. Scenario “Real flood”).....	80
Table 21	Comparison of average wet maximum water depths for the particular areas (Scenario “Fences” vs. Scenario “Real flood”).....	85
Table 22	Comparison of average maximum water depths for the particular areas (Scenario “Fences” vs. Scenario “Real flood”).....	87
Table 23	Comparison of flood extent for the particular areas (Scenario “Fences” vs. Scenario “Real flood”)	89
Table 24	Comparison of flooding for the particular areas (Scenario “Fences” vs. Scenario “Real flood”)	89
Table 25	Comparison of average wet maximum water depths for the particular areas (Scenario “Spatially extended rainfall” vs. Scenario “Real flood”)	95
Table 26	Comparison of average maximum water depths for the particular areas (Scenario “Spatially extended rainfall” vs. Scenario “Real flood”)	97
Table 27	Comparison of flood extent for the particular areas (Scenario “Spatially extended rainfall” vs. Scenario “Real flood”).....	99
Table 28	Comparison of flooding for the particular areas (Scenario “Spatially extended rainfall” vs. Scenario “Real flood”).....	99
Table 29	Comparison of average wet maximum water depths for the particular areas (Scenario “Diversion and retention pond” vs. Scenario “Real flood”)	106
Table 30	Comparison of average maximum water depths for the particular areas (Scenario “Diversion and retention pond” vs. Scenario “Real flood”)	108
Table 31	Comparison of flood extent for the particular areas (Scenario “Diversion and retention pond” vs. Scenario “Real flood”)	110
Table 32	Comparison of flooding for the particular areas (Scenario “Diversion and retention pond” vs. Scenario “Real flood”)	111
Table 33	Height difference (m) between the maximum water depths of the different scenarios and the Scenario “Real flood” at the checkpoints	111
Table 34	Goodness of fit criteria	112
Table 35	Goodness of fit criteria	120

Table 36	Summary of input, output and application files for P-DWave, SWMM and the coupling (P-DWave/SWMM).....	149
Table 37	Flood progress with a time step of 30 min (Scenario “Real flood”).....	151

Table of contents

Acknowledgements	i
Abstract	ii
Abbreviations	ii
List of figures	iv
List of tables	xi
Table of contents	xiv
1. Introduction	1
1.1 Flood event – Scope of work	1
1.2 Outline of work	1
2. Study Area	Error! Bookmark not defined.
2.1 Generally.....	3
2.2 Soures stream	4
2.3 Agia Aikaterini stream.....	5
2.4 Catchment areas (watersheds).....	6
2.5 Description of the flash flood on 15/11/2017.....	7
2.6 Temporal and spatial runoff course – Autopsy results	8
3. Mathematic Models	14
3.1. Hydrological simulation.....	31
3.1.1. Methodology for estimation of flood parameters	14
3.1.2. Parametric synthetic unit hydrograph.....	14
3.1.3. Concentration time	16
3.1.4. Estimation of hydrological losses.....	17
3.1.5. IDF curves	20
3.1.6. Surface reduction	21
3.1.7. Design storms	21
3.2. Hydraulic simulation (Urban flood modelling).....	22
3.2.1. 2D parallel diffusive wave model (P-DWave)	25
3.2.2. Storm Water Management Model SWMM.....	28
3.2.3. Coupling of SWMM and P-DWave.....	29
4. Methodology – Case of Mandra	31
4.1. Rainfall selection	33
4.2. Concentration time	34
4.3. Results	35

4.3.1.	Hydrological simulation area.....	Error! Bookmark not defined.
4.3.2.	Hydraulic simulation area	37
4.4.	Synthetic hydrographs.....	40
4.4.1.	IDF curves	40
4.4.2.	Computational process	41
4.4.3.	Hydrological simulation area results	42
4.5.	1D/2D coupled model.....	43
4.5.1.	Scenarios and impacts – Influence of return period	43
4.5.2.	1D closed conduit model	51
4.5.3.	2D overland flow model P-DWave	52
4.5.4.	Validation, evaluation and assessment.....	57
5.	Results	61
5.1.	Basic Scenario “Real flood”	61
5.1.1.	Checkpoints – Maximum water depths and flood progression	61
5.1.2.	Maximum water depths of area.....	64
5.1.3.	Flood extent and flooding	70
5.2.	Scenario “Fully operated conduits”	72
5.2.1.	Checkpoints – Maximum water depths and flood progression	72
5.2.2.	Maximum water depths of area.....	75
5.2.3.	Flood extent and flooding	78
5.3.	Scenario “Fences”	81
5.3.1.	Checkpoints – Maximum water depths and flood progression	81
5.3.2.	Maximum water depths of area.....	84
6.5.3.3.	Flood extent and flooding	87
5.4.	Scenario “Spatially extended rainfall”	90
5.4.1.	Checkpoints – Maximum water depths and flood progression	90
5.4.2.	Maximum water depths of area.....	94
5.4.3.	Flood extent and flooding	97
5.5.	Scenario “Diversion and retention pond”	100
5.5.1.	Checkpoints – Maximum water depths and flood progression	100
5.5.2.	Maximum water depths of area.....	105
5.5.3.	Flood extent and flooding	109
5.6.	Influence of return period – Scenario “Real flood”.....	116
5.6.1.	Checkpoints – Maximum water depths	116
5.6.2.	Maximum water depths of area.....	120
5.6.3.	Flood extent and flooding	126
5.7.	Alternative Scenarios “Diversion, retention pond and METRO fence” and “New diversion and retention pond”	129
5.7.1.	Maximum water depths of area.....	129

5.7.2.	Flood extent and flooding	132
6.	Discussion	134
6.1.	Basic Scenario “Real flood” – Model validation and evaluation	134
6.1.1.	Checkpoints – Maximum water depths and flood progression	134
6.1.2.	Maximum water depths of area, flood extent and flooding	134
6.2.	Impact of Scenario “Fully operated conduits”	135
6.2.1.	Checkpoints – Maximum water depths and flood progression	135
6.2.2.	Maximum water depths of area.....	136
6.2.3.	Flood extent and flooding	136
6.3.	Impact of Scenario “Fences”	137
6.3.1.	Checkpoints – Maximum water depths and flood progression	137
6.3.2.	Maximum water depths of area.....	137
6.3.3.	Flood extent and flooding	138
6.4.	Impact of Scenario “Spatially extended rainfall”	138
6.4.1.	Checkpoints – Maximum water depths and flood progression	138
6.4.2.	Maximum water depths of area.....	139
6.4.3.	Flood extent and flooding	139
6.5.	Impact of Scenario “Diversion and retention pond”	139
6.5.1.	Checkpoints – Maximum water depths and flood progression	139
6.5.2.	Maximum water depths of area.....	140
6.5.3.	Flood extent and flooding	140
6.6.	Influence of the return period – Scenario “Real flood”	141
6.6.1.	Checkpoints – Maximum water depths	141
6.6.2.	Maximum water depths of area.....	141
6.6.3.	Flood extent and flooding	142
6.7.	Evaluation of Scenario “Diversion and retention pond” and the alternative Scenarios for T=50 years	143
6.7.1.	Maximum water depths of area.....	143
6.7.2.	Flood extent and flooding	144
7.	Conclusion	145
	Appendix	149
	Bibliography	xvii
	Declaration of Authorship	

1. Introduction

1.1. Flood event – Scope of work

On 14th and on 15th November 2017, a very intense storm at Thriasio Plateau in Western Attica, Greece, resulted in the occurrence of a flash flood at towns close to the sea and mainly at the town of Mandra, which is located exactly at the exit of two basins. The flash flood caused significant property damage and, sadly, the loss of 23 people, making it the third deadliest flood in the western suburbs of the Attica Prefecture, Greece. Flash floods are caused by extraordinary heavy rain events, which occur locally and form rapidly rising water levels (LfU 2018). In comparison to other flood types, some of which can be predicted hours to days in advance, these are difficult to predict meaning that good precautions are much more important than predictions (Thieken et al. 2016; Disse and Kaiser 2018).

The objective of this thesis is to simulate the flash flood of 2017 at the town of Mandra using a 1D/2D coupled model and to assess the impact of the proper maintenance of the closed conduits, the implementation of private protection measures, the extension of the rainfall zone over the flooded area and the incorporation of a stream diversion and a retention pond. Additionally, the model is applied to four rainfall scenarios in order to investigate the influence of the return period. Finally, solutions without canalisation works are examined.

1.2. Outline of work

This work can be outlined as follows:

- **Chapter 2** deals with a description of the study area, the streams and the mountain basins used in the hydrological analysis as well as a description of the November 2017 flash flood and the temporal and spatial runoff course.
- **Chapter 3** deals with a description of the tools used in the hydrological simulation, a literature review of urban flood modeling approaches, the presentation of the theory of 2D parallel diffusive wavemodel (P-DWave) and of Storm Water Management Model SWMM as well as their coupling into a 1D/2D model, which is applied to the hydraulic simulation.
- **Chapter 4** deals with the data and set up of the inflow hydrographs generation according to the hydrological simulation. Additionally, the hydraulic simulation is presented as a model set up of a 1D/2D coupled model using SWMM and the 2D

overland flow model P-DWave. Conclusively, the evaluation and assessment criteria are shown.

- **Chapter 5** deals with the presentation of the simulation results for the flash flood of 2017. Also, it deals with the model application in different scenarios in order to assess the impact of the proper maintenance of the closed conduits, the extension of the rainfall zone over the flooded area, the implementation of private protection measures, the incorporation of a stream diversion and a retention pond and the influence of the return period. Finally, solutions without canalisation works are presented.
- **Chapter 6** deals with the model validation and evaluation, the assessment of the impact of the different Scenarios, the assessment of the influence of the return period and the examination of the solutions without canalisation works.
- **Chapter 7** deals with summarizing the conclusions of this thesis as well as suggestions for further research and improvement.

2. STUDY AREA

2.1. Generally

Mandra is the seat of the municipality of Mandra - Idyllia, which is administratively part of the Western Attica Regional Unit of the Attica Prefecture. The population of the town is 11,327 residents according to the 2011 census by the Hellenic Statistical Authority (ELSTAT). The town is located at the outlet of two catchment areas, these of Soures and Agia Aikaterini, which are the streams that caused the flood on 15/11/2017. These basins, like the town, are located in the surrounding area of the Raryo-Thrace field, which is described below. Figure 1 shows the location of the study area at the town of Mandra in Greece.

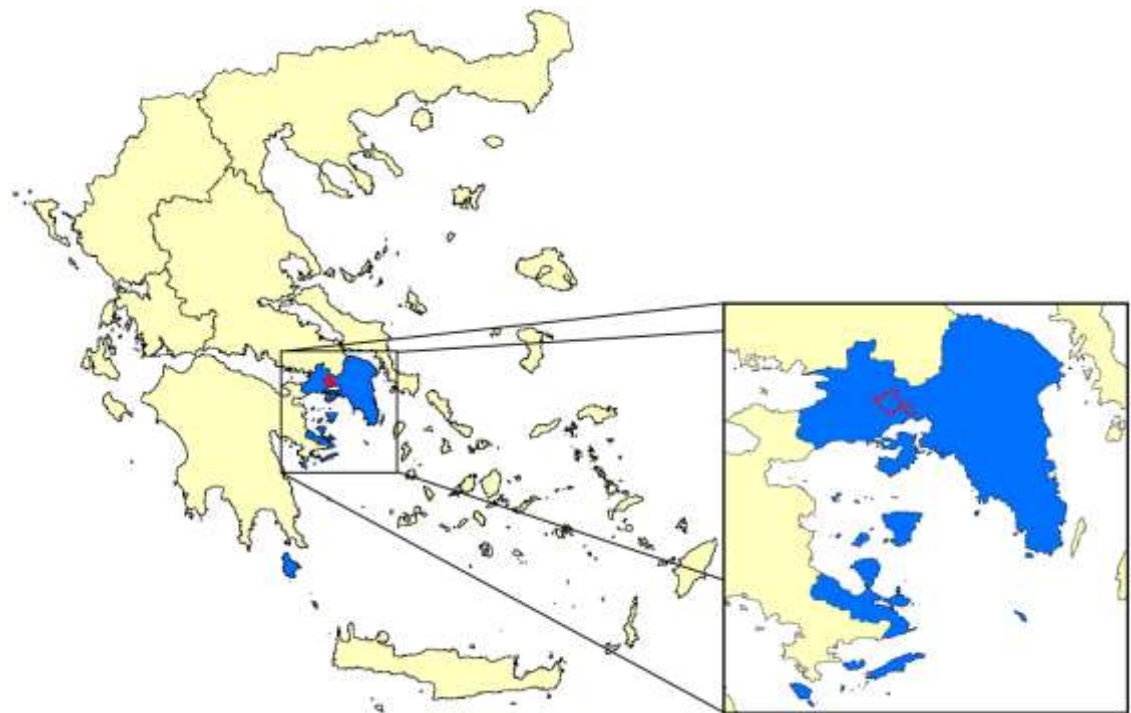


Figure 1 Location of the study area in Greece, Attica and town of Mandra

Generally, the Raryo-Thrace field is a lowland area west of Athens bounded by Mount Parnitha to the north, Mount Aigaleo to the east, Mount Pateras to the west and the Gulf of Eleusis to the south. The main water bodies in the Raryo-Thrace field, from east to west, are:

1. The stream of Agios Georgios or Giannoula, emanating from the southwestern outskirts of Parnitha, flows east of Aspropyrgos and flows into the sea near the state refineries (Flood risk management plan, YPEKA 2017).

2. The stream of Agios Ioannis, which originates from the southwestern outskirts of Parnitha, moves west of Aspropyrgos and flows into the sea in the area of Halivourgiki.
3. The Sarantapotamos torrent originating from the confluence of two stream branches, the Pelkas stream that originates from Mount Kithaironas and crosses the Oinoi Valley and the Agios Georgios stream which flows from the eastern slope of Mount Patera and crosses the homonymous valley next to the valley of Oinoi. The Sarantapotamos torrent, after the contribution of the aforementioned branches, runs through the Raryo-Thrace field and eventually flows into the Gulf of Eleusis in the area of Halivourgiki. The main torrents which contribute to Sarantapotamos are Ag. Vlasios, Ksirorema and Megalo Katerini.
4. The stream Soures, with contributor streams the streams of Agia Aikaterini and Mikro Katerini, which is the subject of this study and is described in detail below.

2.2. Soures stream

The stream of Soures comes from the confluence of two water courses, which unite at the location of Agios Charalambos. It is the Skylorema torrent that originates from the southeastern outskirts of Mount Patera and the Agia Sotira torrent that originates from the Rachi Sotiros region (Apostolidis et al. 2017). The Skylorema torrent has a length of 6.7 km and that of Agia Sotira has a length of 4.7 km. Following the union of the above water courses (see Figure 2) the Soures stream crosses the old Athens-Thebes National Highway (PEOATH) at the technical works (1) and (2), continues along the PEOATH, passes by Michelin factory and underpasses a rural road (3), then underpasses the Vakontios factory (4), the Municipality of Mandra's depot (5) and meets the PEOATH again which it underpasses (6) besides the Logistics METRO factory. Then, it crosses Psiloritou street (7) and V. Douka street (8) besides the Municipality of Mandra's cemetery, crosses the bridge at Louka street (9), and eventually confluences to Agia Aikaterini stream (Vageli Koropouli's closed conduit) at (10), 6.5 km after the town of Mandra entrance. The extent of the stream Soures catchment area at the location of the confluence is equal to 19.35 km². About 100 meters from the confluence, Soures stream crosses again the PEOATH and after about 125 meters having passed by the DHL factory (11) transitions into an artificial river channel, constructed as part of the Attica Road works. The project consists of a twin rectangular concrete channel with dimensions 2 x 4.00 x 3.00 m and length L=2.200 m. The project captures the flows of the two Mandra streams, incorporates the technical works at (12), (13) and the underpassing of the Attica

Road (14), captures the flow of Mikro Katerini stream and finally diverts all the aforementioned flows to Sarantapotamos stream (15). In the past, the Soures stream, after joining the Mikro Katerini stream, was flowing in the direction N-S towards Eleusis, passing through the town and reaching the sea on the western boundary of the town. The diversion of Soures to Sarantapotamos had already been proposed in 1979 with the study « MELETI ANTIPLIMMYRIKIS PROSTASIAS THRIASIOU PEDIU N. ATTIKIS » («STUDY OF FLOODPLAIN PROTECTION IN THE RARYO-THRACE FIELD OF THE ATTICA PERFECTURE») (Peppas and Karavokyris 2004) and was finally constructed by Attiki Odos SA (Attica Road SA).

Figure 2 shows the town of Mandra with its hydrographic network and the technical works. The Sarantapotamos stream, in which the stream Soures runs into, is shown with blue color.



Figure 2 The town of Mandra with the hydrographic network and technical works

2.3. Agia Aikaterini stream

The stream of Agia Aikaterini comes from the confluence of two streams. These are the Katsimidi stream and the Osios Meletios stream (Apostolidis et al. 2017). The length of Katsimidi stream is 6.4 km, that of Osios Meletios is 4.2 km and that of the Agia Aikaterini stream, from the union to the town boundary on Omirou Street, is 3.0 km. In the last 500 m upstream of Omirou Street, the stream of Agia Aikaterini did not have a shaped bed

before the flood event. This is confirmed by orthophoto maps of Greek Land Registry and the available digital elevation model. From Omirou Street, the stream's historic riverbed was converted into road axes, and the waters were driven through a concrete-bounded conduit (16) with dimensions 2.00 m x 1.70 m and length $L=2.300$ m approximately, to the point of confluence with Soures stream. The conduit crosses the streets of Omirou, Agia Aikaterini, Stratigou Nikolaou Rokka and Vageli Koropouli and flows into Soures stream in the town entrance. The extent of the catchment area of Agia Aikaterini stream at the site of the confluence equals to 22.80 km².

2.4. Catchment areas (watersheds)

The basins of interest for hydrological analysis were mapped using the digital elevation model (DEM), with a resolution of 5 m x 5 m (see Figure 3), given by the Greek Land Registry (Mavrogeorgos 2019), which is considered to be appropriate for modelling purposes taking into consideration that resolution meshes with values between one and five meters capture all the main topographic features (Mark et al. 2004). The outlets of the two basins were selected given the respective basins of the area from « FLOOD RISK MANAGEMENT PLAN » of YPEKA for the water department of Attica (GR06). Thus, the catchment area for the Soures stream is identical with the basin «GR0626FR00197» and the basin for the Agia Aikaterini stream is the sum of basins «GR0626FR00155» and «GR0626FR00157».

The catchment area of Agia Aikaterini stream in the selected place is 18.30 km² and its elevation varies from 123.8 to 591.2 m. The length and the average slope of the main stream are 8.7 km and 4.85%, respectively. The catchment area of Soures stream is 16.06 km² and its elevation varies from 161.5 to 841.4 m. The length and the average slope of the main stream are 10.03 km and 5.13%, respectively.

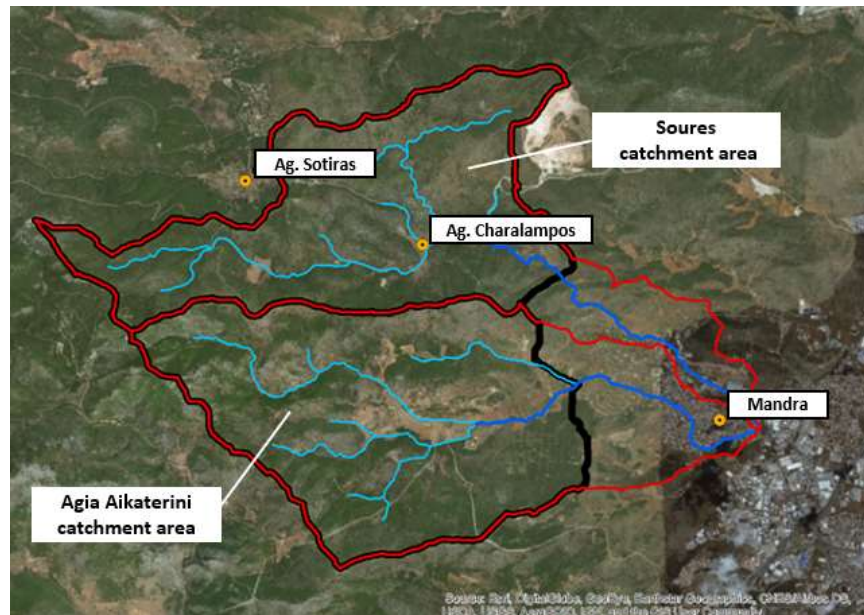


Figure 3 The catchment areas of the study area (Mavrogeorgos 2019)

2.5. Description of the flash flood on 15/11/2017

On 14th and on 15th November 2017, a very intense storm occurred at the mountain Pateras causing sudden floods in the area's watersheds and specifically in that of Yioryi torrent (or Zoireza) basin, which runs into Nea Peramos, in the basins of Soures and Agia Aikaterini streams, which run into Mandra and in the basin of Sarantapotamos stream. However, the majority of the volume of the storm fell into the Soures and Agia Aikaterini basins and caused major disasters at the town of Mandra.

The rainfall field during the event was recorded by the mobile Doppler polarimetric weather radar (XPOL) of the National Observatory of Athens. Although radar estimations are quite uncertain as to the height of the total precipitation, they provide important information on the spatial and temporal evolution of the event. So, according to the radar recordings, the rainfall accumulation was mainly restricted in a quite narrow rainfall zone of 18 km x 4 km in the windward (southeast) slope of the Mt. Pateras (about 1100 m height), indicating a fairly local and at the same time intense phenomenon. The rainfall zone which corresponds to the study area is limited upstream the black border line, as it is shown in Figure 3. The storm started on the night of Tuesday 14 November with a short and quite a small event around 20:00 EET. From midnight onwards, as it is shown in Figure 4, the rain continued for about 8 hours while the storm core occurred between 05:00 and 08:00 EET. This high rain localised event was mainly due to orographic rain and not to rain advection with a weather front.

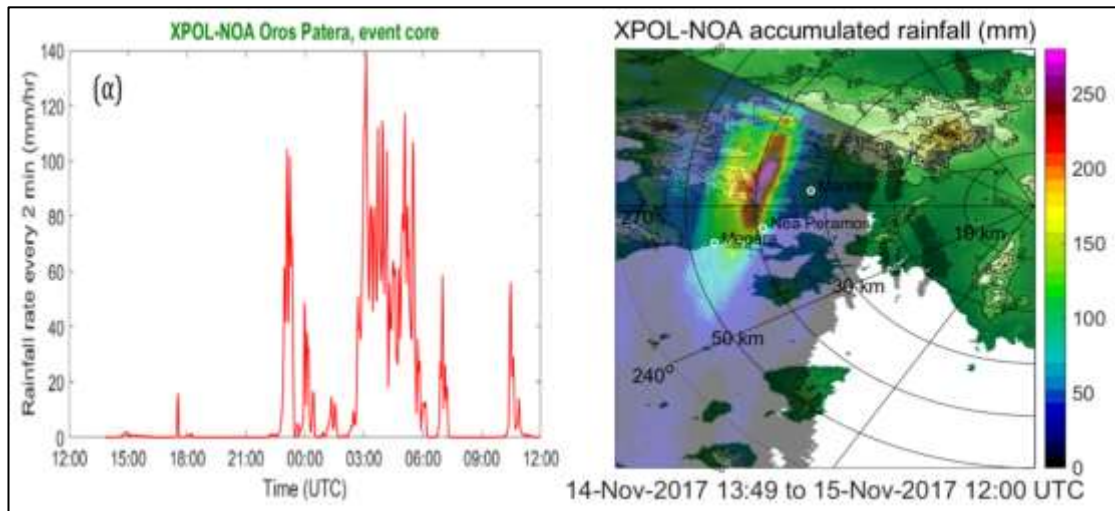


Figure 4 Rainfall hyetograph (left) and accumulative rainfall depth (right) from the estimations of X-POL (Kalogiros et al. 2017)

The total amount of rain exceeded 200 mm in 6 hours (Kalogiros et al. 2017; Kontoes et al. 2018).

2.6. Temporal and spatial runoff course – Autopsy results

The flood wave from Agia Aikaterini stream reached the western boundary of the town at about 06:00 while the flood wave from Soures stream reached the technical work (1) (see Figure 5) and the northwestern boundary of the town at about 06:45. The waves were accompanied by large quantities of debris which gave them the characteristic brown color seen in photographs and video recordings. From the point of extinction of the riverbed of Agia Aikaterini stream at (A) and afterwards, a very large flood wave created a flood that occupied the lowland area upstream of the town and then hit the urban area along its entire length. In the Soures stream, morphological changes have played a decisive role in the spread of the flood due to the intense construction activities in the wider area that have resulted in a dramatic reduction in the available cross-sectional area of the stream (Stamou A. 2018). The flood wave overflowed from the riverbank all the way from the northwest entrance of the town (at the site of the new PEOATH bridge (B)) up to the junction of Rokka street & Koropouli street intersection. All adjacent facilities were affected by the flood, such as the Vakontios building (4), the Municipality of Mandra's depot (5), the Logistics METRO (6) building and the Mandra cemetery (7). Much of the flooding followed the PEOATH axis and from there it spread out to the town entrance and towards the Magoula area via Louka (Stamou) street (8). Flood runoff from the two streams reached the confluence of the streams (C) at 7:05 am (Apostolidis et al., 2017). Consequently, a part of the flood runoff underpassed the

PEOATH (10), entered the artificial channel (11), reached the Attica Road (14) and finally outflowed into Sarantapotamos stream (D). Another part of the runoff overflowed at (10), due to the small cross-section of PEOATH bridge. Subsequently, the industrial area of Mandra flooded and eventually the waters were trapped behind the Attica Road. Finally, the runoff drained under the bridge of Attica Road (E) and flooded the Papakosta area.



Figure 5 Course of Agia Aikaterini and Soures streams

The extent of the flooded areas was captured by a scientific team from the FloodHub service (<http://beyond-eocenter.eu/index.php/floods>) of the BEYOND Center of EO Research and Satellite Remote Sensing of the National Observatory of Greece. Figure 6 shows the mapping of the maximum extent of the flood, as a hybrid result of satellite image classification with automatic unobservable classification (with an algorithm detecting water saturated soils), photo-correction (in case of automatic confusion), and the utilization of data collected during the field survey (21-23 / 11/2017), as well as additional elements that have seen the light of day (Kontoes et al. 2018). The imaging was mainly based on a multi-spectral image from the optical receiver of the World View-4 satellite, which was taken on 21/11/2017 and is a high spatial resolution image with a resolution of 31 cm. It was also based on the combined use of unattended image classification and photo interpretation methods. These procedures were carried out in appropriate combinations of satellite image spectral channels in order to obtain the most accurate and detailed impression of the flooded areas.



Figure 6 Mapping of the maximum extent of the flood (Mavrogeorgos 2019)

The final mapping of the maximum extent of the flood is used in the present work for the evaluation of the hydraulic model.

Undergraduate and postgraduate students of the NTUA's Applied Hydraulics Laboratory, under the coordination and scientific guidance of Professor Anastasios Stamou undertook four autopsies to the town of Mandra from September to November 2018. During these visits several positions (checkpoints) along the two streams were chosen in order to determine the depth of the flow according to the available video recordings of the flood event. However, in addition to the intended sites, flow depths were also measured on the structural elements that had been traced to the flood, months after it, due to the debris. In addition, residents were interviewed during the visits which were extremely useful in understanding the spatio-temporal evolution of the flood. Finally, the maximum extent of the flood, as recorded by the National Observatory of Greece team, was confirmed.

The checkpoint positions are shown in the following Figure 7. The checkpoint positions and the corresponding water depths ultimately used for the evaluation of the results of this work are given in Table 1. The reference point for the mileage of the intersections is the confluence of the two streams at the intersection of Rokka & Koropouli streets.



Figure 7 Checkpoints mapping

Table 1 Water depths at the checkpoints (Mavrogeorgos 2019)

Checkpoint	Position (m)	Description	Water Depth (m)
AA3	2810	Old factory	1.75 (max)
AA4	2120	Aiantos & 25 Martiou	0.80 (6:45)
			1.55 (7:38)
			1.25 (8:30)
			0.10 (10:30)
AA5	2090	Ikarou & 25 Martiou	0.10 (6:30)
			0.50 (6:45)
			1.00 (7:00)
			1.38 (7:15)
			1.45 (7:30)
			1.30 (7:42)
			0.50 (8:45)

AA6	1710	Super market Galaxias	0.20 (6:30)
			0.55 (6:46)
			0.76 (6:55)
			0.90 (7:01)
			1.03 (7:09)
			1.15 (7:13)
			1.15 (7:42)
			0.85 (8:08)
0.20 (9:21)			
AA7	1430	Vageli Koropouli 10	1.45 (7:03) 1.55 (8:15)
AA8	466	Vageli Koropouli 81 (School)	1.55 (max)
S1	3930	1 st technical work	0.15 (6:15)
			0.50 (6:30)
			1.20 (6:45)
			2.50 (7:00)
3.70 (7:15)			
S2	2060	Michelin	2.85 (max)
S3	1690	Nea ethniki odos (Bridge)	0.15 (6:15)
			0.25 (6:30)
			0.50 (6:45)
			1.50 (6:55)
			1.90 (7:00)
			3.50 (7:15)
			2.70 (9:15)
S4	1140	Vakontios downstream	0.1 (6:30)
			1.20 (6:45)
			2.17 (7:00)
			2.90 (7:30)
			3.04 (8:30)
			2.52 (9:15)
1.90 (10:00)			
S5	1020	Municipality of Mandra's depot	
S6	763	Logistics METRO	4.00 (max)
S7	526	Cemetery upstream	3.00 (max)
S8	316	Louka street	3.60 (max)

S9	0	Confluence of the streams	0.50 (6:46) 0.50 (7:00) 3.65 (7:30)
S10	-120	PEOATH downstream	5.50 (max)
S11	-439	Technical work of DHL downstream	5.20 (max)
S12	-1340	Attika road upstream	3.80 (max)
S13	-2230	Outflow into Sarantapotamos stream	2.50 (max)

3. MATHEMATIC MODELS

3.1. Hydrological simulation

3.1.1. Methodology for estimation of flood parameters

The analysis of each flood event aims at extracting the rainfall characteristics (such as active rainfall, runoff coefficient and return period) and the runoff characteristics (time distribution, peak discharge).

The results of each analysis are a useful source of data for future work. The most common method of transforming rainfall into runoff is that of unit hydrograph. The unit hydrograph of d hours is the hydrograph produced by active rainfall of d hours of 10 mm and constant intensity in space and time. The theory of unit hydrograph is based on two basic principles (Mimikou and Baltas 2012):

- **The principle of proportion:** Two active rains of the same duration but with different intensities create hydrographs with the same time base and ordinates which at each time have a ratio equal to the ratio of the intensities.
- **The principle of superposition:** The total hydrograph obtained from individual rainfall is the hydrograph with ordinates equal to the sum of the ordinates of the individual hydrographs.

The establishment of the unit hydrograph in a basin of interest requires hydrometric data from actual flood events. In most basins there are no proper measurements, but even when there are, the direct establishment of the unit hydrograph poses risks because of the reliability of the measurements on the one hand and the assumptions to be made for its extraction on the other. So, the synthetic unit hydrograph is applied almost exclusively to hydrological analysis. Its establishment is based on the physiological characteristics of the study area. In the literature there are numerous methods for its estimation. In Greece, the triangular synthetic unit hydrograph of the British Institute of Hydrology is being implemented (Sutcliffe 1978), that of Snyder (Snyder 1938) and the dimensional (smooth) (USDA Soil Conservation Service 1972).

3.1.2. Parametric synthetic unit hydrograph

For the Greek basins, the parametric synthetic unit hydrograph developed from events analysis in the framework of the DEUCALION research program (Efstratiadis et al., 2014), as it is shown in Figure 8, can also be used. This is composed of a linear upward

branch and an exponentially decreasing downward branch. In order to compile it, the time of the upward branch is calculated by the following equation:

$$t_p = \frac{d}{2} + \beta t_c \quad (1)$$

and the downward branch from the equation:

$$t_b = d + \gamma t_c \quad (2)$$

where,

β, γ : dimensionless parameters with $0 < \beta < 1$ and $\gamma \geq 1$

d : the duration of the unit rainfall and

t_c : the concentration time of the basin (catchment area).

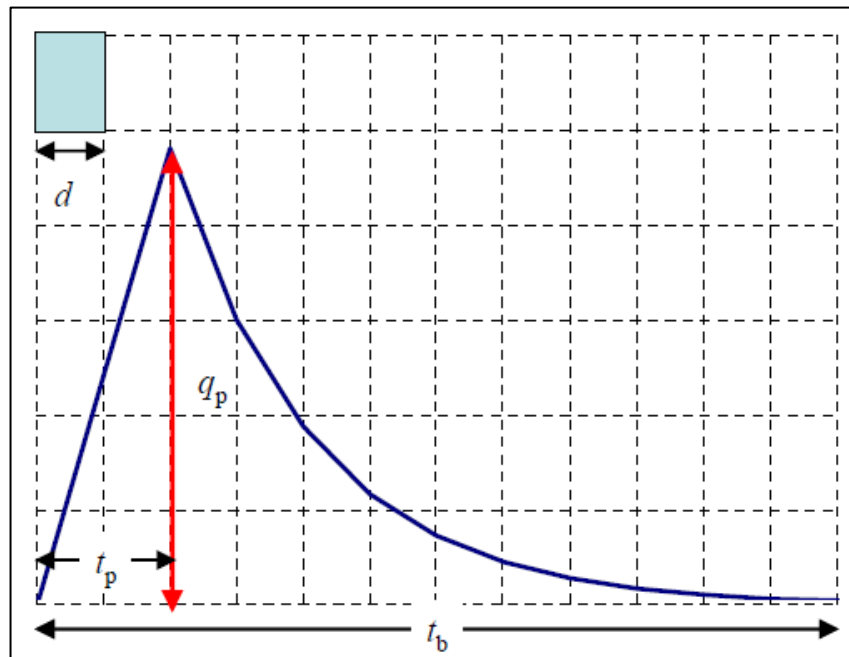


Figure 8 The parametric synthetic unit hydrograph with its characteristics (Efstratiadis et al. 2014)

The above characteristic times are rounded to be integer multiples of the duration d , then the peak discharge Q_p is calculated and the hydrograph ordinates of each time step as well. The discharge Q_p is calculated from the volume of the unit hydrograph for which $V_0 = h_0 \cdot A$, where $h_0 = 10$ mm the height of the unit rainfall and A the basin. There is no analytical formula for the flow peak because the volume equation derives a complex relation, which is numerically solved.

For $t \leq t_p$ the discharge is calculated from the equation:

$$u(t) = Q_p t / t_p \quad (3)$$

For $t > t_p$, the discharge is calculated from the exponential equation:

$$u(t) = Q_p \exp\left(\frac{-k t}{t_b}\right) \quad (4)$$

where k is a coefficient calculated such, so that for $t=t_b$ the discharge Q_p will receive a minimum value, usually equal to $0.01 \text{ m}^3/\text{s}$. After the equation (4) is applied, the coefficient k is a result of the following equation:

$$k = -\ln(Q_0/Q_p) \quad (5)$$

From the analysis of the flood events in the study research mentioned above, the use of values $\beta=0.30$ for basins with steep slopes and $\beta=0.60$ for basins with mild slopes is suggested. The suggested values for the base time parameter γ are the following:

- $\gamma=1$ for dense urban basins, with a developed rainwater network
- $\gamma=5$ for low permeability basins
- $\gamma=10$ for medium to high water permeability basins
- $\gamma=20$ for karst basins, dominated by hypodermic flow.

3.1.3. Concentration time

The concentration time is defined as the time required, so that the water from the farthest point of the basin reaches the outlet. It is a fundamental coefficient of the watershed and is of high importance in hydrological design as it affects a variety of coefficients, such as the time step of the calculations, the duration of the designed storm, the shape and the peak of the unit hydrograph.

For the estimation of the concentration time exists a variety of empirical equations which is available in the literature. In hydrological studies in Greece, it is a common practice to use Giandotti's equation:

$$t_c = \frac{4\sqrt{A} + 1.5L}{0.8\sqrt{\Delta z}} \quad (6)$$

where,

$A \text{ (km}^2\text{)}$: the basin

$L \text{ (km)}$: the length of the main stream

Δz (m) : the difference between the mean altitude of the basin and the altitude of its outlet and

t_c : given in hours.

Concentration time should not be considered constant as it depends on the velocity of surface runoff. So, bigger heights of precipitation lead to higher velocities at the basin and at the hydrographic network, thus, decrease of the concentration time, respectively. In the framework of the DEUCALION research program (<http://deucalionproject.itia.ntua.gr/>), it is suggested to reduce the time resulting from Giandotti's equation, according to the following empirical equation:

$$t_c(T) = t_c \sqrt{\frac{i(5)}{i(T)}} \quad (7)$$

where $i(5)$ is the rainfall intensity that corresponds to a return period of 5 years, for which the estimation of the concentration time, according to Giandotti, is considered representative and $i(T)$ is the rainfall intensity for the return period of the study.

3.1.4. Estimation of hydrological losses

Unit hydrograph is a tool for transforming active rainfall into flood runoff. Therefore, prior to its application, it is necessary to separate the hydrological losses from the hyetograph, that is, the part of the rainfall retained by the soil and the vegetation. The most common method for estimating hydrological losses is that of the runoff curve number – CN developed by Soil Conservation Service (USDA Soil Conservation Service 1972). The basic assumptions of the method are the following:

- From the beginning of the episode to the time t_0 all the amount of rainfall is completely transformed into losses. This amount is called initial abstraction I_α and is a parameter of the method. Therefore, after time t_0 , the active precipitation P_e can not exceed the potential runoff $P - I_\alpha$, where P is the total rainfall.
- Also, after the time t_0 the additional amount of water retained in the basin F_α can not exceed an upper limit called maximum potential retention S , which is a parameter of the method.
- At anytime $t > t_0$, the relation between the active rainfall precipitation P_e and the additional loss F_α to the corresponding potential values ($P - I_\alpha$ and S respectively), are equal.

Therefore:

$$\frac{F_a}{S} = \frac{P_e}{P - I_a} \quad (8)$$

The equation of the water balance of the basin is as follows:

$$P = P_e + I_a + F_a \quad (9)$$

Combining the two above equations yields in the calculation of active precipitation P_e :

$$P_e = \begin{cases} 0, & P \leq I_a \\ \frac{(P - I_a)^2}{P - I_a + S}, & P > I_a \end{cases} \quad (10)$$

Usually, the initial abstraction is taken as a percentage of the maximum potential retention. With this simplification, the above relation is transformed as:

$$P_e = \begin{cases} 0, & P \leq \alpha S \\ \frac{(P - \alpha S)^2}{P + (1 - \alpha)S}, & P > \alpha S \end{cases} \quad (11)$$

Generally, the percentage α is taken equal to 20% of S , a value obtained from experimental results in small US rural basins with mild slopes. However, from analysis of rainfall runoff samples of the DEUCALION project, in most pilot basins (mainly mountainous) the percentage varied between 2-5%. Finally, the application of the above equation requires only one parameter, the value of which can be estimated from runoff measurements or the following empirical relationship:

$$S = 254 \left(\frac{100}{CN} - 1 \right) \quad (12)$$

The runoff curve number ranges from 0 to 100 and depends on the soil type, the land uses in the basin and previous soil moisture conditions, as determined by the SCS method.

According to SCS method, soils are classified into 4 Hydrological Soil Groups (Koutsyiannis and Xanthopoulos 2016):

HSG Group A: Soils with high infiltration rates even when thoroughly wetted. These consist chiefly of deep, well-drained sands and gravels.

HSG Group B: Soils with moderate infiltration rates when thoroughly wetted. These consist chiefly of soils that are moderately deep to deep, moderately well drained to well drained with moderately fine to moderately coarse textures.

HSG Group C: Soils with slow infiltration rates when thoroughly wetted. These consist chiefly of soils with a layer that impedes downward movement of water or soils with moderately fine to fine textures.

HSG Group D: Soils with very slow infiltration rates when thoroughly wetted. These consist chiefly of clay soils with a high swelling potential, soils with a permanent high water table, soils with a clay pan or clay layer at or near the surface, and shallow soils over nearly impervious materials.

Still according to the SCS standard, three types of humidity conditions are considered (Koutsyiannis and Xanthopoulos 2016):

Type I: The soils in the drainage basin are practically dry (dry soil, but the soil moisture content is at wilting point), which refers to the case that the cumulative rainfall of the former 5 days is <13 mm (or <35 mm, for vegetation under growing conditions).

Type II: Average condition, which refers to the case that the cumulative rainfall of the former 5 days is between 13 and 38 mm (or between 35 and 53 mm, for vegetation under growing conditions).

Type III: Practically saturated from antecedent rainfalls, which refers to the case that the cumulative rainfall of the former 5 days is >38 mm (or >53 mm, for vegetation under growing conditions).

Depending on the type of soil and land use the value of the coefficient CN_{II} is selected, for medium humidity conditions, from appropriate literature tables, where as for the other conditions a reduction is made through the following relationships:

$$C_I = \frac{4.2 CN_{II}}{10 - 0.058CN_{II}} \quad (13)$$

$$C_{III} = \frac{23 CN_{II}}{10 + 0.13CN_{II}} \quad (14)$$

Since the values of the coefficient CN, given in the literature, are applied for $\alpha=0.2$, if a different value is selected, a modification of the maximum potential retention S is required. For this purpose, the following process is followed:

1. With the value of CN_{20} , via the Equation (12) the maximum potential retention S_{20} is calculated, which is referred as a percentage of initial abstraction 20%.

2. Via the equation (11) the total active rainfall height P_e is calculated as a function of P , α and S_{20} .
3. For the desired percentage α , given the P and the P_e , the corrected value S_a is calculated, solving the Equation (11) depending on S_a as follows (Risva, 2018):

$$S(\alpha) = \frac{2\alpha P + (1 - \alpha)P_e - \sqrt{P_e[P_e(1 - \alpha)^2 + 4\alpha P]}}{2\alpha^2} \quad (15)$$

The following Table 2 shows the suggested values of initial abstraction percentage α .

Table 2 The suggested values of initial abstraction percentage α (Efstratiadis et al. 2014)

α (%)	Basin Type
5	Urban basins, basins with significant slope, low permeability soils
10	Non-urban basins of moderate water permeability and vegetation
20	Rural and forest basins, basins with important blocking works

3.1.5. IDF curves

In the general case of the dimensioning of hydraulic works the flood peaks are estimated using the intensity duration frequency curves (IDF curves). These curves are mathematical expressions that give the intensity of rainfall i as a function of the duration of rainfall d and the return period T . The establishment of IDF curves is based on the statistical analysis of maximum recorded storms for different time scales from 5 minutes to 48 hours. The general relation of the IDF curves is of the form (Koutsoyiannis et al. 1998):

$$i = \frac{\alpha(T)}{b(d)} \quad (16)$$

where $\alpha(T)$ is the function of the return period resulting from the distribution function fitted to the sample of measurements and $b(d)$ is the function of duration, given from empirical relationships. Depending on the relationships chosen for the functions $\alpha(T)$ and $b(d)$, the final shape of the IDF curves varies. In the issue «Drawing up IDF curves at country level» drafted by the YPEKA (Greek Ministry of Environment and Development) in the context of the implementation of the Directive 2007/60/EK, it is suggested to use a single methodology for all water bodies as developed by (Koutsoyiannis et al., 1998). According to YPEKA, the established IDF curves can be used to calculate the design rainfall

intensity, for a selected duration and return period, at any location or basin of the country. The final form of the curve is based on the Generalized extreme value (Gev) distribution and it is as follows:

$$i(d, T) = \frac{\lambda'(T^\kappa - \psi')}{\left(1 + \frac{d}{\theta}\right)^\eta} \quad (17)$$

where λ' , ψ' and κ are the scale, position and shape parameters respectively, of the Gev distribution.

3.1.6. Surface reduction

The establishment of IDF curves is based on point measurements at rainfall sites. However, the hydrological design should use the average surface rainfall of the basin. Due to the spatial variability of rainfall over a basin, it is impossible to record maximum rainfall intensity simultaneously throughout the basin. For the surface reduction of intensity, the values of the IDF curve are multiplied with the areal reduction factor ϕ . The factor ϕ has the following properties:

1. It is always <1 .
2. It is a decreasing function of the extent of the basin.
3. It is an increasing function of the rainfall duration.

In Greece the following relation is given by (Koutsoyiannis and Xanthopoulos 2016):

$$\phi = \max\left(1 - \frac{0.048 A^{0.36-0.01 \ln A}}{d^{0.35}}, 0.25\right) \quad (18)$$

where,

- ϕ : the areal reduction factor,
- A : the catchment area in km^2 and
- d : the rainfall duration in h.

The relationship was based on tabulated results of National Environmental Research Council (1975) of Great Britain.

3.1.7. Design storms

The synthesis of a design storm involves determining its overall duration, the determination of the time step and the partial rainfall heights at each time step. It should be mentioned that the total duration of the storm should be taken as an integer multiple

of the concentration time of the catchment area (indicatively $d > 3t_c$) and the time step should be taken as an aliquot part of the concentration time of the catchment area (indicatively $dt < 3t_c$).

The methods for the time distribution of design storms are divided into three main categories:

- **Dimensional cumulative curves:** At each time step, the amount of rain is given as a percentage of the total.
- **Simplified methods of partial rainfall heights:** At each time step, the amount of precipitation height is estimated through the IDF curve with the same return period as the total height.
- **Stochastic division models:** The time distribution is derived from a multitude of scenarios that reproduce the statistical structure of recorded storms.

In practice, the second method is more commonly applied and particularly the alternating block method (Sutcliffe 1978; Chow et al. 1988) and the worst profile – U.S. Department of the Interior, 1977.

In the alternating block method, the maximum segment height is set in the middle of the storm and the rest are in descending order left and right of the central block.

In the worst profile method, the partial heights are initially fitted correspondingly to the ordinates of the unit hydrograph, so, the maximum height of rainfall is at the same time placed as the maximum ordinate of the unit hydrograph, the immediately lower height in the same position as the immediately lower ordinate etc. The layout is then reversed and the final hyetograph is obtained.

3.2. Hydraulic simulation (Urban flood modelling)

Flood risk is expected to significantly increase in the twenty-first century and beyond, due to the ongoing rapid urbanisation and climate change (IPCC 2014). Urban flood modelling, that simulates the water movement in urban space and provides reliable flood mapping and inundation extent predictions has become an indispensable tool to support flood risk assessment and management (Ernst et al. 2010; Dawson et al. 2011; Dottori et al. 2013; Coles et al. 2017).

One-dimensional (1D) hydrodynamic models are easy to set up, calibrate and explain and provide good approximation in urban flood modelling with less computational effort.

These are the main reasons 1D models are preferred for more than 30 years by the industry and even nowadays most River Authorities and practitioners rely on them (Crispino et al. 2015; Leandro et al. 2009; Seyoum et al. 2012). Introduced in 1971, the Storm Water Management Model (SWMM) is considered a landmark of urban hydrological models (Delleur 2003). The Storm Water Management Model (SWMM) – an open-source software developed by the U.S. Environmental Protection Agency – is one of the most widely used models. Commercial software such as PCSWMM by Computational Hydraulics International (CHI) and MIKE URBAN by DHI often rely on the SWMM engine (Rossmann 2015; Chen et al. 2016; CHI 2020a; DHI 2020). 1D models when applied to floodplain flows, provide good approximations and they are preferred as long as the water moves in confined surface flow channels and therefore, remains within the street profile and while the surface flow paths can be identified (Mark et al. 2004). However, in many cases the water overtops the street curbs, changes direction and the flow paths are difficult to define. The same happens due to the complexity of the geometry formed by buildings, houses, and roads. Then, 2D surface flow models are preferred although they need more computational time (Mark et al. 2004; Allitt et al. 2009; Leandro et al. 2009; Seyoum et al. 2012). A benchmark test including six two-dimensional (2D) hydraulic models, conducted by Hunter et al. (2008), shows that flows in urban areas are successfully simulated by 2D models, provided that high-resolution terrain data, building topology and land use data are available and combined in the modelling process. When such terrain data are available, uncertainty in friction parameters becomes a more dominant factor than topographic error. However, fine mesh resolution (i.e. 5 m or less) for large areas can lead to unacceptable run times for 2D models simulations, while simultaneously requires a more complex parameterization of flow resistance (Dottori et al. 2013). Street widths appear to be a useful guide for selecting a mesh resolution. 3 cells across street with a mesh resolution of 5 m give a good balance between accuracy and computational effort according to Gallegos et al. (2009), while a mesh resolution of 1 to 2 m leads to an accurate simulation of the water depths but velocity values become inaccurate according to Fewtrell et al. (2011). A cell size between 1 m and 5 m is recommended by Mark et al. (2004). High resolution data are integrated with models. Buildings change the flow directions because they act as impervious obstacles in the flow path. There are several methods of representing buildings in the modelling mesh. The more commonly used method is the building-block method (BB), where ground elevation data are raised to the heights of rooftops. Alternatively, in the building-hole method (BH) the computational mesh can be generated with holes aligned with building walls, in the building-resistance method (BR) the flow

resistance is upscaled or meshes ignore buildings completely in the no-building method (NB) (Schubert et al. 2008; Schubert and Sanders 2012; Dottori et al. 2013; Leandro et al. 2016).

1D and 2D models cannot properly simulate the complex phenomenon of the interaction between the flow in the sewerage system and the urban overland flow. (Gallegos et al. 2009) approached the phenomenon modifying the 2D continuity equation with a set of point sink and source terms corresponding to curb inlets and sub-surface pipe outlets, respectively. 1D/1D models simulate the sewerage system and the urban overland flow using a one-dimensional approach. 1D/1D models use the dual drainage concept. A 1D surface network of channels that represents the natural flow paths and retention basins (major system) and a 1D pipe network that represents the sewer system (minor system) are linked by through manholes that allow a bi-directional flow between the two systems (Leandro and Martins 2016). However, the first attempts to model the interactions between the major and the minor system were one-directional and the surcharging water was lost from the system (Ellis et al. 1982). Later, the 1D/1D coupled hydraulic model used was simulation of interaction between pipe flow and overland flow in networks (SIPSON) (Djordjević et al. 2004). Djordjević et al. (1999) and Djordjević et al. (2005) presented a mathematical formula that solves simultaneously the continuity equation for network nodes, the complete St. Venant equations for the 1D sewer and 1D surface networks, and the links equations including the use of energy and mass conservation at the system interactions. 1D/1D models are widely used in practice due to their fast computational time and their sufficient accuracy. Yet, the same limitations apply to them as to the above-mentioned 1D models (Leandro et al. 2009; Seyoum et al. 2012).

1D/2D coupled hydrodynamic models overcome these limits, are easier and faster to set up, and model urban floodings very well (Allitt et al. 2009; Leandro et al. 2011). They combine a 1D sewer system model with a 2D hydrodynamic model to simulate overland flow and allow interaction between the systems using weir and orifice equations for linking according to the flow direction, which depends on the hydraulic conditions (Hsu et al. 2002; Chen et al. 2005; Bazin et al. 2014). Martins et al. (2017) compare three coupled models and find that models simplifying the Shallow Water Equations (SWE) produce comparable results to models that solve the complete shallow water equations with less computational effort. The heterogeneity of structures and land surfaces in urban environments and the complex interaction between the sewer system and the overland surface cause a high degree of uncertainty at urban flood modelling and are major challenges for the modeller (Salvadore et al. 2015; Leandro et al. 2016). As an example, the direct coupling of the building runoff to the sewer system – instead of being routed

by 2D overland flow to the sewer – closes the gap between the simulated sewer capacity and the design standards (Leandro et al. 2016). Also, the type of manhole and of the inlets affects the inflow as well as the surcharge and potential displacement of the manhole by surcharging water would impact the flow characteristics (Lopes et al. 2012; Chen et al. 2015; Beg et al. 2017).

The understanding of the physics of water during flooding is nowadays at a very advanced level due to experimental modelling of urban flooding through laboratory experiments (Mignot et al. 2019). However, according to Bates et al. (2014) there are still great uncertainties concerning urban flood modelling. Main causes of inaccurate models are the faulty input files, incorrect observations of real events leading to incorrect calibration, structural model errors and conceptual model uncertainty.

3.2.1. 2D parallel diffusive wave model (P-DWave)

The growing advances in remote sensing technologies in conjunction with the availability of Digital terrain models (DTM) have led the research to two-dimensional (2D) inundation models (Bradbrook et al. 2004). If catastrophic scenarios of dam break are excluded, where the full dynamic equations and the corresponding dynamic models must be applied, flooding over plain areas (floodplain inundation) is characterized by a slow moving phenomenon whereby the inundation can be modelled by the diffusive equations (Chen et al. 2005). The diffusive wave simplification neglects the inertia terms allowing a simplified set of equations to be solved leading to faster computational times.

P-DWave was developed by J. Leandro, A.S. Chen and A. Schumann. The formulas as a basis for the program were taken from their work "A 2D parallel diffusive wave model for floodplain inundation with variable time step (P-DWave)" (Leandro et al. 2014).

The basic equations of P-DWave are the 2D Shallow Water Equations. The 2D Shallow Water Equations (SWE) can be written in the conservative form as:

$$\frac{dh}{dt} + \nabla(uh) = R \quad (19)$$

$$\frac{dh}{dt} + (\mathbf{u}\nabla)\mathbf{u} + \frac{v_t}{h}(h\nabla\mathbf{u}) + g\nabla(h+z) = gS_f \quad (20)$$

where,

h : the water depth

\mathbf{u} : the depth-averaged flow velocity vector where, $\mathbf{u} = [u_x \ u_y]^T$

g : the acceleration due to gravity

- z : the bed elevation
 ν_t : the turbulent eddy viscosity
 R : the source/sink term (e.g. rainfall or inflow)
 \mathbf{S}_f : the bed friction vector where, $\mathbf{S}_f = [S_{fx} \ S_{fy}]^T$.

The Diffusive wave model neglects all the forces in the momentum equations except for the gravity term $g\nabla(h+z)$ and bed friction \mathbf{S}_f . Compared to the version discussed by Leandro et al., in the paper, the version of P-DWave used in this study also includes the new feature that both the water depth h and the height of the riverbed z are variable over time. The momentum Equation (20) simplifies to:

$$g\nabla(h+z) = g\mathbf{S}_f \quad (21)$$

The continuity Equation (19) is solved using an explicit first order finite volume discretization on a regular grid. The spatial domain of P-DWave is discretized in cell-centered control volumes:

$$\frac{h_i^{t+1} - h_i^t}{\Delta t} + \frac{1}{A_i} \sum_{j=1}^4 h_{ij} u_{ij} L_{ij} = R \quad (22)$$

where,

- A_i : the cell area
 L_{ij} : the contact face between cells
 u_{ij} : the water velocity at each of the four cell faces
 h_{ij} : the water-depth at each of the four cell faces and h_{ij} , u_{ij} evaluated as following:

$$h_{ij} = \frac{h_i + h_j}{2} \quad (23)$$

$$\mathbf{u}_{ij} = \frac{h_{ij}^{4/3}}{n_{ij}^2 |\mathbf{u}_{ij}|} I_{n,ij} \quad (24)$$

where,

- u_{ij} : the velocity in the direction perpendicular to each cell face
 $I_{n,ij}$: the water-level surface-gradient vector multiplied with the face unit normal vector $\tilde{n} = [\tilde{n}_x \ \tilde{n}_y]^T$ where, $I_{n,ij} = (S_{wx}\tilde{n}_x + S_{wy}\tilde{n}_y)_{ij}$.

For the sake of simplicity all variables without the time index are evaluated at the current time (t).

Explicit schemes must have the time step limited in order to ensure stability. In order to study the stability of the proposed numerical scheme, Equation (22) is re-written as (for the sake of simplicity R will be set to zero):

$$h_i^{t+1} = h_i^t \left(1 - \frac{\Delta t}{2A_i} \sum_{j=1}^4 a_{ij} \right) + \frac{\Delta t}{2A_i} \sum_{j=1}^4 a_{ij} h_j^t \quad (25)$$

where, $a_{ij} = u_{ij} L_{ij}$ and after u_{ij} replacement:

$$a_{ij} = \frac{h_{ij}^{2/3} I_{n,ij}}{n_{ij} \sqrt{I_{m,ij}}} L_{ij} \quad (26)$$

All coefficients in Equation (26) must be positive in order to ensure that the scheme remains stable and monotonic:

$$1 - \frac{\Delta t}{2A_i} \sum_{j=1}^4 a_{ij} > 0 \quad (27)$$

For a regular grid $A_i = \Delta x^2$ the final expression for the variable time step Δt in x-direction can be obtained by replacing the water-level surface gradient vector in Equation (26):

$$\Delta t < \text{ArgMax} \left(\text{ArgMin} \left(2\Delta x^2 n_{ij} \frac{\sqrt{I_{m,ij}}}{h_{ij}^{5/3}} \right), \Delta t_{min} \right) \quad (28)$$

for all i, j.

During a flood event, there are always dry cells at the beginning which change to a wet state and vice versa, resulting in moving boundary conditions. For this purpose, the parameter φ is introduced in the continuity equation (22).

$$\frac{h_i^{t+1} - h_i^t}{\Delta t} + \frac{1}{A_i} \sum_{j=1}^4 \varphi_j h_{ij} u_{ij} L_{ij} = R \quad (29)$$

If the water depth is greater than 0 in the next time step φ is always 1. If the water depth becomes negative, values between 0 and 1 are assumed for φ . Equation (30) shows the valid conditions under which the model remains completely conservative:

$$\varphi = \varphi_{1...4} = \begin{cases} 1 & \text{for } h_i^{t+1} < 0 \\ \frac{\Delta x^2 (h_i^t + R\Delta t)}{\Delta t \sum_{j=1}^4 h_{ij} u_{ij} L_{ij}} & \text{for } h_i^{t+1} > 0 \end{cases} \quad (30)$$

3.2.2. Storm Water Management Model SWMM

The Storm Water Management Model SWMM (version 5.1.001) is a 1D dynamic rainfall-runoff model created by the United States Environmental Protection Agency (USEPA). The runoff is generated by subcatchments that receive precipitation and the routing takes place in a system of pipes, channels, storage devices and pumps amongst others (Rossmann 2015). It is based on the gradually varied unsteady flow equations – the Saint-Venant equations.

SWMM offers steady flow, kinetic wave and dynamic wave routing for modelling the flow in the pipes or channels. The dynamic wave method that is used in the present study applies the continuity equation at the nodes and the continuity and momentum equation in the links. At every time step a combination of the momentum and the continuity Equation (31) must be solved for each link (Rossmann 2017):

$$\frac{dQ}{dt} = 2V \frac{dA}{dt} - V^2 \frac{dA}{dx} + gA \frac{dH}{dx} - gAS_f \quad (31)$$

where,

- x : the distance [m]
- A : the flow cross-sectional area [m²]
- V : the velocity [m/s]
- Q : the flow rate [m³/s]
- H : the hydraulic head of water in the conduit (Z+Y) [m]
- Z : the conduit invert elevation [m]
- Y : the conduit water depth [m]
- S_f : the friction slope (head loss per unit length)
- g : the acceleration of gravity [m/s²].

The spatial discretization dx is set to be equal to the length of the link L to be discretized in a finite difference form. The conduit cross-section area A and the velocity V are averages of the end values of the conduit at time t. The continuity Equation (32) shows that V and A are dependent on the discharge Q, the head in the node H, the surface area of the node and half the length of each attached link A_S and the node storage A_{Store} (Rossmann 2017):

$$\frac{dH}{dt} = \frac{\sum Q}{\sum A_S + A_{Store}} \quad (32)$$

The Equations (31) and (32) are then solved sequentially in order to derive the head at each node and the discharge in each link. To do so, Picard iterations are used to

integrate the continuity equation of the nodes over time step Δt . SWMM 5 uses an implicit backward Euler method to provide stability. The time steps are limited to the time it takes for the wave to propagate the whole length of the pipe with the so-called Courant-Friedrichs-Lewy condition (Rossmann 2017):

$$\Delta t \leq \frac{L}{|V|} \left(\frac{Fr}{1 + Fr} \right) Cr \quad (33)$$

where,

Fr : the Froude number

Cr : the Courant number.

Surcharge would result in equation (34) having no solution. Therefore, Equation (31) replaces it when there is no more volume available in the conduits that are connected to the node (Rossmann 2017):

$$\Delta H = \frac{-\sum Q}{\sum \frac{dQ}{dH}} \quad (34)$$

Should the surcharging exceed the node's maximum depth H_{max} the node becomes flooded and the overflow rate Q_{ovfl} is the average net flow rate (inflow – outflow) at the current time step, as Equation (35) shows:

$$Q_{ovfl} = 0.5 \left(\sum Q^t + \sum Q^{t+\Delta t} \right) \quad (35)$$

3.2.3. Coupling of SWMM and P-DWave

SWMM 5.1 consists of functions that are inside of Dynamic Link Libraries (DLL) which enable an easier linkage to other models compared to earlier versions (Leandro and Martins 2016). The idea of the presented linking method is to keep the original code and to only add functions that provide the ability to communicate with the 2D overland model: SWMM-Link, SWMM-to-2D and 2D-to-SWMM (Leandro and Martins 2016). SWMM-Link enables the extraction of the ID, the crest and elevations of the nodes that should be linked, as well as the simulation time and the time step. That initiates the linking time steps between the overland flow model and the SWMM model (Leandro and Martins 2016). SWMM-to-2D extracts the water levels at each time step of the nodes and takes the nodes' ID to exchange the flow. 2D-to-SWMM then exchanges the discharges between the two models (Leandro and Martins 2016).

The 2D overland model P-DWave includes two subroutines (Chen et al. 2007; Seyoum et al. 2012; Chen et al. 2015). The 1D/2D link discharges subroutine is in control of the bidirectional discharge between the models. The discharge is determined by either a

weir Equation (36), if the hydraulic head at the manhole h_{1D} is smaller than the ground surface elevation Z_{2D} or an orifice Equation (37), if $h_{1D} > Z_{2D}$:

$$Q = c_w w h_{2D} \sqrt{2g h_{2D}} \quad (36)$$

$$Q = c_o A_{mh} \sqrt{2g(h_{2D} + Z_{2D} - h_{1D})} \quad (37)$$

where,

Q : the discharge between the models

c_w : the weir discharge coefficient

w : the weir crest width [m]

A_{mh} : the manhole area [m²]

c_o : the orifice discharge coefficient.

Surcharging discharge is determined by another orifice Equation (38) (Leandro and Martins 2016):

$$Q = -c_o A_{mh} \sqrt{2g(h_{1D} - Z_{2D} - h_{2D})} \quad (38)$$

The second routine is used to synchronize the two models because the timestep in SWMM Δt_{1D} is always larger than in P-DWave Δt_{2D} . Therefore, the run time of SWMM is used as a synchronization time T_{sync} and the P-DWave timestep is adjusted when the 2D model run time should exceed T_{sync} (Leandro and Martins 2016):

$$\Delta t_{2D} = \min\left\{T_{sync} \Delta t_{1D} \sum \Delta t_{2D}; \Delta t_{2D}\right\} \quad (39)$$

Alternatively, one could set the time step in SWMM equal to time step in P-DWave. This, however, would increase the communication time between the models (Leandro and Martins 2016).

4. Methodology – Case of Mandra

This chapter deals with the data and set up of the inflow hydrographs generation according to the hydrological simulation presented in the previous chapter. Additionally, the hydraulic simulation is presented as a model set up of a 1D/2D coupled model using SWMM and the 2D overland flow model P-DWave. Conclusively, the evaluation and assessment criteria are shown.

Figure 9 displays the main processes and interactions between the singular models.

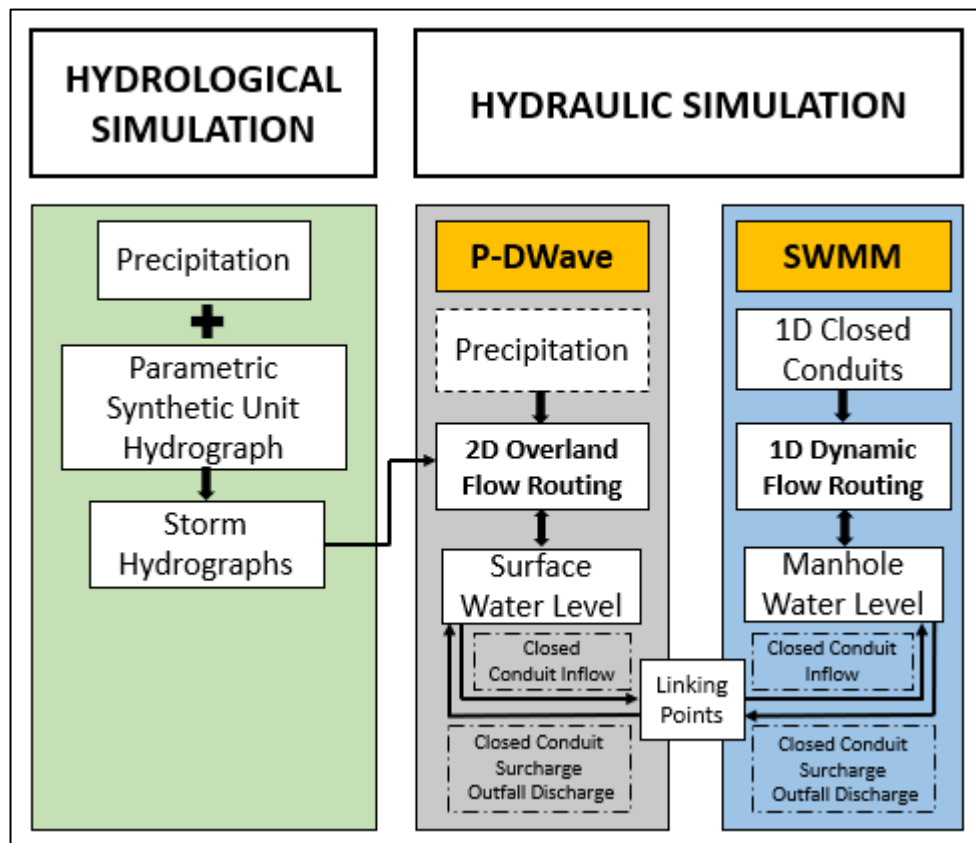


Figure 9 Model interaction scheme

Figure 10 presents the input data for the 1D/2D coupled model.

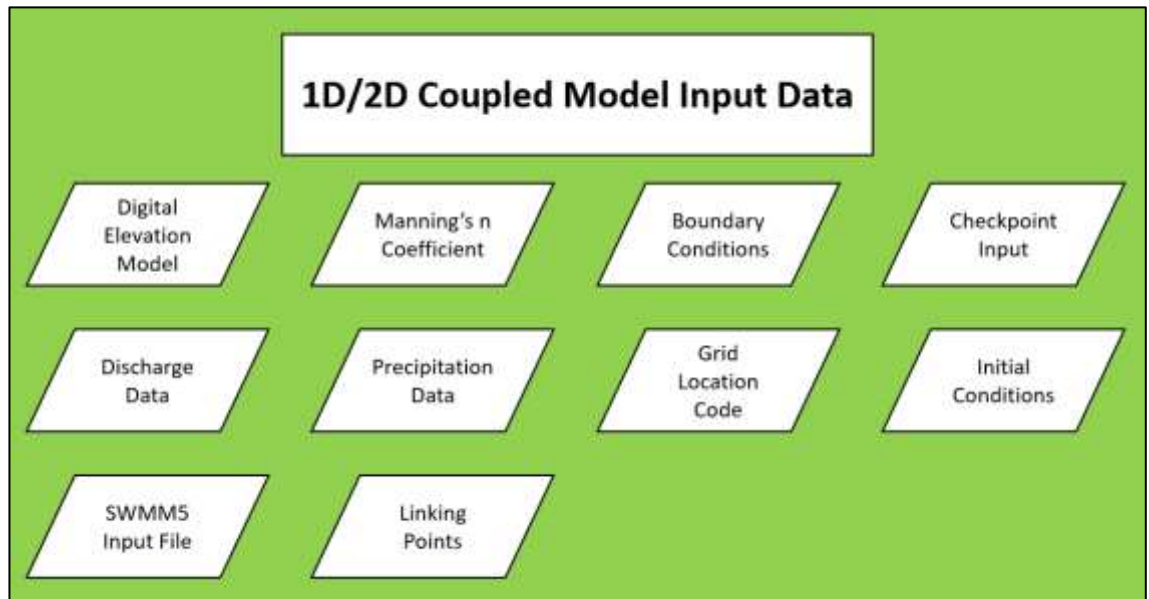


Figure 10 Model input data

Figure 11 shows the spatial distribution of the hydrological simulation area. The two red circles represent the location of the inflow storm hydrographs for the 1D/2D coupled model.

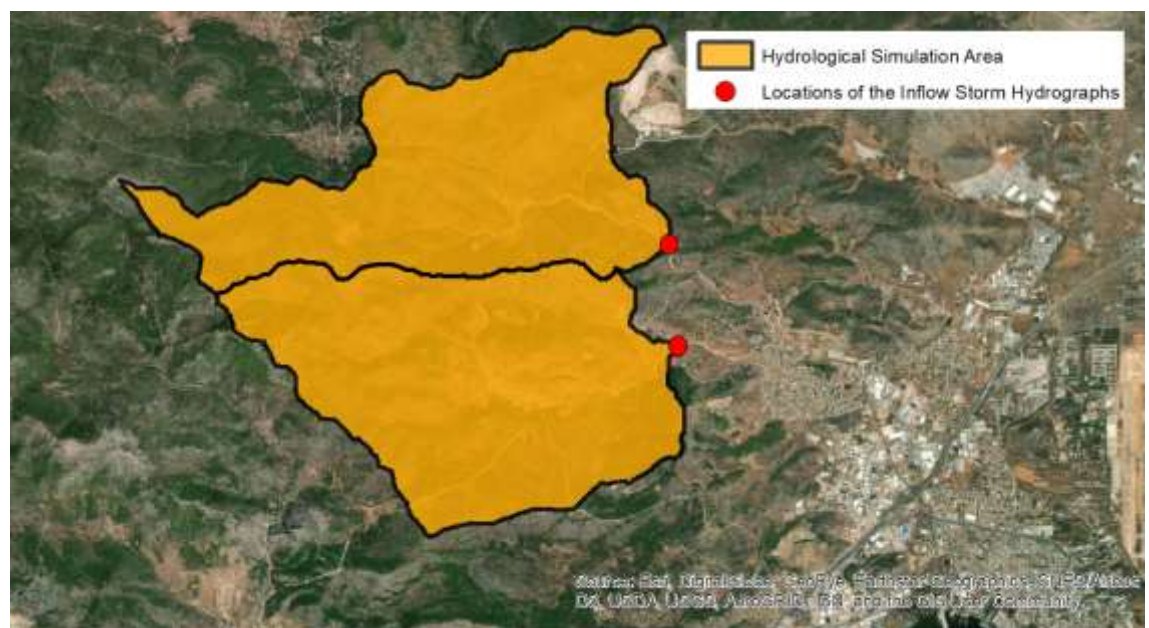


Figure 11 Spatial distribution of the hydrological simulation area where the circles mark the inflow locations generated by the hydrological simulation

Figure 12 shows the spatial distribution of the 1D/2D coupled model for the study area.

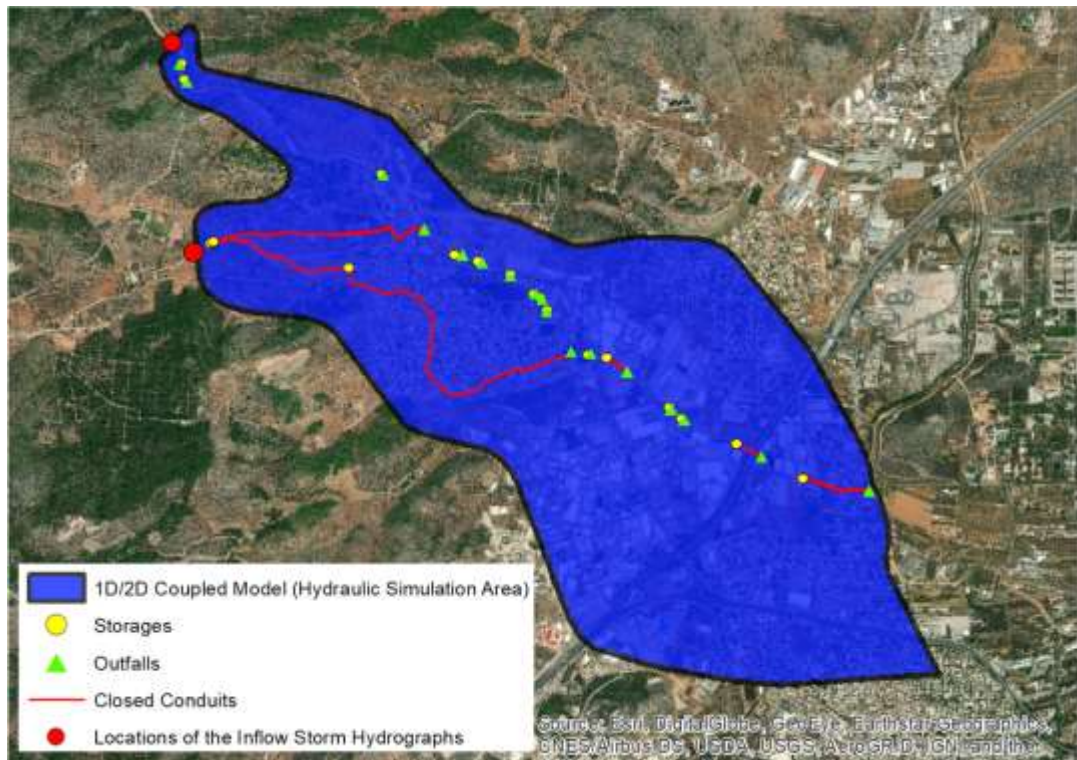


Figure 12 Spatial distribution of the coupled 1D/2D model where the circles mark the inflow locations generated by the hydrological simulation

4.1. Rainfall selection

For the best possible reproduction of the event and the assessment of the maximum discharges that hit the town of Mandra in November 2017, a necessary element is the recording of the rainfall. However, there was no rainfall station in the basins, which would greatly facilitate the hydrological analysis. In addition, from the rainfall stations of eastern Attica, no one is within the rainfall zone, as recorded by the meteorological radar X-POL of National Observatory of Athens. Thus, as a result, the recordings of the nearby stations at Mantra and Eleusis are not considered to be useful for further analysis, in order to calculate the maximum discharges because they have underestimated the event.

An attempt was made, in a diploma thesis, to reproduce the event in terms of size and time evolution through reverse hydrological analysis. Specifically, from level recordings of a conduit at the "Gyra Stefanis" site in the neighboring basin of Sarantapotamos it is attempted to estimate the rainfall time series at a hypothetical station X that is considered representative of the storm. Furthermore, Monte Carlo analysis was applied to better estimate the uncertainty and a total of 1000 time series were produced at station X. As concluded in the above work, although the analysis was based on scarce data, the

results seem reasonable and could be extended for hydrological analysis in the basins of Soures and Agia Aikaterini streams (Mavrogeorgos 2019).

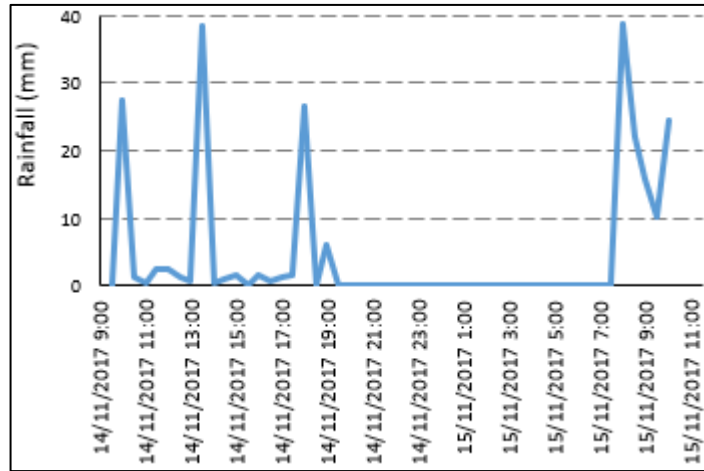


Figure 13 The simulated rainfall for 95% confidence interval on virtual station X (Mavrogeorgos 2019)

In a most recent diploma thesis, the time series of station X derived from the Monte Carlo analysis and corresponding to a 95% confidence interval were used after testing. The same time series of station X is adopted in the present work. This time series is from November 14, 09:30 am until November 15, 10:00 am and is shown in Figure 13 (Mavrogeorgos 2019).

4.2. Concentration time

In the present work, as in the above thesis, the Equation (7) can not be applied to reduce the concentration time as the return period of the event is not known. However, in order to take into account the dependence of the concentration time with the rainfall intensity, the reduction relationship recommended by Michailidi et. al. (2018) is used. In this work the calculation of concentration time was based on data from 30 basins in Greece, Cyprus and Italy. According to this, the final concentration time is obtained by applying the following three relationships:

$$t_c = t_0 \cdot i_e^{-\beta} \quad (40)$$

where,

t_0 : the unit concentration time (h)

i_e : the active rainfall intensity (mm/h)

β : a factor of recession and t_0 , β evaluated as following:

$$t_0 = 9.00 nA^{0.028}L^{0.216}b^{0.081}J^{-0.5} \quad (41)$$

$$\beta = 0.40 - 0.80 A^{0.186}L^{-0.5}b^{-0.356} \quad (42)$$

where,

- A : the catchment area (km²)
- L : the length of the maximum path (km)
- b : the mean width of the main stream (m)
- J : the mean slope of the main stream
- n : the average Manning's coefficient.

The calculation of concentration time, according to Giandotti, and the calculation of concentration time, after the reduction, appear in Table 3 and Table 4, respectively.

Table 3 Calculation of concentration time according to Giandotti

Basin	A (km ²)	L (km)	H _{mean} (m)	H _{exit} (m)	ΔH (m)	Concentration Time t _c (h)
Agia Aikaterini	18.30	8.7	302.5	123.8	178.7	2.82
Soures	16.06	10.03	377.8	161.5	216.3	2.65

Table 4 Calculation of concentration time

Basin	A (km ²)	L (km)	n	b _{aver} (m)	J (%)	t ₀ (h)	β	i _e (mm/h)	t _c (h)	Reduction from Giandotti
Agia Aikaterini	18.30	8.7	0.04	4.30	4.85	3.18	0.123	53.80	1.95	0.69
Soures	16.06	10.03	0.04	5.60	5.13	3.25	0.171	41.30	1.72	0.65

4.3. Results

4.3.1. Hydrological simulation area

The calculations were made using a suitable program that calculates the active hyetogram by applying the method SCS, synthesizes the parametric synthetic unit hydrograph and it combines them to produce the storm hydrograph. The time step of calculations was taken to be equal to 0.5 h, equal to the discretion time of the selected storm. For the establishment of the synthetic unit hydrograph, the rise time parameter β

was considered equal to 0.3 and the base time parameter γ equal to 3 for both basins. The synthetic unit hydrographs appear in Figure 14.

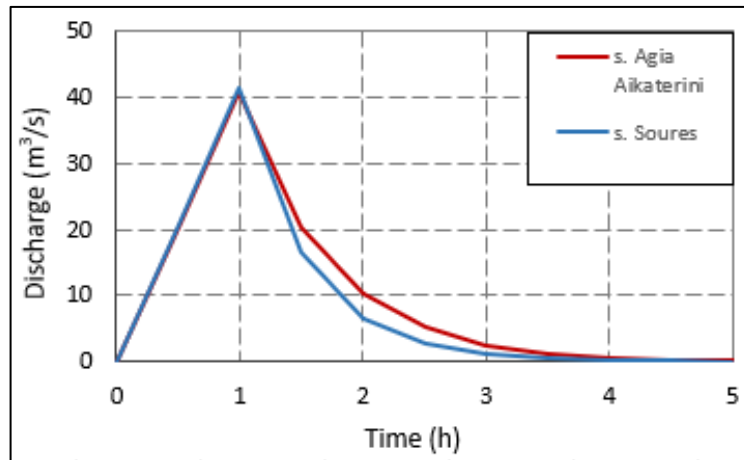


Figure 14 Synthetic unit hydrographs for rainfall duration $d=0.5$ h (Mavrogeorgos 2019)

Losses were calculated for the total selected event, with duration from 14/11/2017 09:30 to 15/11/2018 10:00. At the stations of Eleusis and Villia of the National Observatory of Athens, which are located closer to the study area, the total amount of rainfall of the 5 last days is 20.6 mm and 26.2 mm, respectively. Therefore, average conditions of previous soil moisture were selected. The parameter CN_{II} was obtained from the hydrology study of HYDROMENT (2018). In this study the CN number for the Soures stream was calculated based on the hydrogeologic map and land uses of the area but also on field surveys. According to this study, the value of CN_{II} in the basin of Soures stream equals to 60. The value of CN_{II} in the basin of Agia Aikaterini stream is 70, through proper reference to the given information (Mavrogeorgos 2019).

The percentage of initial abstractions α is taken equal to 20%. So, from the process described above, the hydrographs of the two streams (see Figure 15), which will be used by the hydraulic model, were calculated. The peak discharges were equal to 160 m³/s and 128.4 m³/s for Agia Aikaterini stream and Soures stream, respectively. The base time of the flood for the two streams is equal to 7 h. The hydrograph's inlet hours are determined so that the calculated flow depths match the available measurements and are not strictly identical to those obtained from the hydrological analysis. In this case, the inlet hours were equal to 05:40 a.m. for Agia Aikaterini stream and 06:15 a.m. for Soures stream.

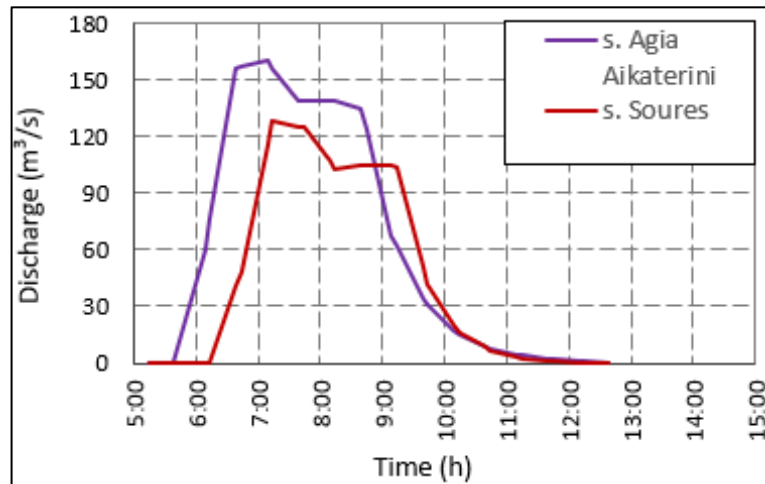


Figure 15 Inlet hydrographs for the hydraulic model (Mavrogeorgos 2019)

4.3.2. Hydraulic simulation area

As it turns out from the soil map of the former Greek Special Secretariat for Water, the soils of the area are primarily soil type A (sandy, clay, sandy, silty) and secondary B (silty). (http://thyamis.itia.ntua.gr/egyfloods/gr06/gr06_maps_jpg_p01/GR06_P01_S6_soil.jpg)

For average conditions, which refer to the case that the cumulative rainfall of the former 5 days is between 13 and 38 mm (or between 35 and 53 mm, for vegetation under growing conditions), the SCS method gives detailed tables with CN values (CN_{II}) for each hydrological soil group and for different land uses. The following Table 5 shows the range of CN_{II} values per land use and Hydrological Soil Group (A, B, C, D).

Table 5 CN_{II} according to Land use and Hydrological Soil Groups (Mavrogeorgos 2019)

Land Use	Hydrological Soil Group			
	A	B	C	D
Impervious Areas and Water Bodies	100	100	100	100
Wide Linear Croplands	62-66	71-74	78-80	81-82
Dense Croplands	51-63	67-73	76-80	80-83
Tree-Crops	35-57	58-73	72-82	79-86
Forests with Sparce Vegetation	36-61	59-75	73-83	79-87
Forests with Dense Vegetation	33-53	57-71	71-80	78-85
Urban Areas	80	87	91	93
Peak Discharge Q_{peak} (m^3/s)	33.8	35.3	36.9	38.7

The land uses of the hydraulic simulation area are shown in the following Figure 16:

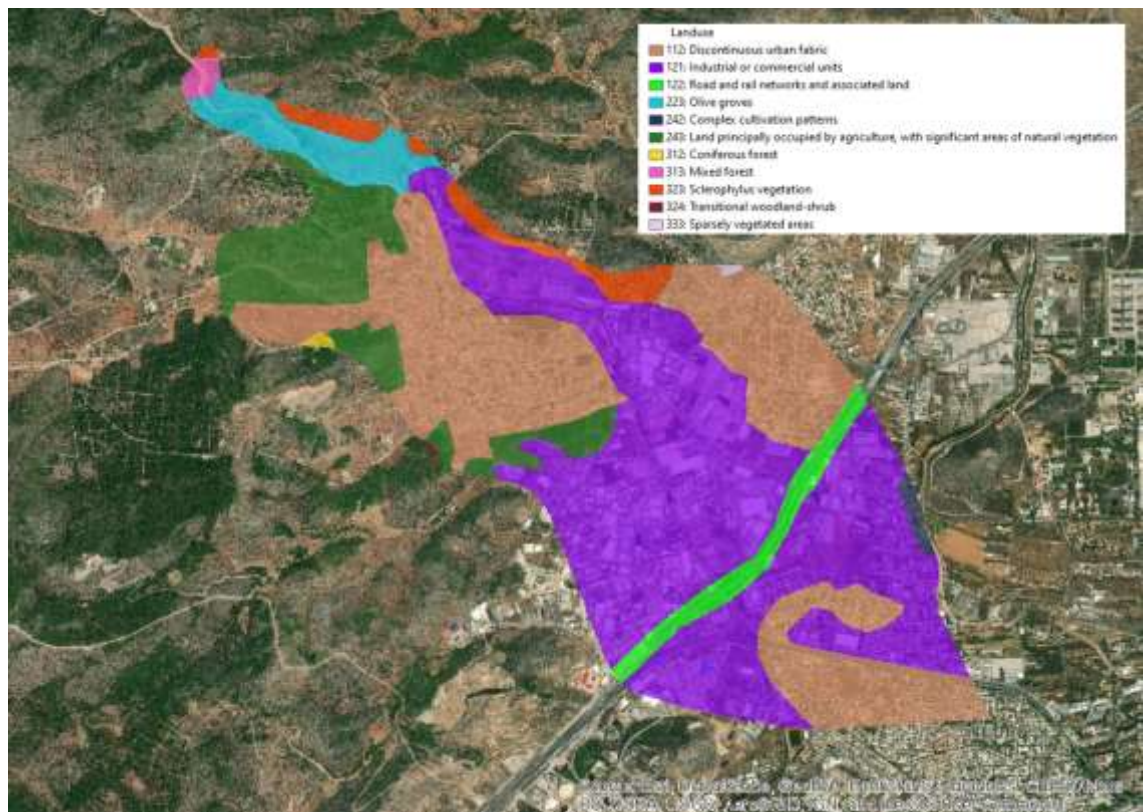


Figure 16 Land uses of the hydraulic simulation area

Table 6 Runoff curve number CN_{II} of the hydraulic simulation area

Code	Description	Area (m ²)	CN_{II}	Weight	CN_{II} Weighted	CN_{II} (Hydraulic Simulation Area)
112	Discontinuous urban fabric	3473414	83.5	0.3207	26.78	79
121	Industrial or commercial units	4912592	83.5	0.4535	37.87	
122	Road and rail networks and associated land	342165	83.5	0.0316	2.64	
223	Olive groves	455834	55.75	0.0421	2.35	
242	Complex cultivation patterns	52303	55.75	0.0048	0.27	

243	Land principally occupied by agriculture, with significant areas of natural vegetation	1180399	63.5	0.1090	6.92
312	Coniferous forest	15274	57.75	0.0014	0.08
313	Mixed forest	59821	57.75	0.0055	0.32
323	Sclerophylus vegetation	323628	57.75	0.0299	1.67
324	Transitional woodland-shrub	7404	43	0.0007	0.03
333	Sparsely vegetated areas	8777	72.5	0.0008	0.06

Taking into account all the above, the value of the runoff curve number CN_{II} of the simulation area is calculated to be equal to 79 according to Table 6.

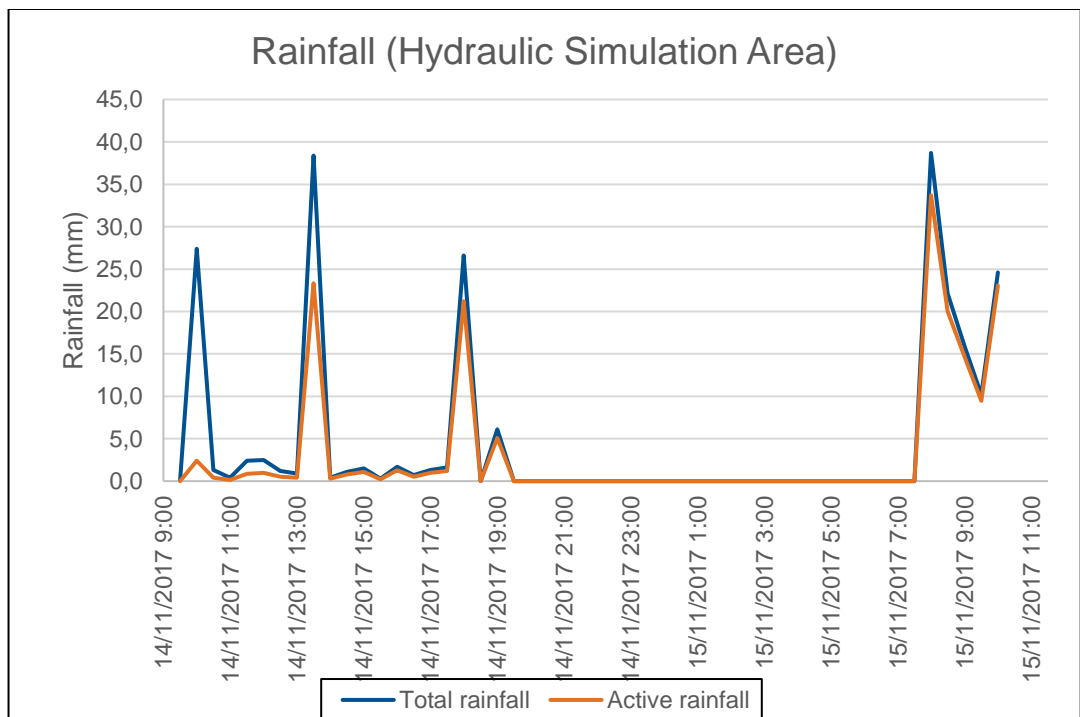


Figure 17 Rainfall for the hydraulic simulation area

The maximum potential retention S of the hydraulic simulation area is calculated according to the Equation (12) and then the time series of the active precipitation P_e of the simulation for the 15/11/2017 event is calculated. The time series of the real event is shown in Figure 17. Then, the rainfall intensity is calculated as it is shown in Figure 18.

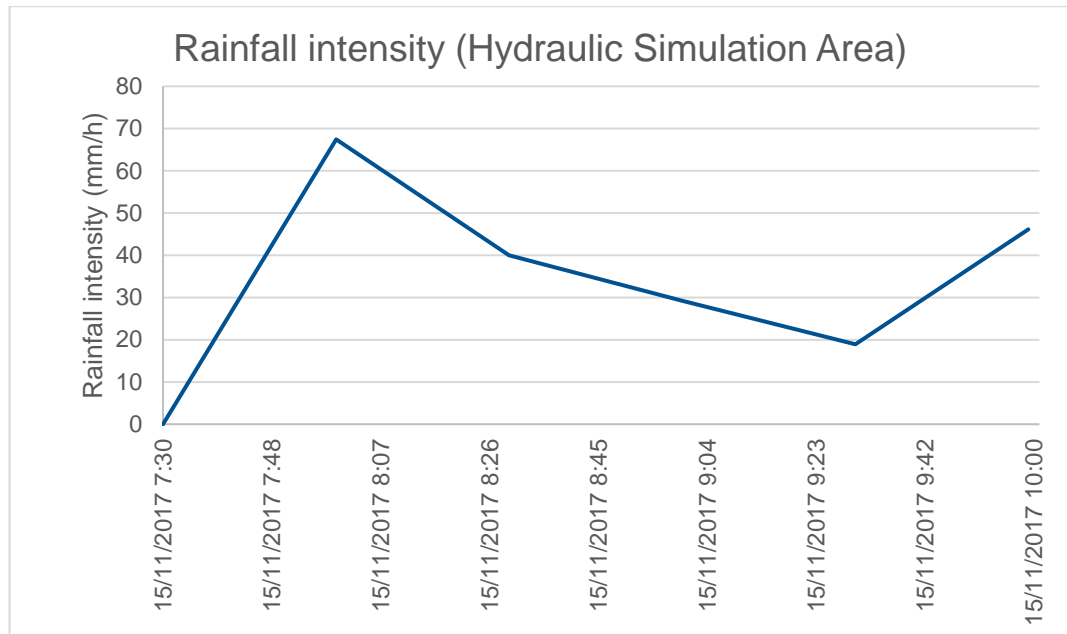


Figure 18 Rainfall intensity for the hydraulic simulation area

4.4. Synthetic hydrographs

4.4.1. IDF curves

For the calculation of the synthetic hydrographs, the meteorologic stations in which the IDF curves were produced from YPEKA, according to the implementation of the Directive 2007/60/EK, are needed. The Mandra Water Treatment Plant station, property of the National Technical University of Athens, with an altitude of 258 m and the Eleusis station, property of the National Meteorologic Service of Athens with an altitude of 31 m are located in the study area. The distances of the two stations from the centers of gravity of the two basins are approximately the same. Taking into account that the mean elevation of the two basins (377.8 m for Soures stream and 302.5 m for Agia Aikaterini stream), Mandra station was considered more suitable because it had the smallest elevation difference with both basins. As it is shown in Figure 19 below, the Mandra's IDF curve gives the highest values of rainfall intensity for the selected storm duration (12 h), which is another reason for the selection of this curve.

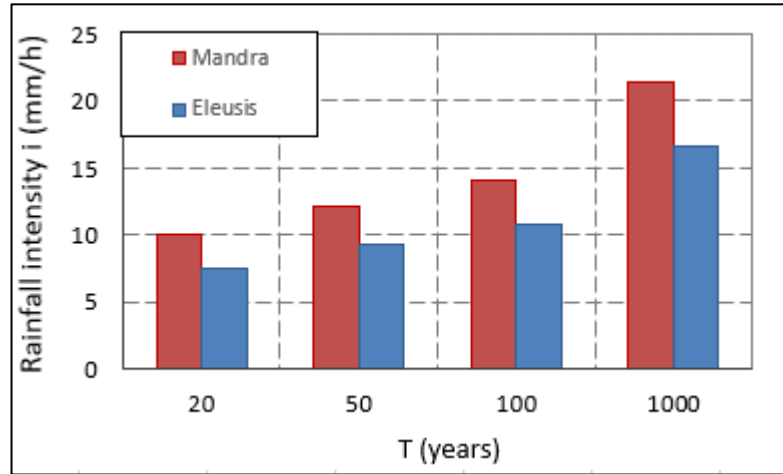


Figure 19 Comparison of IDF curves for rainfall duration ($d=12$ h) for the four examined return periods T (Mavrogeorgos 2019)

Finally, the equation of the used IDF curve is the following:

$$i(d, T) = \frac{213.4 (T^{0.125} - 0.641)}{\left(1 + \frac{d}{0.124}\right)^{0.622}} \quad (43)$$

4.4.2. Computational process

For the synthesis of the hyetographs, the total amount of rainfall is taken equal to 12 h (far greater than the longer concentration time of the two basins) and the time step of the calculations is taken equal to 0.5 h (much shorter than the smaller concentration time of the two basins). Rainfall time distribution was done by the alternating block method which is most commonly used for small return periods. After that, the SCS-CN method was applied, with a consideration of average conditions of previous soil moisture and the active hyetograph and the duration of active rainfall were calculated. Subsequently, the intensity of active rainfall was calculated and the concentration time was reduced for each return period by applying the Equation (40). From the concentration time, synthetic unit hydrographs were produced using the methodology presented in the unit 3.1.2, the characteristics of which are shown in Table 7 for Soures stream and in Table 8 for Agia Aikaterini stream. Finally, the hydrographs for all return periods were calculated (see Figure 20 and Figure 21) and the peak discharges as well (Table 9). The base flow was considered zero, a value not far from the reality, since the flow in the two streams is transient.

4.4.3. Hydrological simulation area results

Table 7 Assessment of the characteristics of unit hydrograph of s. Soures examined return periods (Mavrogeorgos 2019)

Return Period T (years)	20	50	100	1000
Total Amount of Point Rainfall (mm)	120.4	146.5	168.4	256.2
Total Height of Surface Rain, h (mm)	114.3	139.1	159.9	243.2
Total Active Rainfall Height, h_e (mm)	25.9	40.3	53.8	115.8
Intensity of Active Rainfall, i_e (mm/h)	3.70	5.38	6.72	12.86
Final Concentration Time, t_c (h)	2.60	2.44	2.35	2.10
Raising Time t_p (h)	1	1	1	1
Base Time t_b (h)	8.5	8	7.5	7
Peak Discharge Q_{peak} (m^3/s)	30.6	32.1	33.6	35.3

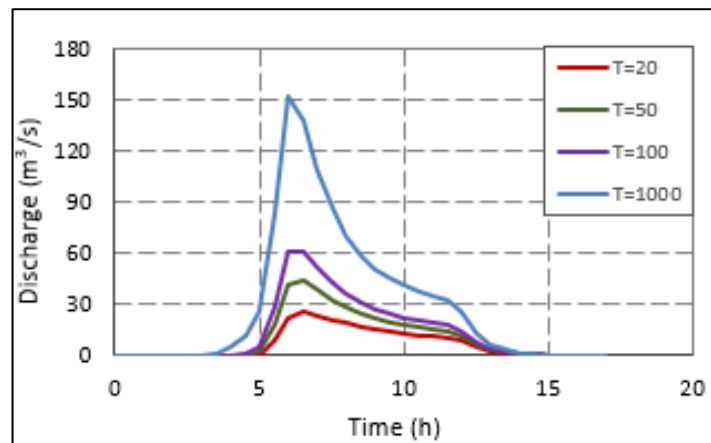


Figure 20 Inlet storm hydrographs for the hydraulic model for s. Soures (Mavrogeorgos 2019)

Table 8 Assessment of the characteristics of unit hydrograph of s. Agia Aikaterini examined return periods (Mavrogeorgos 2019)

Return Period T (years)	20	50	100	1000
Total Amount of Point Rainfall (mm)	120.4	146.5	168.4	256.2
Total Height of Surface Rain, h (mm)	114.1	138.8	159.5	242.7
Total Active Rainfall Height, h_e (mm)	42.4	60.7	77.0	148.0
Intensity of Active Rainfall, i_e (mm/h)	5.29	7.14	8.55	14.80

Final Concentration Time, t_c (h)	2.59	2.50	2.44	2.28
Raising Time t_p (h)	1	1	1	1
Base Time t_b (h)	8.5	8	8	7.5
Peak Discharge Q_{peak} (m³/s)	33.8	35.3	36.9	38.7

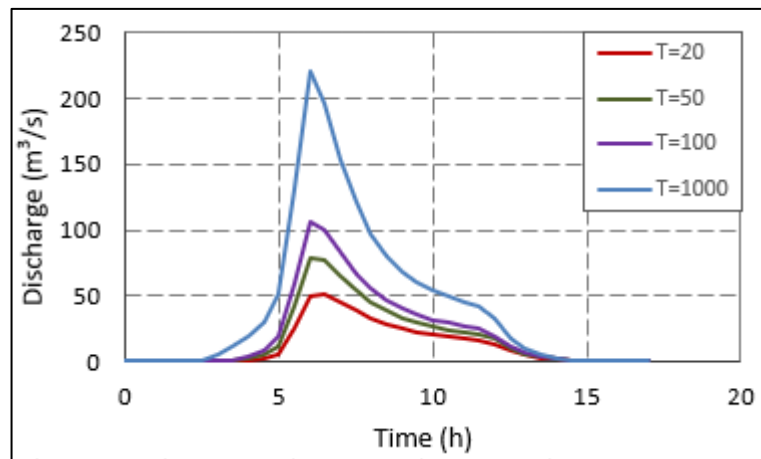


Figure 21 Inlet storm hydrographs for the hydraulic model for s. Agia Aikaterini (Mavrogeorgos 2019)

Table 9 Peak discharges of storm hydrographs (m³/s) for the examined return periods (Mavrogeorgos 2019)

Return Period T (years)	S. Soures	S. Agia Aikaterini
20	25.5	51.6
50	43.5	78.7
100	61.0	106.4
1000	151.1	220.8

4.5. 1D/2D coupled model

4.5.1. Scenarios and impacts – Influence of return period

The objective of this thesis is to simulate the flash flood of 2017 at the town of Mandra using a 1D/2D coupled model and to assess the impact of the proper maintenance of the closed conduits, the implementation of private protection measures, the extension of the rainfall zone over the flooded area and the incorporation of additional technical works of

a stream diversion and a retention pond in conjunction with properly maintained closed conduits. Additionally, the return period is investigated and finally, the last case and two alternatives are compared with the simulated flash flood for the return period of T=50 years. For this purpose, 13 different scenarios are conducted.

The basic Scenario, which is referred as “Real flood”, features the actual flash flood of 2017. A number of technical works (1, 2, 3, 4, 5, 7, 8, 16) is fully clogged and the technical work (10) is partially clogged and operates with an active cross section of 4.50 m x 3.50 m instead of 5.50 m x 4.50 m, as it is shown in Figure 22 and verified by the autopsy records (<http://beyond-eocenter.eu/index.php/floods>). All the technical works and their operational situation are shown in the following Table 10.

Table 10 Technical works of Agia Aikaterini and Soures streams (Mavrogeorgos 2019 adjusted)

Technical Work	Location	Diameter/Width (m)	Height (m)	Length (m)	Cross-Section (m)	Active Cross-Section
1	Model entrance	3.00	1.50	15	Rectangular	0
2	Just downstream of technical work 1	3.00	1.50	35	Rectangular	0
3	Michelin	2.00	1.00	12	Rectangular	0
4	Vakontios SA	4.00	1.25	61	Twin rectangular	0
5	Municipality of Mandra's depot	0.80	-	30	Twin circular	0
6	Logistics METRO	3.50	2.00	15	Rectangular	Full
7	Cemetery upstream	1.20	-	14	Circular	0
8	V. Douka street	1.20	-	13	Circular	0
9	Louka street	5.00	1.90	15	Rectangular	Full
10	PEOATH	5.50	4.50	18	Rectangular	4.50 x 3.50
11	DHL downstream Channel 1	4.00	3.00	185	Twin Rectangular	Full
12	Channel 2	4.00	3.00	16	Twin Rectangular	Full

13	Psiloriti street-Channel 3	4.00	3.00	31	Twin Rectangular	Full
14	Attica Road-Channel 4	4.00	3.00	200	Twin Rectangular	Full
15	Channel 5	4.00	3.00	497	Twin Rectangular	Full
16	Vageli Koropouli closed conduit	2.00	1.70	2319	Rectangular	0



Figure 22 Technical works (Scenario “Real flood”)

The Scenario “Fully operated conduits” features the actual flash flood but it assumes a proper maintenance of all the closed conduits in order to ensure the operation with their full cross-sectional area. So, all the technical works, including the partially clogged (10) and the fully clogged (1, 2, 3, 4, 5, 7, 8, 16) of the Scenario “Real flood”, operate with their full cross-sectional area.

The Scenario “Fences” features the actual flash flood but it assumes that private protection measures have been undertaken. More precisely, the flooded properties

(basements) are protected with raising the surrounding fences at a height of 1 to 3 m, as it is shown in Figure 23.

The Scenario “Spatially extended rainfall” features the actual flash flood but it assumes that the rainfall is not restricted only in the upstream area (hydrological simulation area), but also extends in the downstream area (hydraulic simulation area). The rain starts at 05:45 ie coincides with the start of the input hydrograph of Agia Aikaterini stream, which is half an hour earlier than the Soures hydrograph.

The Scenario “Diversion and retention pond”, deals with properly maintained closed conduits, as in the Scenario “Fully operated conduits”, combined with new technical works of a stream diversion and a retention pond (17, 18, 19 and 20), as they are shown in Figures 24 and 25 and in Table 11.

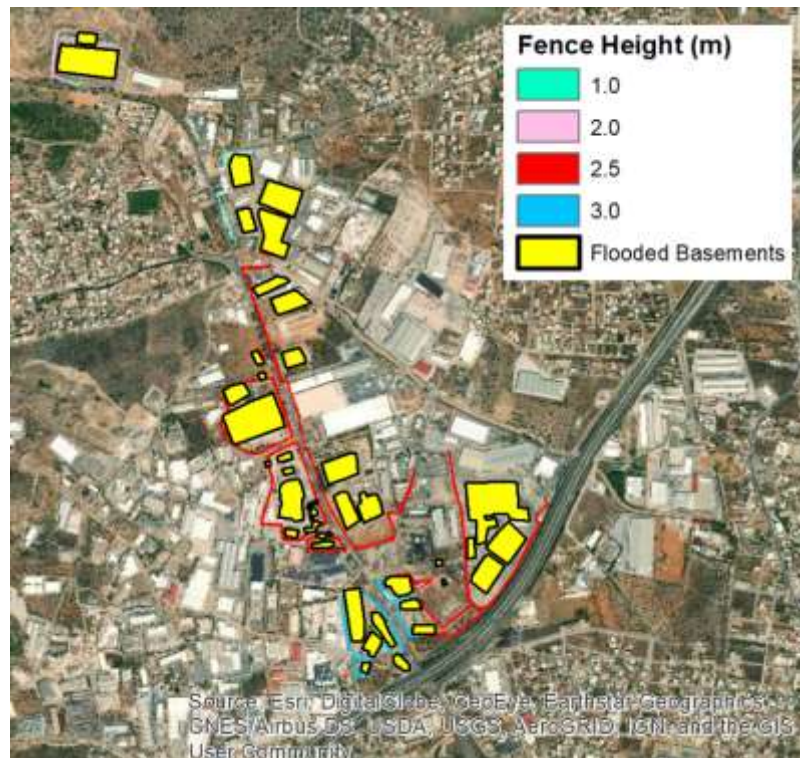


Figure 23 Mapping of fences (Scenario “Fences”)



Figure 24 New technical works of diversion and retention pond (Scenario “Diversion and retention pond”)

The technical works aim to prevent the main residential area of Mandra from flooding due to Agia Aikaterini stream’s runoff. The design period is T=50 years.

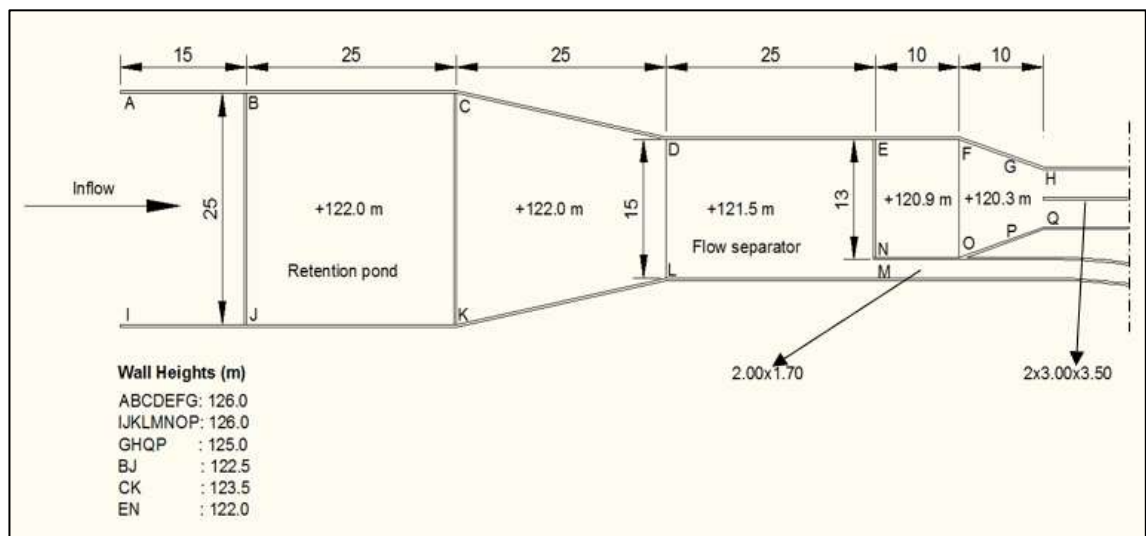


Figure 25 Plan of the new technical works of diversion and retention pond (Scenario “Diversion and retention pond”)

Table 11 Existing and new technical works of Agia Aikaterini and Soures streams

Technical Work	Location	Diameter/ Width (m)	Height (m)	Length (m)	Cross-Section (m)	Active Cross-Section
1	Model entrance	3.00	1.50	15	Rectangular	Full

2	Just downstream of technical work 1	3.00	1.50	35	Rectangular	Full
3	Michelin	2.00	1.00	12	Rectangular	Full
4	Vakontios SA	4.00	1.25	61	Twin rectangular	Full
5	Municipality of Mandra's depot	0.80	-	30	Twin circular	Full
6	Logistics METRO	3.50	2.00	15	Rectangular	Full
7	Cemetery upstream	1.20	-	14	Circular	Full
8	V. Douka street	1.20	-	13	Circular	Full
9	Louka street	5.00	1.90	15	Rectangular	Full
10	PEOATH	5.50	4.50	18	Rectangular	Full
11	DHL downstream Channel 1	4.00	3.00	185	Twin Rectangular	Full
12	Channel 2	4.00	3.00	16	Twin Rectangular	Full
13	Psiloriti street-Channel 3	4.00	3.00	31	Twin Rectangular	Full
14	Attica Road-Channel 4	4.00	3.00	200	Twin Rectangular	Full
15	Channel 5	4.00	3.00	497	Twin Rectangular	Full
16	Vageli Koropouli closed conduit	2.00	1.70	2319	Rectangular	Full
17	Retention pond	25.00		25.00		
18	Flow separator	15.00		25.00		
19	Diversion closed conduit	3.00	3.50	1585	Twin Rectangular	Full

20	Extention of Vageli Koropouli closed conduit	2.00	1.70	1063	Rectangular	Full
-----------	--	------	------	------	-------------	------

A proper design would anticipate an open channel capable of carrying the flow with a retention period $T=50$ years, taking into consideration the contribution of the existing closed conduit of Vageli Koropouli, which can take a discharge around $10 \text{ m}^3/\text{s}$. This channel had to flow into Soures as far as downstream aiming to minimize the respective Soures technical works. However, the geomorphology of the region and the urban plan of the study area force to a different design. The diversion of Agia Aikaterini stream to Soures stream has been proposed by the study «MELETI EKTROPIS CHIMARROU AG. AIKATERINIS KAI DIEYTHETISIS CHIMARROU SOURES THRIASIOU PEDIU» («STUDY OF AG. AIKATERINI DIVERSION TO SOURES STREAM AND CANALISATION OF SOURES STREAM IN THE RARYO-THRACE FIELD») (ETME – Peppas et al. 2014). The present study focuses in the diversion of Agia Aikaterini stream to Soures stream, an initial phase A of the technical interventions which include as another phase B the canalisation of Soures stream according to the above study (ETME – Peppas et al. 2014). All the relative technical works of the diversion case are adjusted according to the different hydrological data of the present study. The return period ($T=50$ years) remains the same. The total design includes the following technical works. A twin rectangular closed conduit with dimensions $2 \times 3.00 \text{ m} \times 3.50 \text{ m}$, which flows into Soures fairly upstream of the confluence and more specifically downstream the technical work (3) and the checkpoint S3 and upstream the technical work (4). Also, another closed conduit with dimensions $2.00 \text{ m} \times 1.70 \text{ m}$ is designed as an extention of the Vageli Koropouli closed conduit (16) (see Figure 24). A suitable separation of the flow is incorporated which leads the flow firstly to the extension of Vageli Koropouli closed conduit and then to the diversion conduit in order to reduce the overflow along Soures stream between the location of the diversion and the confluence with Agia Aikaterini stream (Vageli Koropouli closed conduit). A retention pond is designed just upstream the technical work of the flow separation. All the technical works are located just downstream of the location of the inflow storm hydrograph, where the riverbed of Agia Aikaterini stream is still fairly narrow and favours to catch the flow. Also, the Scenario “Diversion and retention pond” is examined with flash floods having a return period of $T=50$ and 100 years for validation of the design of the new technical works.

Additionally, the model is applied to four (4) rainfall scenarios in order to investigate the influence of the return period. The Scenario “Real flood” is compared with flash floods having a return period of T=20, 50, 100 and 1000 years. Finally, the Scenario “Diversion and retention pond” and two alternative scenarios are examined and compared with the Scenario “Real flood” for a return period T=50 years. The first alternative incorporates fence raising of the Logistics METRO (see Figure 26) and the second alternative the diversion to Soures at a location downstream of the technical work S6. The new diversion, as shown in Figure 27, has a length of 2273 m. All the aforementioned simulations are shown in Tables 12, 13 and 14.



Figure 26 New technical works of diversion and retention pond (Scenario “Diversion, retention pond and METRO fence”)



Figure 27 New technical works of diversion and retention pond (Scenario “New diversion and retention pond”)

Table 12 Summary of the simulation scenarios

Real Flood	Fully Operated Conduits	Fences	Spatially Extended Rainfall	Diversion and Retention Pond
------------	-------------------------	--------	-----------------------------	------------------------------

Scenario "Real Flood"	✓			
Scenario "Fully Operated Conduits"	✓	✓		
Scenario "Fences"	✓		✓	
Scenario "Spatially Extended Rainfall "	✓			✓
Scenario "Diversion and Retention Pond"	✓	✓		✓

Table 13 Summary of the simulations concerning the influence of the return period

	T=20	T=50	T=100	T=1000
Real Flood	✓			
Real Flood		✓		
Real Flood			✓	
Real Flood				✓

Table 14 Summary of the simulations concerning the alternatives and the validation of the design of the new technical works

	T=50	T=100
Diversion and Retention Pond	✓	✓
Diversion, Retention Pond and METRO Fence	✓	
New Diversion and Retention Pond	✓	

4.5.2. 1D closed conduit model

There are 15 technical works along Soures stream and 1 more (Vageli Koropouli closed conduit) along Agia Aikaterini stream. The technical works are shown in Figure 2. Table 10 points out important characteristics of the technical works. It is clarified that due to sediment transport a significant number of technical works is clogged partially or fully as

it has already been shown in Table 10 (active cross-section 0 for fully clogged section). The above number of technical works and their characteristics remain the same for the Scenarios “Real flood”, “Fences” and “Spatially extended rainfall”. Also, the number of technical works remains the same but the characteristic of the active cross-section changes from 0/4.50 m x 3.50 m to full in the Scenario “Fully operated conduits”. Finally, the new technical works (19 and 20), as they are shown in Table 11, are incorporated keeping the full cross-section in the Scenario “Diversion and retention pond”. The other characteristics of the technical works are: elevation, manning’s n coefficient and the coordinates of each storage and outfall. All the characteristics are included in the SWMM5 .inp file.

The model which incorporates all the aforementioned characteristics consists of 46 nodes (23 of them are storages and the other 23 are outfalls) and 23 conduits with a total length of 4,496 meters for the Scenarios “Real flood”, “Fully operated conduits”, “Fences” and “Spatially extended rainfall”. Concerning the Scenarios “Diversion and retention pond” and “Diversion, and retention pond and METRO fence” the model consists of 51 nodes (26 of them are storages and the other 25 are outfalls) and 26 conduits with a total length of 8,730 meters. Finally, the Scenario “New diversion and retention pond” consists of a total length of 10,106 meters.

4.5.3. 2D overland flow model P-DWave

P-DWave model requires a Digital Elevation Model (DEM), the initial and boundary conditions, a location code for every cell and the manning’s roughness as ASCII (American Standard Code for Information Interchange) files. Additionally, the discharge (m^3/s) data, the precipitation data as a list of intensities [mm/h] and the checkpoints are needed as .txt files. The location code file and the initial conditions (initial water depths) file are created automatically and therefore not further explained.

The coupling needs as an input a linking points .txt file which includes the id, the coordinates as well as the cross-section’s perimeter and area of the storages and outfalls. A summary of all input, output and application files for SWMM, P-DWave and the coupling process is given in Table 36 in the appendix. An exemplary P-DWave master file is displayed in Figure 115 in the appendix.

Digital Elevation Modell

The Digital Elevation Model is used to initialize bathymetry. The spatial discretization of the DEM is selected according to the morphology of the study area and the desired accuracy in hydraulic calculations. Then, additional topographic maps can be used to

better represent the terrain in places where the DEM presents lack of information or errors. Additional topographic data is also used for more realistic representation and optimal modeling of various flow-influencing infrastructures, such as highways, railways, embankments, drainage networks, culverts and canals. In order to achieve a compromise between computing effort, precision and accuracy, a cell size of 5 m x 5 m is chosen for the simulations (Mark et al. 2004; Gallegos et al. 2009). The DEM was granted by the Greek land registry in raster format. All the underpasses of the Attica Road are modelled manually as open channels. The streets in the DEM are reduced by 0.1 m to simulate the natural canalisation of roads and similarly, the buildings in DEM are added as blocks of 8 m height incorporating the building-block method (BB) (Mark et al. 2004; Schubert and Sanders 2012). More specifically, taking a satellite image from ArcGis as a backdrop image, polygons in the shape of buildings were designed in the whole area. Then, with a tool from ArcMap the elevation of the terrain model was extracted in these polygons and raised for another 8 meters which approximates the height of buildings. As for the roads, with the same process the elevation of the terrain model was extracted and then decreased for 0.1 meters in order to be represented more realistically.

It has also been observed that the natural riverbed of Soures stream 70 m downstream of (S3) (1620 m upstream of the confluence with Agia Aikaterini stream) up to the technical work (11) (245 m downstream of the confluence with Agia Aikaterini stream) in many parts is not represented correctly by the DEM. In addition, the same phenomenon is observed at the artificial open channel of Soures stream in its whole length (Mavrogeorgos 2019). In order to alleviate the above problems, a point shapefile from Mavrogeorgos thesis was used. The point shapefile was converted into a raster file with 5 x 5 m resolution with an interpolation tool in ArcMap and the final riverbed of Soures stream was merged into the DEM. Finally, all the existing technical works (see Figure 2 and Table 20) were properly represented according to the elevations taking into account Google Earth Pro.

After several consecutive runs of the model, the water depth in several streets was observed to be unexpectedly high preventing partially or fully the flood evolution. It was found that the display of the elevation in the DEM was incorrect, mainly because of the presence of trees and after a proper search using the tools of Google Earth Pro and Google Maps, the DEM was corrected manually. Moreover, fences which blocked partially or fully the flood evolution were added (even in 5 x 5 m resolution) in order to ensure a better representation of the flood inundation (e.g. Logistics METRO, on either side of Soures stream downstream of (S11)).

Finally, regarding the amount of water retained due to flooding into the properties, it was considered that the water flooded the properties mainly in the non-residential areas and especially the ones where a significant water depth was observed. The residential area of the town of Mandra which was flooded by the Agia Aikaterini stream is not supposed to retain significant water volume taking into consideration that the residents were inside their houses during the flood time (early in the morning) and undertook all the necessary protection measures to prevent flooding into their houses. On the contrary, the non-residential properties were empty of people, thus no protection measures could be taken. The elevation in the DEM of the corresponding buildings in this area was reduced by 1.5 - 2 meters taking into consideration the magnitude of the surrounding water depths. Figure 28 shows the DEM of the hydraulic simulation area.

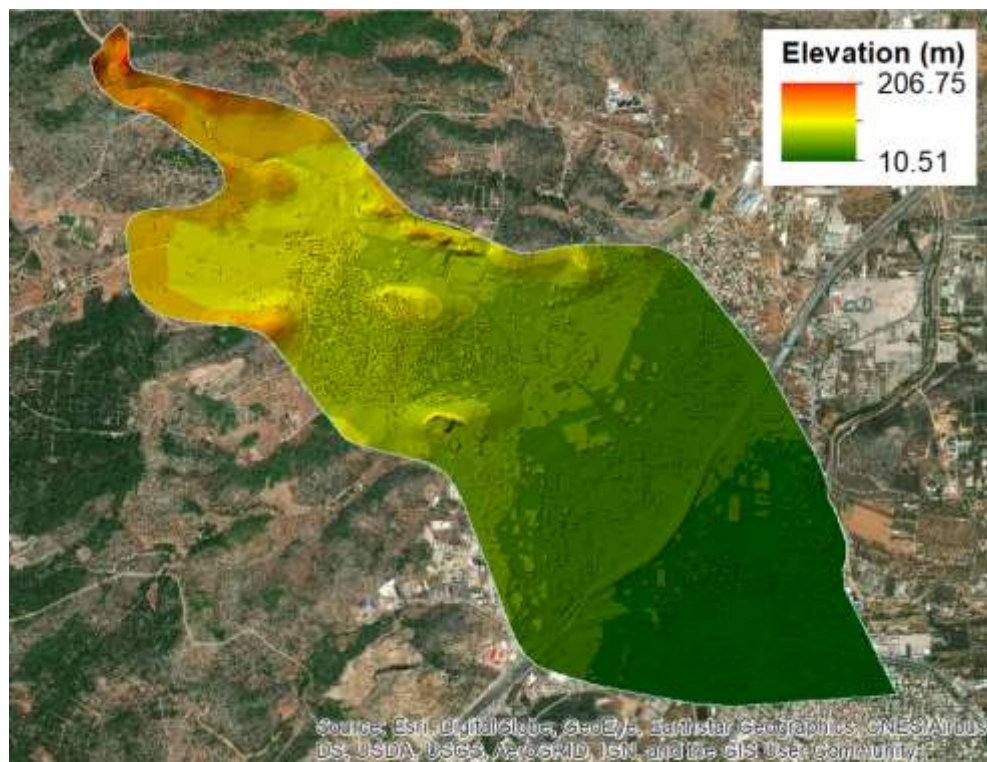


Figure 28 **Display of the DEM of the hydraulic simulation area**

Manning's roughness

The Manning's roughness is needed by P-DWave to accurately model the routing and potential retention effects of the soil material (Hunter et al. 2008). In order to represent the Manning's n coefficient, spatial data from Corine Land Cover 2012 were used which were provided from the Greek Land Registry. The data are given in shapefile format in which each different land use is delimited by a closed polygon of which only the area within the boundaries of the hydraulic simulation area is preserved. A specific Manning's

roughness value was given in all cells inside each polygon according to the landuse, as shown in the following Table 15:

Table 15 Selected Manning's n coefficient according to the land uses (1) (Mavrogeorgos 2019 adjusted)

Code	Description	Literature	Selected
112	Discontinuous urban fabric	0.060-0.115	0.100
121	Industrial or commercial units	0.115-0.230	0.180
122	Road and rail networks and associated land	0.013-0.038	0.020
223	Olive groves	0.043-0.050	0.045
242	Complex cultivation patterns		0.023
243	Land principally occupied by agriculture, with significant areas of natural vegetation	0.058-0.100	0.060
312	Coniferous forest	0.100-0.200	0.127
313	Mixed forest	0.100-0.230	0.140
323	Sclerophylus vegetation	0.072-0.125	0.100
324	Transitional woodland-shrub	0.045-0.700	0.058
333	Sparsely vegetated areas	0.050-0.070	0.070

In addition to the areas specified by Corine, four additional zones of roughness were used and a separate Manning's n value for each zone was assigned. These four zones are the riverbed of Agia Aikaterini stream, the natural riverbed of Soures stream, the artificial riverbed of Soures stream and the PEOATH. The final values of the n coefficient are shown in the following Table 16:

Table 16 Selected Manning's n coefficient according to the land uses (2) (Mavrogeorgos 2019)

Streams	Description	Literature	Selected
Agia Aikaterini	Rocky channel with growth of weeds and grass	0.050-0.080	0.065
Soures (Natural Riverbed)	Rocky channel with growth of weeds and grass	0.050-0.080	0.065
Soures (Artificial Riverbed)	Concrete channel (float finish)	0.013-0.016	0.016
PEOATH	Asphalt	0.012-0.020	0.013

Based on the above, the grid with the Manning's n coefficient is illustrated for the hydraulic simulation area in Figure 29.

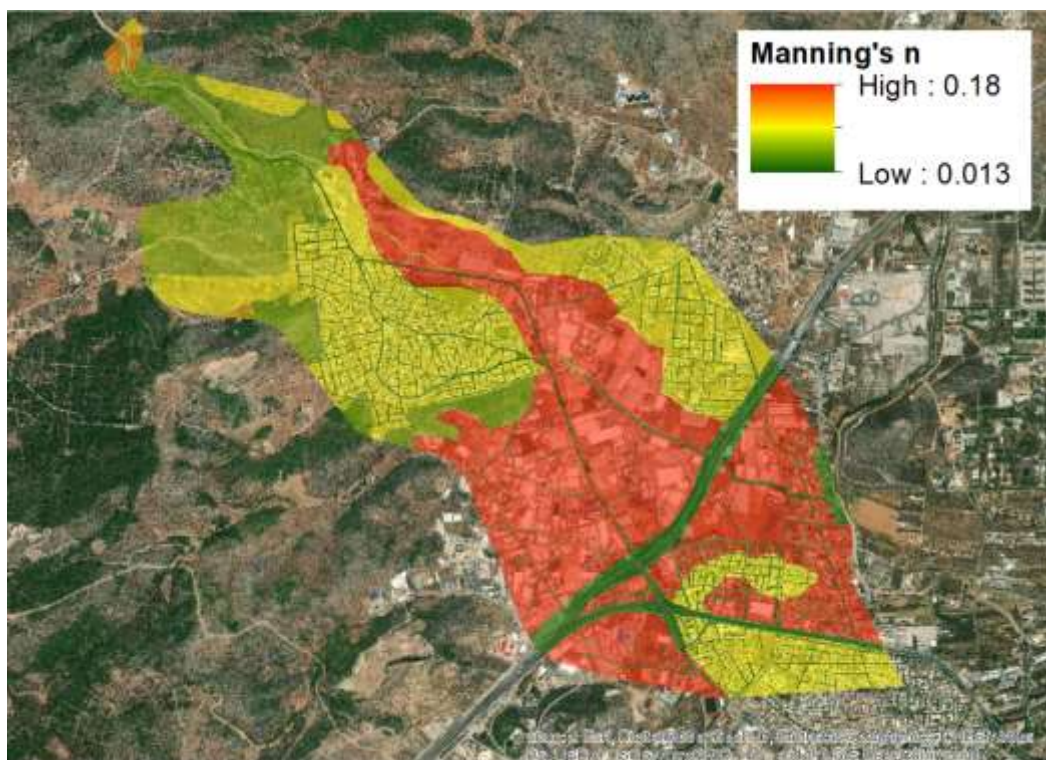


Figure 29 Display of the Manning's roughness value in the hydraulic simulation area (Mavrogeorgos 2019 adjusted)

Boundary Conditions

In the beginning of the computational field (upstream), two boundary conditions are defined with predetermined flows, that is the storm hydrographs of Agia Aikaterini stream and Soures stream, respectively. All the other area which corresponds to the borders of the hydraulic simulation area is assigned a free outflow boundary condition so no unnecessary ponding will form. This includes the areas where Sarantapotamos stream and Mikro Katerini stream intersect the hydraulic simulation area since there are no available flow data and it is assumed that there is no flow.

Discharge data

The storm hydrographs of Agia Aikaterini stream and Soures stream (see Figure 15) or the storm hydrographs for T=20, T=50, T=100 and T=1000 years (see Figure 20 and Figure 21) are used as inlet storm hydrographs to the model, according to the examined Scenarios.

Precipitation data

As it has been explained the rainfall was restricted only in the upstream area (hydrological simulation area) and it was not extended in the downstream area (hydraulic simulation area). Therefore, the precipitation data as a list of intensities [mm/h] are used for the 1D/2D coupled model only in the Scenario "Spatially extended rainfall". In all the other Scenarios the intensities were assumed as zero.

Checkpoints

The x,y coordinates of each checkpoint were used.

4.5.4. Validation, evaluation and assessment

Observation data generally allow for evaluating only some variables of interest, such as water depth and flooding extent. The velocity field is difficult to estimate and point measurements are rarely available (Schubert and Sanders 2012). The model results are analysed regarding their water depths, flood progression, flood extent and flooding.

Checkpoint evaluation

For validation purposes, the simulated maximum water depths at the checkpoints are compared with the measured data. Here the Nash-Sutcliffe-Efficiency (NSE) (Nash and Sutcliffe 1970), the Root-Mean-Square-Error (RMSE) and the Mean-Average-Error (MAE) are used as a measure of fitness.

$$NSE = 1 - \frac{\sum(y'_i - y_i)^2}{\sum(y_i - \bar{y})^2} \quad (45)$$

$$RMSE = \sqrt{\frac{\sum(y'_i - y_i)^2}{n}} \quad (46)$$

$$MAE = \frac{\sum|y'_i - y_i|}{n} \quad (47)$$

where,

y'_i : a single simulated value

y_i : a single observed value

\bar{y} : the observed mean

n : the number of value pairs

For evaluation purposes, the simulated maximum water depths at the checkpoints are used instead of the measured data. Also, the time change of water depths at the checkpoints of the other scenarios is compared with the corresponding time change of the scenario “Real flood” to assess flood progression.

Maximum water depth of area evaluation

Besides singular points, average maximum water depths of particular areas are of interest to validate and evaluate the coupled 1D/2D model. For this purpose, the following particular areas are analyzed: the study area of the coupled 1D/2D model (hydraulic simulation area), the main residential area of the town of Mandra (placed in the northwestern part of the hydraulic simulation area upstream of the confluence of the two streams) and the main industrial area of the town of Mandra. The latter ones are considered areas of weakness regarding flood. More precisely, the main residential area is the area where the Agia Aikaterini stream's historic riverbed was converted into road axes and only a small part of the flow is driven through Vageli Koropouli closed conduit to the point of confluence with Soures stream. The main industrial area is the area with many large industrial and commercial properties seriously damaged by the flood. All the three mentioned particular areas are shown illustratively in Figure 30.

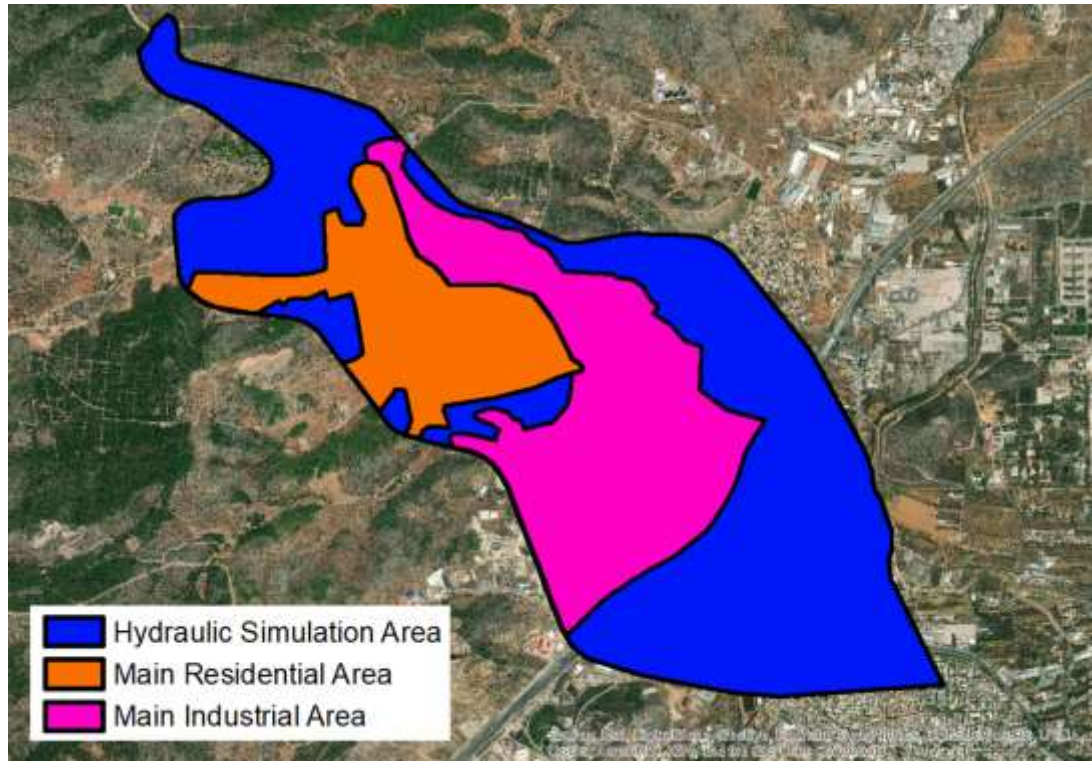


Figure 30 Mapping of the particular areas

The magnitude of the flood regarding the water depth for each area is presented using, as indexes, the average wet maximum water depth (AWMWD) and the average maximum water depth (AMWD) for the particular areas, which are defined according to the Equations (48) and (49):

$$AWMWD = \frac{\sum_i \max h_i}{\sum_i A_i} \quad (48)$$

$$AMWD = \frac{\sum_i \max h_i}{\sum_i A_i + \sum_j A_j} \quad (49)$$

where,

h_i : water depth of wet cell i

A_i : area of wet cell i

A_j : area of dry cell j

It must be mentioned that the AWMWD is not representative, as an impact quantification index, in cases of relatively large flood extent differentiations.

Flood extent and flooding evaluation

Another tool to validate and evaluate the coupled 1D/2D model is the flood extent of the different Scenarios. The flood extent is derived by the contour line of a flooded area and

includes both the wet and dry parts of the area. For validation purposes, the flood extent of the Scenario “Real flood” (real flood extent) is compared with the final mapping of the recorded maximum extent of the flood (recorded flood extent). For evaluation purposes, the flood extent of the other Scenarios within the particular areas is compared with the real flood extent, respectively.

Also, the magnitude of the flood regarding the flood spatial distribution for each particular area is considered using the term “flooding”, where flooding considers only the wet parts of the areas. The flooding of the other Scenarios within the particular areas are compared with the real flood flooding, respectively.

5. Results

5.1. Basic Scenario "Real flood"

5.1.1. Checkpoints-Maximum water depths and flood progression

The following Figures show the results of the 1D/2D model in terms of water depths for all the checkpoints. Figures 31, 32 and 33 give the time evolution of the water depths compared to the observations.

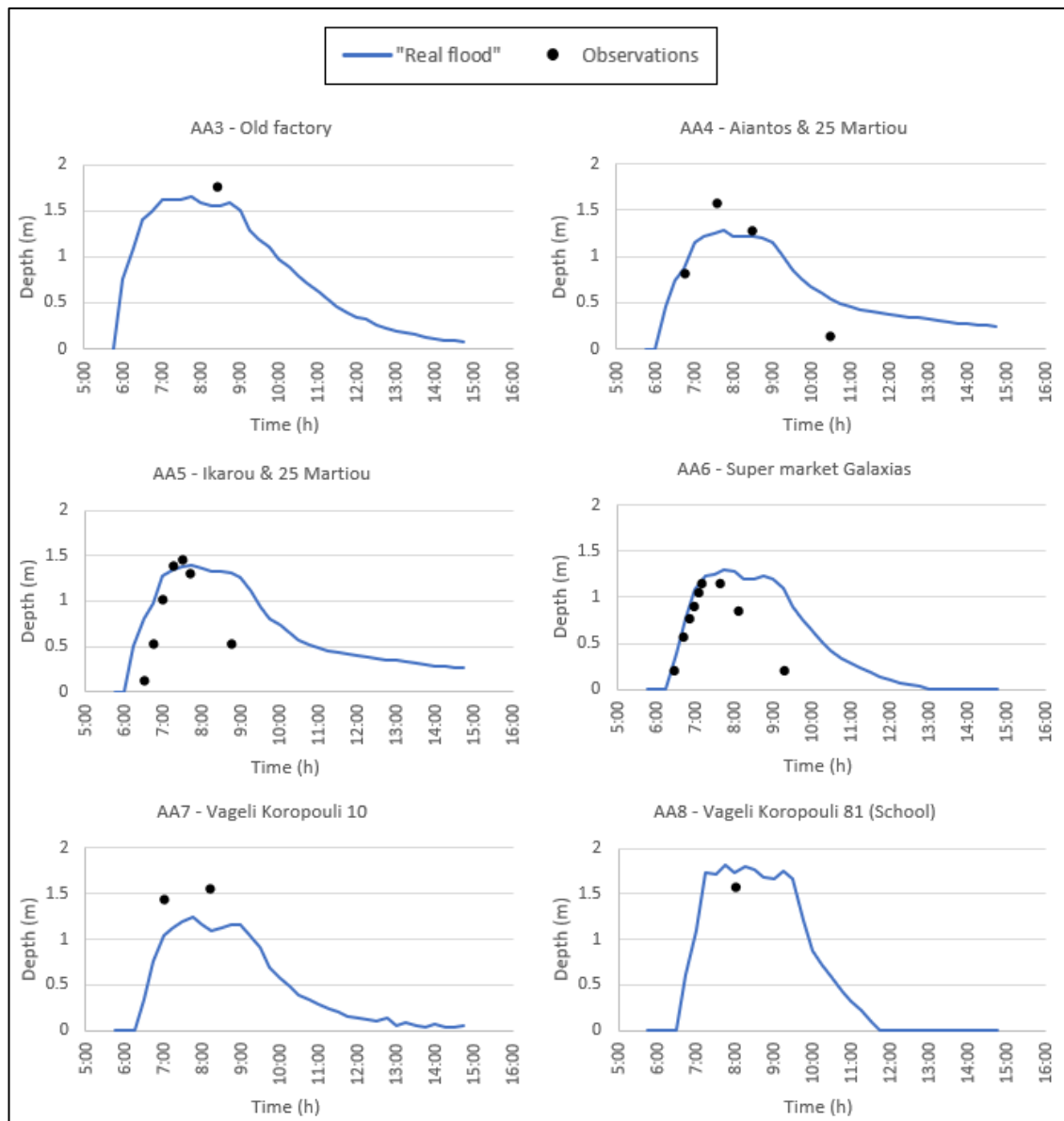


Figure 31 Time change of water depths at the checkpoints of Agia Aikaterini stream

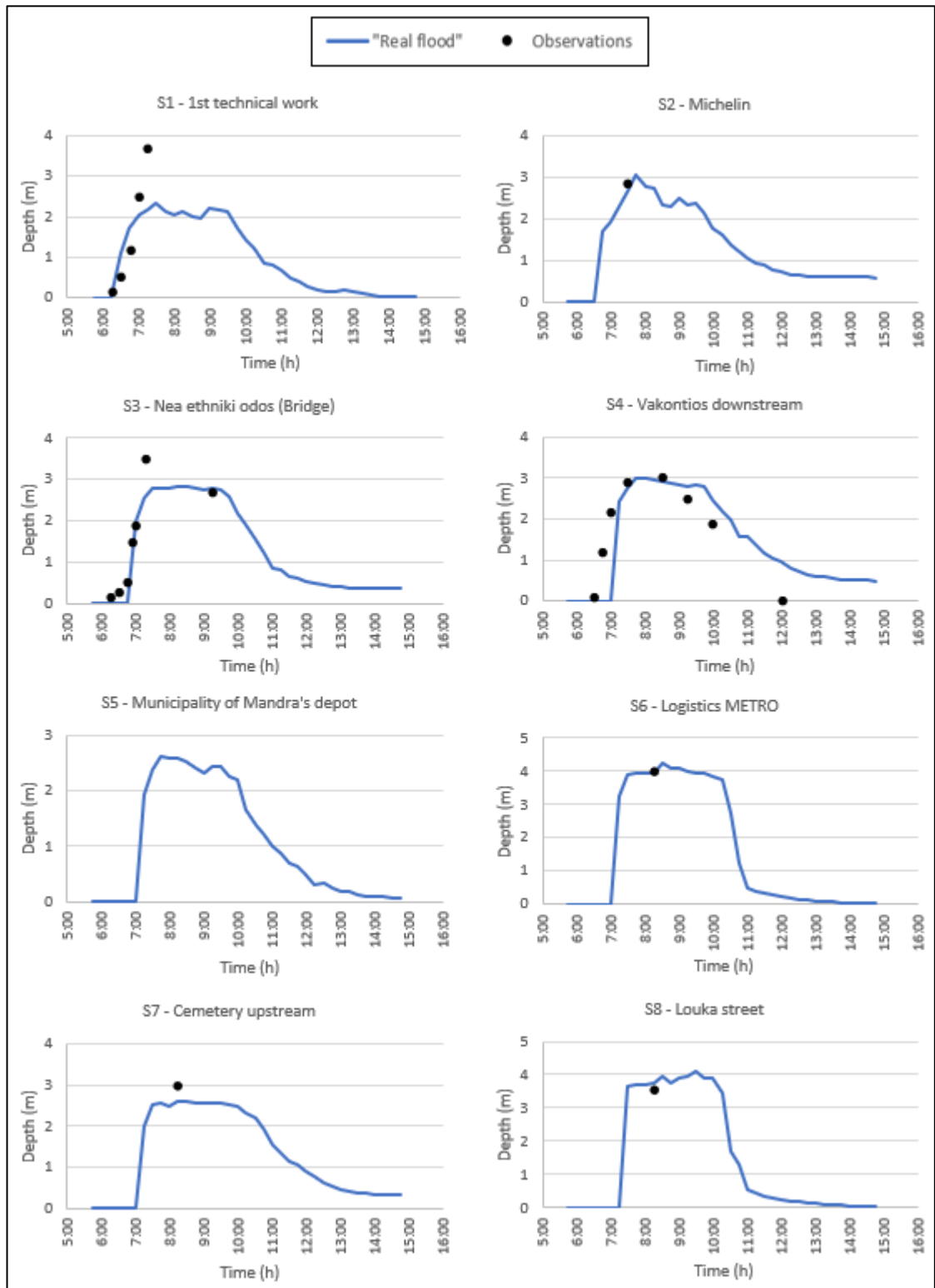


Figure 32 Time change of water depths at the checkpoints of Soures stream upstream of the confluence with Agia Aikaterini stream

The model underestimates the observed maximum water depths at checkpoints AA3, AA4, AA5 and AA7 and overestimates the observed maximum depths at checkpoints

AA6 and AA8. Specifically, the range of deviation extends from a slight difference of 5 cm at AA5 up to a small difference of 30 cm at AA7.

Figures 32 and 33 show that the model underestimates the maximum water depths at checkpoints S1, S3, S4, S7, S11 and S12 and overestimates the maximum depths at checkpoints S2, S6, S8, S10 and S13. Specifically, the range of deviation extends from a slight difference of 5 cm at S4 up to a difference of 1.39 m at S1.

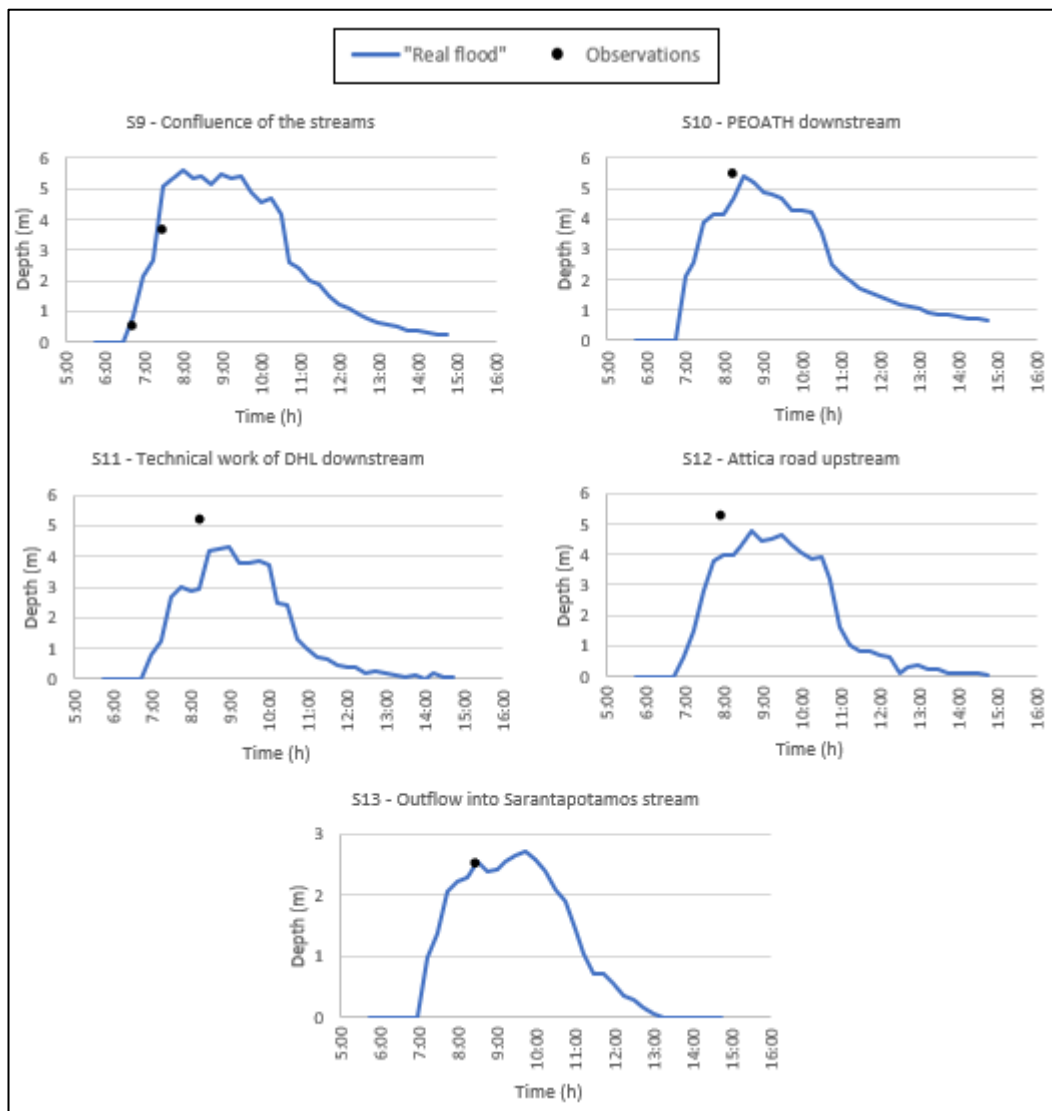


Figure 33 Time change of water depths at the checkpoints of Sores stream downstream of the confluence with Agia Aikaterini stream

A comparison of the simulated values to the observed values of the maximum water depth at the checkpoints are shown in Figures 34 and 35. The RMSE, NSE, and MAE are 0.494, 0.871 and 0.362, respectively.

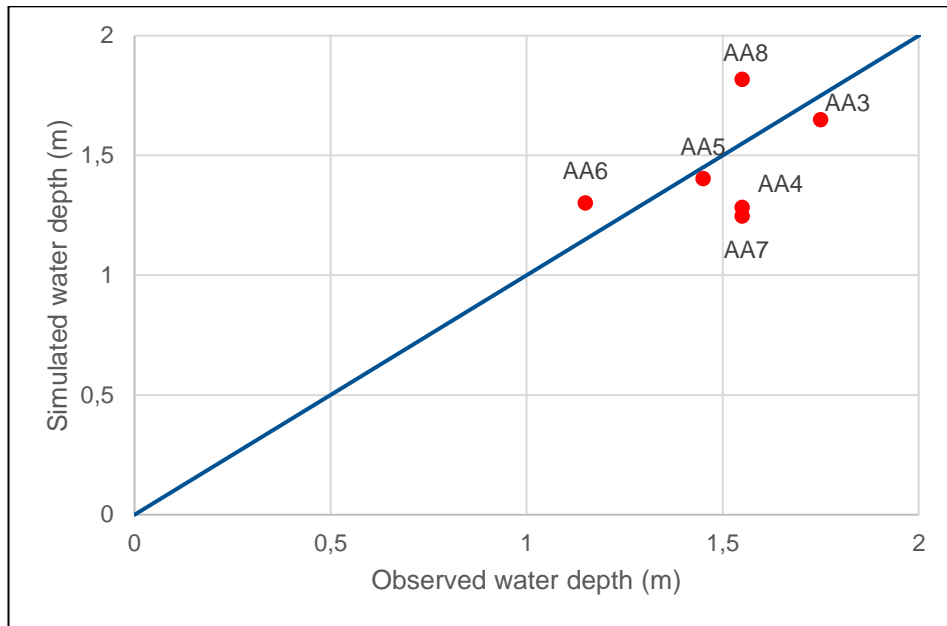


Figure 34 Simulated maximum water depths compared to the maximum observed water depths for Agia Aikaterini stream (Scenario “Real flood”)

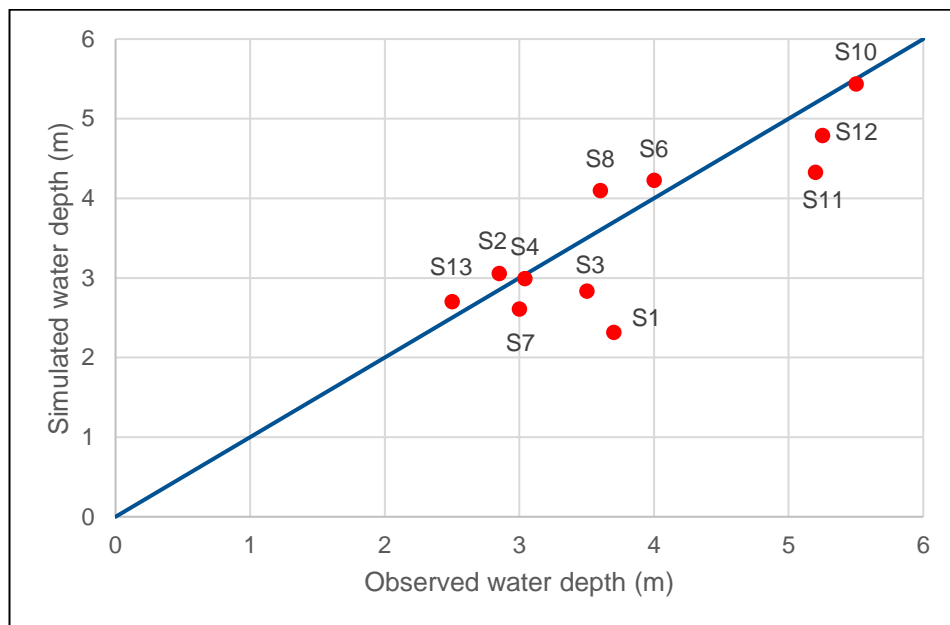


Figure 35 Simulated maximum water depths compared to the maximum observed water depths for Soures stream (Scenario “Real flood”)

The flood progression with a time step of 30 min is shown in Table 37 in the appendix.

5.1.2. Maximum water depths of area

Figure 36 presents the display of the maximum water depths and actually shows the flood extent that results from the 1D/2D model (Scenario “Real flood”) compared to the mapping of the maximum recorded extent of the flood (recorded flood extent) and then

Figures 37 to 41 present the ones in the individual areas (sections 1 to 5). All the wet (due to the flood) parts of the hydraulic simulation area, are depicted with different colour according to the magnitude of the respective water depth.

The maximum water depths range from 0.03 m to 6.70 m.

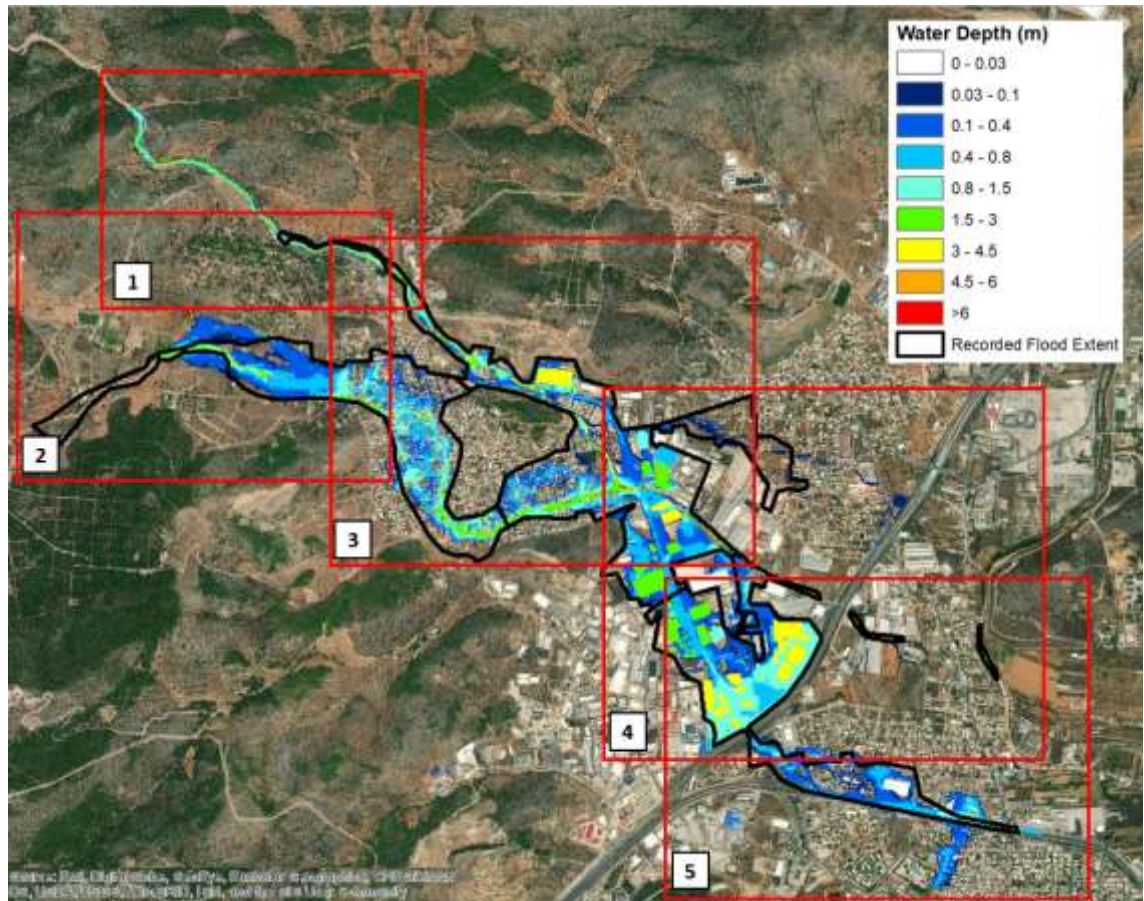


Figure 36 Simulated maximum water depths and the recorded flood extent in a five sections spatial distribution (Scenario "Real flood")

In section 1, there is no flood recording along the initial length of the stream, where the flood is confined within a narrow strip. Large slopes rise beyond the banks of the stream holding the water between them. At the entrance of the hydraulic simulation area, the water overflows from the very narrow bed of the stream, flooding the road (PEOATH) and occupying the whole area between the hills on either side. In section 1, there are also the blocked technical works 1, 2 and 3 in which the flow passed over as it was also revealed by the on-site autopsy.

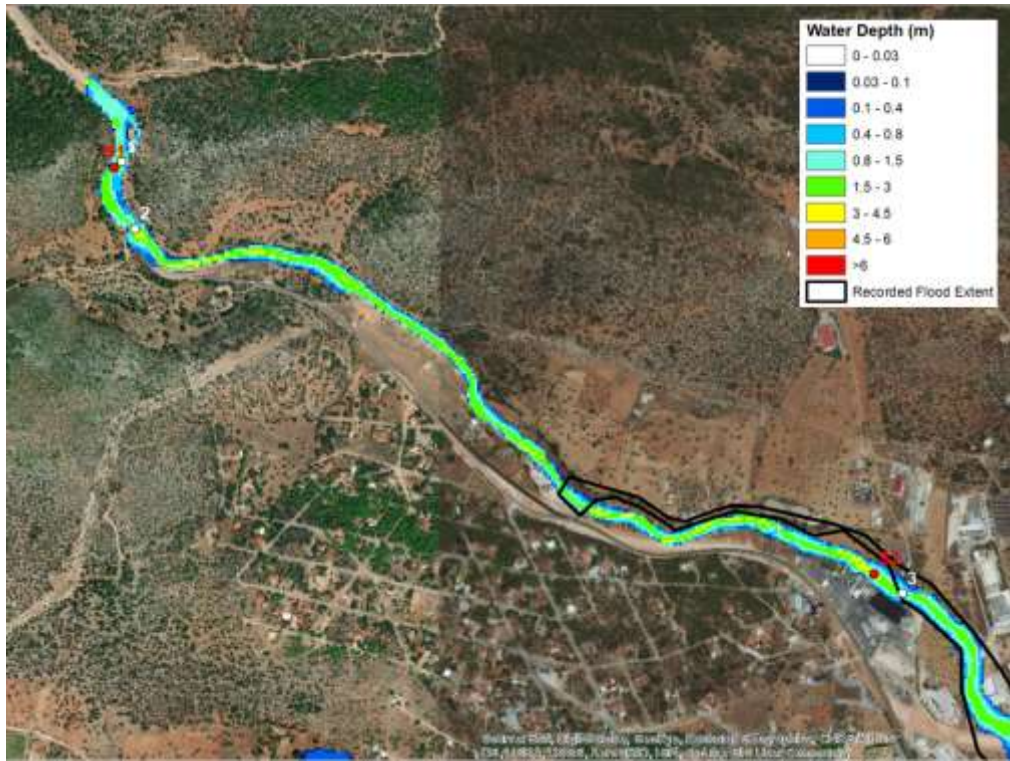


Figure 37 Simulated maximum water depths and the recorded flood extent – Section 1 (Scenario “Real flood”)

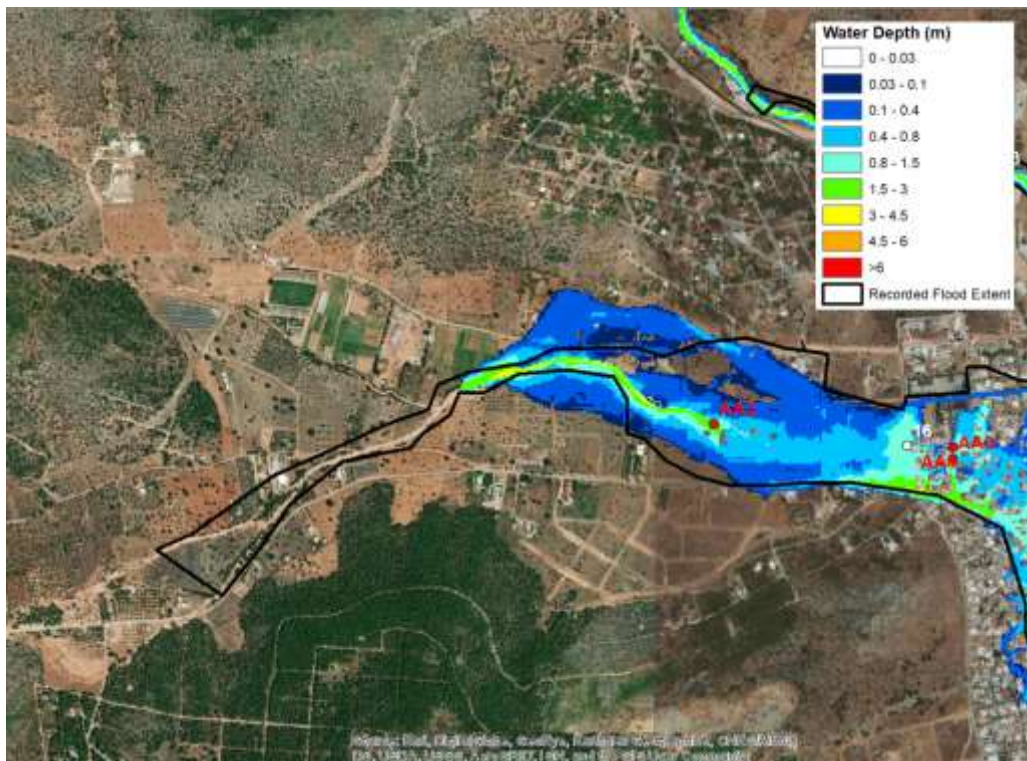


Figure 38 Simulated maximum water depths and the recorded flood extent – Section 2 (Scenario “Real flood”)

In section 2, shortly after the entrance in the hydraulic simulation area, at the northwestern part of the main residential area (urban fabric) of the town of Mandra, the water overflows on either side of the current bed and then the flow is divided into 2 branches.

Then, the flood wave moves, passing the old factory (checkpoint AA3), to the east and hits the northwestern residential part of the town of Mandra.

Section 3 focuses to the main residential area of the town of Mandra up to the confluence of the two streams.

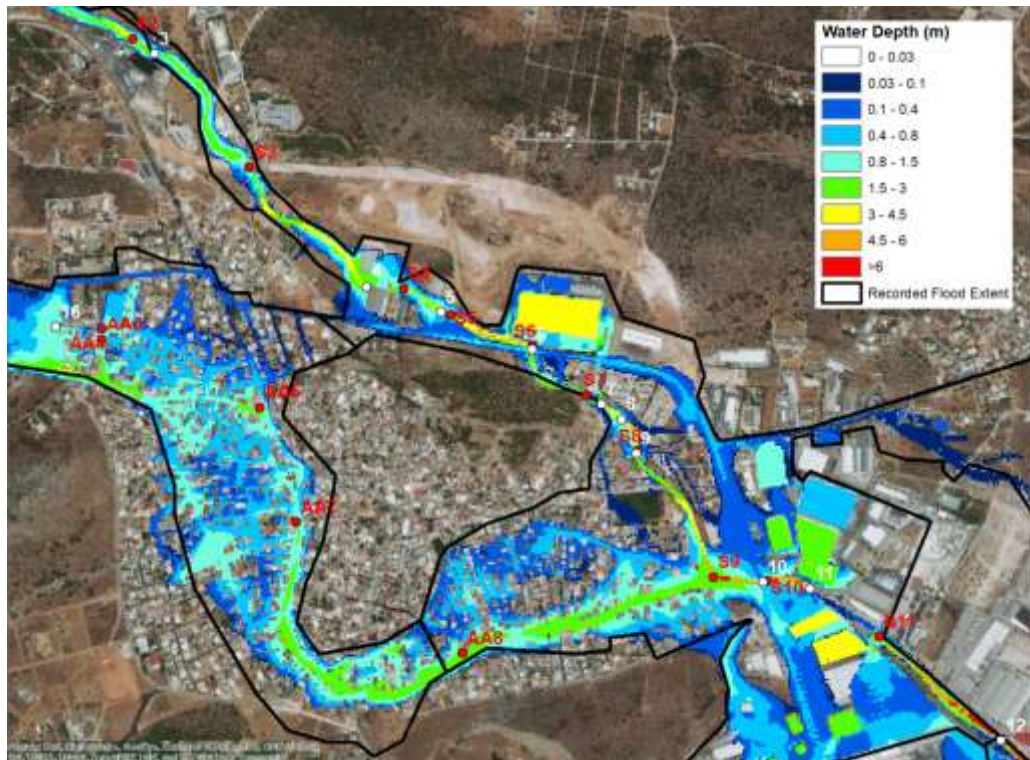


Figure 39 Simulated maximum water depths and the recorded flood extent – Section 3 (Scenario “Real flood”)

As soon as the wave reaches the facilities of the Vakontios unit at (4), its intense spread begins and floods all the neighboring buildings and the PEOATH. The wave then overpasses at (5) the Municipality of Mandra’s Depot and proceeds to the area of Logistics METRO (6) where the stream forms a right angle. Obviously the wave is unable to follow the axis of the stream and the flow is divided into three parts. Part of it overflows the relatively low fence of the Logistics METRO property to the north, flooding the whole area and then flooding the PEOATH to the east but also returning to Soures stream at (7). Another part follows the axis of the PEOATH to the east, partly flooding the surrounding industrial area and the residential area to the east, but mainly following the PEOATH axis to the south reaching the bridge at (10). There, the flood is divided, partially

reenters Soures stream and partially moves to the south. Also, a third part overflows (6) and moves to the southeast along the Soures stream. After overpassing (7) the flood moves to the southeast joining the flood produced by Agia Aikaterini stream and eventually reaching the confluence of the two streams and the bridge at (10).

The flood wave from Agia Aikaterini stream, after passing AA5, partially flows to the east but the large part is mainly driven through Koropouli street, where it forms the largest flow depths, and the surrounding part of the main residential area of the town of Mandra and eventually reaches the junction where, a part "falls" on the bed of the Soures stream and the rest moves to the industrial area of Mandra and Attica Road.

Section 4 focuses mainly at the industrial area (industrial or community units) up to Attica Road. The water does not overflow from Soures stream. On the other hand, the flood evolves from (10) and inundates almost the entire industrial area up to Attica Road, where the slopes trap the water in significant depths exceeding 0.8 m.

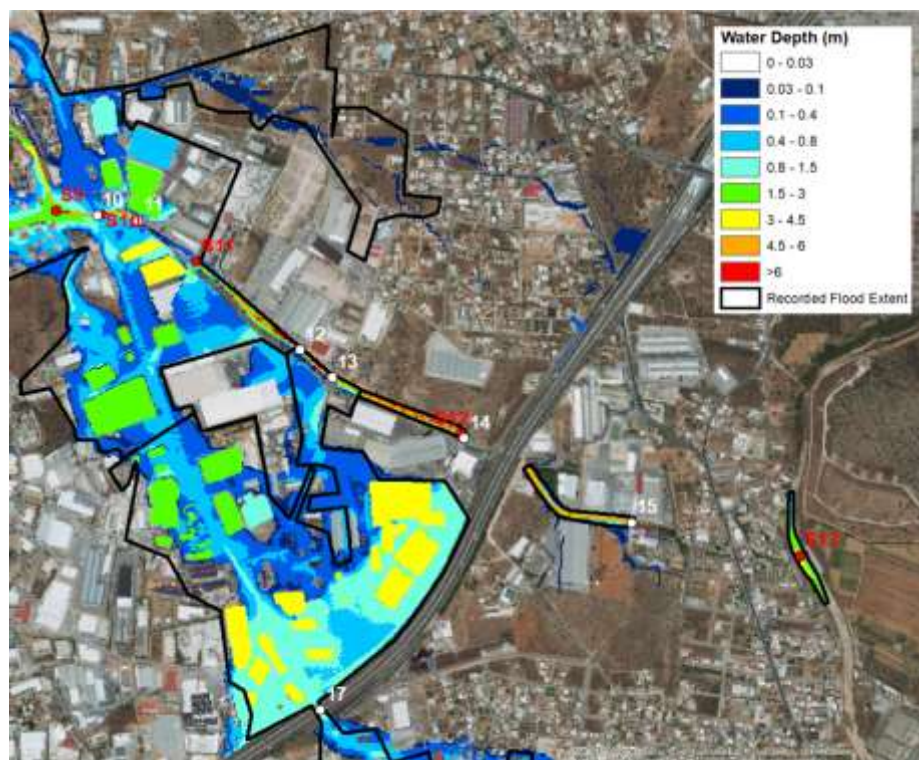


Figure 40 Simulated maximum water depths and the recorded flood extent – Section 4 (Scenario “Real flood”)

Section 5 focuses on the area that is placed east of Attica Road. The flow of Soures stream after underpassing Attica Road, inundates a tiny area with water depths lower than 0.1 m. Also, the water that moved along the PEOATH passes under the bridge of Attica Road and floods the Papakosta settlement.

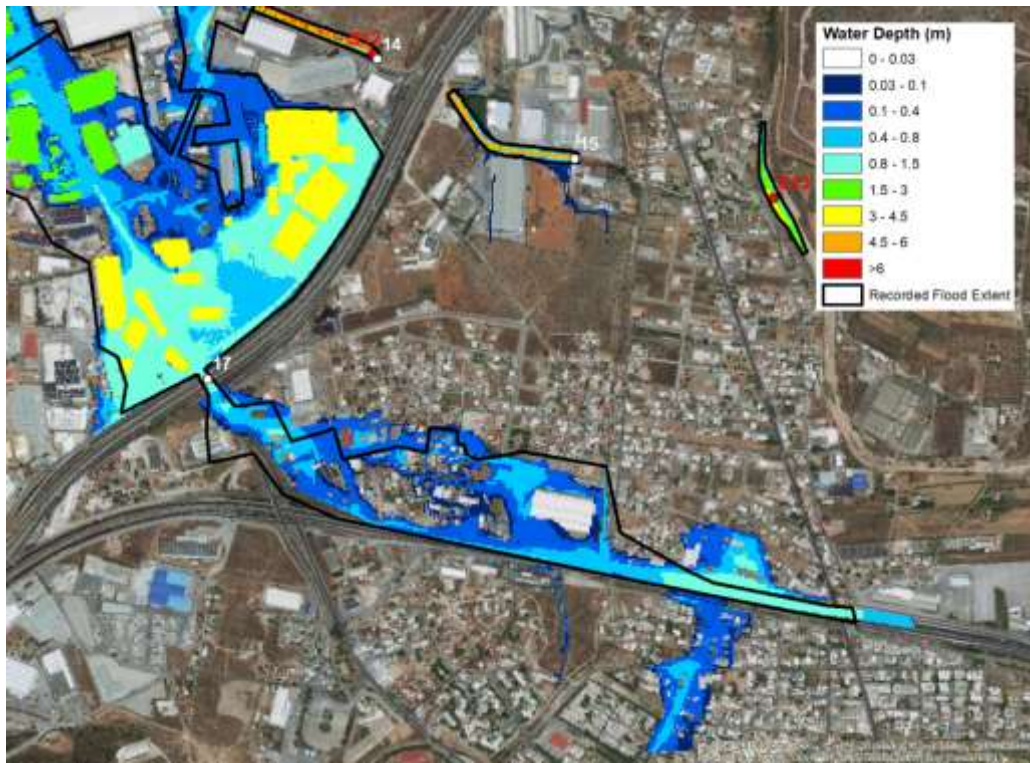


Figure 41 Simulated maximum water depths and the recorded flood extent – Section 5 (Scenario “Real flood”)

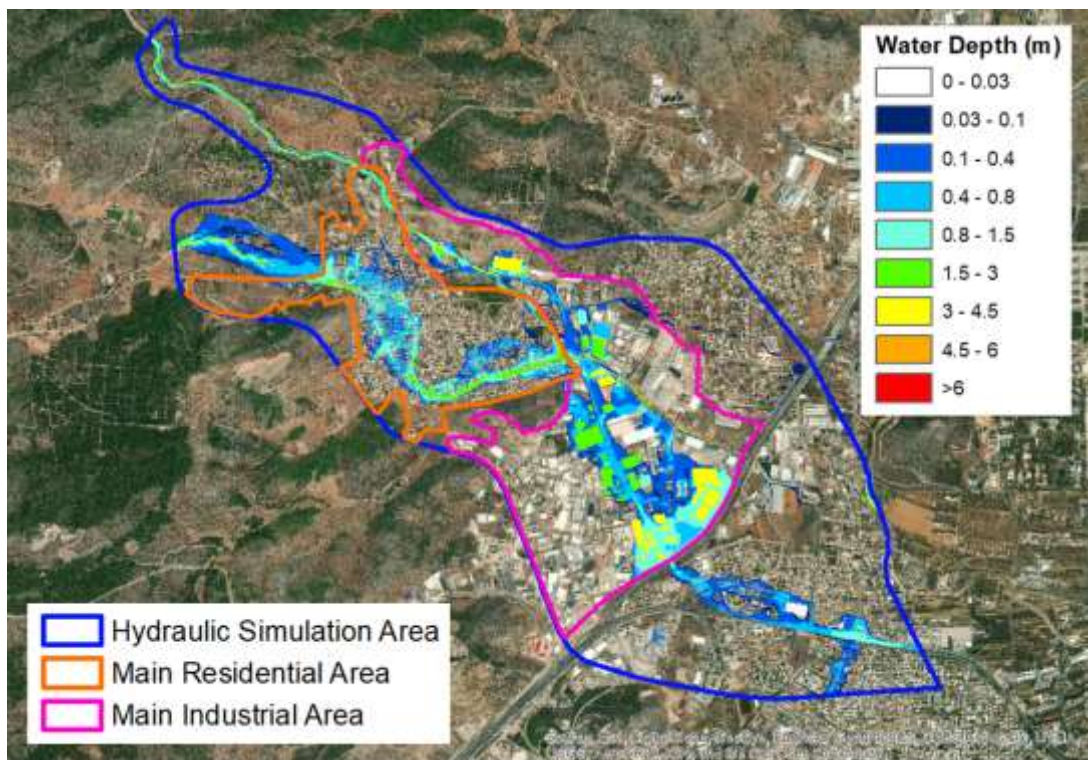


Figure 42 Simulated maximum water depths within the particular areas (Scenario “Real flood”)

The average wet maximum water depth, which corresponds only to the wet parts, of the whole hydraulic simulation area is 0.883 m. The average wet maximum water depth of the main residential area is 0.784 m and the average wet maximum water depth of the main industrial area is 1.166 m, respectively. The maximum water depths in these particular areas are shown in Figure 42.

Taking into consideration not only the wet parts but also the dry ones, then the corresponding average maximum water depth of the hydraulic simulation area is 0.160 m. The average maximum water depth of the main residential area is 0.201 m and the average maximum water depth of the industrial area is 0.335 m, respectively.

5.1.3. Flood extent and flooding

The flood extent is derived by the contour line that shows the continuous flooding of the area with at least 0.03 m. The real flood extent is compared with the recorded flood extent, as it is shown in Figure 43. The relative commentary has already been done extensively in unit 5.1.1.

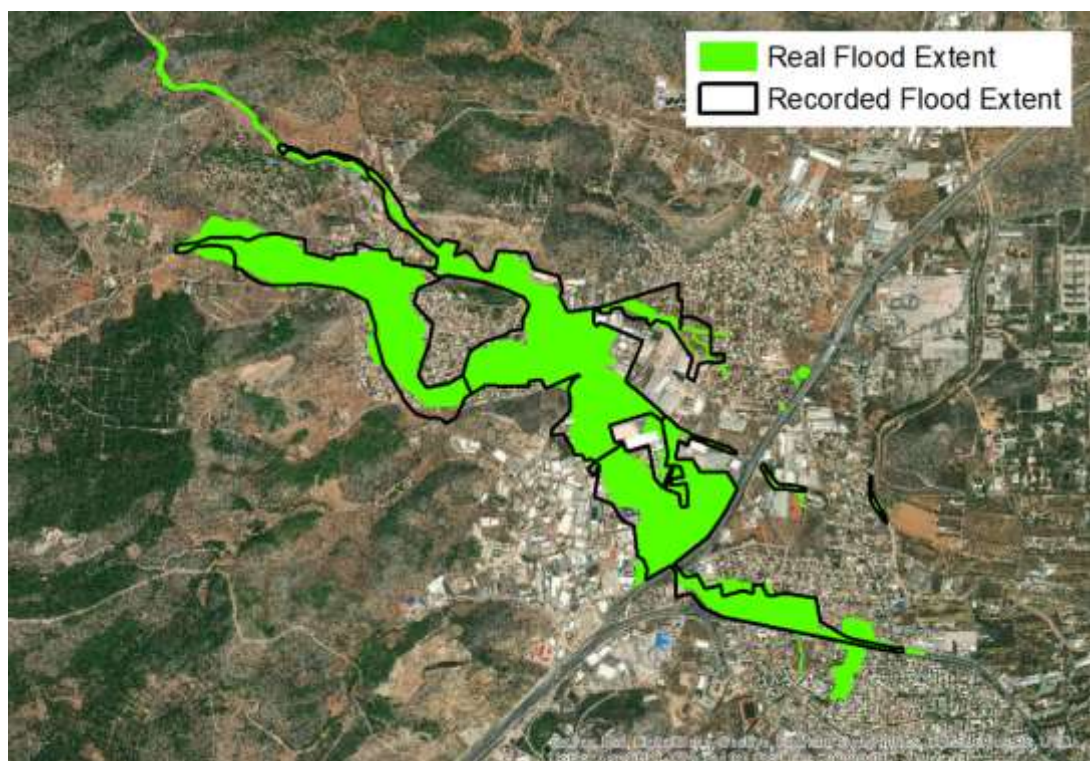


Figure 43 Comparison of real flood extent with recorded flood extent (Scenario “Real flood”)

The real flood extent covers an area of 2.535 km² very close to the recorded flood extent, which covers an area of 2.598 km². As it is shown in Figure 43, the recorded flood extent does not cover the northwestern part of the area and therefore, for the reliability of the comparison, the corresponding part of the real flood extent is ignored reducing the real

flood extent to an area of 2.494 km². This corresponds to a 96.0% of the recorded flood extent. The relative surplus and deficit are 12.4% and 16.4%, respectively.

Figure 44 shows the real flood extent within the hydraulic simulation area, the main residential area and the main industrial area , so called particular areas. The real flood extent covers an area of 2.535 km², as previously mentioned, of the hydraulic simulation area at a rate of 23.4%. It, also, covers an area of 0.711 km² at a percentage of 41.1% of the main residential area and an area of 1.097 km² at a percentage of 35.5% of the main industrial area.

Flooding is the area of the wet parts with a maximum water depth at least 0.03 m.

Flooding covers an area of 1.964 km² of the hydraulic simulation area at a percentage of 18.1%. It, also, covers an area of 0.444 km², at a percentage of 25.7%, of the main residential area and an area of 0.888 km², at a percentage of 28.7% of the main industrial area.

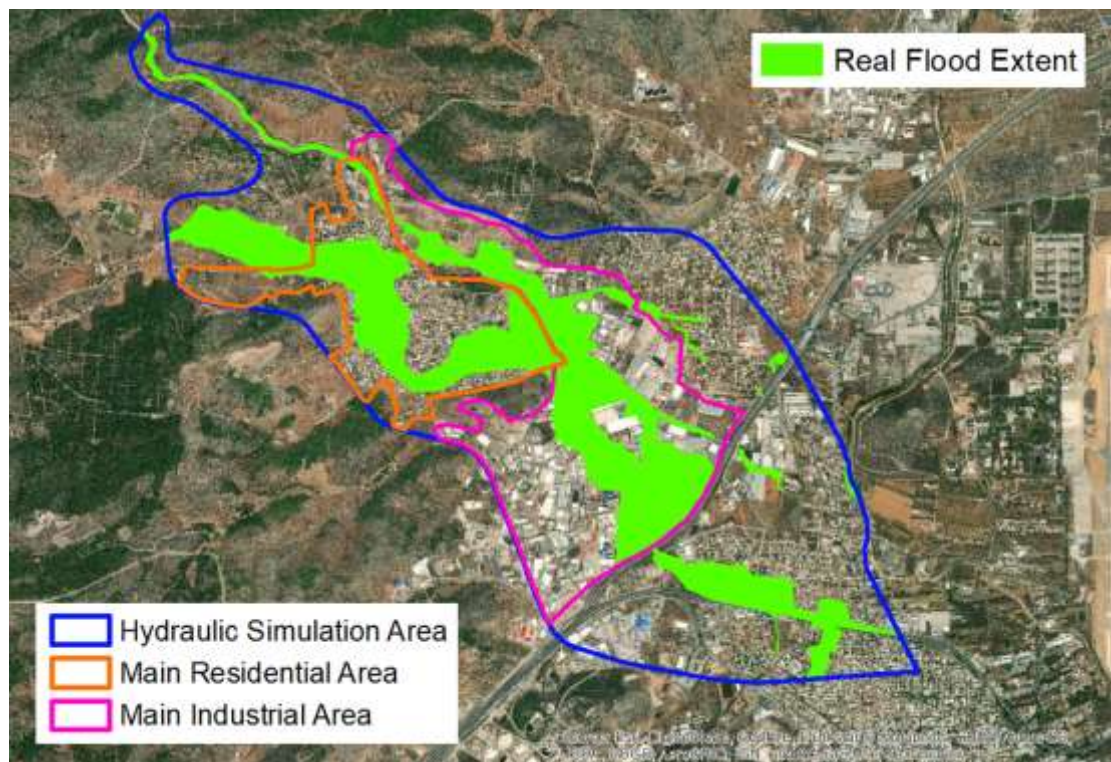


Figure 44 Flood extent within the particular areas (Scenario “Real flood”)

5.2. Scenario “Fully operated conduits”

5.2.1. Checkpoints – Maximum water depths and flood progression

Figures 45, 46 and 47 give the time evolution of the water depths of the Scenario “Fully operated conduits” compared to the water depths of the Scenario “Real flood”.

As it is shown in Figure 45, the model underestimates the simulated maximum depths of the Scenario “Real flood” at all checkpoints of Agia Aikaterini stream except AA3, where it is the same, from a slight difference of 4 cm at AA5 up to a slight difference of 9 cm at AA7.

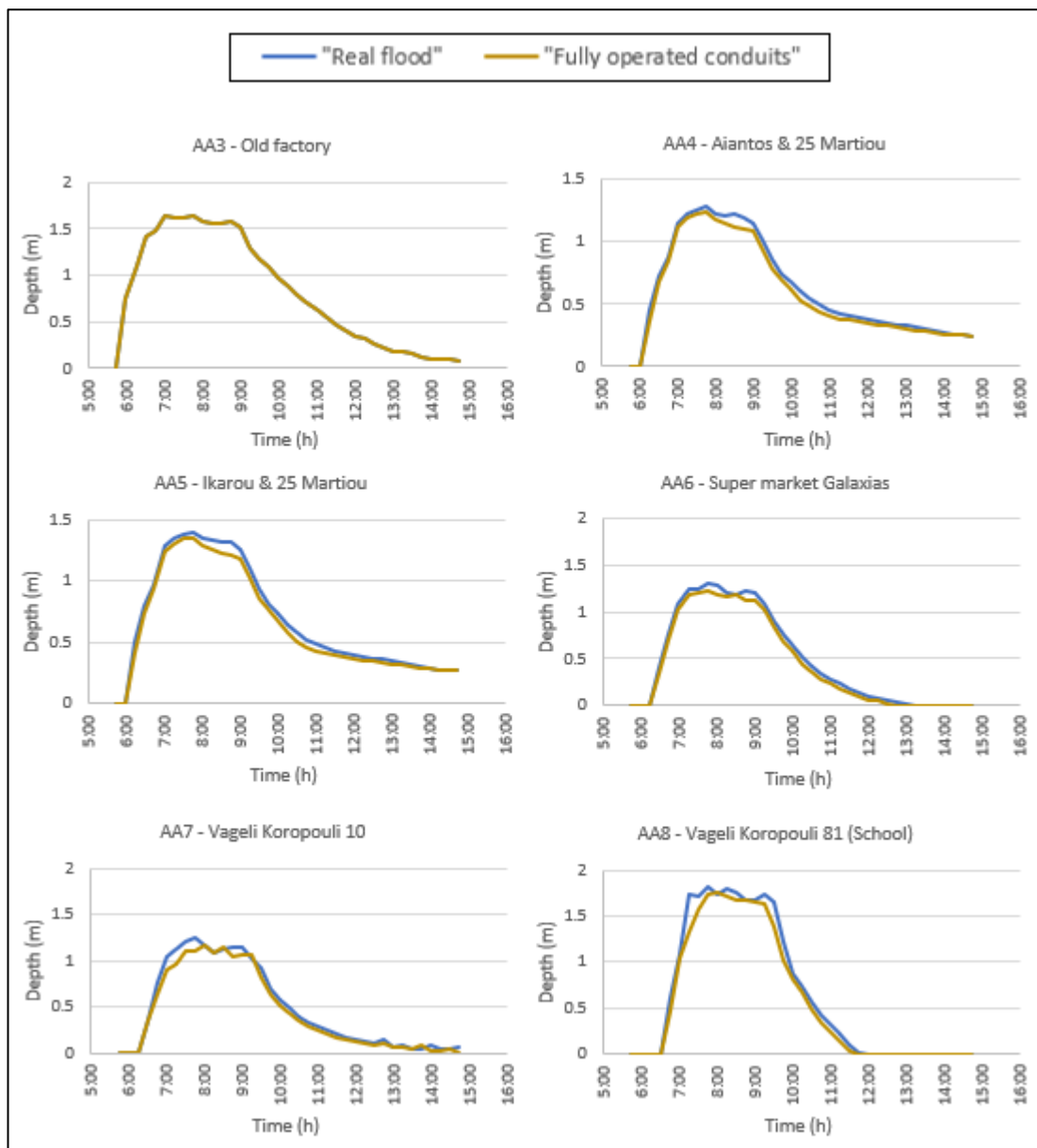


Figure 45 Time change of water depths at the checkpoints of Agia Aikaterini stream

The checkpoint AA3 presents an identical time change of the water depth. Generally, there are insignificant deviations regarding the flood progress compared to Scenario "Real flood".

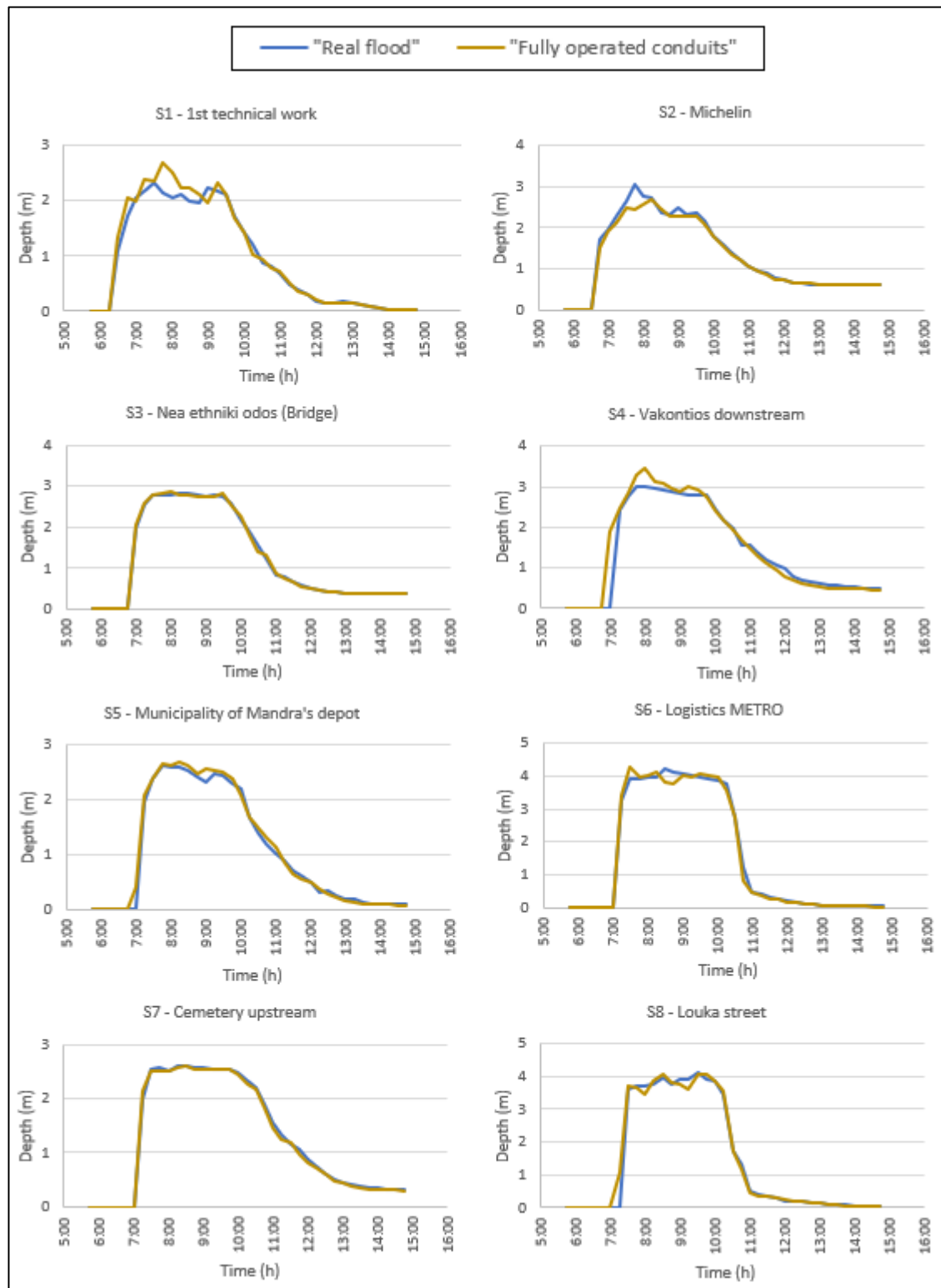


Figure 46 Time change of water depths at the checkpoints of Soures stream upstream of the confluence with Agia Aikaterini stream

Figures 46 and 47 show that the model underestimates the simulated maximum depths of the Scenario “Real flood” at checkpoints S2 and S7 of Soures stream and overestimates the maximum depths at checkpoints S1, S3, S4, S5, S6, S8, S10, S11, S12 and S13. The range of deviation extends from a slight difference of 2 cm at S7 up to a difference of 0.96 m at S11. Regarding the flood progress, an earlier rising of the upward branch is observed in the cases S4, S5, S8 and particularly in the cases S9, S10, S11, S12 and S13. It should be mentioned that generally, the earlier rising of the upward branch is not followed by an earlier lowering of the downward branch.

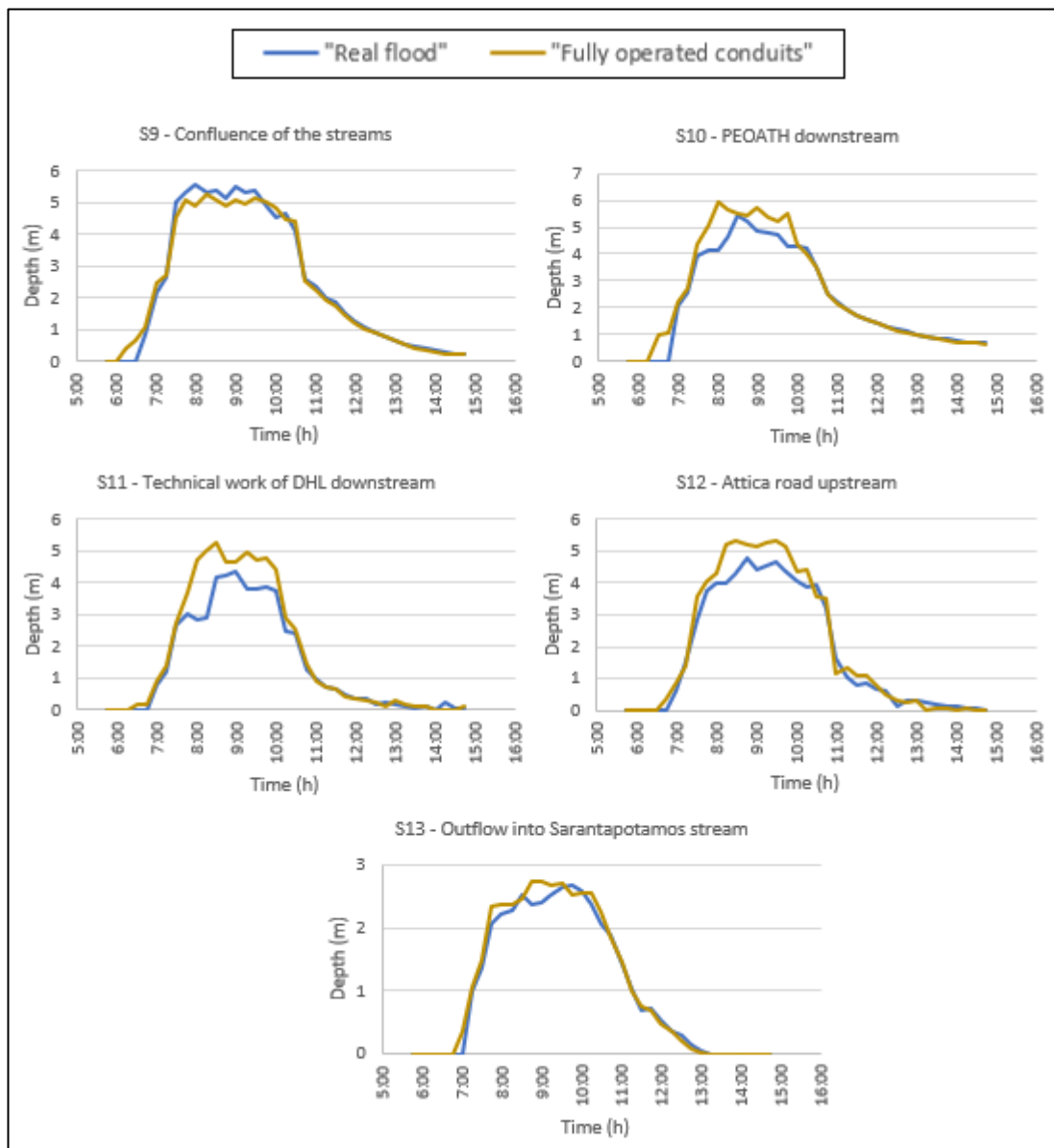


Figure 47 Time change of water depths at the checkpoints of Soures stream downstream of the confluence with Agia Aikaterini stream

A comparison of the maximum water depths at the checkpoints is shown in Figures 48 and 49. The RMSE, NSE, and MAE are 0.353, 0.941 and 0.242, respectively.

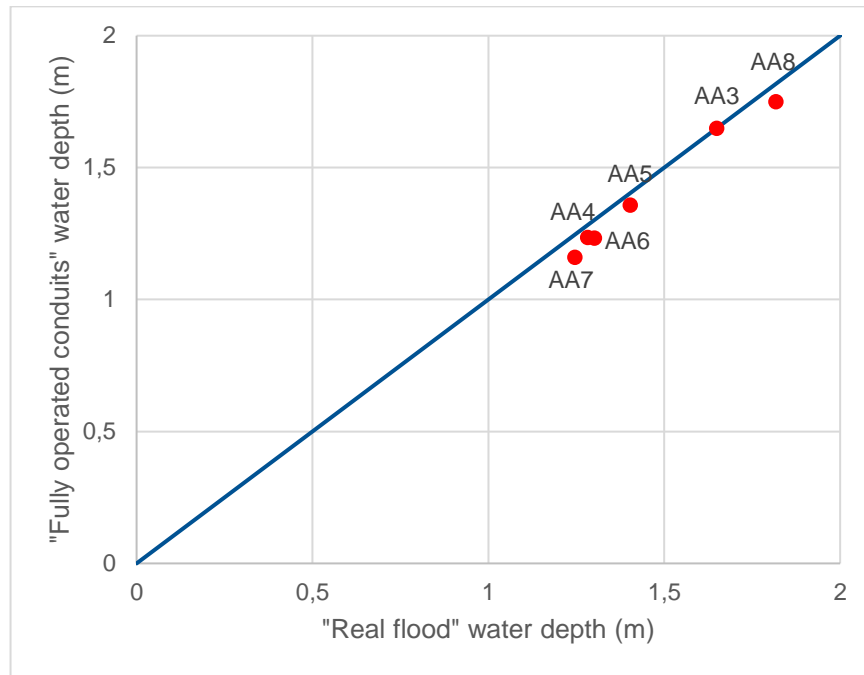


Figure 48 Comparison of maximum water depths for Agia Aikaterini stream (Scenario “Fully operated conduits”)

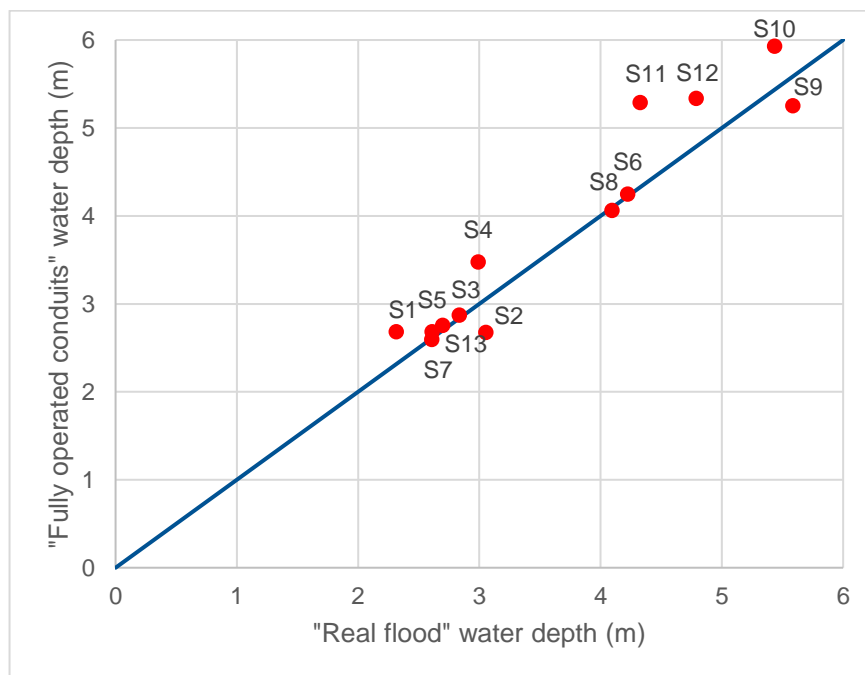


Figure 49 Comparison of maximum water depths for Soures stream (Scenario “Fully operated conduits”)

5.2.2. Maximum water depths of area

Figure 50 shows the maximum water depths within the hydraulic simulation area, the main residential area and the main industrial area.

The maximum water depths range from 0.03 m to 7.03 m

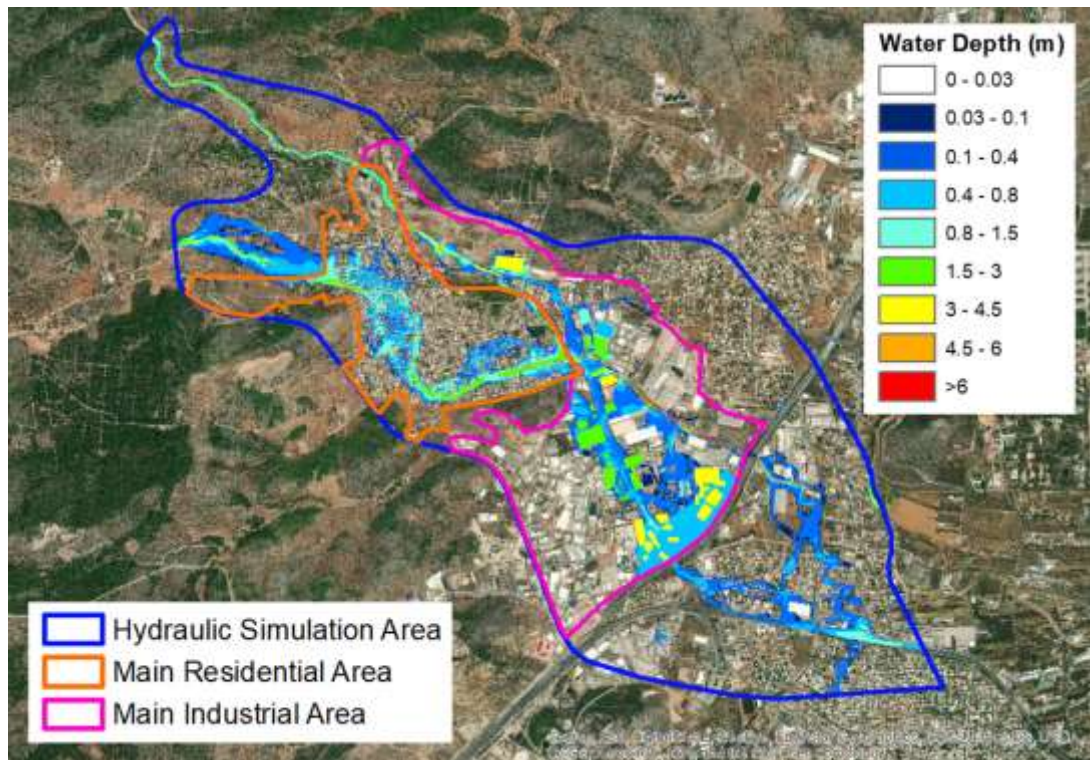


Figure 50 Maximum water depths within the particular areas (Scenario “Fully operated conduits”)

Table 17 presents the comparison of average wet maximum water depths for the particular areas between Scenario “Fully operated conduits” and Scenario “Real flood”.

Table 17 Comparison of average wet maximum water depths for the particular areas (Scenario “Fully operated conduits” vs. Scenario “Real flood”)

Area	Average Wet Maximum Water Depth		Depth Difference (m) (1)-(2)	Depth Percentage (%) $100*(1)/(2)$
	(m)			
	Scenarios			
	“Fully Operated Conduits” (1)	“Real Flood” (2)		
Hydraulic Simulation Area	0.767	0.883	-0.116	86.9
Main Residential Area	0.760	0,784	-0.024	96.9

Main Industrial Area	1.038	1.166	-0.128	89.0
-----------------------------	-------	-------	--------	------

The average wet maximum water depth of the hydraulic simulation area is 0.767 m. The average wet maximum water depth of the main residential area is 0.760 m and the average wet maximum water depth of the main industrial area is 1.038 m, respectively. The average wet maximum water depth difference ranges from a small difference of -11.6 cm in the hydraulic simulation area and -12 cm in the main residential area to a slight difference of -2.4 cm in the main industrial area with corresponding depth percentages 86.9%, 89% and 96.9%, respectively. The results of the comparison of Table 17 are confirmed in Figure 51.

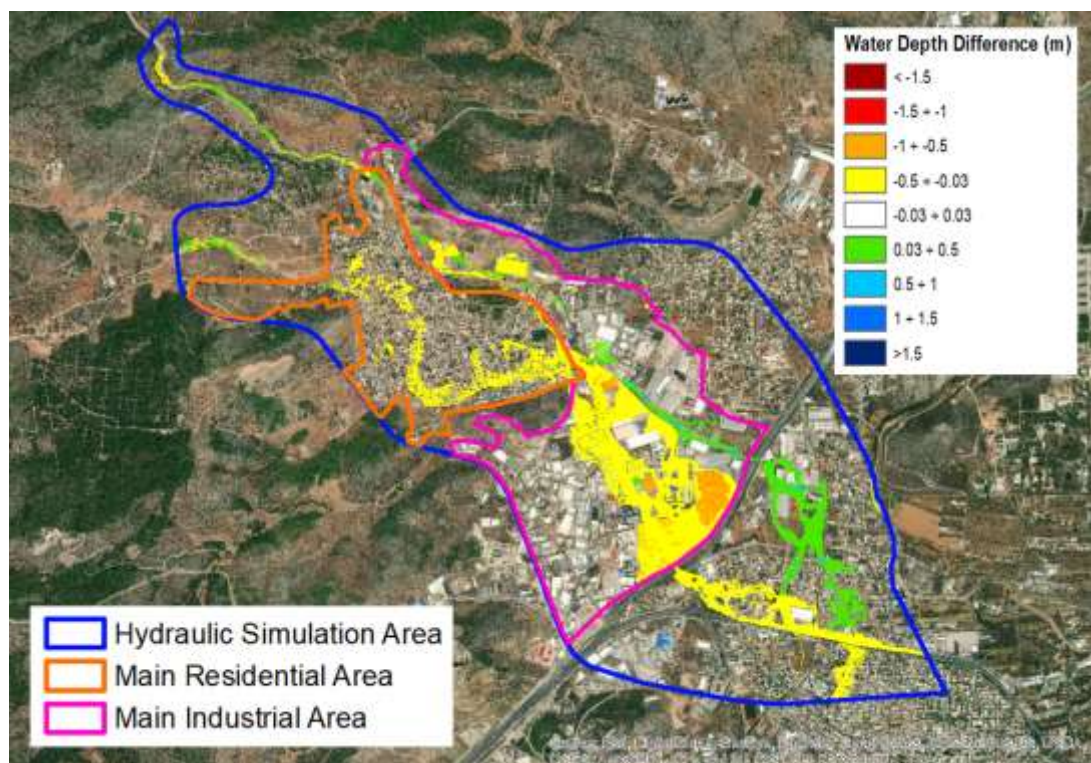


Figure 51 Differences of maximum water depths between Scenario “Fully operated conduits” and Scenario “Real flood”

There is a slight difference on the maximum water depths in the main residential area, where the difference in a significant portion is almost zero (less than 3 cm) and in the other portion it does not exceed -50 cm. On the other hand, in the main industrial area, the majority of the region presents differences less than -50 cm. In the main industrial area there is a reduction of the maximum depths and on the contrary, an increase in the surrounding areas of Soures stream and particularly in the area downstream of Attica Road, where a flooding with maximum depths up to 50 cm is presented as it is shown

illustratively in Figure 51. Finally, Figure 51 confirms the choking of the flow upstream the clogged technical works.

Table 18 presents the comparison of average maximum water depths for the particular areas between Scenario “Fully operated conduits” and Scenario “Real flood”. The results of the comparison confirm the previous results.

Table 18 Comparison of average maximum water depths for the particular areas (Scenario “Fully operated conduits” vs. Scenario “Real flood”)

Area	Average Maximum Water Depth		Depth Difference (m) (1)-(2)	Depth Percentage (%) $100*(1)/(2)$
	(m)			
	Scenarios			
	“Fully Operated Conduits” (1)	“Real Flood” (2)		
Hydraulic Simulation Area	0.148	0.160	-0.012	92.2
Main Residential Area	0.192	0.201	-0.009	95.4
Main Industrial Area	0.293	0.335	-0.042	87.5

5.2.3. Flood extent and flooding

Figure 52 shows the comparison of the flood extent of Scenario “Fully operated conduits” with the real flood extent.

The flood extent covers an area of 2.774 km² larger than the real flood extent, which covers an area of 2.535 km². This corresponds to a percentage 109.4% of the real flood extent.

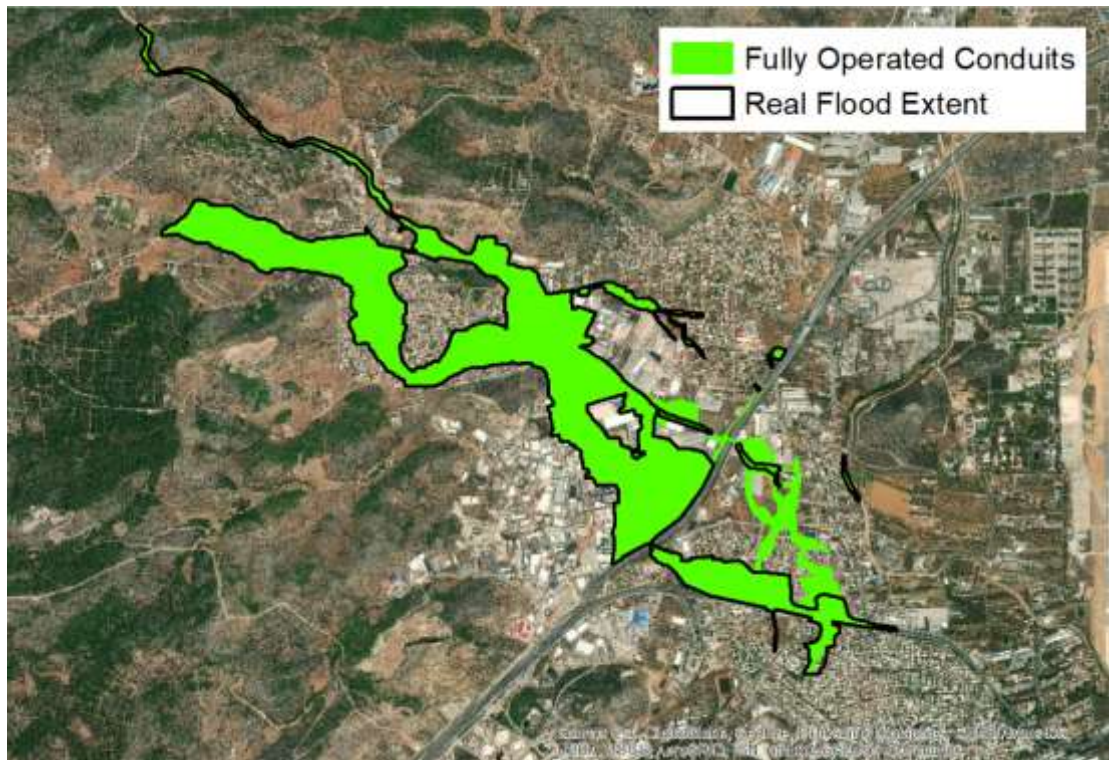


Figure 52 Comparison of the flood extent with the real flood extent (Scenario “Fully operated conduits”)

Figure 53 shows the flood extent within the particular areas.

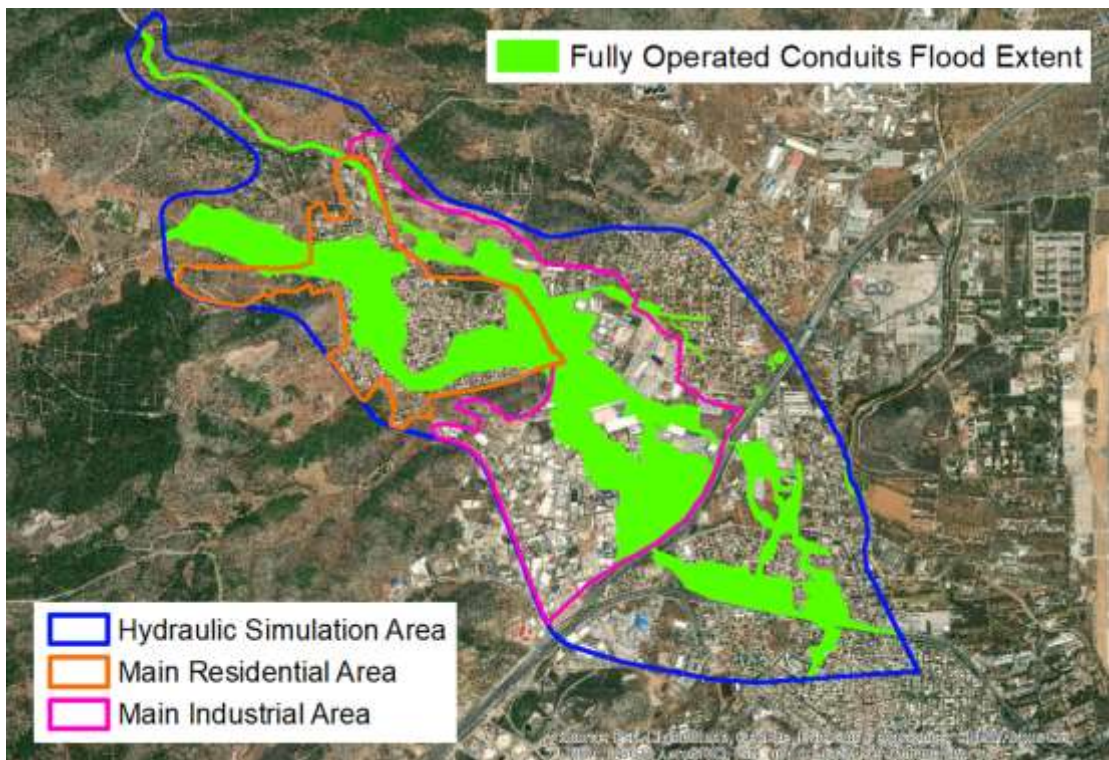


Figure 53 Flood extent within the particular areas (Scenario “Fully operated conduits”)

Table 19 presents the comparison of flood extent for the particular areas between Scenario “Fully operated conduits” and Scenario “Real flood”.

Table 19 Comparison of flood extent for the particular areas (Scenario “Fully operated conduits” vs. Scenario “Real flood”)

Area	Flood Extent Percentage (%)		Difference of Flood Extent Percentages (%) (1)-(2)	Percentage of Flood Extents (%) $100*(1)/(2)$
	Scenarios			
	“Fully Operated Conduits” (1)	“Real Flood” (2)		
Hydraulic Simulation Area	25.6	23.4	2.2	109.4
Main Residential Area	40.9	41.1	-0.2	99.5
Main Industrial Area	36.6	35.5	1.1	103.0

The flood extent covers an area of 2.774 km², as previously mentioned, of the hydraulic simulation area at a percentage of 25.6%. It, also, covers an area of 0.707 km² at a percentage of 40.9% of the main residential area and an area of 1.130 km² at a percentage of 36.6% of the main industrial area. The difference of flood extent percentages ranges in a spectrum of slight differences from 2.2% in the hydraulic simulation area to -0.2% in the main residential area and 1.1% in the main industrial area with corresponding percentage of flood extents of 109.4%, 99.5% and 103.0%, respectively.

Table 20 presents the comparison of flooding for the particular areas between Scenario “Fully operated conduits” and Scenario “Real flood”.

Table 20 Comparison of flooding for the particular areas (Scenario “Fully operated conduits” vs. Scenario “Real flood”)

Area	Flooding Percentage (%)		Difference of Flooding Percentages	Percentage of Floodings (%)
	Scenarios			

	“Fully Operated Conduits” (1)	“Real Flood” (2)	(%) (1)-(2)	100*(1)/(2)
Hydraulic Simulation Area	19.2	18.1	1.1	106.0
Main Residential Area	25.3	25.7	-0.4	98.4
Main Industrial Area	28.2	28.7	-0.5	98.3

5.3. Scenario “Fences”

5.3.1. Checkpoints – Maximum water depths and flood progression

Figures 54 and 55 give the time evolution of the water depths of the Scenario “Fences” compared to the water depths of the Scenario “Real flood”.

The time evolution of the water depths is identical with that of Scenario “Real flood” at all checkpoints of Agia Aikaterini stream, as it is shown in Figures 31. The model overestimates the simulated maximum depths of the Scenario “Real flood” at all checkpoints of Soures stream downstream S3. The range of deviation extends from a slight difference of 6 cm at S4 and S13 up to a difference of 1.21 m at S12. Also, the flood progress is the same regarding the two branches. Small differences are observed comparing the occurrences of the maximum depths downstream of S6.

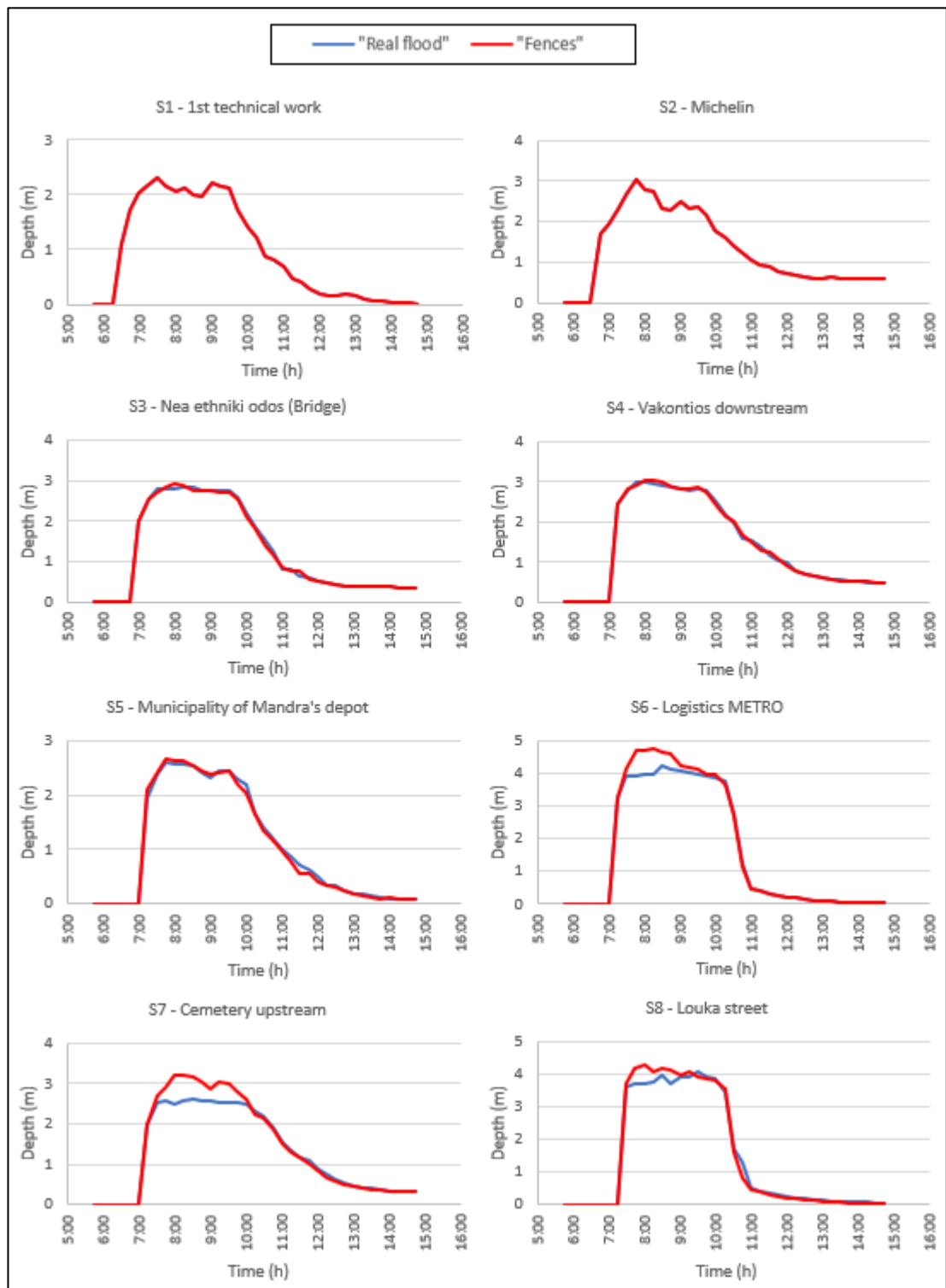


Figure 54 Time change of water depths at the checkpoints of Soures stream upstream of the confluence with Agia Aikaterini stream

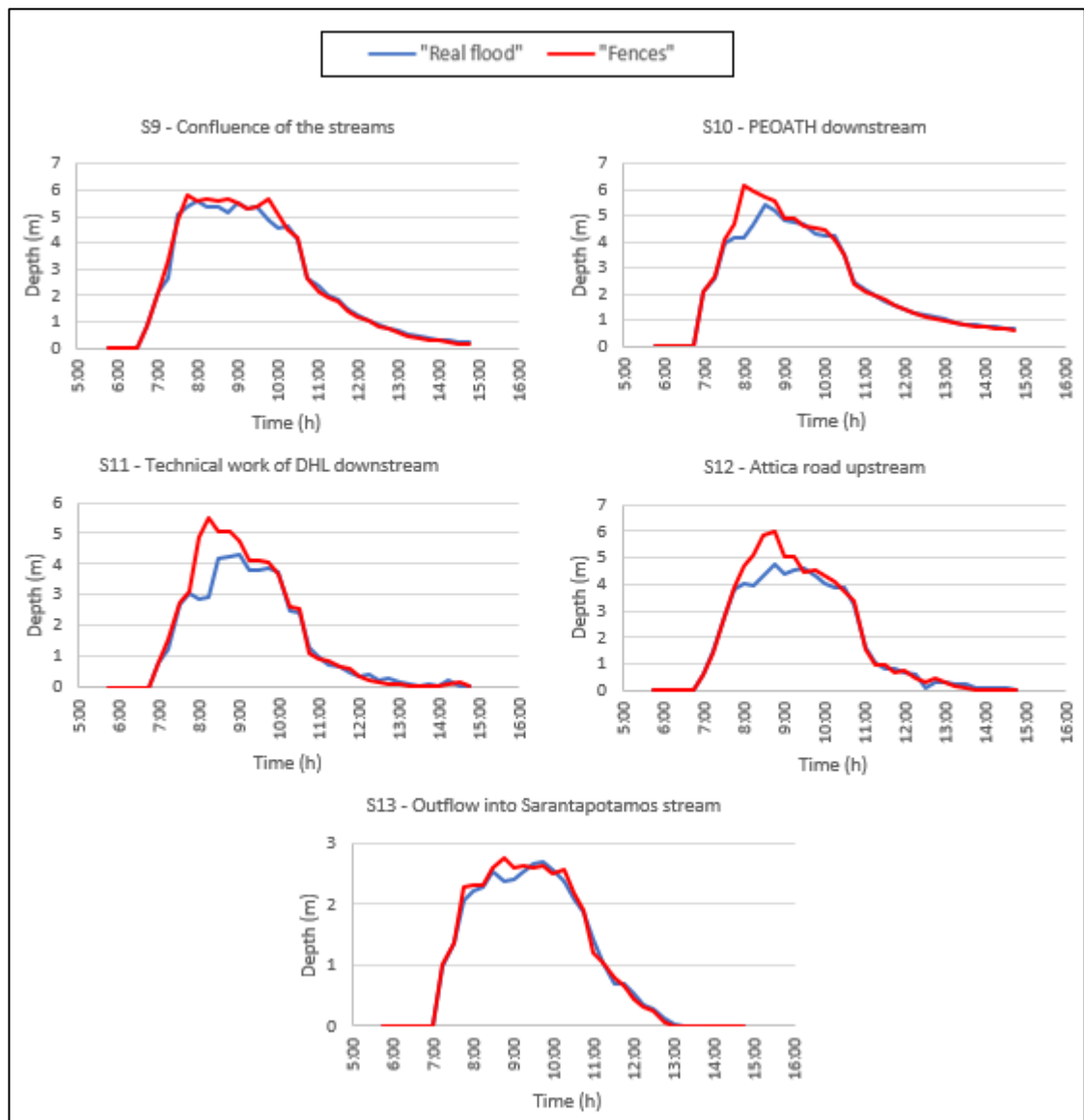


Figure 55 Time change of water depths at the checkpoints of Soures stream downstream of the confluence with Agia Aikaterini stream

A comparison of the maximum water depths at the checkpoints is shown in Figures 56 and 57. The RMSE, NSE, and MAE are 0.492, 0.885 and 0.289, respectively.

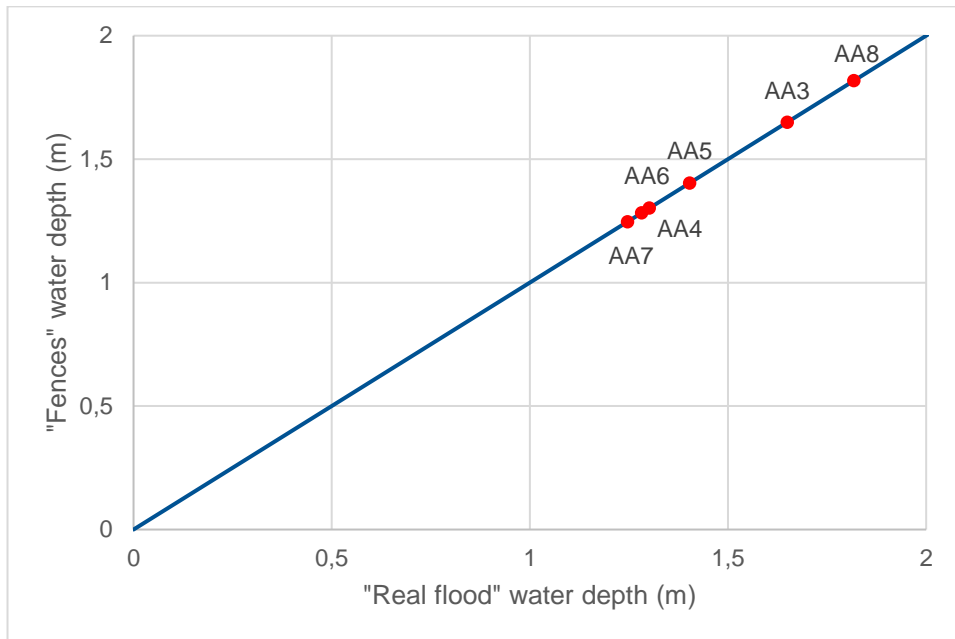


Figure 56 Comparison of maximum water depths for Agia Aikaterini stream (Scenario "Fences")

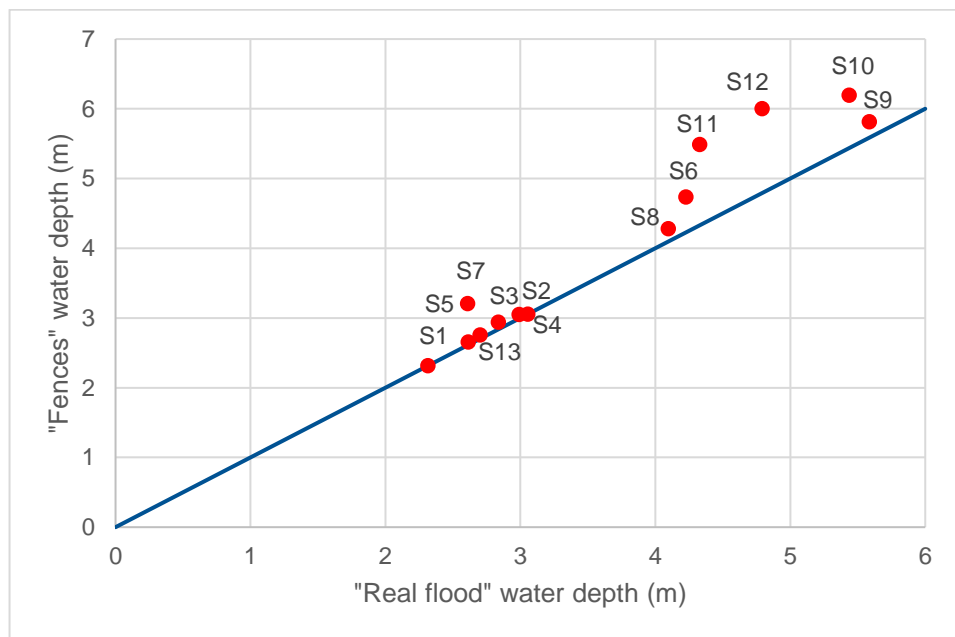


Figure 57 Comparison of maximum water depths for Soures stream (Scenario "Fences")

5.3.2. Maximum water depths of area

The maximum water depths in the particular areas are shown in Figure 58.

The maximum water depths range from 0.03 m to 7.12 m.

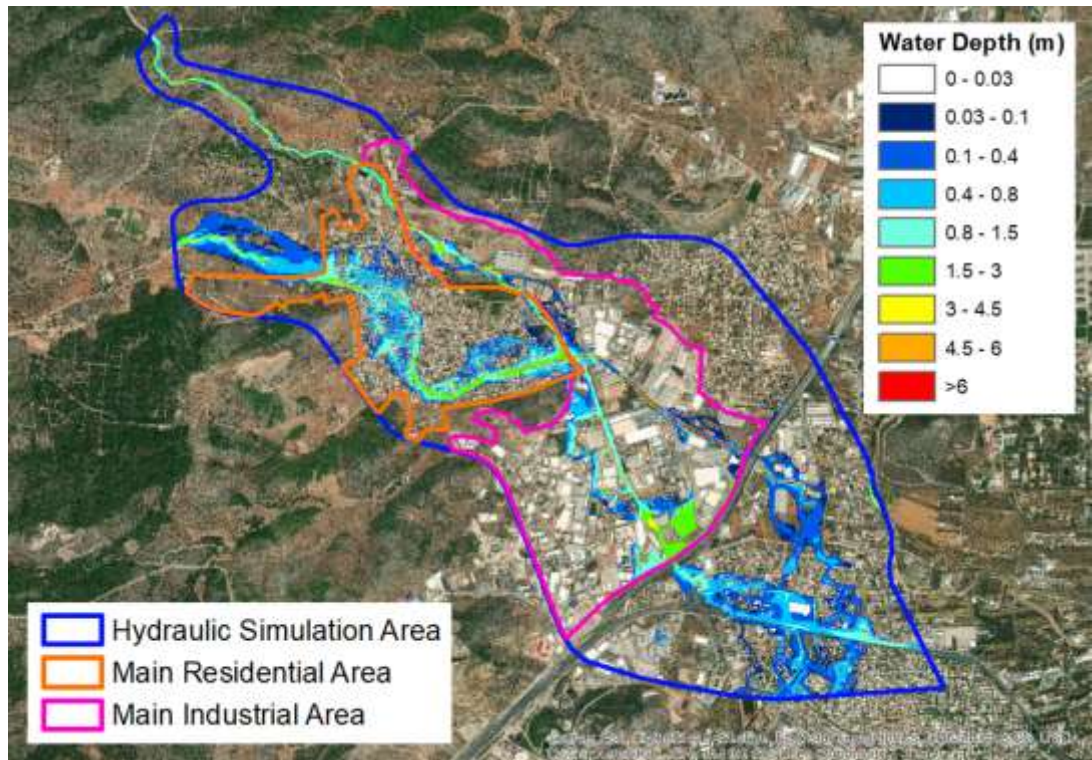


Figure 58 Maximum water depths within the particular areas (Scenario “Fences”)

Table 21 presents the comparison of average wet maximum water depths for the particular areas between Scenario “Fences” and Scenario “Real flood”.

Table 21 Comparison of average wet maximum water depths for the particular areas (Scenario “Fences” vs. Scenario “Real flood”)

Area	Average Wet Maximum Water Depth (m)		Depth Difference (m) (1)-(2)	Depth Percentage (%) $100*(1)/(2)$
	Scenarios			
	“Fences”	“Real Flood”		
	(1)	(2)		
Hydraulic Simulation Area	0.695	0.883	-0.188	78.7
Main Residential Area	0.790	0,784	0.006	100.8
Main Industrial Area	1.067	1.166	-0.098	91.6

The average wet maximum water depth of the hydraulic simulation area is 0.695 m. The average wet maximum water depth of the main residential area is 0.790 m and the average wet maximum water depth of the industrial area is 1.067 m, respectively. The average wet maximum water depth difference ranges from a difference of -18.8 cm in the hydraulic simulation area and 0.6 cm in the main residential area to a difference of -9.8 cm in the main industrial area with corresponding depth percentages of 78.7%, 100.8% and 91.6%, respectively. The results of the comparison of Table 21 are confirmed in Figure 59. Very slight differences are observed on the maximum water depths in the main residential area (see Figure 59).

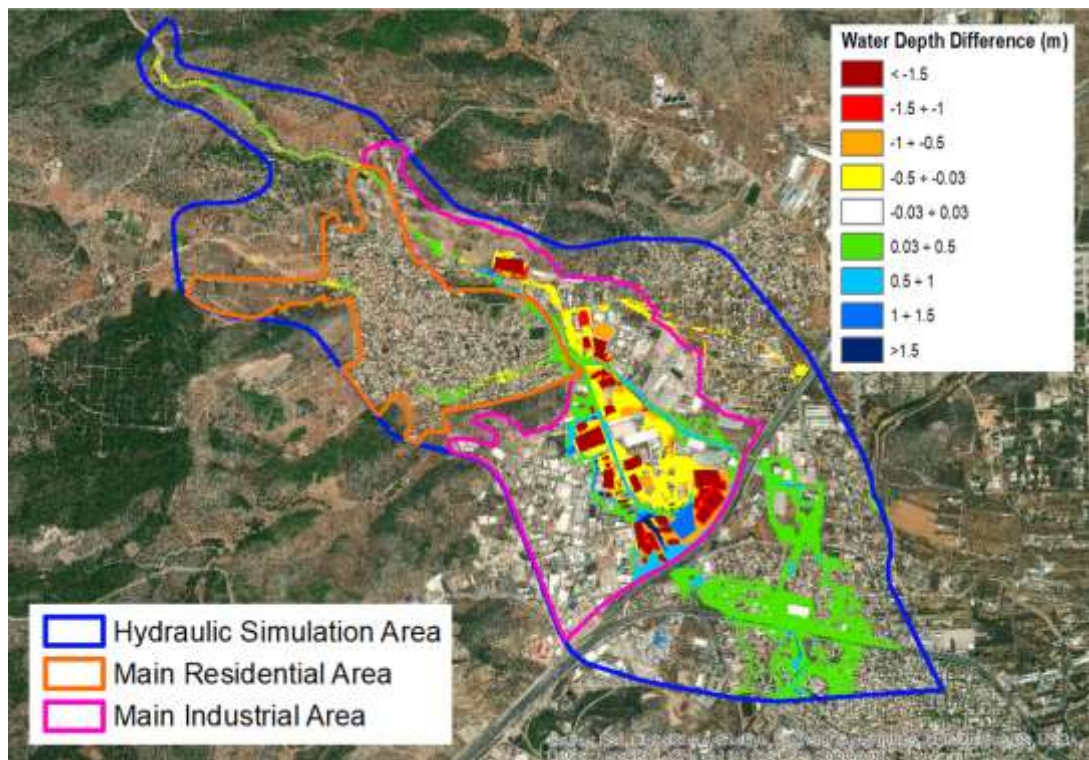


Figure 59 Differences of maximum water depths between Scenario “Fences” and Scenario “Real flood”

In the main industrial area, the depth differences range from less than -1.50 m inside the protected properties to greater than 1.50 m along the PEOATH besides Attica Road (see Figure 59). More precisely, the depth differences are less than 0.5 m southeast of Attica Road.

Table 22 presents the comparison of average maximum water depths for the particular areas between Scenario “Fences” and Scenario “Real flood”. The results of the comparison confirm the previous results.

Table 22 Comparison of average maximum water depths for the particular areas (Scenario “Fences” vs. Scenario “Real flood”)

Area	Average Maximum Water Depth (m)		Depth Difference (m)	Depth Percentage (%)
	Scenarios			
	“Fences”	“Real Flood”	(1)-(2)	100*(1)/(2)
	(1)	(2)		
Hydraulic Simulation Area	0.120	0.160	-0.040	75.0
Main Residential Area	0.207	0.201	0.006	103.0
Main Industrial Area	0.140	0.335	-0.195	41.9

5.3.3. Flood extent and flooding

Figure 60 shows the comparison of the flood extent of Scenario “Fences” with the real flood extent.

The flood extent covers an area of 2.489 km² very close to the real flood extent, which covers an area of 2.535 km². This corresponds to a 98.2% of the real flood extent.

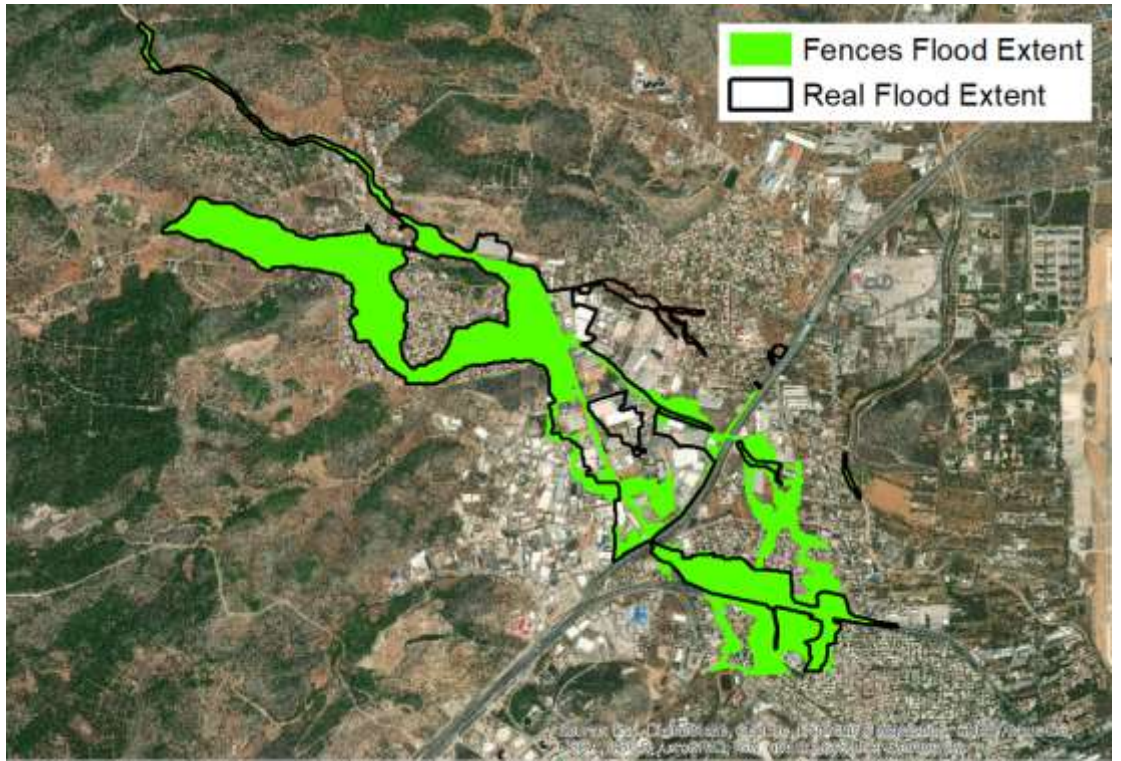


Figure 60 Comparison of the flood extent with the real flood extent (Scenario “Fences”)

Figure 61 shows the flood extent within the particular areas.

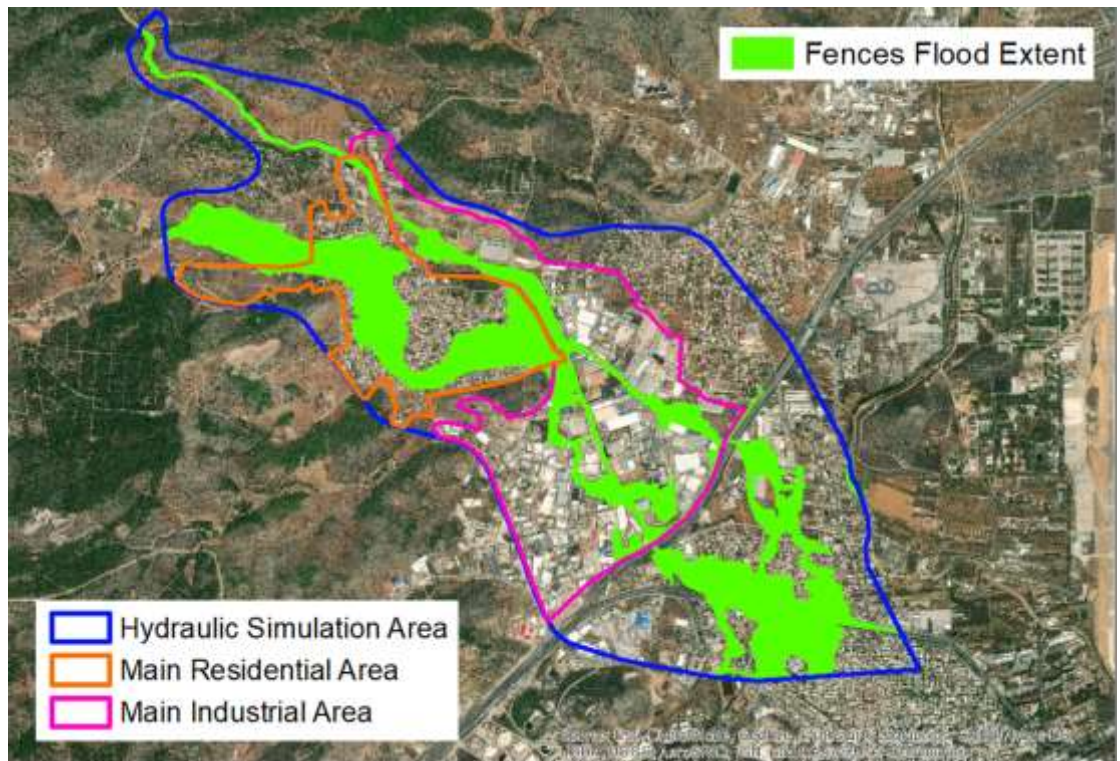


Figure 61 Flood extent within the particular areas (Scenario “Fences”)

Table 23 presents the comparison of flood extent for the particular areas between Scenario “Fences” and Scenario “Real flood”.

Table 23 Comparison of flood extent for the particular areas (Scenario “Fences” vs. Scenario “Real flood”)

Area	Flood Extent Percentage (%)		Difference of Flood Extent Percentages (%)	Percentage of Flood Extents (%)
	Scenarios			
	“Fences” (1)	“Real Flood” (2)	(1)-(2)	100*(1)/(2)
Hydraulic Simulation Area	23.0	23.4	-0.4	98.2
Main Residential Area	41.4	41.1	0.3	100.8
Main Industrial Area	18.3	35.5	-17.2	51.5

The flood extent covers an area of 2.489 km² as previously mentioned, of the hydraulic simulation area at a percentage of 23.0%. It, also, covers an area of 0.716 km² at a percentage of 41.4% of the main residential area and an area of 0.565 km² at a percentage of 18.3% of the main industrial area. The difference of flood extent percentages ranges from slight differences of -0.4% in the hydraulic simulation area and 0.3% in the main residential area to the difference of -17.2% in the main industrial area with corresponding percentage of flood extents of 98.2%, 100.8% and 51.5%, respectively.

Table 24 presents the comparison of flooding for the particular areas between Scenario “Fences” and Scenario “Real flood”. The results of the comparison confirm the previous results.

Table 24 Comparison of flooding for the particular areas (Scenario “Fences” vs. Scenario “Real flood”)

Area	Flooding Percentage (%)		Difference of Flooding Percentages (%)	Percentage of Floodings (%)
	Scenarios			
	“Fences”	“Real Flood”	(1)-(2)	100*(1)/(2)

	“Fences”	“Real Flood”	(%)	100*(1)/(2)
	(1)	(2)	(1)-(2)	
Hydraulic Simulation Area	17.3	18.1	-0.8	95.3
Main Residential Area	26.2	25.7	0.5	102.2
Main Industrial Area	13.1	28.7	-15.6	45.7

5.4. Scenario “Spatially extended rainfall”

5.4.1. Checkpoints – Maximum water depths and flood progression

Figures 62, 63 and 64 give the time evolution of the water depths of the Scenario “Spatially extended rainfall” compared to the water depths of the Scenario “Real flood”.

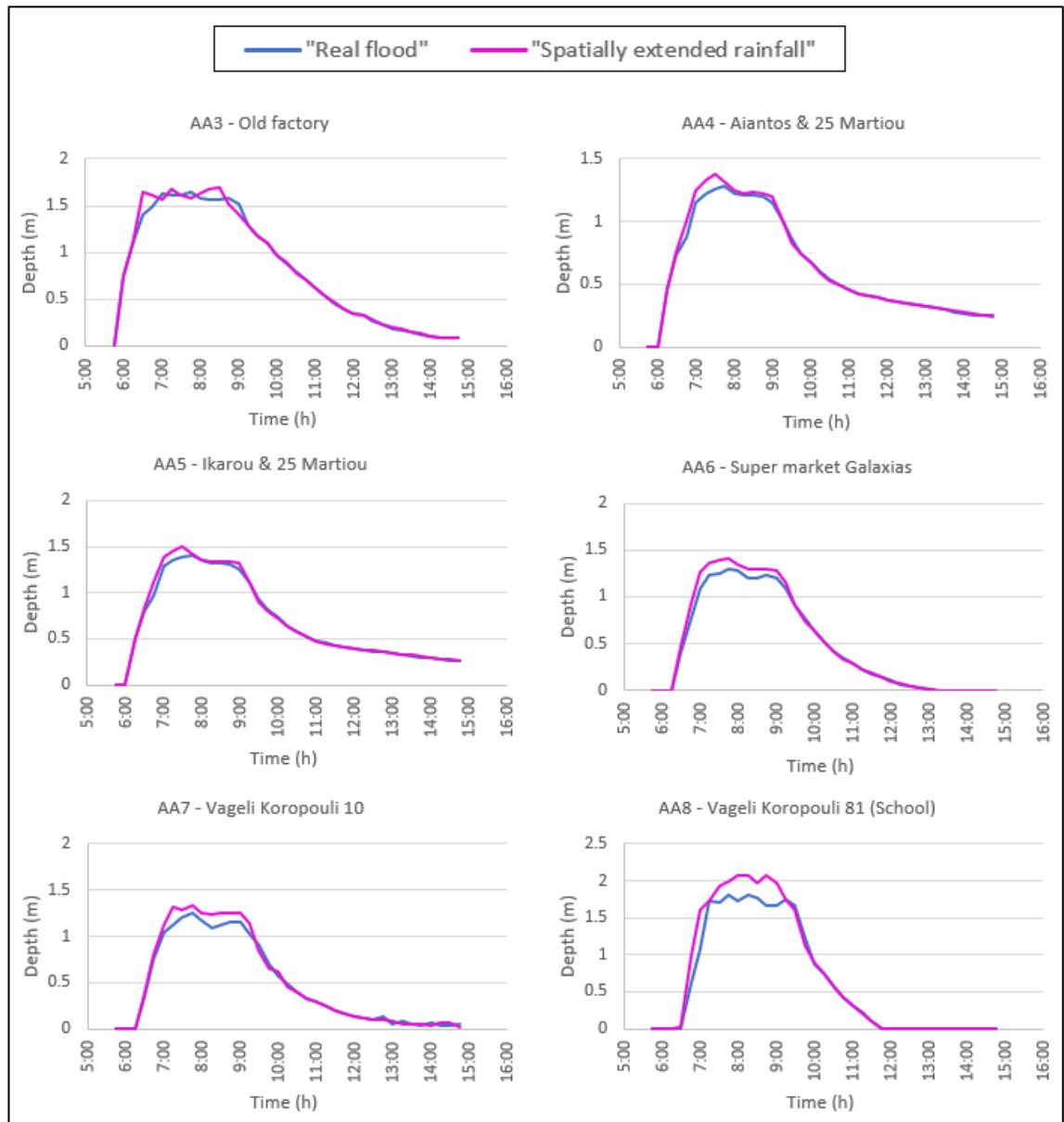


Figure 62 Time change of water depths at the checkpoints of Agia Aikaterini stream

The model, due to the rainfall extension, overestimates the simulated maximum depths of the Scenario "Real flood" at all checkpoints of Agia Aikaterini stream, from a slight difference of 4 cm at AA3 up to a small difference of 25 cm at AA8. An earlier rising of the upward branch is observed.

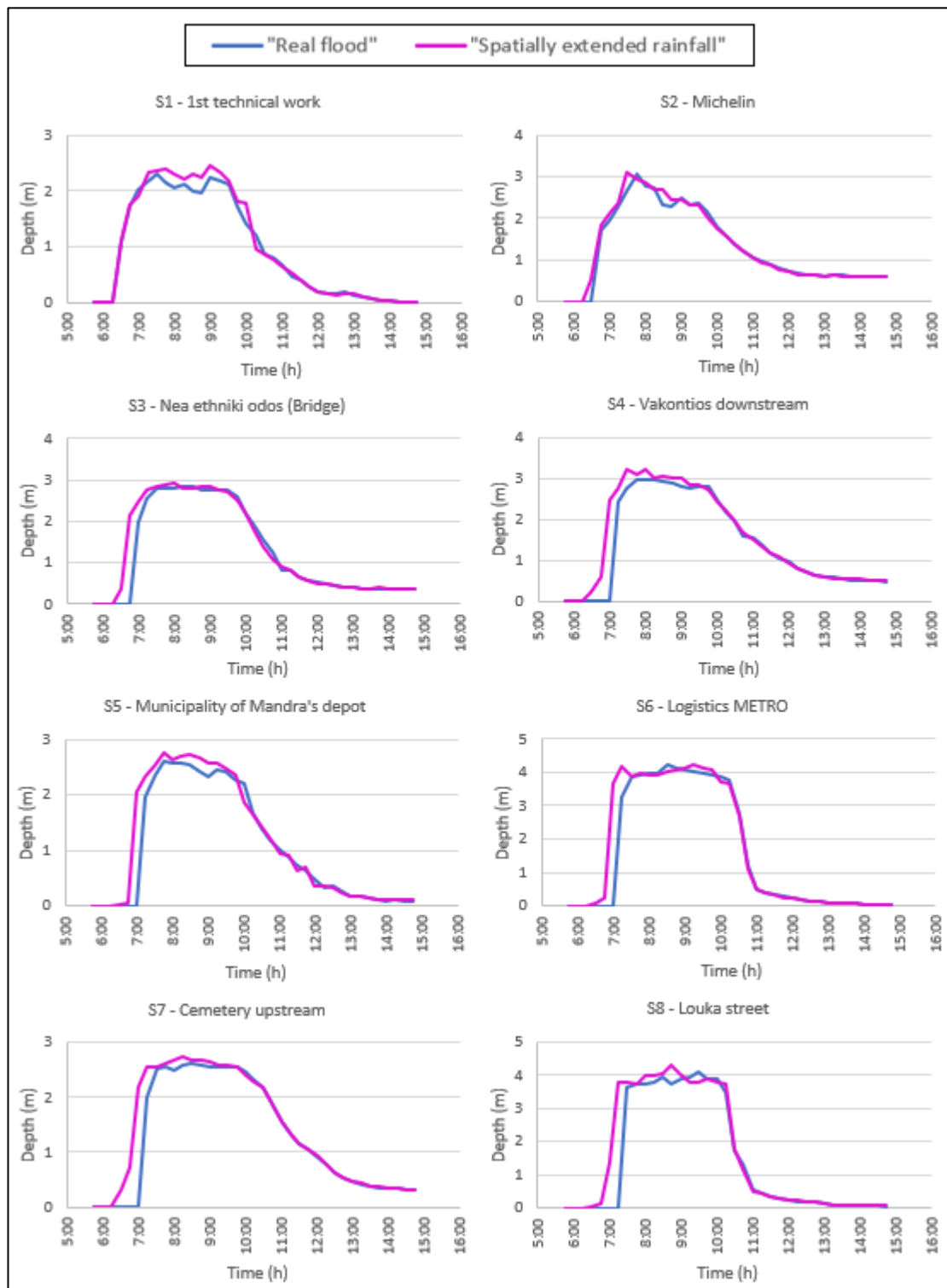


Figure 63 Time change of water depths at the checkpoints of Sores stream upstream of the confluence with Agia Aikaterini stream

The model overestimates the simulated maximum depths of the Scenario "Real flood" at all checkpoints of Sores stream except for S6 from a slight difference of 6 cm at S2 up to a difference of 1.07 m at S11.

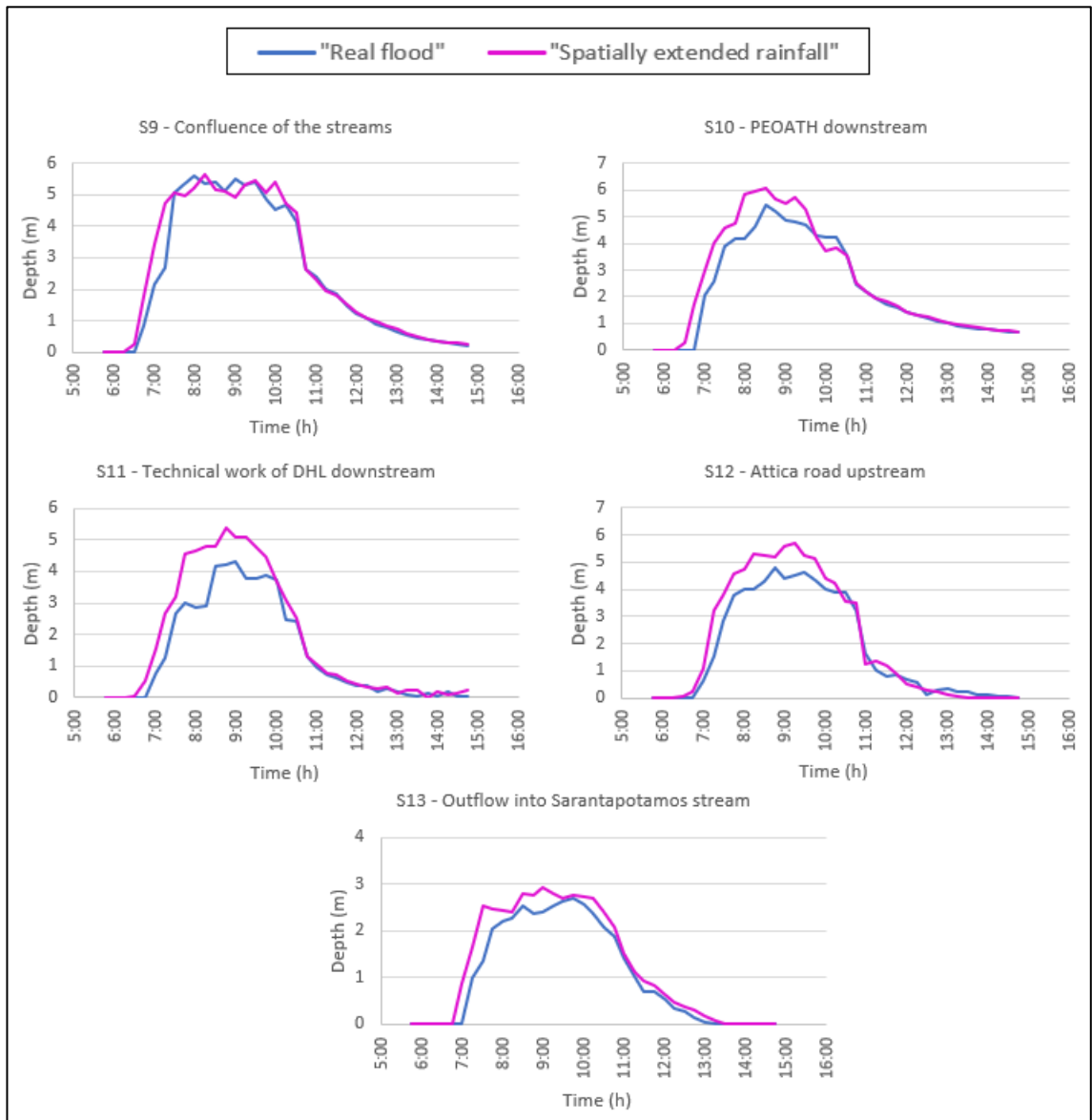


Figure 64 Time change of water depths at the checkpoints of Soures stream downstream of the confluence with Agia Aikaterini stream

A comparison of the maximum water depth at the checkpoints is shown in Figures 65 and 66. The RMSE, NSE, and MAE are 0.403, 0.923 and 0.271, respectively.

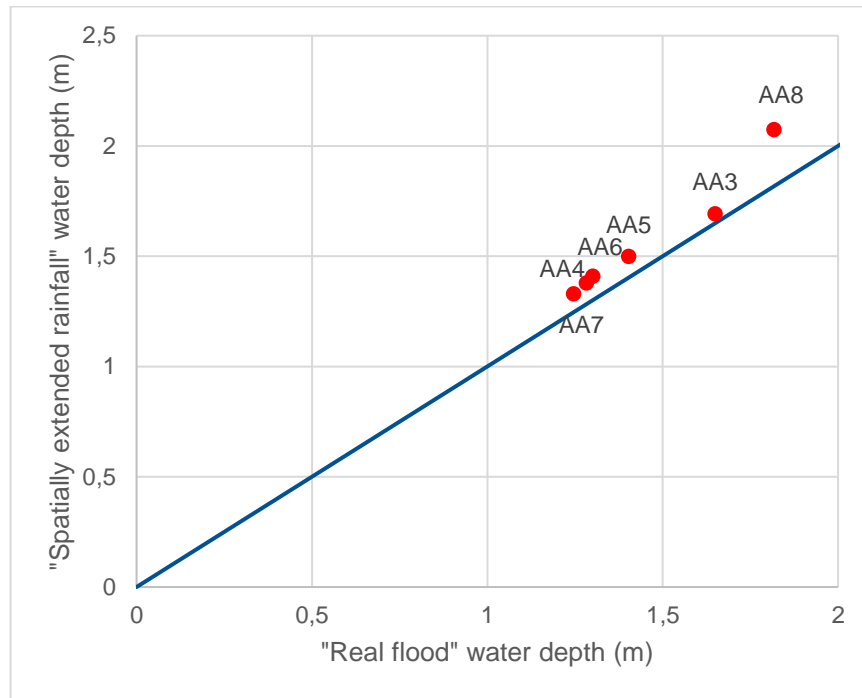


Figure 65 Comparison of maximum water depths for Agia Aikaterini stream (Scenario "Spatially extended rainfall")

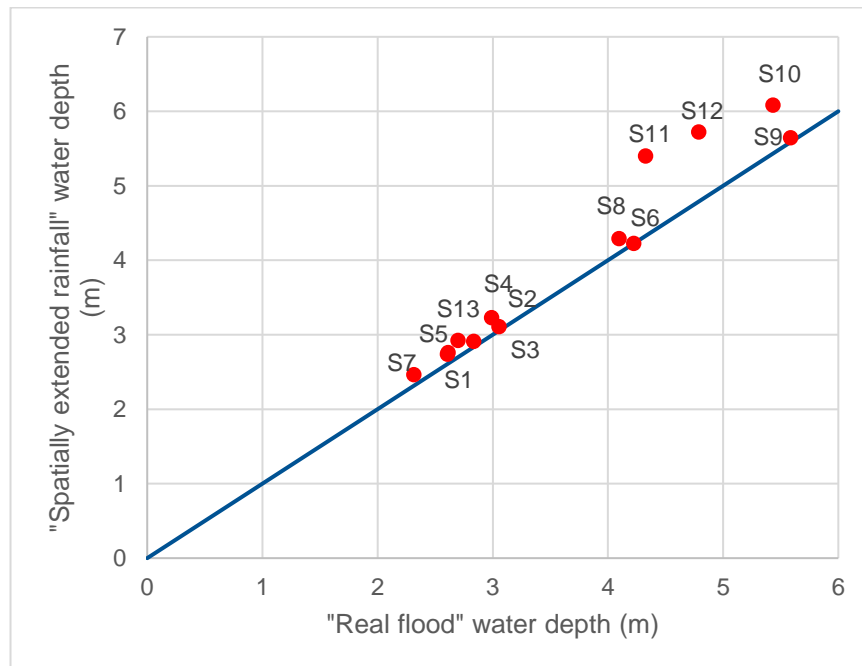


Figure 66 Comparison of maximum water depths for Soures stream (Scenario "Spatially extended rainfall")

5.4.2. Maximum water depths of area

The maximum water depths range from 0.03 m to 7.65 m.

The maximum water depths in the particular areas are shown in Figure 67.

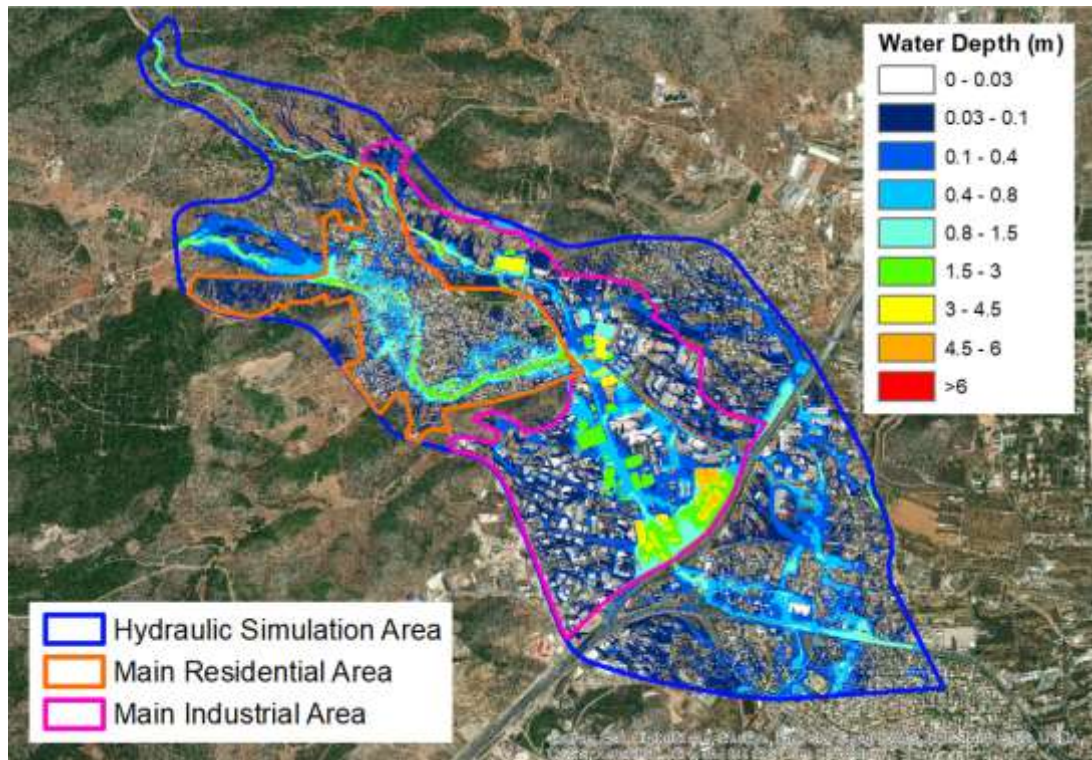


Figure 67 Maximum water depths within the particular areas (Scenario “Spatially extended rainfall”)

Table 25 presents the comparison of average wet maximum water depths for the particular areas between Scenario “Spatially extended rainfall” and Scenario “Real flood”.

Table 25 Comparison of average wet maximum water depths for the particular areas (Scenario “Spatially extended rainfall” vs. Scenario “Real flood”)

Area	Average Wet Maximum Water Depth		Depth Difference (m) (1)-(2)	Depth Percentage (%) $100*(1)/(2)$
	(m)			
	Scenarios			
	“Spatially Extended Rainfall” (1)	“Real Flood” (2)		
Hydraulic Simulation Area	0.501	0.883	-0.382	56.7
Main Residential Area	0.571	0.784	-0.213	72.8

Main Industrial Area	0.728	1.166	-0.437	62.5
-----------------------------	-------	-------	--------	------

The average wet maximum water depth of the hydraulic simulation area is 0.501 m. The average wet maximum water depth of the main residential area is 0.571 m and the average wet maximum water depth of the main industrial area is 0,728 m, respectively. The average wet maximum water depth difference ranges from a difference of -38.2 cm in the hydraulic simulation area and -21.3 cm in the main residential area to a difference of -43.7 cm in the main industrial area with corresponding depth percentages of 56.7%, 72.8% and 62.5%, respectively. The results of the comparison of Table 25 are confirmed in Figure 68.

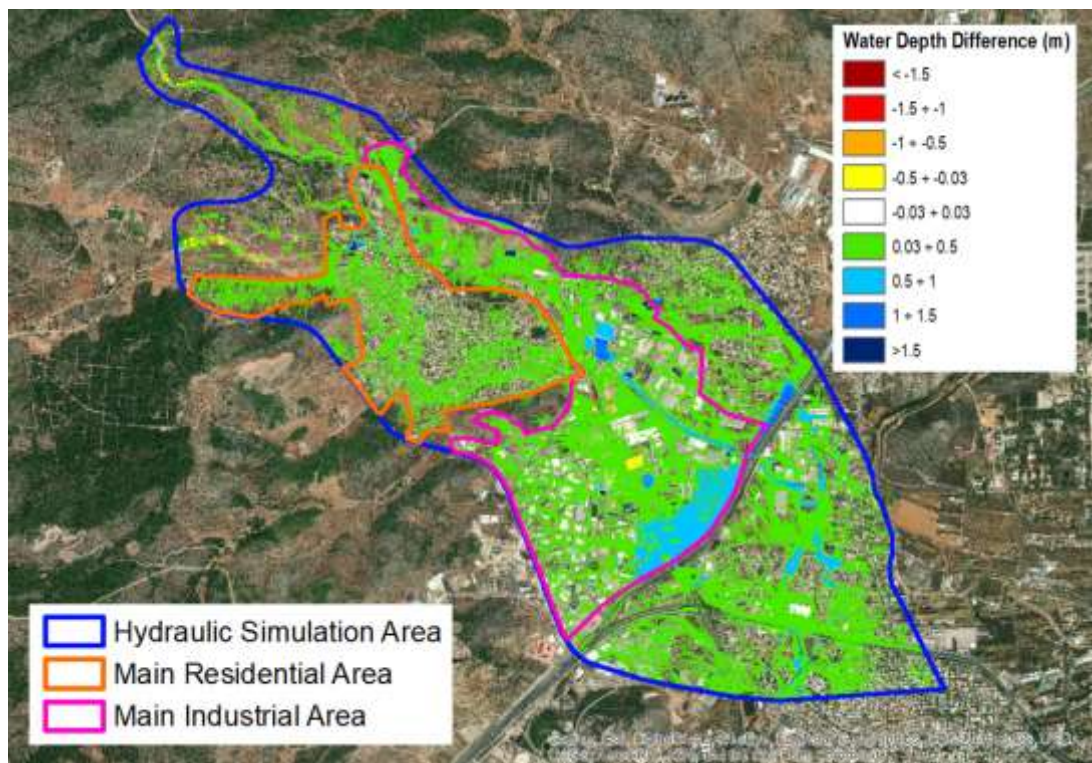


Figure 68 Differences of maximum water depths between Scenario “Spatially extended rainfall” and Scenario “Real flood”

Generally, the water covers the whole area except of some specific parts with high altitude, mainly in the northern part of the hydraulic simulation area out of the main residential area and the main industrial area. The depth difference is usually below 50 cm, but in some basements mainly located besides Attica Road, exceeds 1.0 m. The differences are negative and consecutively the depth percentages are much lower than 100%.

Table 26 presents the comparison of average maximum water depths for the particular areas between Scenario “Spatially extended rainfall” and Scenario “Real flood”.

Table 26 Comparison of average maximum water depths for the particular areas (Scenario “Spatially extended rainfall” vs. Scenario “Real flood”)

Area	Average Maximum Water Depth (m)		Depth Difference (m) (1)-(2)	Depth Percentage (%) $100*(1)/(2)$
	Scenarios			
	“Spatially Extended Rainfall” (1)	“Real Flood” (2)		
	Hydraulic Simulation Area	0.234		
Main Residential Area	0.251	0.201	0.050	124.6
Main Industrial Area	0.443	0.335	0.108	132.2

The average maximum water depth of the hydraulic simulation area is 0.234 m. The average maximum water depth of the main residential area is 0.251 m and the average maximum water depth of the industrial area is 0.443 m, respectively. The average maximum water depth difference ranges from a difference of 7.4 cm in the hydraulic simulation area and 5 cm in the main residential area to a difference of 10.8 cm in the main industrial area with corresponding depth percentages of 146.1%, 124.6% and 132.2%, respectively.

5.4.3. Flood extent and flooding

Figure 69 shows the comparison of the flood extent of Scenario “Spatially extended rainfall” with the real flood extent.

The flood extent covers an area of 9.006 km² much larger than the real flood extent, which covers an area of 2.535 km². This corresponds to a 355.2% of the real flood extent.

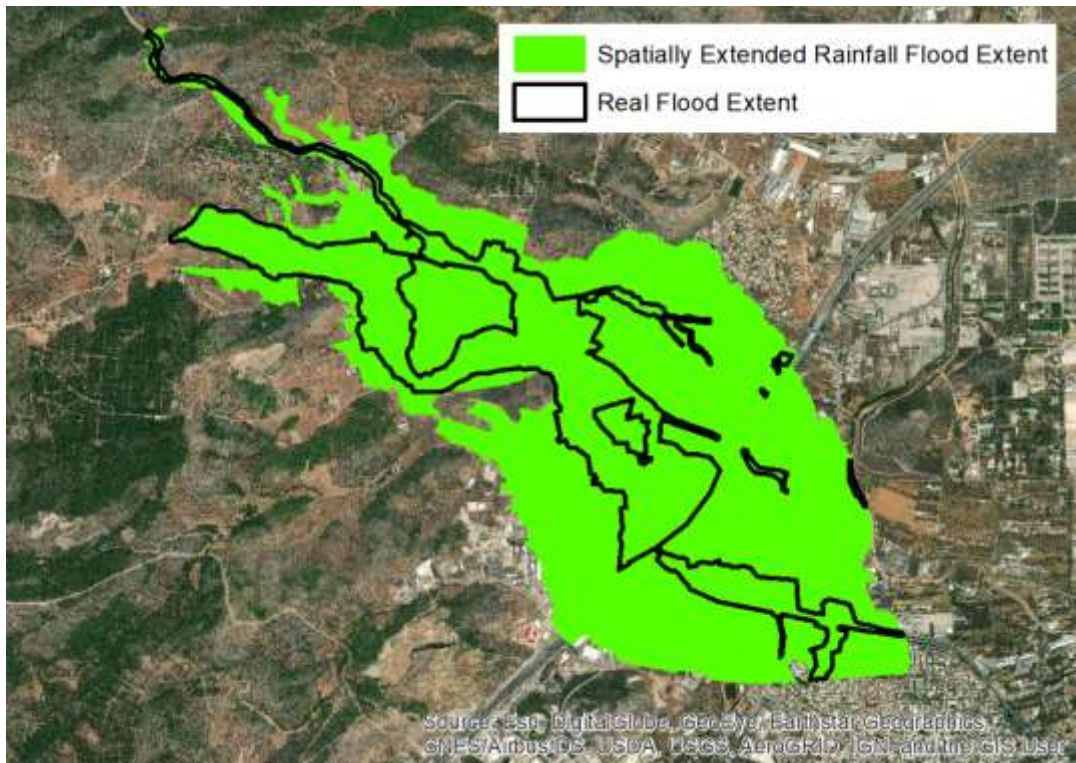


Figure 69 Comparison of the flood extent with the real flood extent (Scenario “Spatially extended rainfall”)

Figure 70 shows the flood extent within the particular areas.

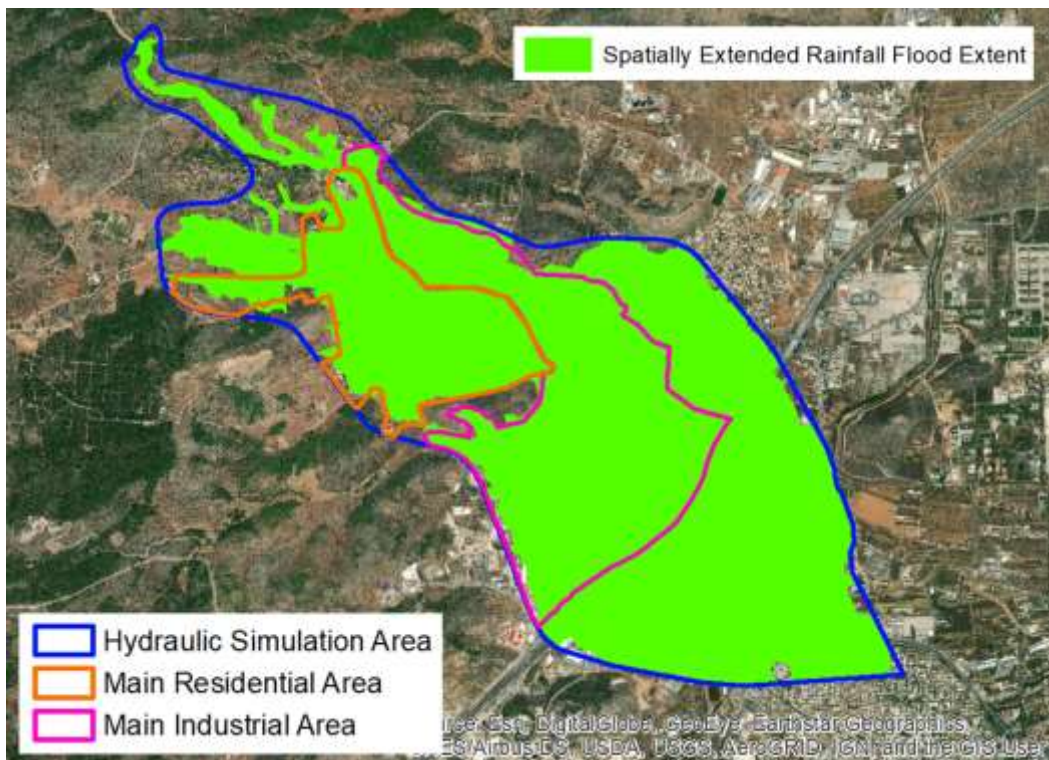


Figure 70 Flood extent within the particular areas (Scenario “Spatially extended rainfall”)

Table 27 presents the comparison of flood extent for the particular areas between Scenario “Spatially extended rainfall” and Scenario “Real flood”.

Table 27 Comparison of flood extent for the particular areas (Scenario “Spatially extended rainfall” vs. Scenario “Real flood”)

Area	Flood Extent Percentage (%)		Difference of Flood Extent Percentages (%)	Percentage of Flood Extents (%)
	Scenarios			
	“Spatially Extended Rainfall” (1)	“Real Flood” (2)	(1)-(2)	100*(1)/(2)
Hydraulic Simulation Area	83.2	23.4	59.8	355.2
Main Residential Area	88.3	41.1	47.2	214.9
Main Industrial Area	96.8	35.5	61.4	273.0

The flood extent covers an area of 9.006 km² as previously mentioned, of the hydraulic simulation area at a percentage of 83.2%. It, also, covers an area of 1.528 km² at a percentage of 88.3% of the main residential area and an area of 3.092 km² at a percentage of 96.8% of the main industrial area. The difference of flood extent percentages ranges from a difference of 59.8% in the hydraulic simulation area and 47.2% in the main residential area to the difference of 61.4% in the main industrial area with corresponding percentage of flood extents of 355.2%, 214.9% and 273.0%, respectively.

Table 28 presents the comparison of flooding for the particular areas between Scenario “Spatially extended rainfall” and Scenario “Real flood”.

Table 28 Comparison of flooding for the particular areas (Scenario “Spatially extended rainfall” vs. Scenario “Real flood”)

Area	Flooding Percentage (%)		Difference of Flooding Percentages	Percentage of Floodings (%)
	Scenarios			
	“Spatially Extended Rainfall” (1)	“Real Flood” (2)	(1)-(2)	100*(1)/(2)

	“Spatially Extended Rainfall” (1)	“Real Flood” (2)	(%) (1)-(2)	100*(1)/(2)
Hydraulic Simulation Area	46.7	18.1	28.6	257.5
Main Residential Area	43.9	25.7	18.2	171.1
Main Industrial Area	60.8	28.7	32.1	211.7

Flooding covers an area of 5.056 km² of the hydraulic simulation area at a percentage of 46.7%. It, also, covers an area of 0.76 km², at a percentage of 43.9%, of the main residential area and an area of 1.880 km², at a percentage of 60.8% of the main industrial area. The difference of flooding percentages ranges from a difference of 28.6% in the hydraulic simulation area and 18.2% in the main residential area to a difference of 32.1% in the main industrial area with corresponding percentage of floodings of 257.5%, 171.1% and 211.7%, respectively.

5.5. Scenario “Diversion and retention pond”

5.5.1. Checkpoints – Maximum water depths and flood progression

Figures 71 and 72 show the maximum water depths of the Scenario “Diversion and retention pond” in the particular areas for a return period of T=50 and T=100 years, respectively. They reveal that there is no overflow at the units of the retention pond and the flow separator only for the return period of T=50 years, therefore the designed diversion works operate proerly.

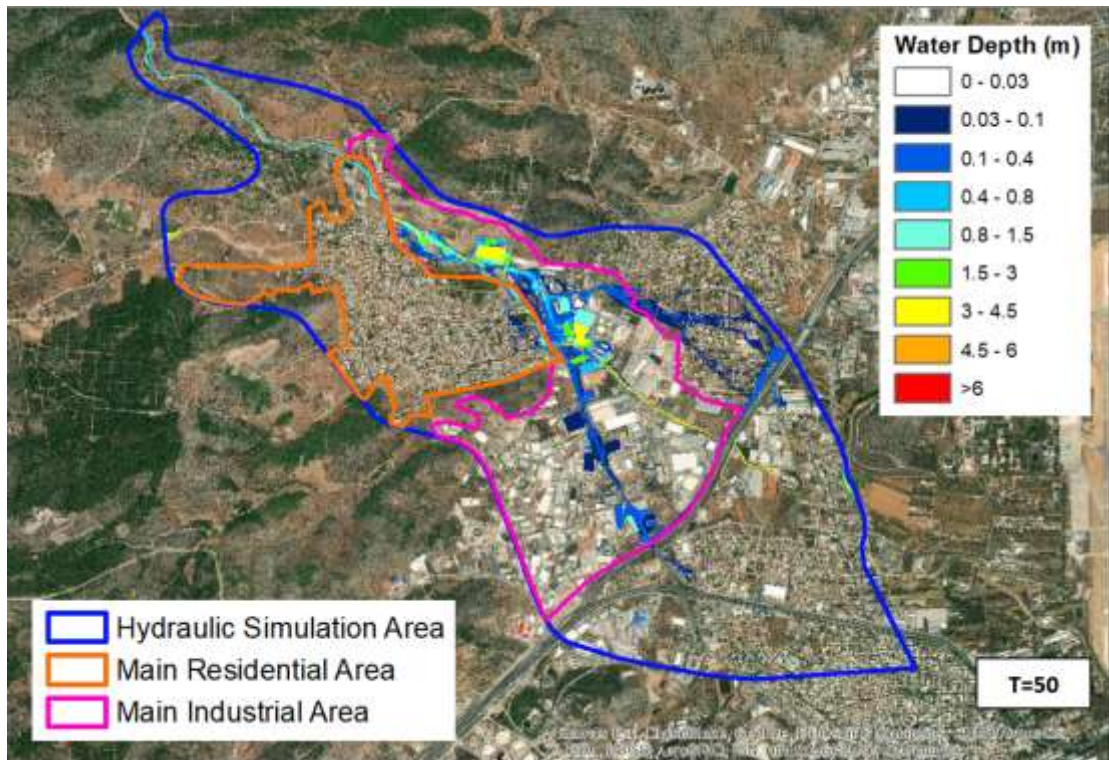


Figure 71 Maximum water depths within the particular areas (Scenario “Diversion and retention pond”)

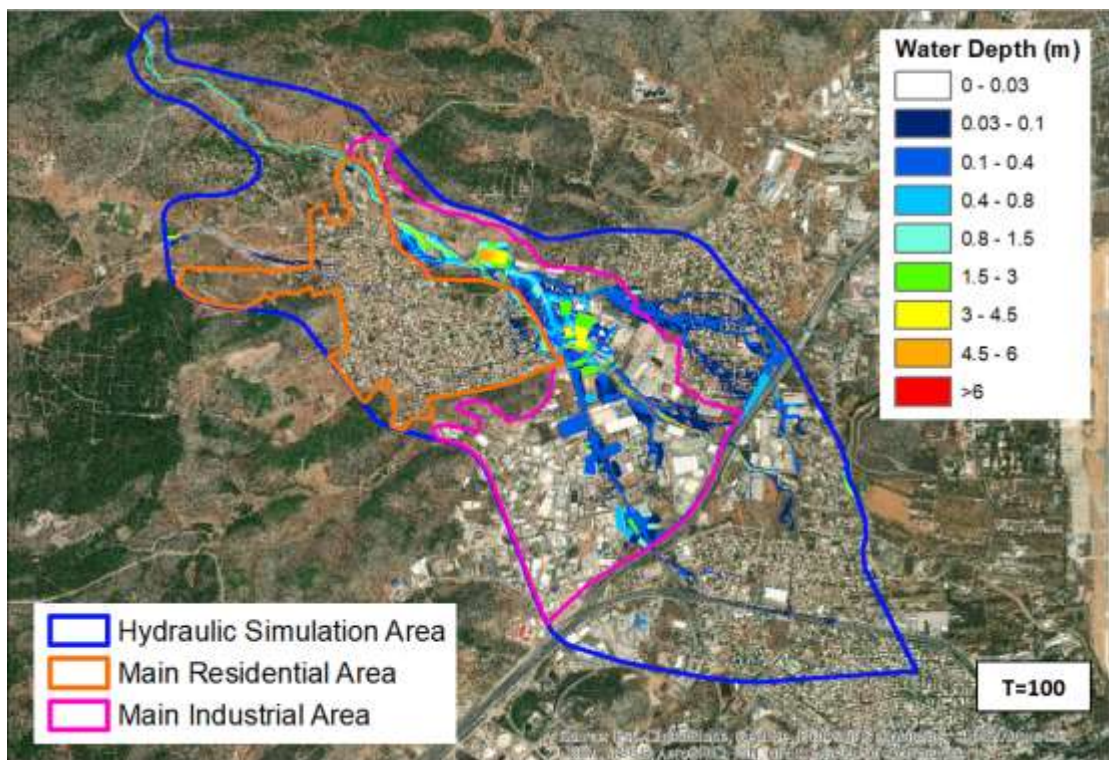


Figure 72 Maximum water depths within the particular areas (Scenario “Diversion and retention pond”)

Figures 73, 74 and 75 give the time evolution of the water depths of the Scenario "Diversion and retention pond" compared to the water depths of the Scenario "Real flood".

As it is shown in Figure 73, the model underestimates the simulated maximum depths of the Scenario "Real flood" at all checkpoints of Agia Aikaterini stream from a difference of 90.4 cm at AA4 up to a difference of 1.82 m at AA8.

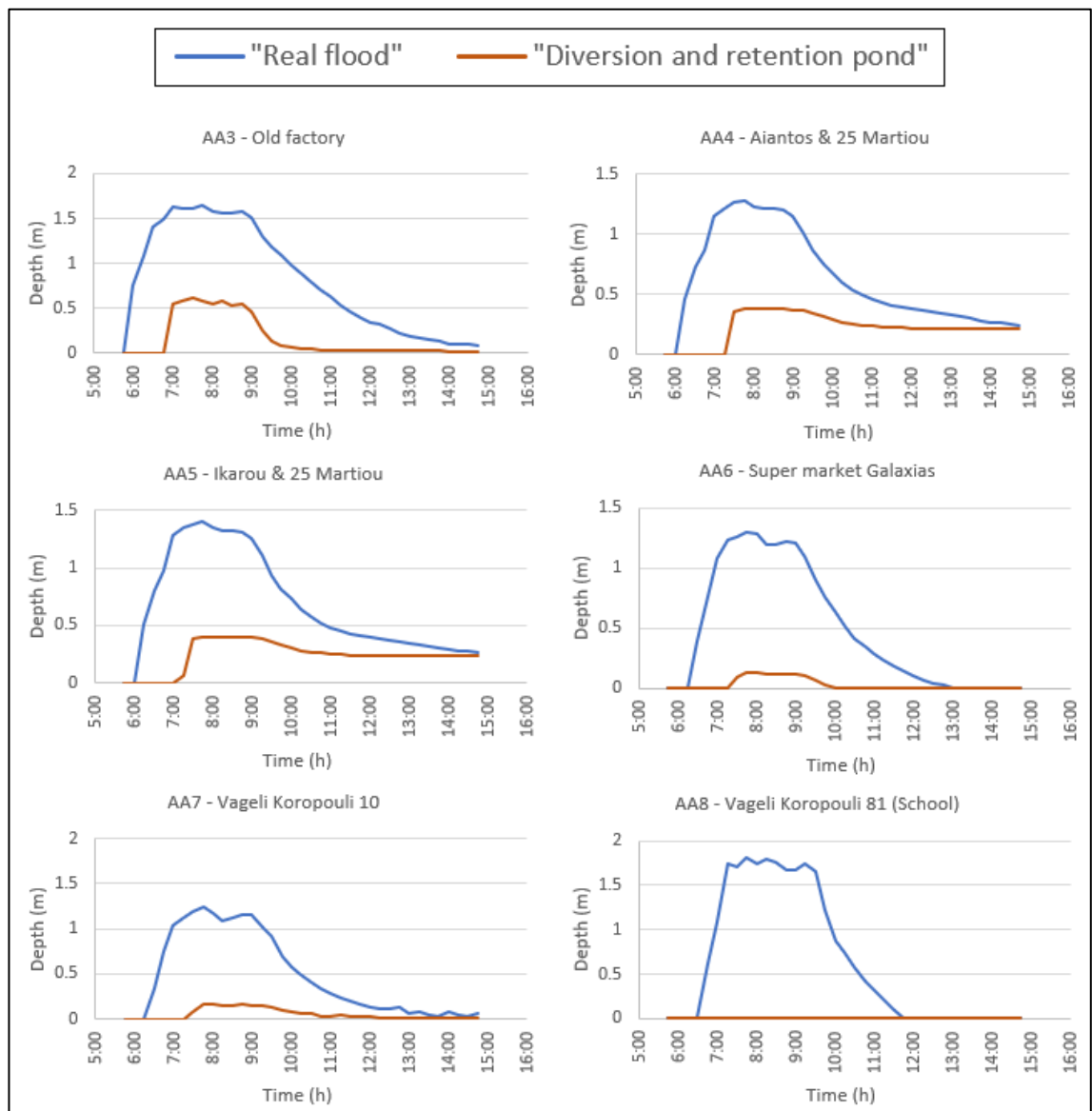


Figure 73 Time change of water depths at the checkpoints of Agia Aikaterini stream

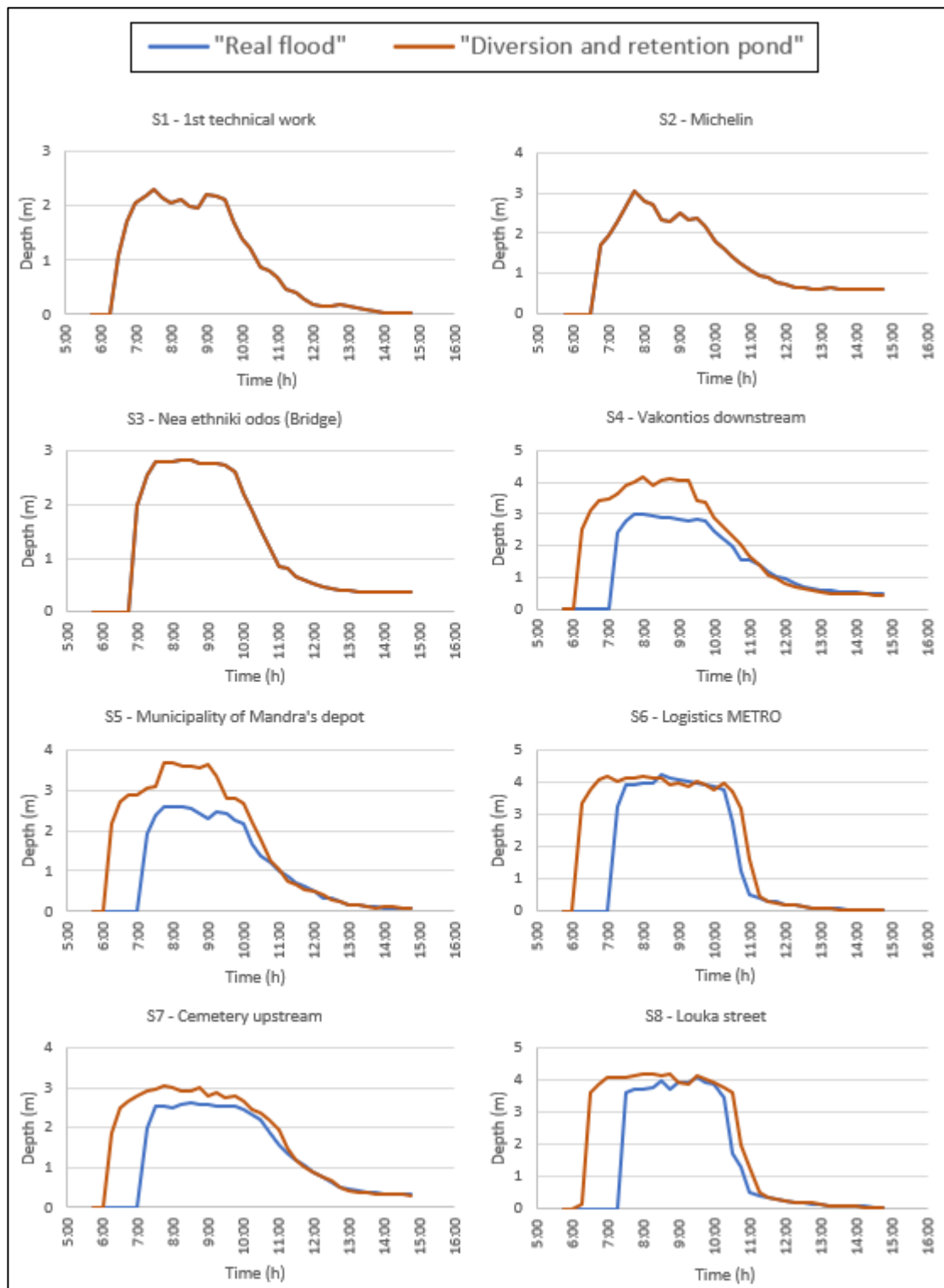


Figure 74 Time change of water depths at the checkpoints of Sores stream upstream of the confluence with Agia Aikaterini stream

All the maximum depths are small and at AA8 is zero. Also, the flood progression at every checkpoint of Agia Aikaterini stream is smaller regarding time and magnitude.

The model overestimates the simulated maximum depths of the Scenario "Real flood" at all checkpoints of Soures stream downstream S3. The range of deviation extends from a slight difference of 4.2 cm at S6 up to a difference of 2.59 m at S11.

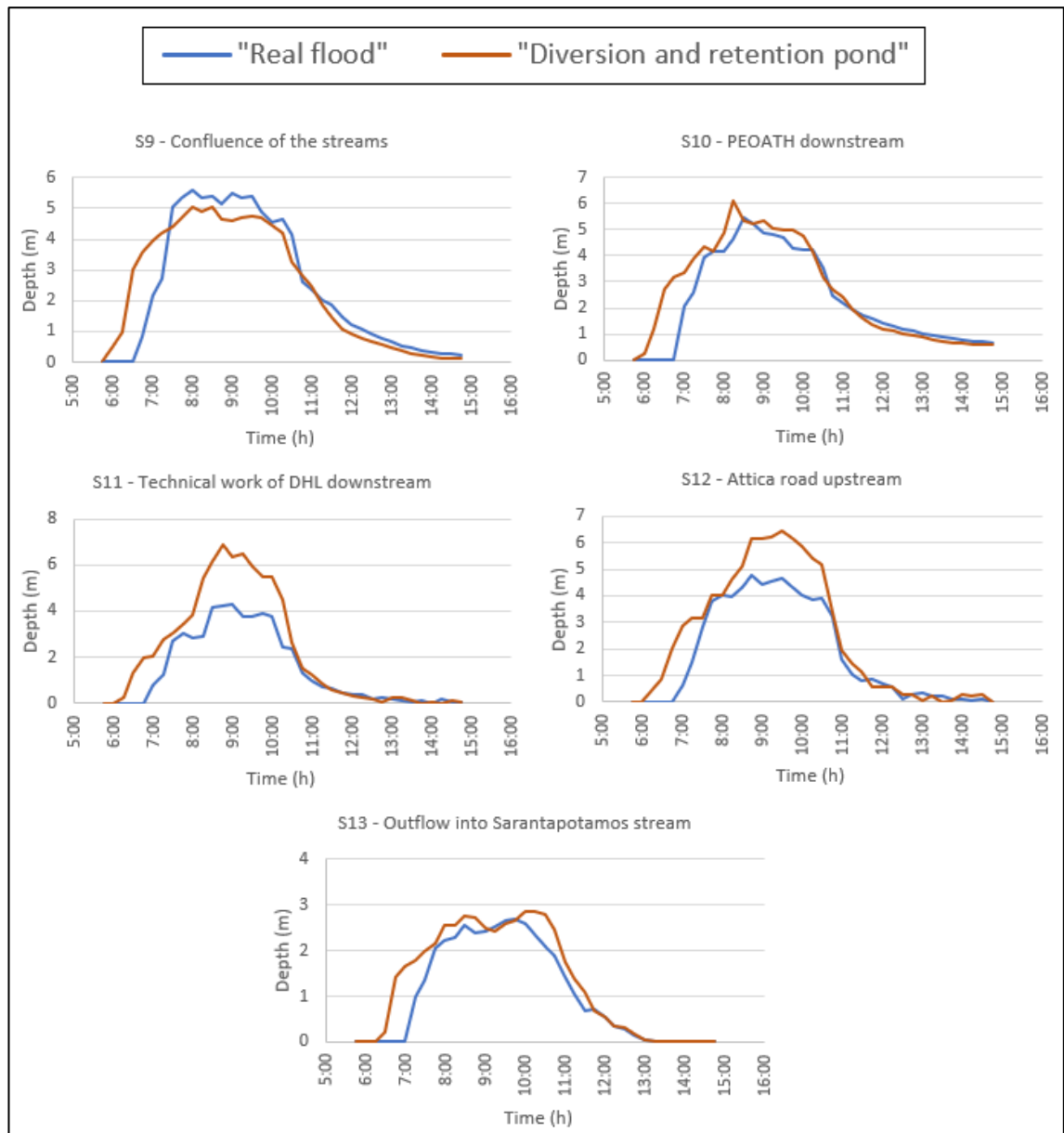


Figure 75 Time change of water depths at the checkpoints of Soures stream downstream of the confluence with Agia Aikaterini stream

Regarding the flood progress, there is an earlier rising of the upward branch downstream S3. Also, the earlier rising of the upward branch is not followed by an earlier lowering of the downward branch.

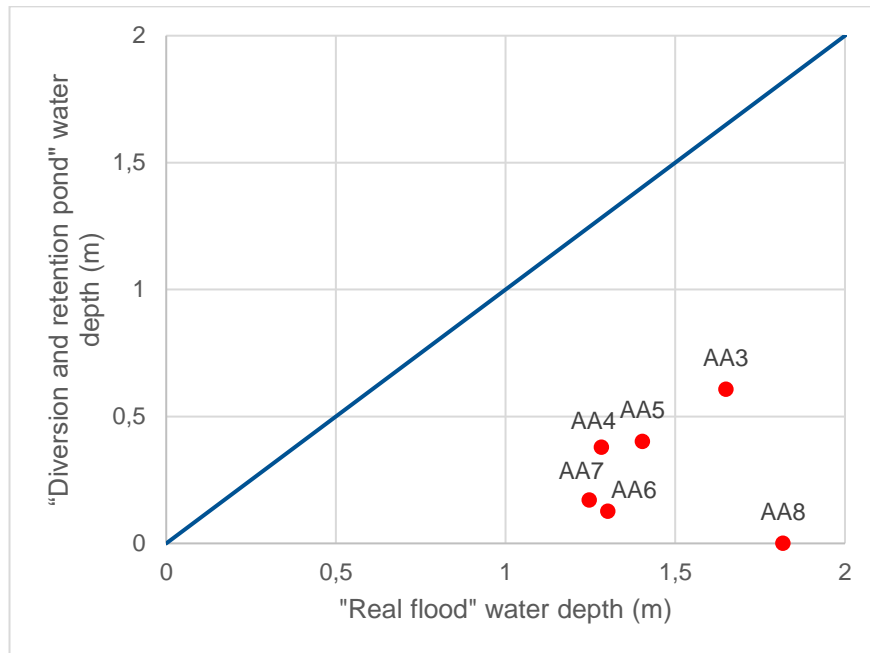


Figure 76 Comparison of maximum water depths for Agia Aikaterini stream (Scenario "Diversion and retention pond")

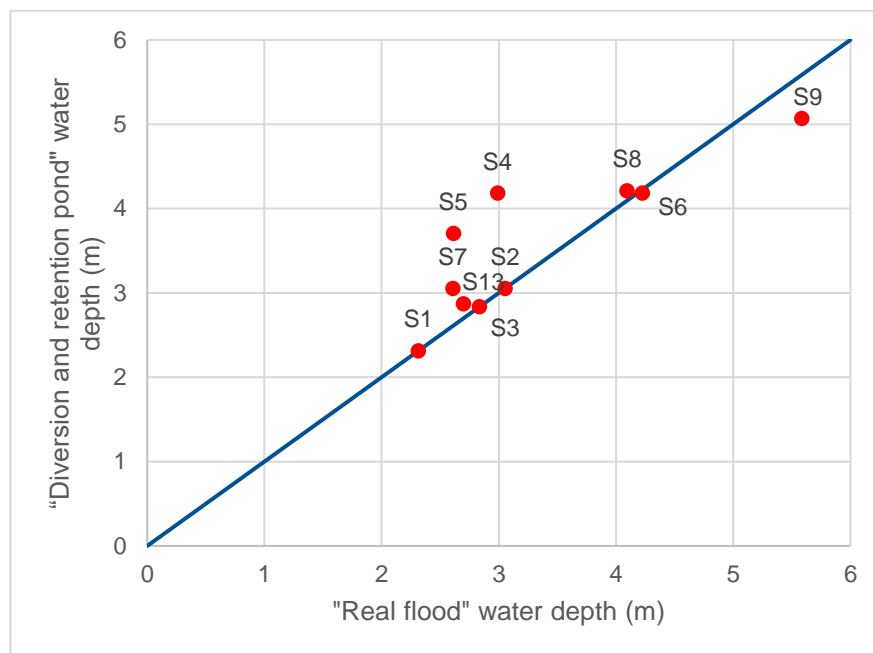


Figure 77 Comparison of maximum water depths for Soures stream (Scenario "Diversion and retention pond")

A comparison of the maximum water depths at the checkpoints is shown in Figures 76 and 77. The RMSE, NSE, and MAE are 1.131, 0.393 and 0.912, respectively.

5.5.2. Maximum water depths of area

The maximum water depths in the particular areas are shown in Figure 78.

The maximum water depths range from 0.03 m to 8.81 m.

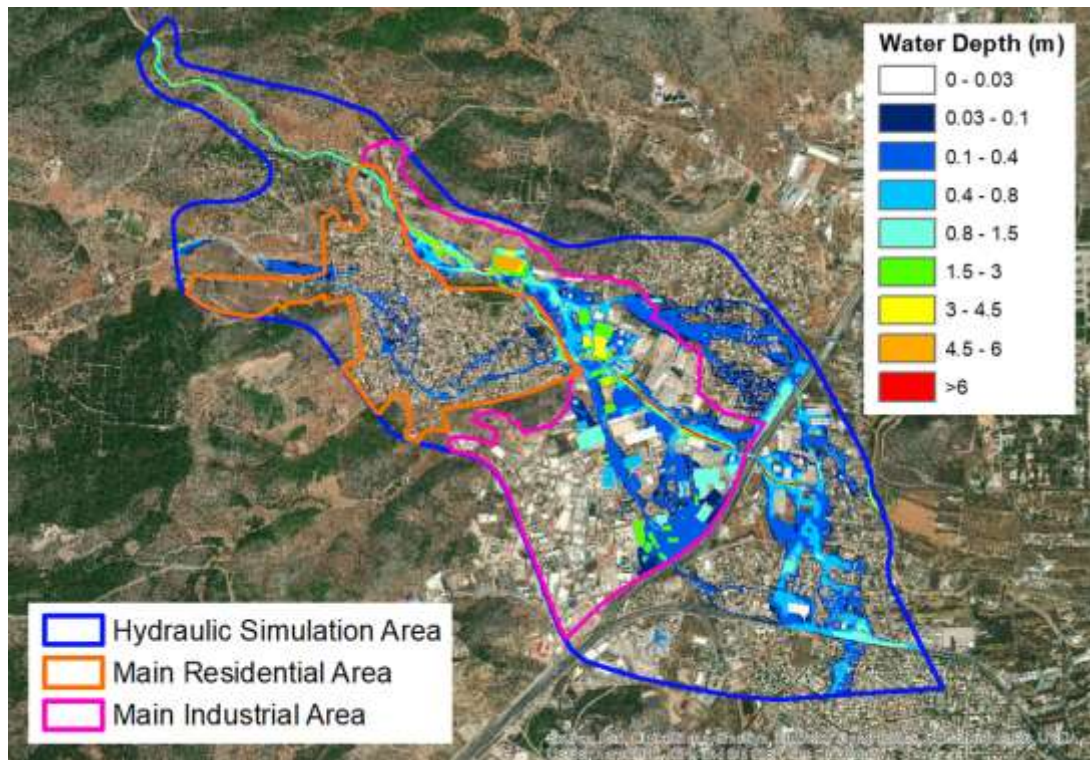


Figure 78 Maximum water depths within the particular areas (Scenario “Diversion and retention pond”)

Table 29 presents the comparison of average wet maximum water depths for the particular areas between Scenario “Diversion and retention pond” and Scenario “Real flood”.

Table 29 Comparison of average wet maximum water depths for the particular areas (Scenario “Diversion and retention pond” vs. Scenario “Real flood”)

Area	Average Wet Maximum Water Depth (m)		Depth Difference (m) (1)-(2)	Depth Percentage (%) 100*(1)/(2)
	Scenarios			
	“Diversion and Retention Pond”	“Real Flood”		
	(1)	(2)		
Hydraulic Simulation Area	0.617	0.883	-0.266	69.9
Main Residential Area	0.410	0,784	-0.374	52.3

Main Industrial Area	0.842	1.166	-0.323	72.3
-----------------------------	-------	-------	--------	------

The average wet maximum water depth of the hydraulic simulation area is 0.617 m. The average wet maximum water depth of the main residential area is 0.410 m and the average wet maximum water depth of the main industrial area is 0.842 m, respectively. The average wet maximum water depth difference ranges from a difference of -26.6 cm in the hydraulic simulation area and -37.4 cm in the main residential area to a difference of -32.3 cm in the main industrial area with corresponding depth percentages of 69.9%, 52.3% and 72.3%, respectively. The results of the comparison of Table 29 are confirmed in Figure 79.

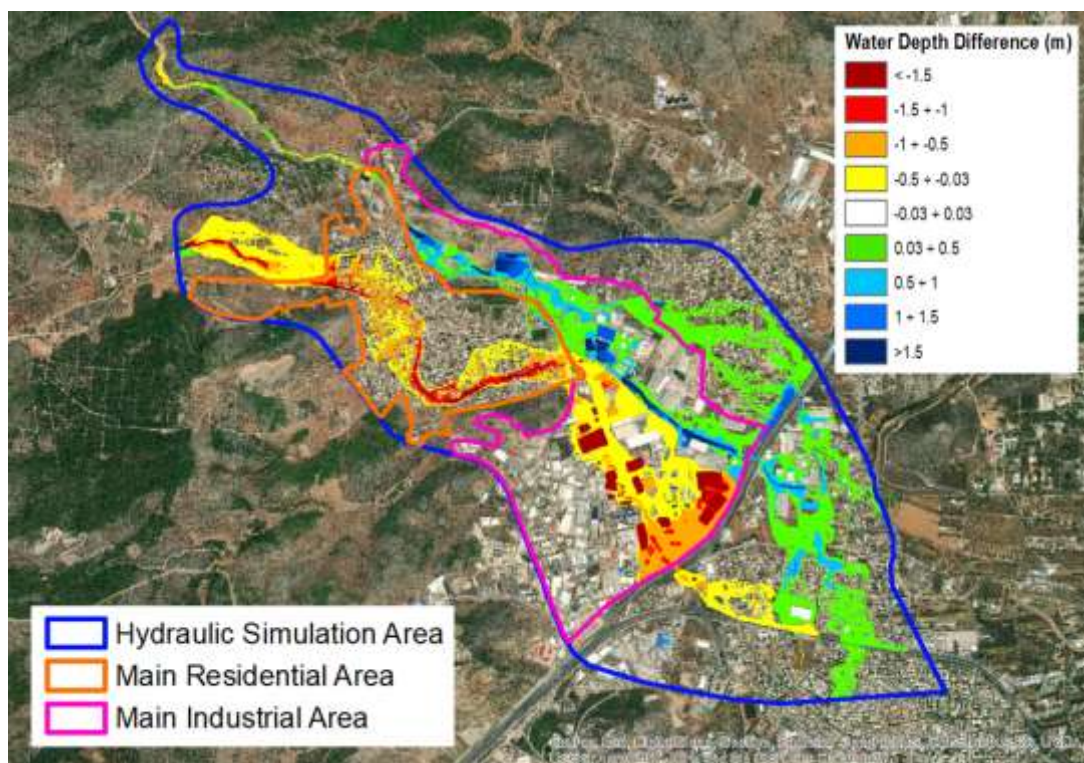


Figure 79 Differences of maximum water depths between Scenario “Diversion and retention pond” and Scenario “Real flood”

The main residential area has significantly lower depths and the water differences exceed -1.5 m along the relatively low altitudes along the path of the Vageli Korropouli closed conduit and the same happens with the part of the main industrial area to the south of the PEOATH bridge. On the contrary, the water differences exceed 1.5 m in the Logistics METRO area. A significant part of the hydraulic simulation area is inundated to the east with water differences mostly lower than 0.5 m but there are still locations like the area east of the Logistics METRO, where they are upper than 0.5 m and even upper

than 1.0 m besides the Attica Road, where the water ponds. Soures stream inundates a relatively large area after underpassing Attica Road with water differences mostly lower than 0.5 m. Also, there are lower water depths in the part of the main industrial area that is south of the PEOATH bridge. The water depths are mostly lower than 0.4 m.

In the main industrial area, the depth differences range from less than -1.50 m inside the protected properties to greater than 1.50 m in the low areas besides Attica Road (see Figure 79).

Table 30 presents the comparison of average maximum water depths for the particular areas between Scenario “Diversion and retention pond” and Scenario “Real flood”. The results of the comparison confirm the previous results.

Table 30 Comparison of average maximum water depths for the particular areas (Scenario “Diversion and retention pond” vs. Scenario “Real flood”)

Area	Average Maximum Water Depth		Depth Difference (m) (1)-(2)	Depth Percentage (%) (1)/(2)
	(m)			
	Scenarios			
	“Diversion and Retention Pond” (1)	“Real Flood” (2)		
Hydraulic Simulation Area	0.133	0.160	-0.027	83.2
Main Residential Area	0.050	0.201	-0.152	24.7
Main Industrial Area	0.300	0.335	-0.038	88.7

5.5.3. Flood extent and flooding

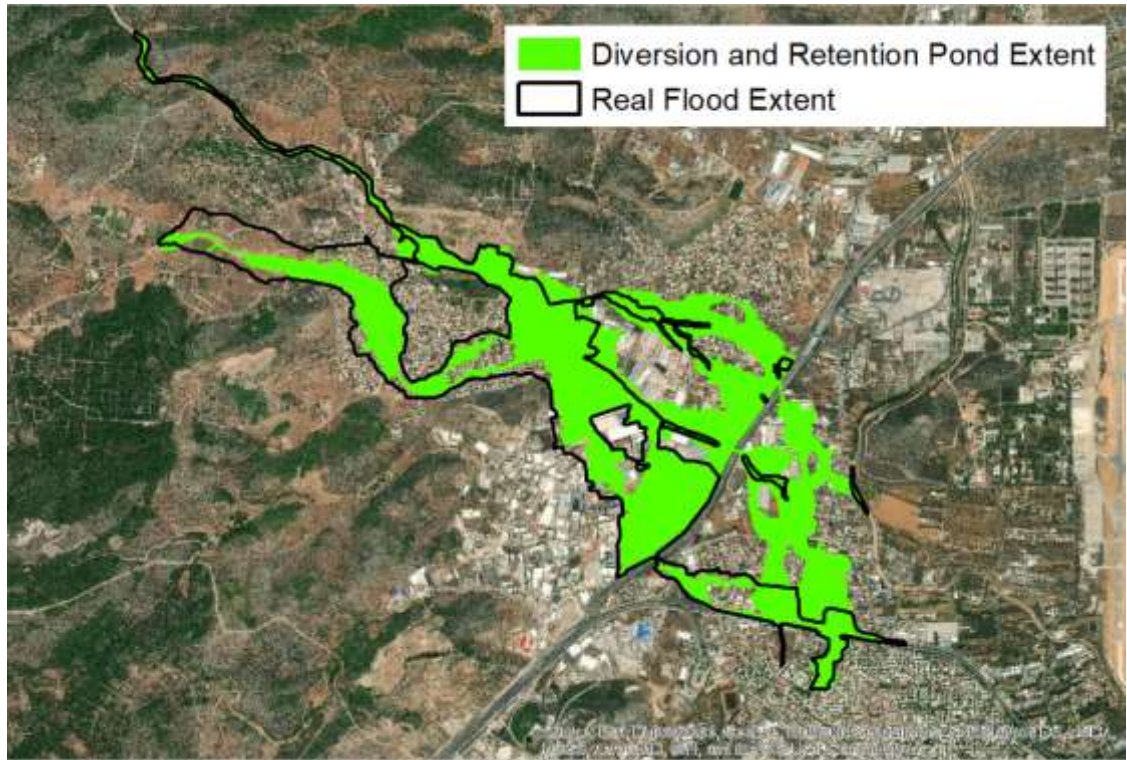


Figure 80 Comparison of the flood extent with the real flood extent (Scenario “Diversion and retention pond”)

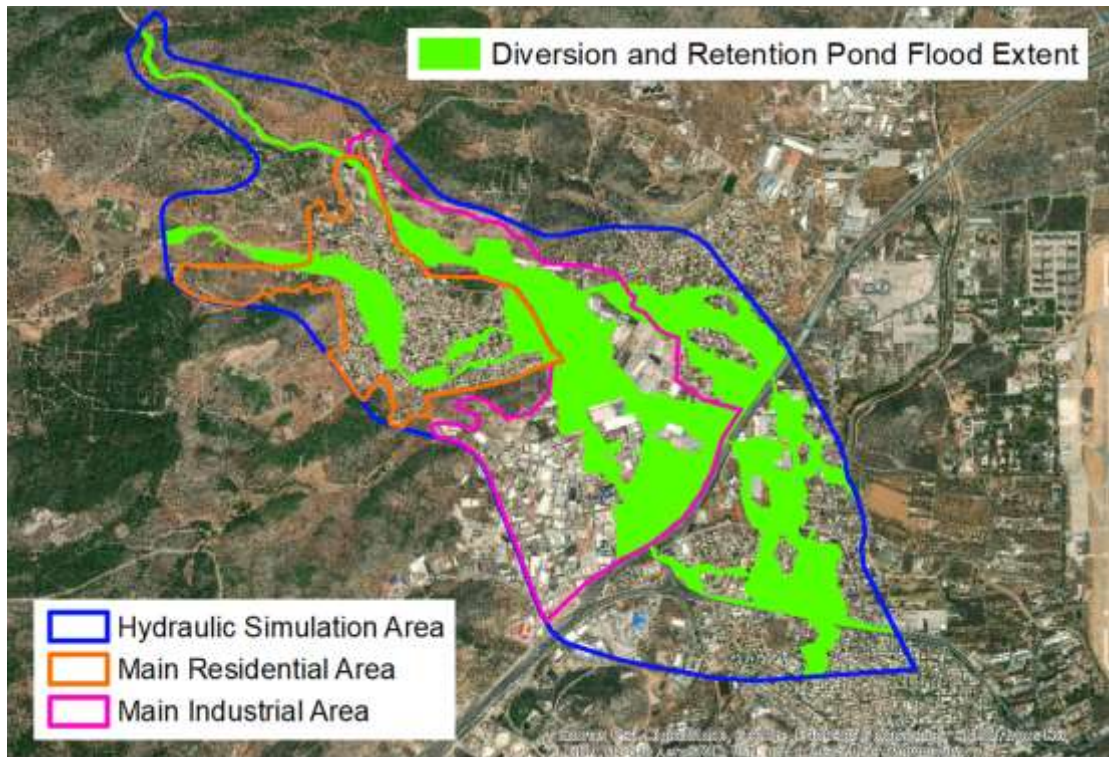


Figure 81 Flood extent within the particular areas (Scenario “Diversion and retention pond”)

Figure 80 shows the comparison of the flood extent of Scenario “Diversion and retention pond” with the real flood extent. The flood extent covers an area of 3.105 km² much larger than the real flood extent, which covers an area of 2.535 km². This corresponds to a percentage 122.5% of the real flood extent.

Figure 81 shows the flood extent within the particular areas.

Table 31 presents the comparison of flood extent for the particular areas between Scenario “Diversion and retention pond” and Scenario “Real flood”.

Table 31 Comparison of flood extent for the particular areas (Scenario “Diversion and retention pond” vs. Scenario “Real flood”)

Area	Flood Extent Percentage (%)		Difference of Flood Extent Percentages (%) (1)-(2)	Percentage of Flood Extents (%) 100*(1)/(2)
	Scenarios			
	“Diversion and Retention Pond”	“Real Flood”		
	(1)	(2)		
Hydraulic Simulation Area	28.7	23.4	5.3	122.5
Main Residential Area	23.8	41.1	-17.3	57.8
Main Industrial Area	42.6	35.5	7.2	120.2

The flood extent covers an area of 3.105 km² as previously mentioned, of the hydraulic simulation area at a percentage of 28.7%. It, also, covers an area of 0.411 km² at a percentage of 23.8% of the main residential area and an area of 1.318 km² at a percentage of 42.6% of the main industrial area. The difference of flood extent percentages ranges from differences of -5.3% in the hydraulic simulation area and -17.3% in the main residential area to the difference of 7.2% in the main industrial area with corresponding percentage of flood extents of 122.5%, 57.8% and 120.2%, respectively.

Table 32 presents the comparison of flooding for the particular areas between Scenario “Diversion and retention pond” and Scenario “Real flood”. The results of the comparison confirm the previous results.

Table 32 Comparison of flooding for the particular areas (Scenario “Diversion and retention pond” vs. Scenario “Real flood”)

Area	Flooding Percentage (%)		Difference of Flooding Percentages (%)	Percentage of Floodings (%)
	Scenarios			
	“Diversion and Retention Pond”	“Real Flood”	(1)-(2)	100*(1)/(2)
	(1)	(2)		
Hydraulic Simulation Area	21.6	18.1	3.5	119.0
Main Residential Area	12.1	25.7	-13.6	47.1
Main Industrial Area	35.3	28.7	6.5	122.7

A summary of all the derived differences between maximum water depths of the different scenarios and the Scenario “Real flood” at the checkpoints is displayed in Table 33.

Table 33 Height difference (m) between the maximum water depths of the different scenarios and the Scenario “Real flood” at the checkpoints

	Fully Operated Conduits	Fences	Spatially Extended Rainfall	Diversion and Retention Pond
AA3	0	0	0.043	-1.042
AA4	-0.047	0	0.096	-0.904
AA5	-0.046	0	0.096	-1.002
AA6	-0.069	0	0.108	-1.175
AA7	-0.086	0	0.083	-1.075
AA8	-0.068	0	0.257	-1.817
S1	0.366	0	0.15	0
S2	-0.378	0	0.051	0
S3	0.036	0.106	0.075	0
S4	0.486	0.06	0.236	1.192

S5	0.071	0.041	0.145	1.095
S6	0.023	0.508	0	-0.042
S7	-0.013	0.596	0.13	0.444
S8	-0.035	0.183	0.195	0.117
S9	-0.333	0.229	0.06	-0.517
S10	0.495	0.762	0.646	0.681
S11	0.961	1.16	1.072	2.585
S12	0.546	1.211	0.932	1.648
S13	0.057	0.056	0.224	0.173

Table 34 shows a summary of the goodness of fit criteria of all scenarios.

Table 34 Goodness of fit criteria

	Fully Operated Conduits	Fences	Spatially Extended Rainfall	Diversion and Retention Pond
RMSE	0.353	0.492	0.403	1.131
NSE	0.941	0.885	0.923	0.393
MAE	0.242	0.289	0.271	0.912

Figures 82 and 83 show the average wet maximum water depth and the average maximum water depth of the different Scenarios for the particular areas, respectively.

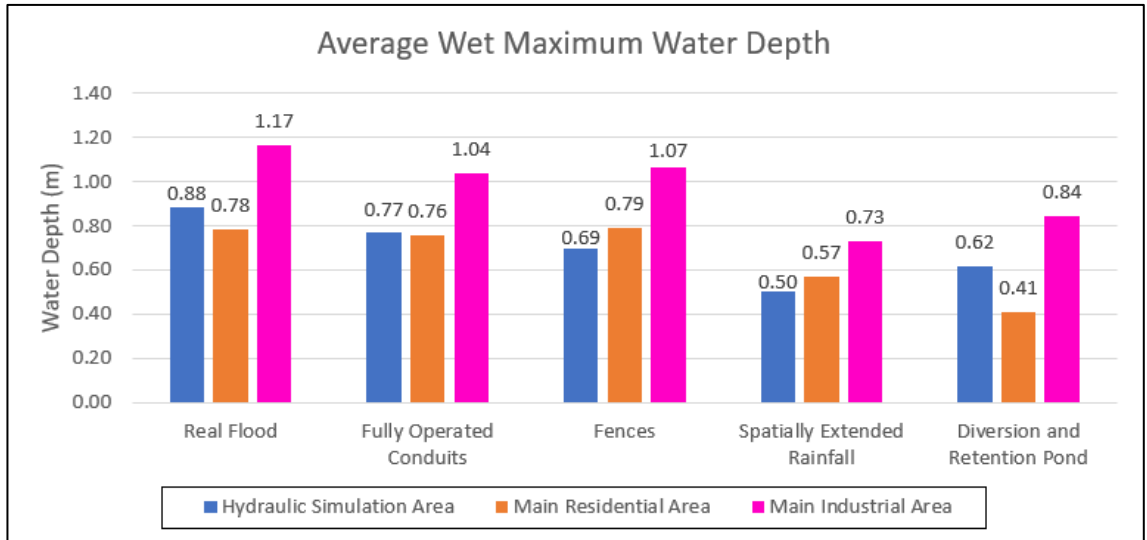


Figure 82 Average wet maximum water depth of the different Scenarios for the particular areas

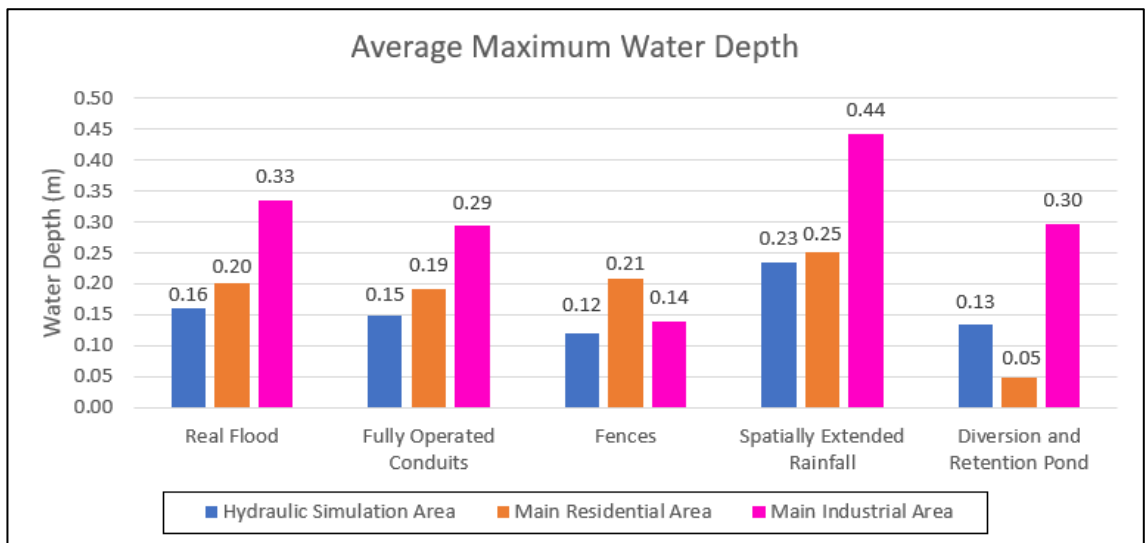


Figure 83 Average maximum water depth of the different Scenarios for the particular areas

Figures 84 and 85 show the average wet maximum water depth percentage and the average maximum water depth percentage of the different Scenarios for the particular areas, respectively.

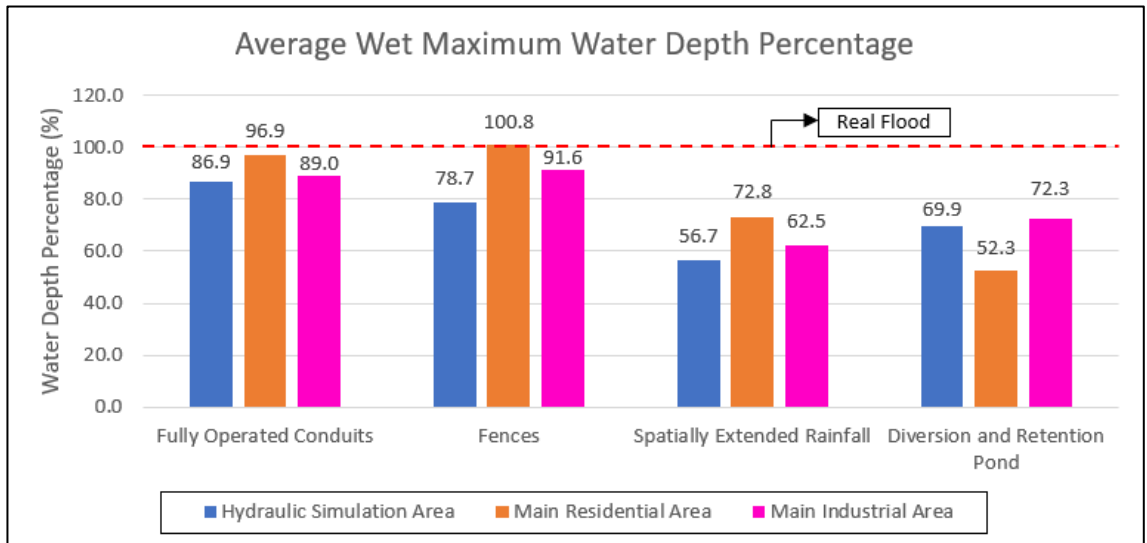


Figure 84 Average wet maximum water depth percentage of the different Scenarios for the particular areas

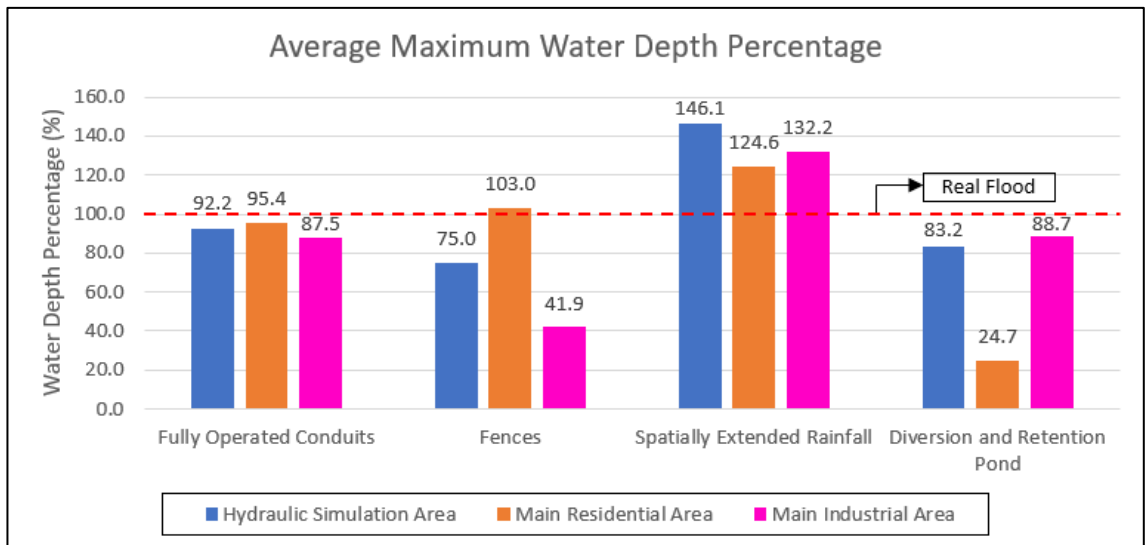


Figure 85 Average maximum water depth percentage of the different Scenarios for the particular areas

Figures 86 and 87 show the flood extent and the flood extents percentage of the different Scenarios for the particular areas, respectively.

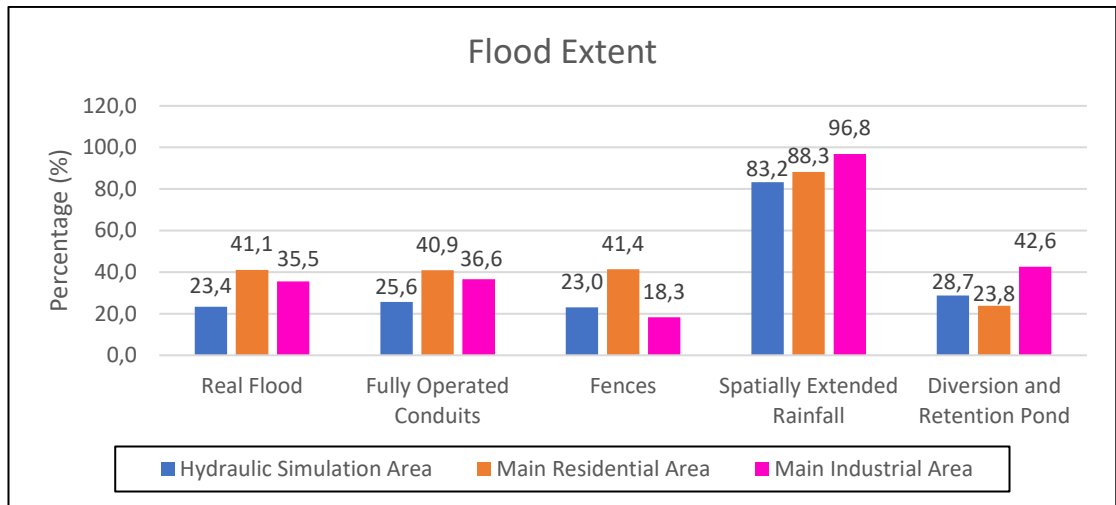


Figure 86 Flood extent of the different Scenarios for the particular areas

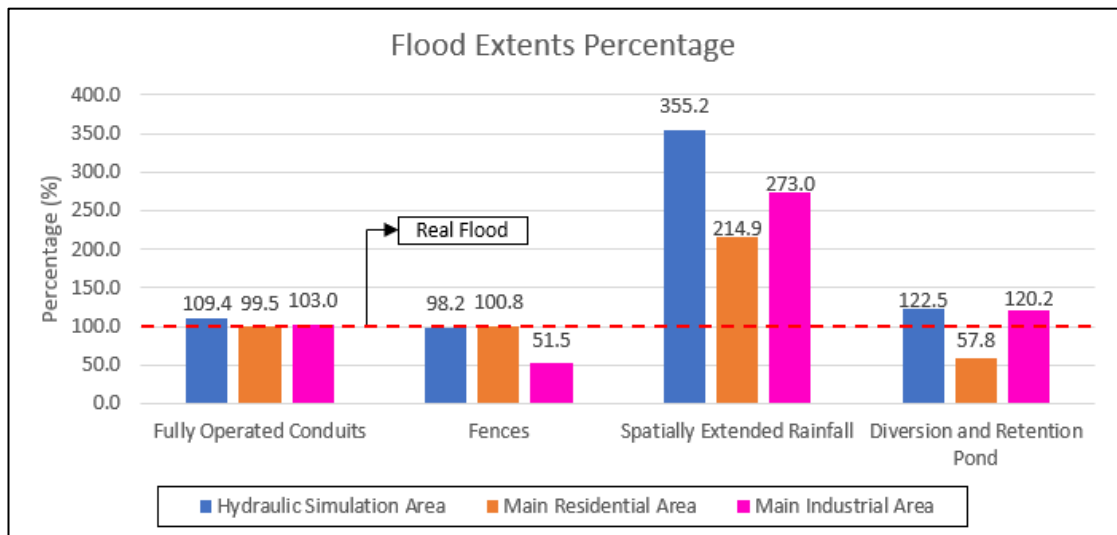


Figure 87 Flood extents percentage of the different Scenarios for the particular areas

Figures 88 and 89 show the flooding and the floodings percentage of the different Scenarios for the particular areas, respectively.

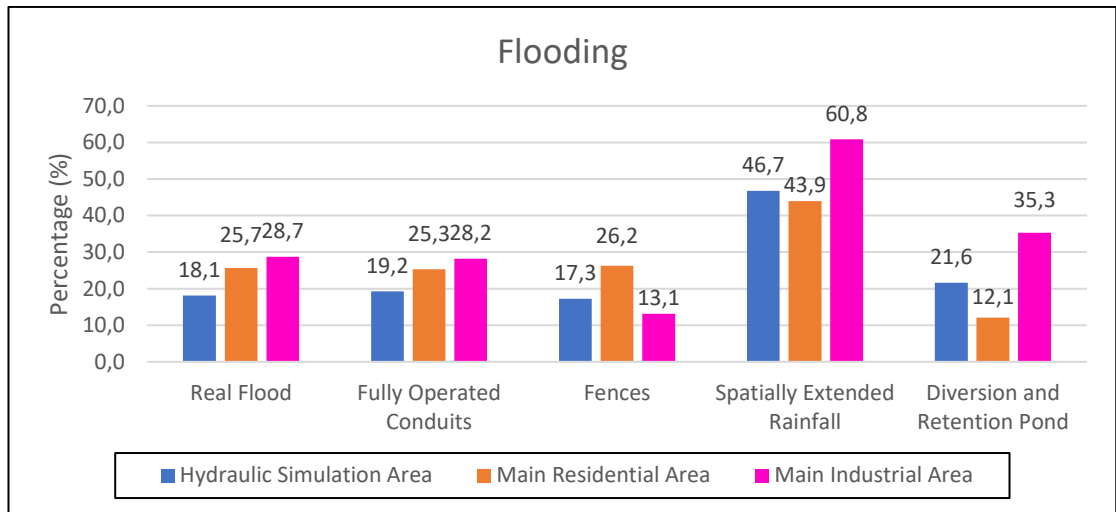


Figure 88 Flooding of the different Scenarios for the particular areas

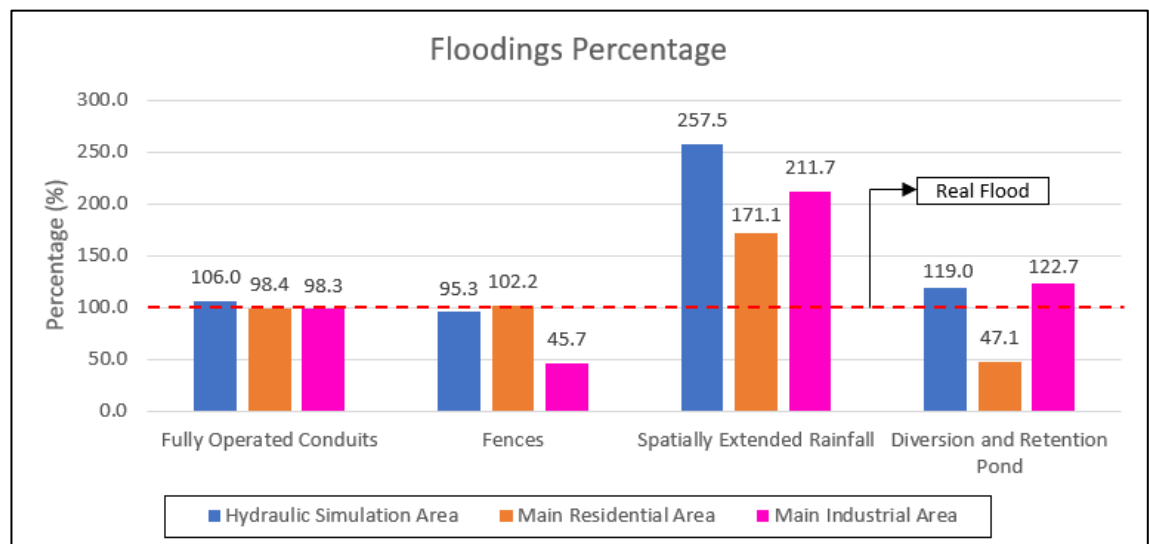


Figure 89 Floodings percentage of the different Scenarios for the particular areas

5.6. Influence of the return period – Scenario “Real flood”

5.6.1. Checkpoints – Maximum water depths

Figures 90, 91 and 92 give the time evolution of the water depths for floods having a return period of T=20, 50, 100 and 1000 years compared to the water depths of the Scenario “Real flood” for all the checkpoints.

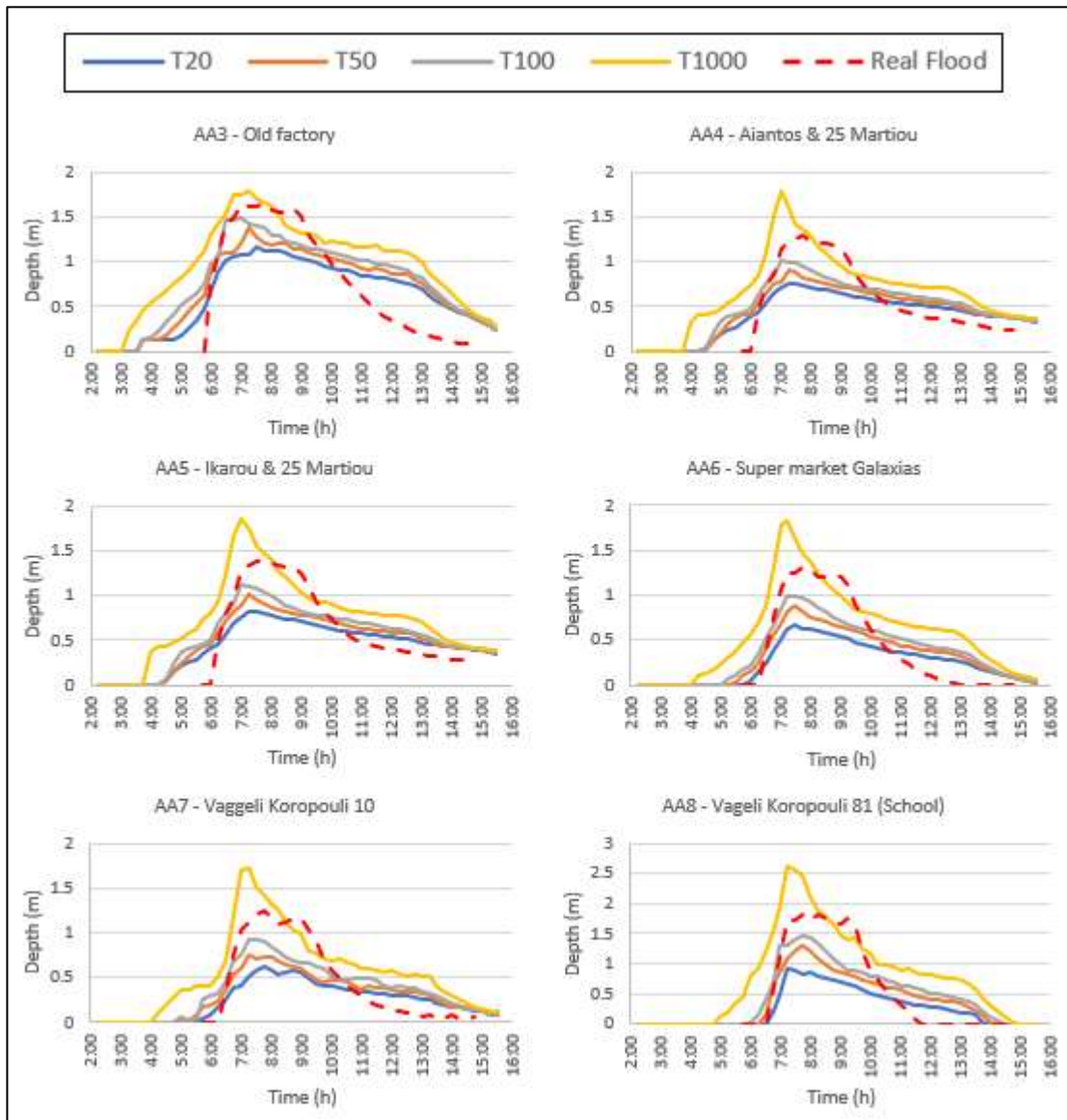


Figure 90 Time change of water depths at the checkpoints of Agia Aikaterini stream

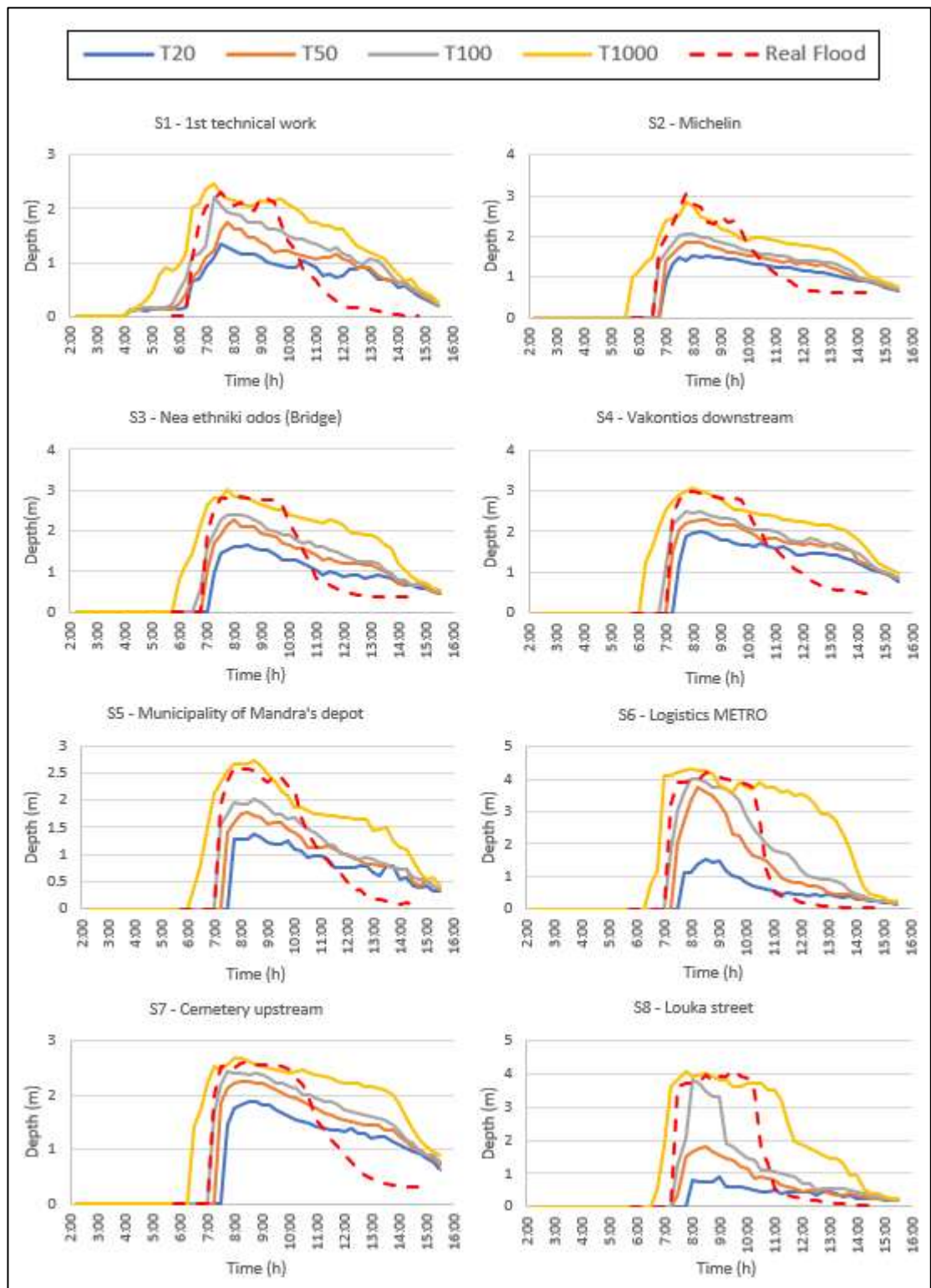


Figure 91 Time change of water depths at the checkpoints of Sores stream upstream of the confluence with Agia Aikaterini stream

As it is shown in Figure 90, the model underestimates the simulated maximum depths of the Scenario “Real flood” at all checkpoints of Agia Aikaterini stream for return period of $T=20, 50$ and 100 years. Also, the model overestimates the simulated maximum depths

of the Scenario “Real flood” at all checkpoints of Agia Aikaterini stream for return period of $T=1000$ years at all checkpoints of Agia Aikaterini stream.

Figure 91 and Figure 92 show that the model underestimates the simulated maximum depths of the Scenario “Real flood” at all checkpoints of Soures stream for return period of $T=20$, 50 and 100 years. Also, the model, generally, overestimates the simulated maximum depths of the Scenario “Real flood” for the return period of $T=1000$, particularly downstream of the confluence of the two streams but still there are few checkpoints (S2, S8 and S9) where the model underestimates the simulated maximum depths of the Scenario “Real flood” with a small difference of 3.1 cm up to a difference of 20.4 cm.

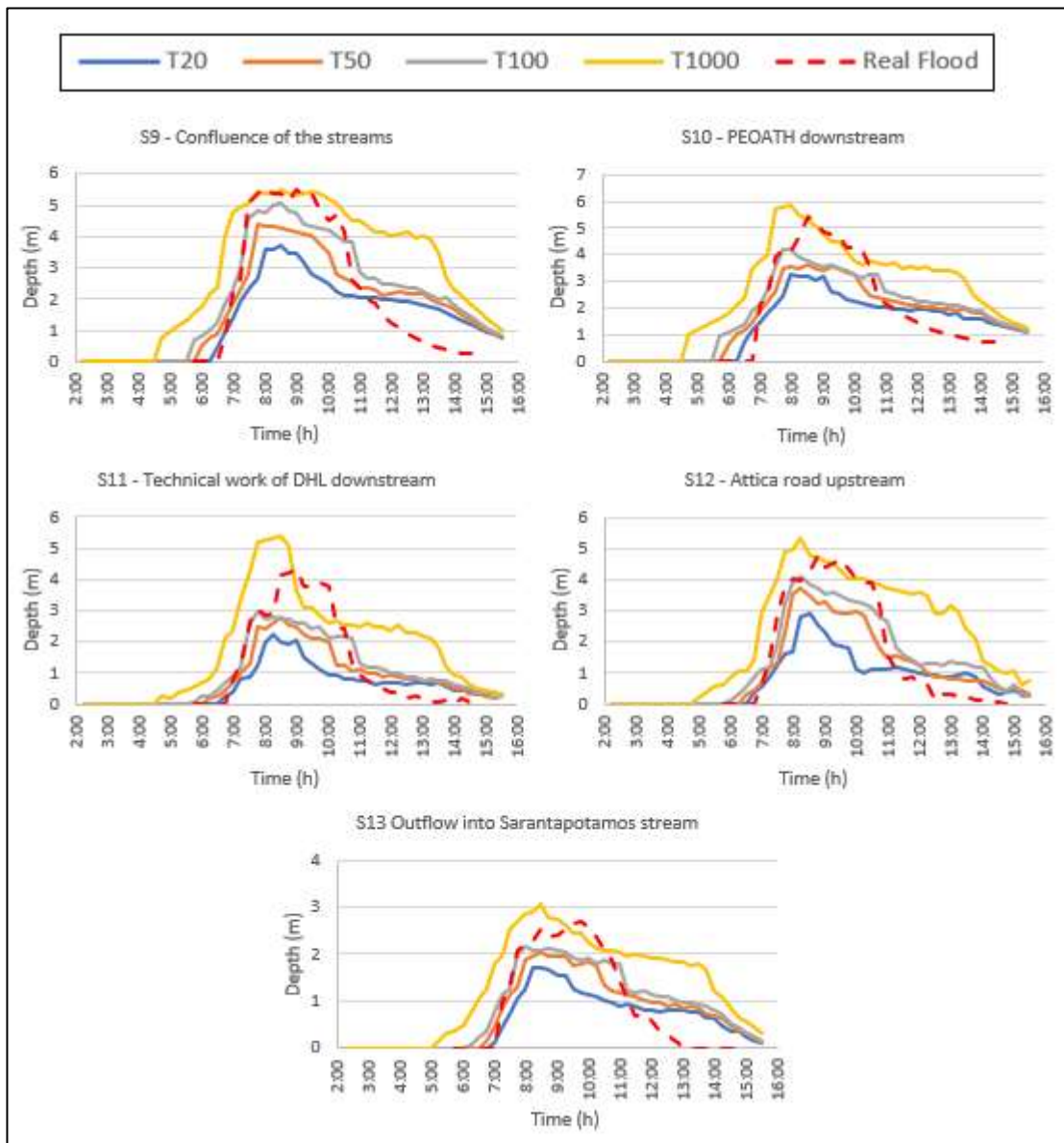


Figure 92 Time change of water depths at the checkpoints of Soures stream downstream of the confluence with Agia Aikaterini stream

Table 35 shows the RMSE, NSE, and MAE of the comparison of the maximum water depths at the checkpoints between flash floods having a return period of T=20, 50, 100 and 1000 years with the maximum water depths of the Scenario “Real flood”.

Table 35 Goodness of fit criteria

	T=20	T=50	T=100	T=1000
RMSE	1,625	1,043	0,634	0,451
NSE	-0,253	0,484	0,809	0,903
MAE	1,490	0,923	0,548	0,372

5.6.2. Maximum water depths of area

Figures 93, 94, 95 and 96 show the maximum water depths of the floods having a return period of T=20, 50, 100 and 1000 years within the hydraulic simulation area, the main residential area and the main industrial area.

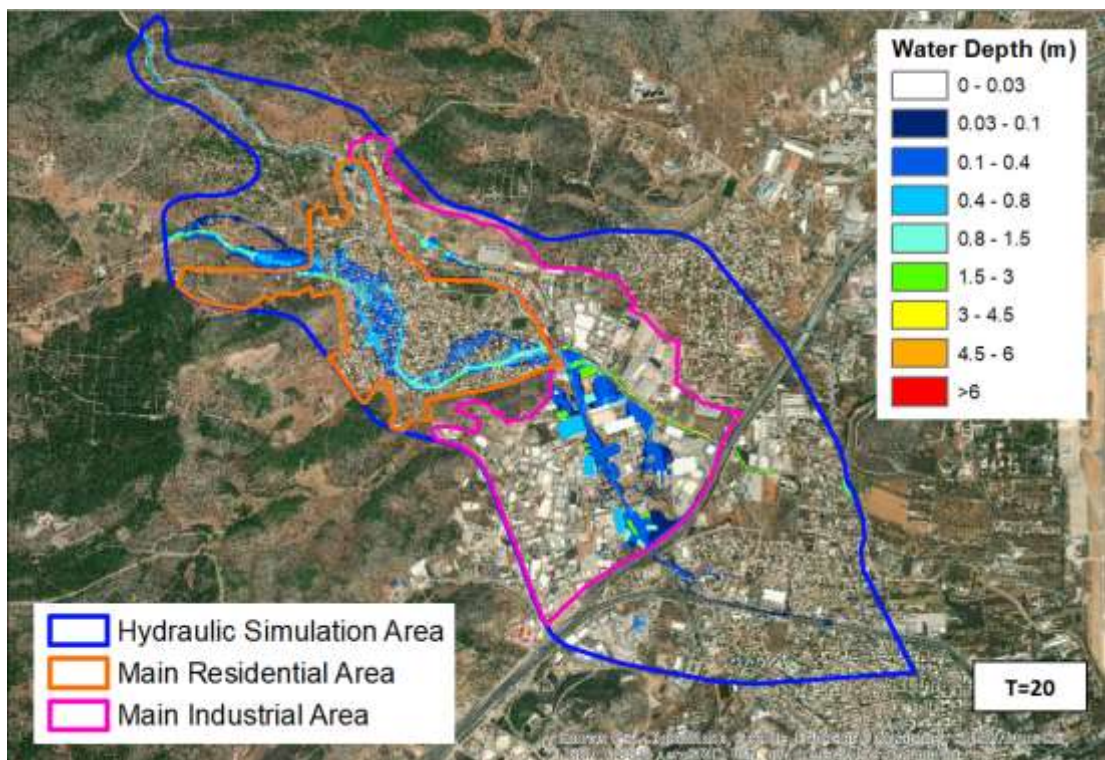


Figure 93 Maximum water depths within the particular areas (Scenario “Real flood”)

The maximum water depths range from 0.03 m to 4.27 m, 5.13 m, 5.92 m and 7.16 m for a return period of T=20, 50, 100 and 1000 years, respectively.

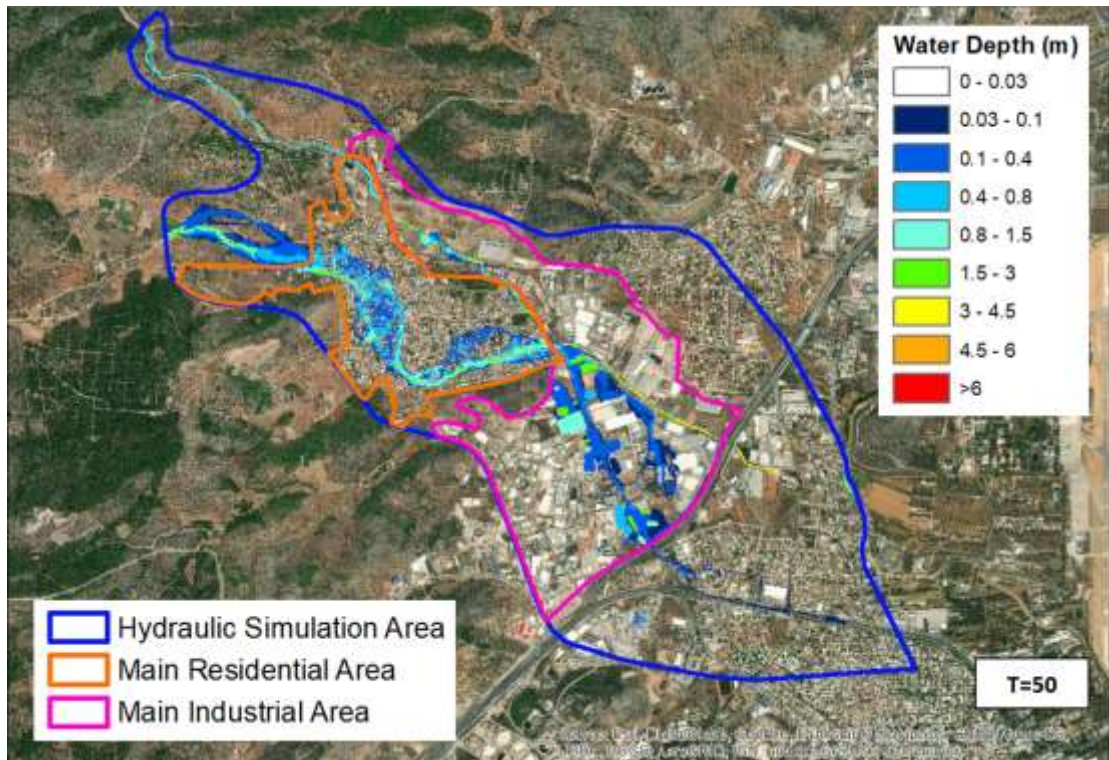


Figure 94 Maximum water depths within the particular areas (Scenario “Real flood”)

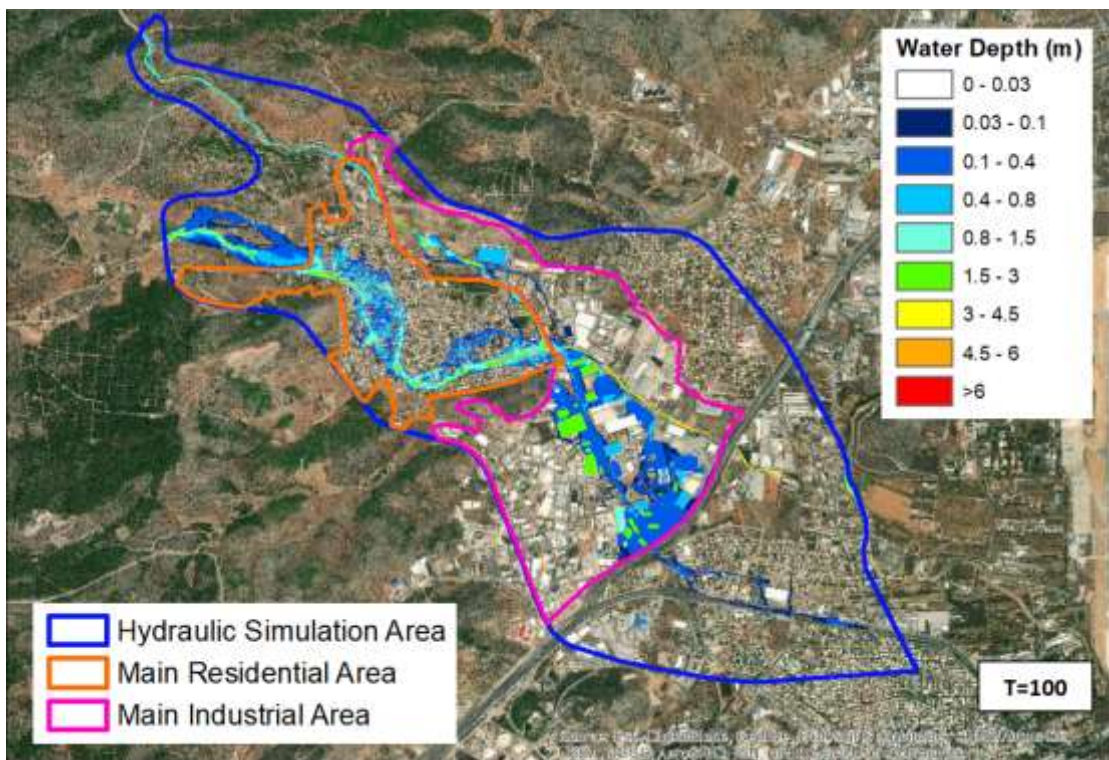


Figure 95 Maximum water depths within the particular areas (Scenario “Real flood”)

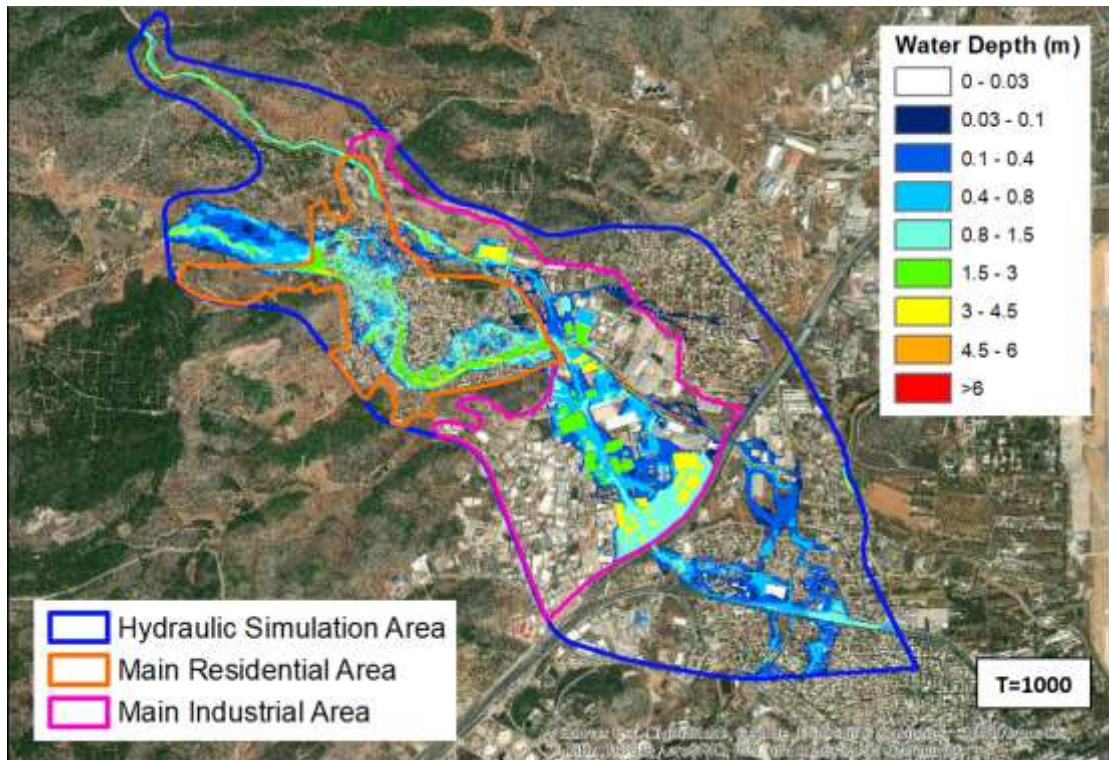


Figure 96 Maximum water depths within the particular areas (Scenario “Real flood”)

Figures 93 and 94 reveal that for T=20 and 50 years the maximum depths are much smaller than the depths of real flood. Figure 95 shows that for T=100 years the maximum depths are still smaller than the depths of real flood. Also, the flood is more evident after underpassing Attica Road in the south, even with water depths lower than 50 cm. Figure 96 shows that for T=1000 years the maximum depths are larger than the depths of real flood.

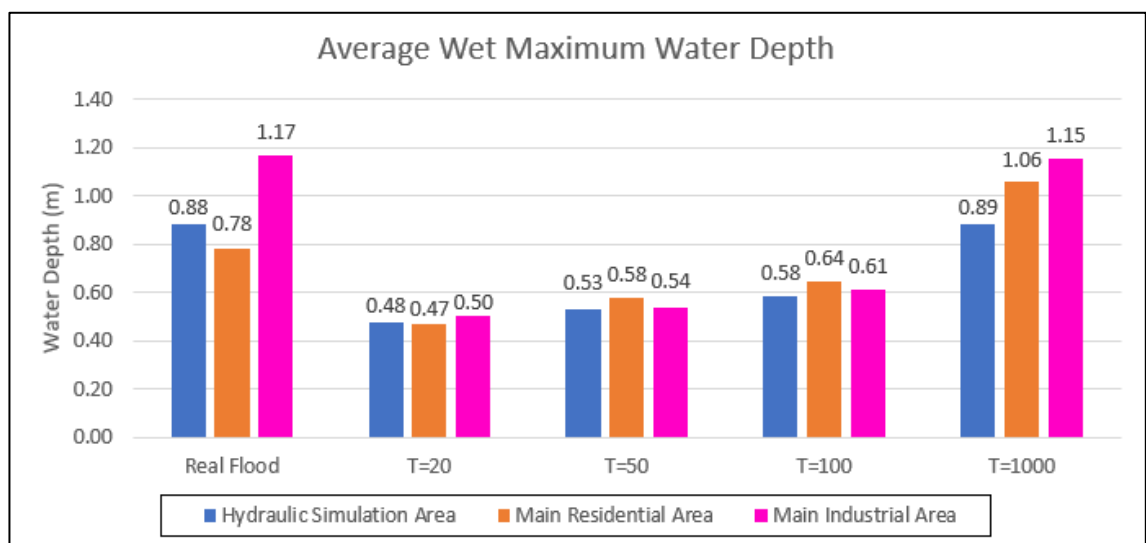


Figure 97 Average wet maximum water depths for the particular areas (Scenario “Real flood”)

Figure 97 presents the comparison of average wet maximum water depths in the particular areas between floods with return period T=20, 50, 100 and 1000 years and real flood. It shows a gradual increase of the average wet maximum water depth for every particular area as the return period increases.

The increase is smooth only for the main residential area.

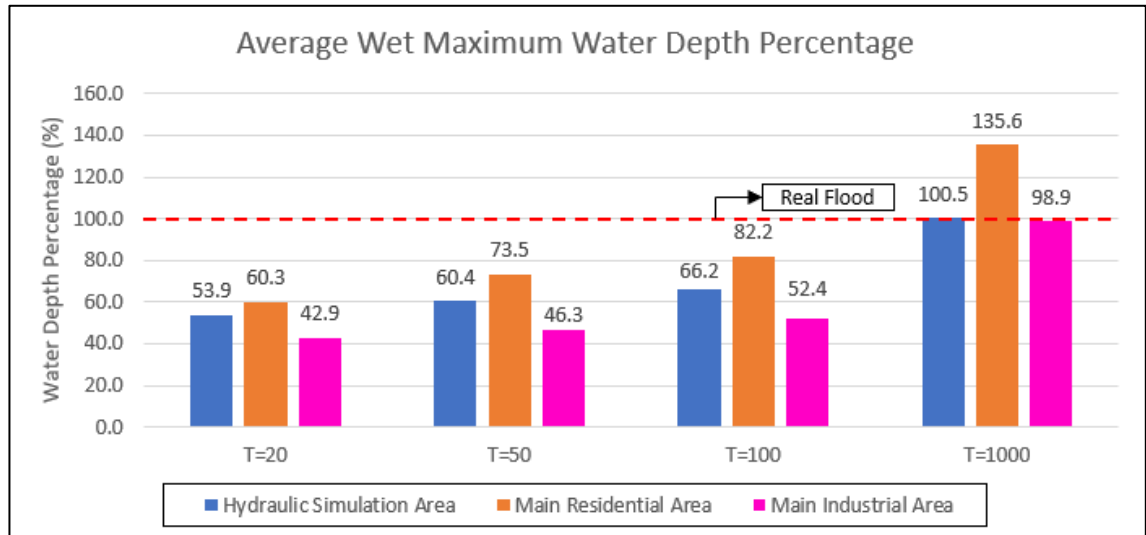


Figure 98 Average wet maximum water depth percentage between floods with return period T=20, 50, 100 and 1000 years and real flood for the particular areas

Also, Figures 98 and 99 present the average wet maximum water depth percentage between floods with return period T=20, 50, 100 and 1000 years and real flood for the particular areas. The return period of the real flood in the main residential area, as a representative one, is 235 years, as it is shown in Figure 99.

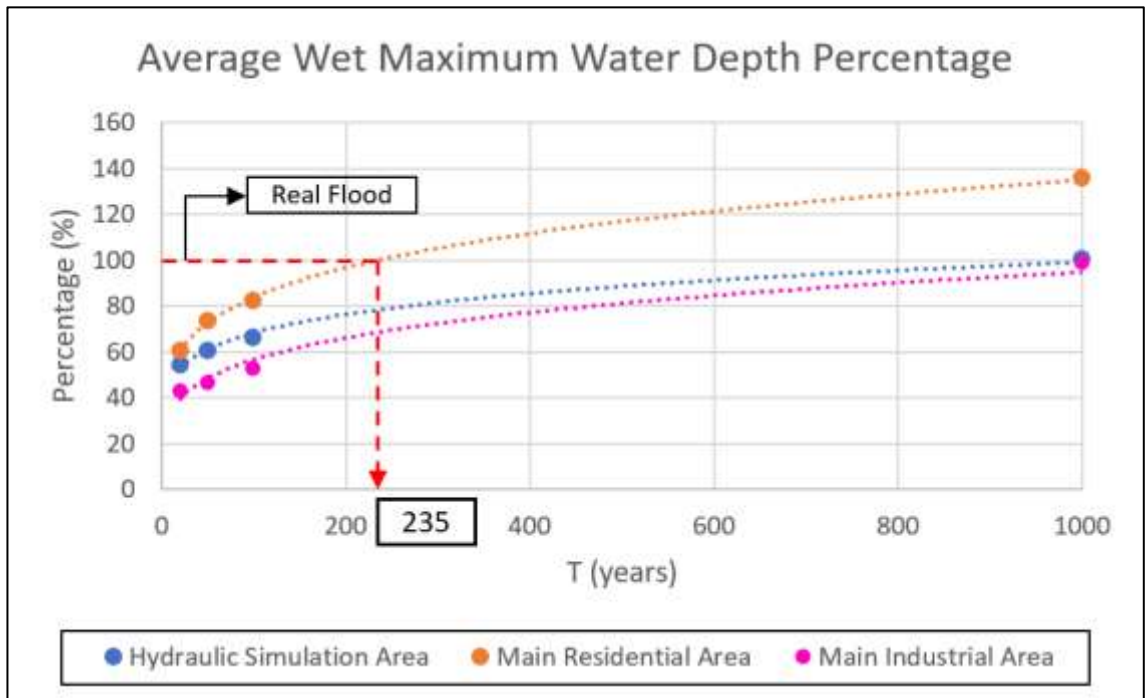


Figure 99 Average wet maximum water depth percentage between floods with return period T=20, 50, 100 and 1000 years and real flood for the particular areas

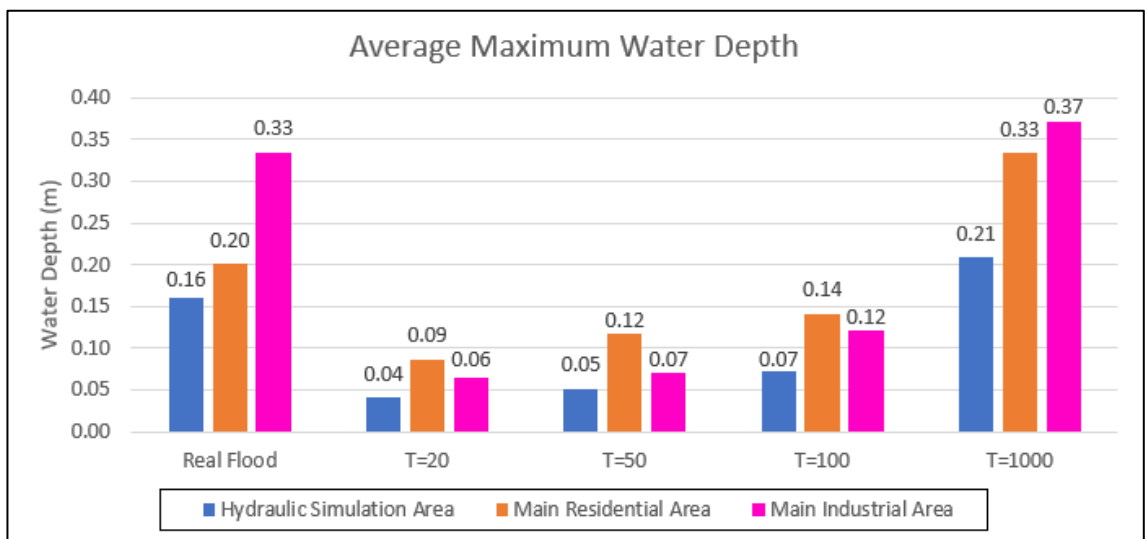


Figure 100 Average maximum water depths for the particular areas (Scenario "Real flood")

Figure 100 presents the comparison of average maximum water depths for the particular areas between floods with return period T=20, 50, 100 and 1000 years and real flood. There is a consistency in the gradual increase of the average maximum water depth, as the return period increases, for all the particular areas. However, it is obvious for the main industrial area that the relative depth increase accelerates for T=100 years and more, like the return period of the real flood, and then it slows for T=1000 years.

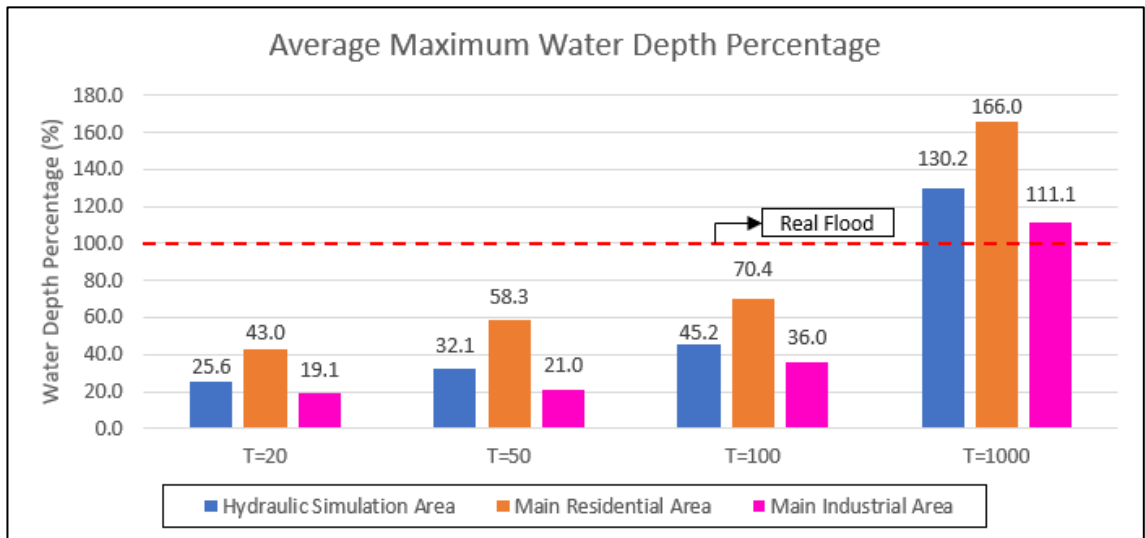


Figure 101 Average maximum water depth percentage between floods with return period T=20, 50, 100 and 1000 years and real flood for the particular areas

Also, Figure 101 and 102 present the average maximum water depth percentage between floods with return period T=20, 50, 100 and 1000 years and real flood for the particular areas. The return period of the real flood in the main residential area is 243 years, as it is shown in Figure 102.

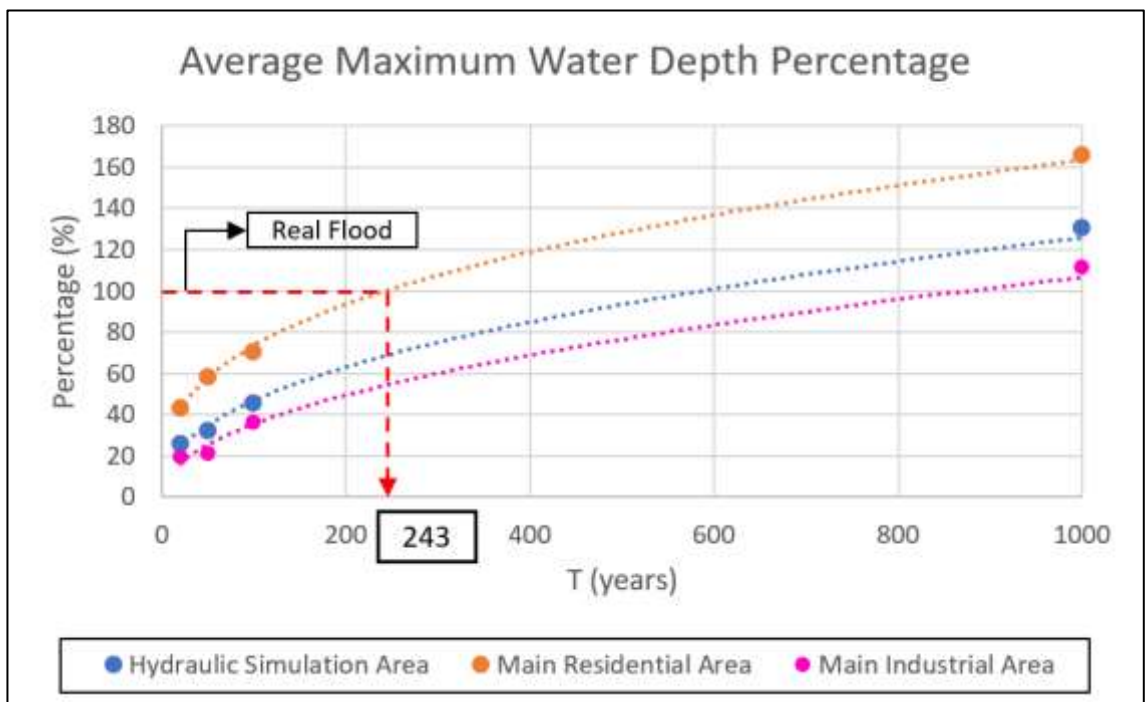


Figure 102 Average maximum water depth percentage between floods with return period T=20, 50, 100 and 1000 years and real flood for the particular areas

5.6.3. Flood extent and flooding

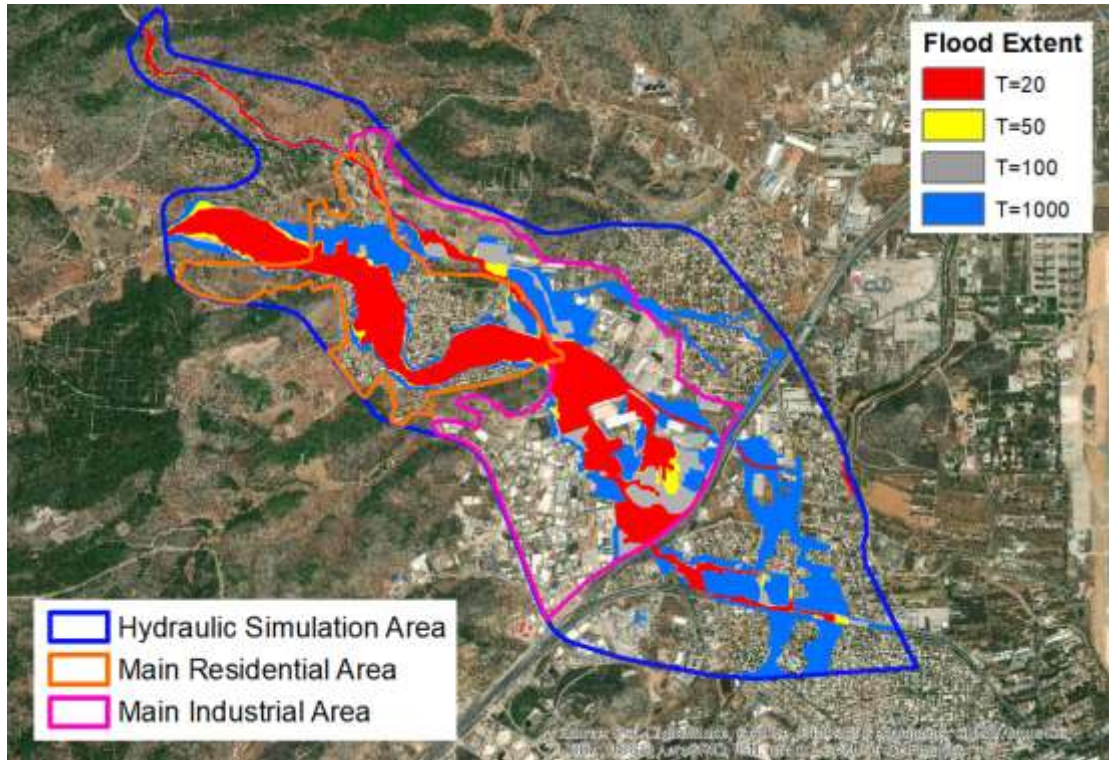


Figure 103 Comparison of flood extent within the particular areas for T=20, 50, 100 and 1000 years (Scenario “Real flood”)

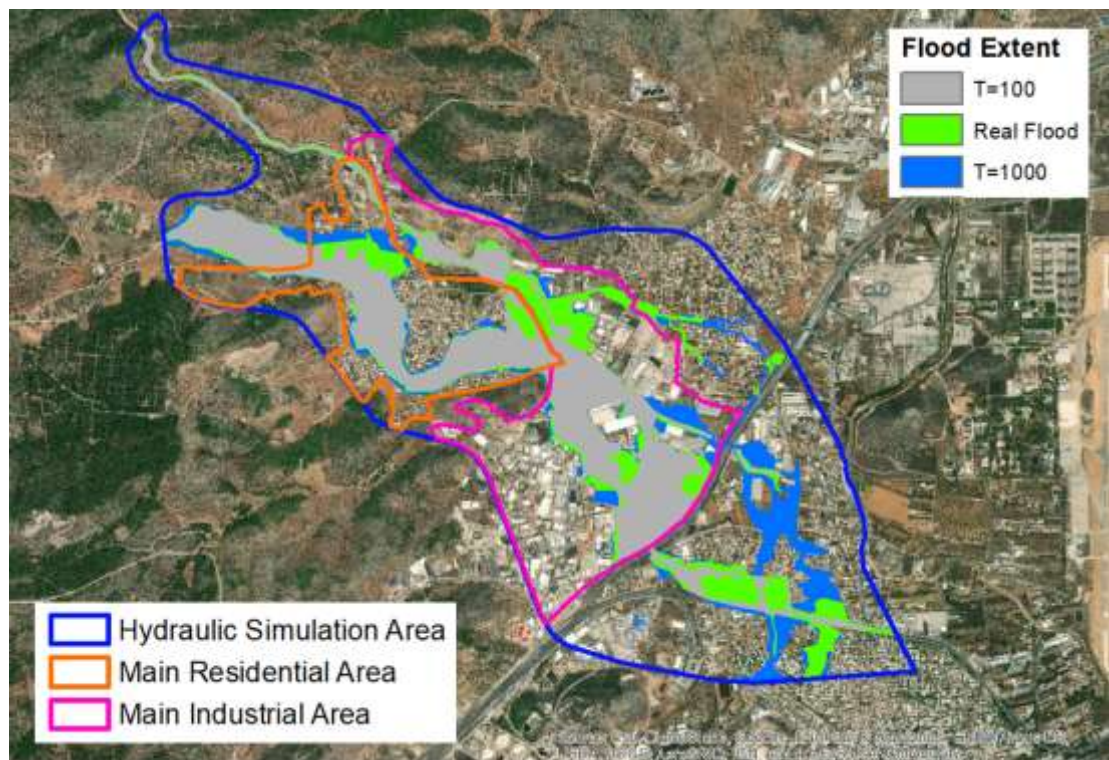


Figure 104 Comparison of flood extent within the particular areas for T=100, 1000 years and real flood (Scenario “Real flood”)

Figure 103 shows the comparison of flood extent for the particular areas for T=20, 50, 100 and 1000 years. It shows illustratively the increase of the flood extent as the return period increases from T=20 to T=1000 years, which has already been mentioned in unit 5.6.2.

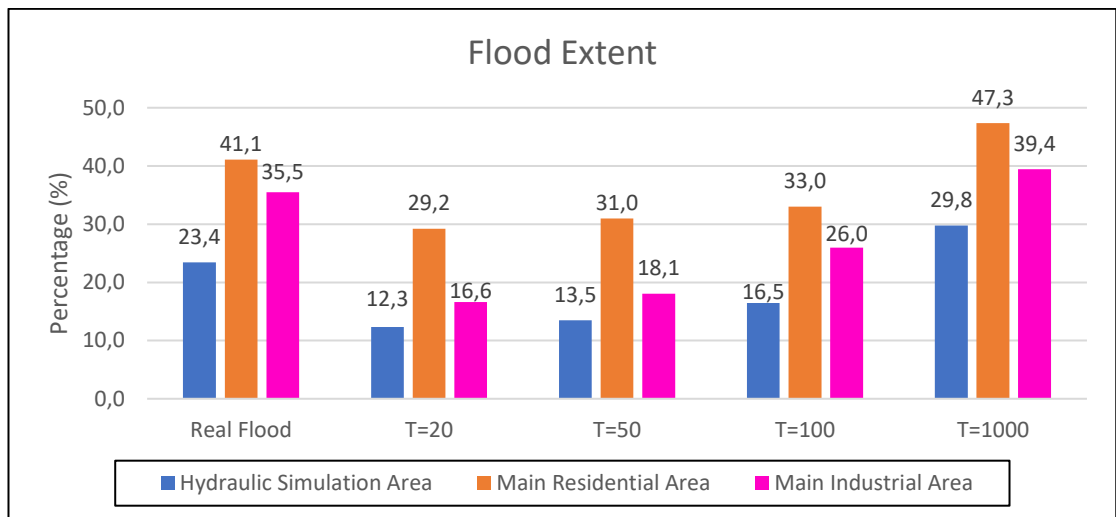


Figure 105 Flood extent for the particular areas (Scenario “Real flood”)

Figure 104 focuses in the comparison of flood extent for the particular areas for T=100, 1000 years and real flood. As it is shown in Figure 105, the real flood extent percentages in the particular areas are 23.4% in the hydraulic simulation area, 41.1% in the main residential area and 35.5% in the main industrial area greater than the corresponding of 16.5%, 33.0% and 26.0% for T=100 years.

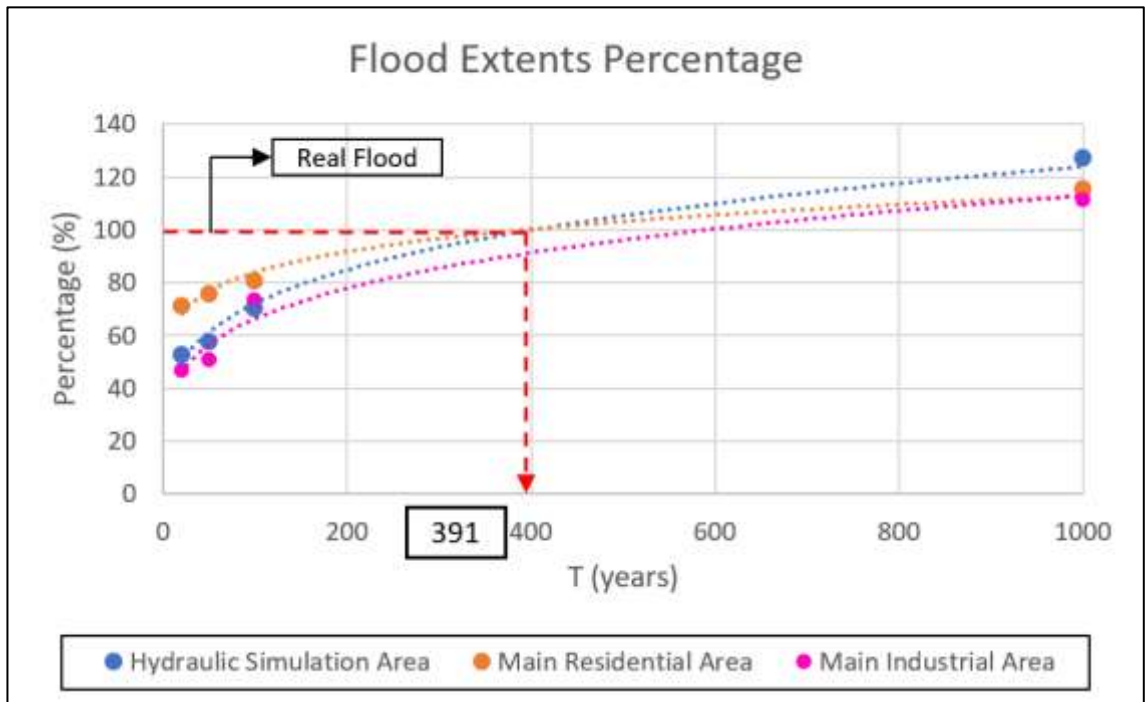


Figure 106 Flood extents percentage of floods with return period T=20, 50, 100 and 1000 years and real flood for the particular areas

Figure 106 presents the flood extents percentage between floods with return period T=20, 50, 100 and 1000 years and real flood for the particular areas. The return period of the real flood in the main residential area is 391 years.

As it is shown in Figure 107, the real flood extent percentages in the particular areas are 18.1% in the hydraulic simulation area, 25.7% in the main residential area and 28.7% in the main industrial area greater than the corresponding of 12.4%, 22.0% and 19.7% for T=100 years.

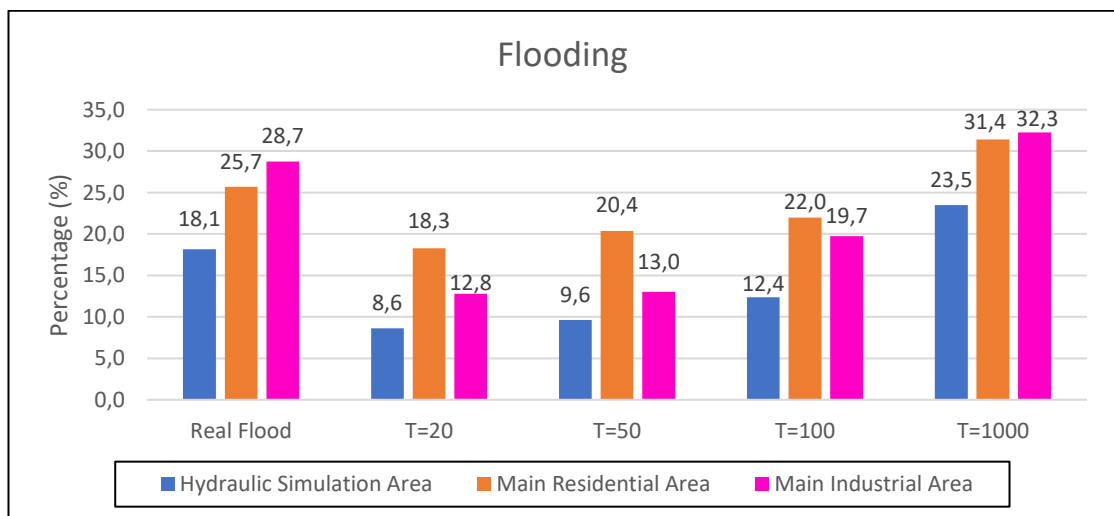


Figure 107 Flooding for the particular areas (Scenario "Real flood")

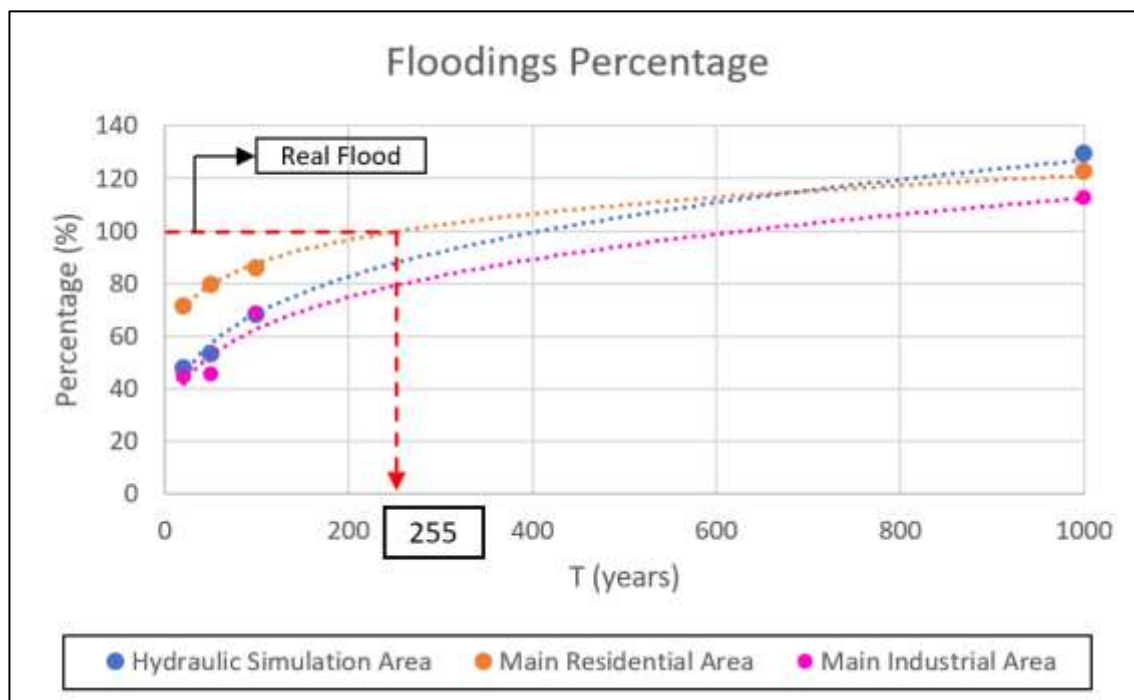


Figure 108 Floodings percentage of floods with return period T=20, 50, 100 and 1000 years and real flood for the particular areas

Figure 108 presents the floodings percentage between floods with return period T=20, 50, 100 and 1000 years and real flood for the particular areas. The return period of the real flood in the main residential area, as a more representative area even in this case, is 255 years.

5.7. Alternative Scenarios “Diversion, retention pond and METRO fence” and “New diversion and retention pond”

5.7.1. Maximum water depths of area

Figures 109 and 110 show the maximum water depths of the alternative scenarios “Diversion, retention pond and METRO fence” and “New diversion and retention pond” having a return period of T=50 years within the hydraulic simulation area, the main residential area and the main industrial area.

The maximum water depths range from 0.03 m to 6.44 m in Figure 109.

The maximum water depths range from 0.03 m to 6.30 m in Figure 110.

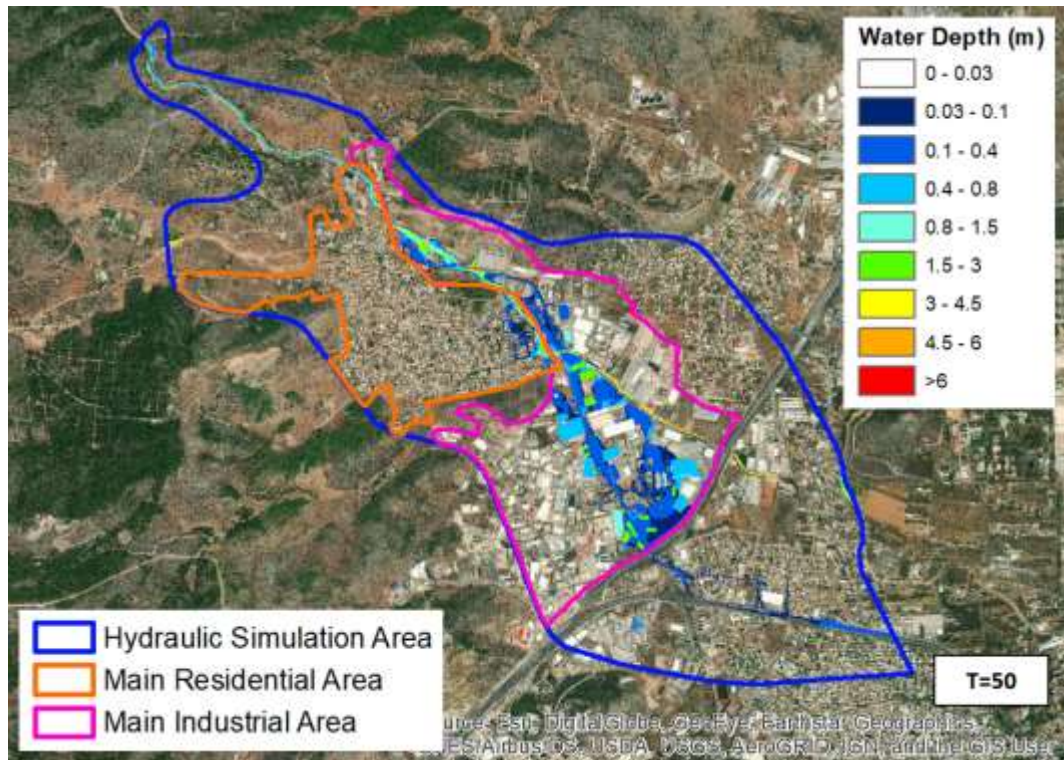


Figure 109 Maximum water depths within the particular areas (Alternative Scenario “Diversion, retention pond and METRO fence”)

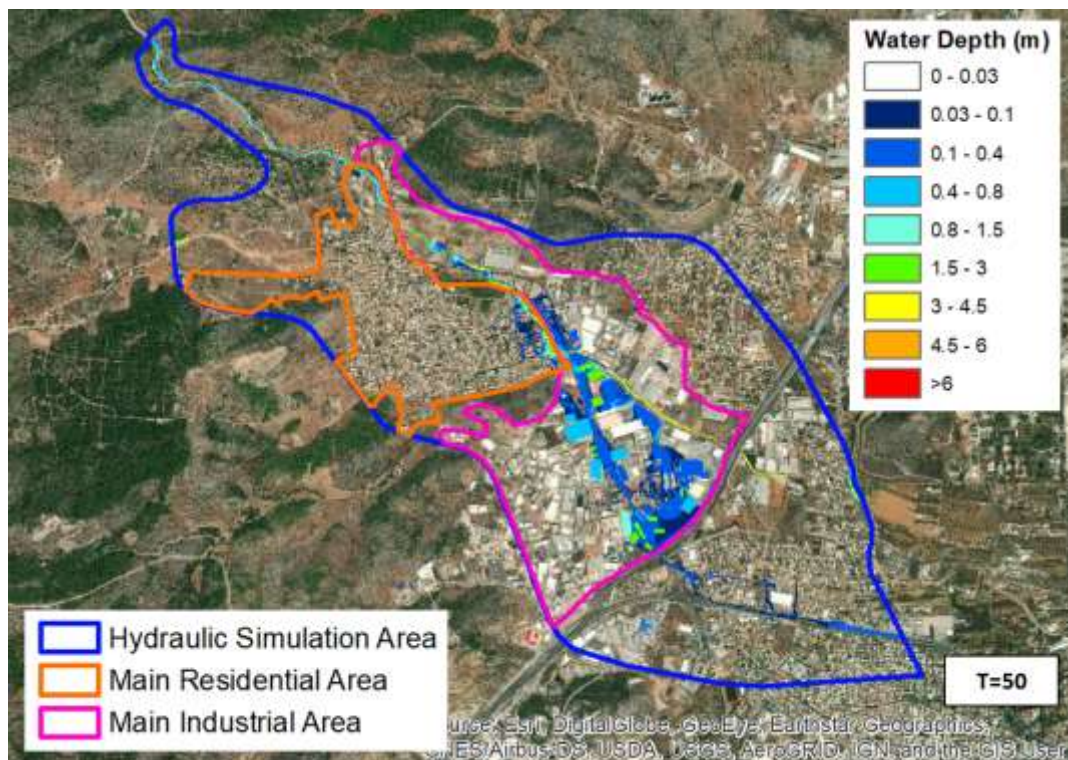


Figure 110 Maximum water depths within the particular areas (Alternative Scenario “New diversion and retention pond”)

Figure 111 presents the comparison of average wet maximum water depths of Scenario “Diversion and retention pond” and alternative Scenarios with average wet maximum water depths of Scenario “Real flood” for the particular areas.

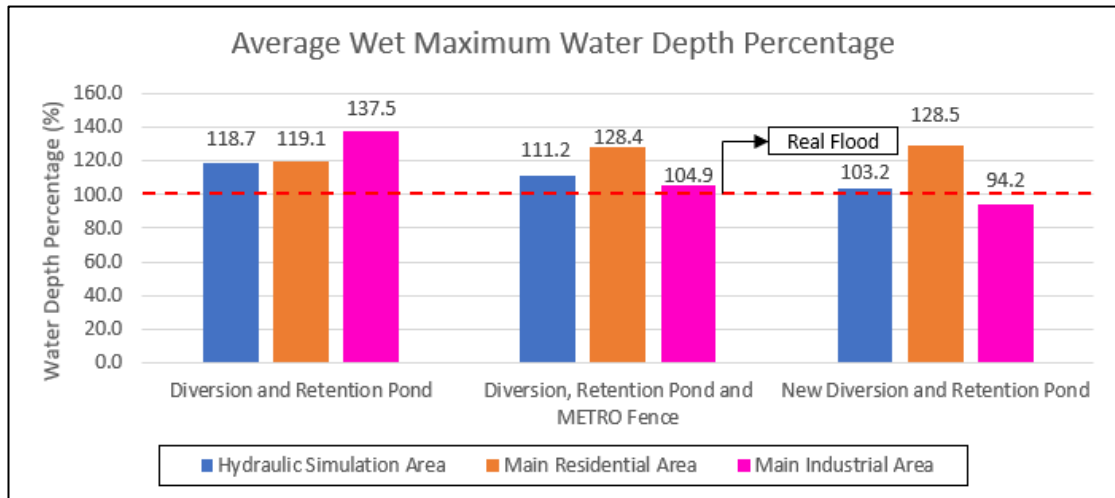


Figure 111 Average wet maximum water depth percentage of Scenarios “Diversion and retention pond” and alternative Scenarios for the particular areas

For the Scenario “Diversion and Retention Pond” the average wet maximum water depth percentages are 118.7% in the hydraulic simulation area, 119.1% in the main residential area and 137.5% in the main industrial area. For the Scenario “Diversion, retention pond and METRO fence” the average wet maximum water depth percentages are 111.2%, 128.4% and 104.9% and for the Scenario “New diversion and retention pond” the average wet maximum water depth percentages are 103.2%, 128.5% and 94.2%, respectively.

Figure 112 presents the comparison of average maximum water depths of Scenario “Diversion and retention pond” and alternative Scenarios with average maximum water depths of Scenario “Real flood” for the particular areas.

For the Scenario “Diversion and Retention Pond” the average maximum water depth percentages are 88.9% in the hydraulic simulation area, 17.9% in the main residential area and 173.5% in the main industrial area. For the Scenario “Diversion, retention pond and METRO fence” the average maximum water depth percentages are 90.2%, 27.9% and 169.0% and for the Scenario “New diversion and retention pond” 76.5%, 26.3% and 135.7%, respectively.

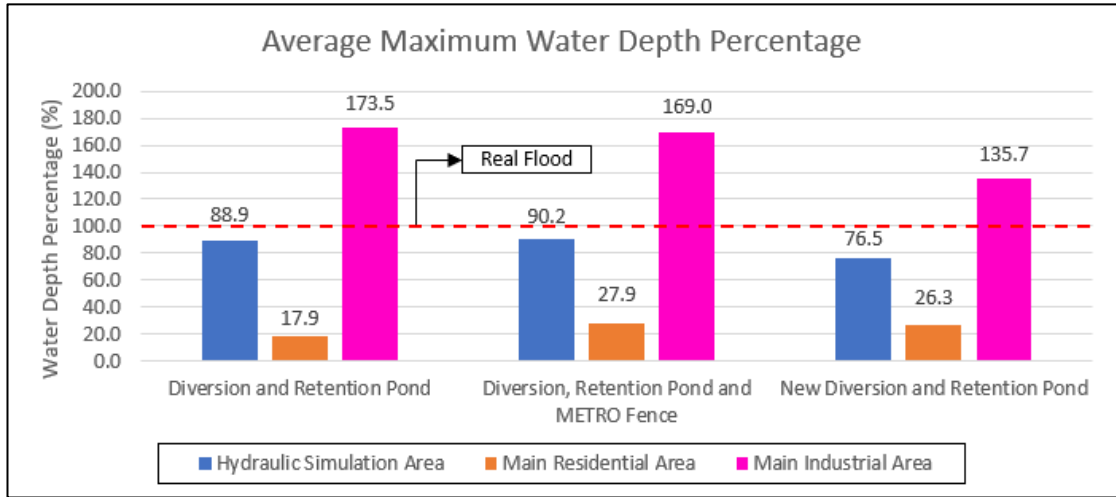


Figure 112 Average maximum water depth percentage of Scenarios “Diversion and retention pond” and alternative Scenarios for the particular areas

5.7.2. Flood extent and flooding

Figure 113 presents the comparison of flood extents of Scenario “Diversion and retention pond” and alternative Scenarios with flood extents of Scenario “Real flood” for the particular areas.

For the Scenario “Diversion and Retention Pond” the flood extents percentages are 74.7% in the hydraulic simulation area, 18.6% in the main residential area and 115.4% in the main industrial area. For the Scenario “Diversion, retention pond and METRO fence” the flood extents percentages are 75.4%, 24.4% and 144.9% and for the Scenario “New diversion and retention pond” 65.7%, 21.9% and 124.4%, respectively.

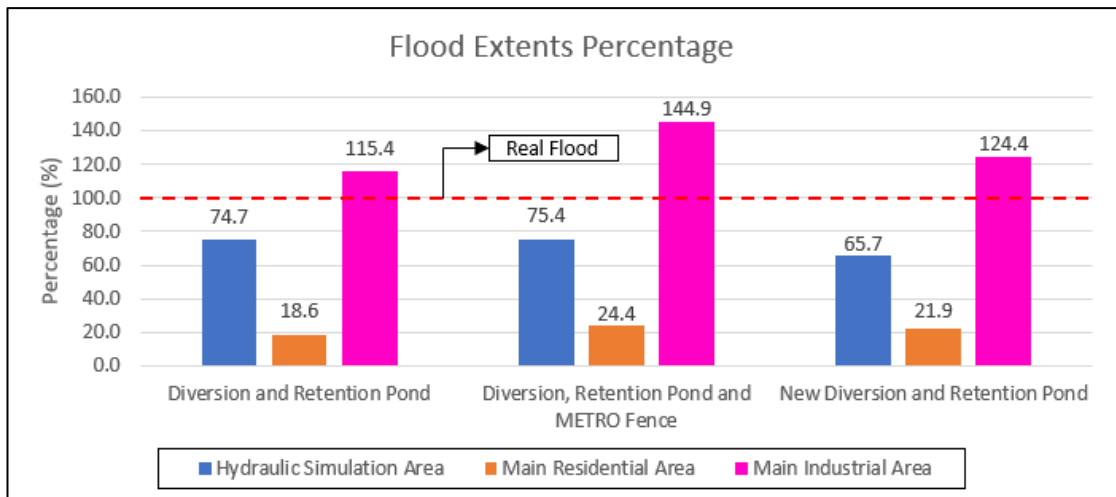


Figure 113 Flood extents percentage of Scenarios “Diversion and retention pond” and alternative Scenarios for the particular areas

Figure 114 presents the comparison of floodings of Scenario “Diversion and retention pond” and alternative Scenarios with floodings of Scenario “Real flood” for the particular areas.

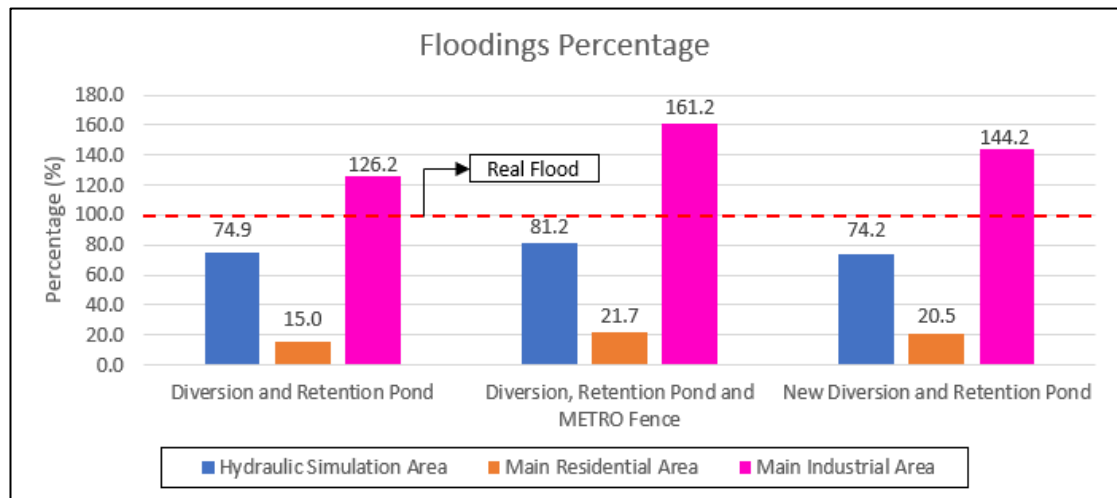


Figure 114 Floodings percentage of Scenarios “Diversion and retention pond” and alternative Scenarios for the particular areas

For the Scenario “Diversion and Retention Pond” the floodings percentages are 74.9% in the hydraulic simulation area, 15.0% in the main residential area and 126.2% in the main industrial area. For the Scenario “Diversion, retention pond and METRO fence” the floodings percentages are 81.2%, 21.7% and 161.2% and for the Scenario “New diversion and retention pond” 74.2%, 20.5% and 144.2%, respectively.

6. Discussion

The 1D/2D coupled model is used and thirteen different scenarios are conducted.

6.1. Basic Scenario “Real flood” – Model validation and evaluation

6.1.1. Checkpoints – Maximum water depths and flood progression

The model satisfactorily represents the observed maximum water depths almost at all checkpoints of Agia Aikaterini and Soures streams. It should be mentioned that the relatively large difference of 1.38 m at S1 is due to the fact that the significantly narrower than 5 m riverbed at S1 can not be properly represented by the 5 m resolution of the DEM. The DEM actually overestimates the cross-section resulting in a much lower water depth. It should be mentioned that the DEM accepts a single value of the Manning’s coefficient $n=0.016$ for all the height along the open twin rectangular concrete channel, where the actual concrete banks extend up to the height of 3 m. Over that height, a natural bank exists with a Manning’s coefficient $n=0.065$ resulting in a much higher water depth for water depths exceeding 3 m. This fact justifies the underestimation of the water depths at the checkpoints S11 and S12, where there is a difference of 0.87 m and 0.46 m at checkpoints S11 and S12 respectively. The RMSE, NSE, and MAE from the comparison of the maximum water depths at the checkpoints for the basic scenario “Real flood” are 0.494, 0.871 and 0.362, respectively.

The flood moves along streets mainly having a width of 8 m modelled with only 2 cells across street. Despite this disadvantage of the DEM, the model satisfactorily represents the flood evolution regarding the upward branch of the flood progression as it is shown at checkpoints AA4, AA5 and AA6 of Agia Aikaterini stream. Also, although there are only few checkpoints and corresponding observations, it seems that there is a delay concerning the downward branch. This is due mostly to the shape of the storm hydrograph of Agia Aikaterini stream and the inherent uncertainty of the rainfall. Additionally, the model satisfactorily represents the upward and downward branch of the flood as it is shown at checkpoints S3, S4 and S9 of Soures stream.

The statistical evaluation validates the coupled 1D/2D model and its set-up.

6.1.2. Maximum water depths of area, flood extent and flooding

The display of maximum water depths gives an idea of the spatial severity of the flood and the flood extent that result from the 1D/2D model (Scenario “Real flood”). The maximum water depths are derived for comparison reasons. The same applies to the

flooding. The display of maximum water depths compared to the mapping of the maximum recorded extent of the flood (recorded flood extent) demonstrates that the model represents the flood inundation highly satisfactorily. All the technical works, even if they are not clogged, are overpassed. This is to be expected because they were constructed to face a storm much milder than the November 2017 one. Yet, the water does not overflow from Soures stream along the length of the artificial channel although the actual concrete banks of the artificial channel, which exist downstream of the technical work (11), extend up to the height of 3 m. Over that height, a natural bank exists at a height of 5.3 m approximately, which protects the surrounding area from flooding. Thus, despite that the water overflows at (12) and (13), it reenters Soures stream. There are only two areas where differences are pointed out. Shortly after the entrance in the hydraulic simulation area the water overflows on either side of the current bed. The examination of the DEM revealed that at this point the cross section of the stream narrows and therefore overflow is caused. Also, it seems that a relatively smaller area is inundated in the residential area close to the town of Magoula, probably due to the inherent inability of the DEM to accurately represent the microtopography of the nearby area. The statistical evaluation, as mentioned in the previous unit 6.1.1 and the very high percentage of 96.0% of the real flood extent compared to the recorded flood extent, taking into consideration that the relative surplus and deficit are only 12.4% and 16.4%, respectively, validate the coupled 1D/2D model and its set-up. They also show that P-DWave is suitable for flash flood simulations as it presents satisfactory results and is fairly easy to set up.

6.2. Impact of Scenario “Fully operated conduits”

6.2.1. Checkpoints – Maximum water depths and flood progression

The operation of the Vageli Koropouli closed conduit (16), with the dimensions of 2.00 m x 1.70 m and length $L=2,300$ m approximately, has a low impact because it receives a relatively small supply of nearly $10 \text{ m}^3/\text{s}$, much lower than the peak discharge of $160 \text{ m}^3/\text{s}$ of Agia Aikaterini stream. Hence, excluding the checkpoint AA3 that is far upstream of the conduit entrance and not affected from the operation of the conduit resulting in an identical time change of the water depth, there are slight differences with regard to the maximum water depths of Agia Aikaterini stream.

The checkpoints S2, S7 and S9 of Soures stream are upstream of the technical works (3), (7) and (10) respectively, which were fully ((3), (7)) or partially clogged (10) in Scenario “Real flood” thus choking the flow and producing relatively higher water depths. The exact opposite happens, as it is expected, with the checkpoints S1, S4, S5, S8 and

S10 which are downstream of the technical works (1), (4), (5) and (9) respectively. Regarding the overestimations of the maximum depths at checkpoints S11, S12 and S13 of the artificial channel, they are due to the full operation of the upstream technical work (10) at the PEOATH bridge.

Generally, there are insignificant deviations with regard to the flood progress compared to the Scenario "Real flood". The earlier rising of the upward branch, meaning faster water movement, is due to the full operation of the technical works and is evident for the cases where the checkpoint is downstream of a technical work (cases S4, S5, S8) and particularly in cases S9, S10, S11, S12 and S13 because of the full operation of the aforementioned closed conduit (16). It should be mentioned that generally, the earlier rising of the upward branch is not followed by an earlier lowering of the downward branch, which is alleviated due to the full operation of the technical works. The low impact is verified from the statistics of the comparison of the maximum water depths at the checkpoints with the Scenario "Real flood". The RMSE and MAE (0.353 and 0.242) are very low and the NSE (0.941) is very close to 1.

6.2.2. Maximum water depths of area

The Vageli Koropouli technical work (16) causes a slight reduction on the maximum water depths in the main residential area. On the other hand, the full operation of the technical works and mainly of the technical work at the PEOATH bridge (10) causes a larger reduction of the maximum depths in the majority of the main industrial area that, locally, besides Attica Road exceeds 0,50 m and on the contrary, it causes an increase of them in the surrounding areas of Soures stream and particularly in the area downstream of Attica Road, where a flooding with maximum depths up to 50 cm is presented. Finally, Figure 51 confirms the choking of the flow upstream the clogged technical works.

Generally, there is a low impact considering the maximum water depths within the particular areas (the hydraulic simulation area, the main residential area and the main industrial area) with average wet water depth percentages 86.9%, 96.9% and 89.0% and average water depth percentages 92.2%, 95.4% and 87.5%, respectively.

6.2.3. Flood extent and flooding

The flood extent is larger although the flood is not so severe, as it was revealed in the previous analysis regarding the water depths. This is justified from the fact that in this case, Soures stream overflows downstream of the technical work (11) contributing to a small increase of the flood extent in both the hydraulic simulation area and in the main

industrial area with flood extents percentages of 109.4% and 103.0%, respectively. In this specific region the inundation is sparsely distributed with very small water depths, even lower than 10 cm upstream Attica Road, thus resulting in floodings percentages of 106.0% and 98.3% in the hydraulic simulation area and in the main industrial area respectively, as it is shown in Table 20.

The low impact is more evident in the main residential area with a flood extents percentage of 99.5% and a floodings percentage of 98.4%.

6.3. Impact of Scenario “Fences”

6.3.1. Checkpoints – Maximum water depths and flood progression

The time evolution of the water depths along Agia Aikaterini stream is identical to the one of Scenario “Real flood” because no protection measures were taken in the main residential area of Mandra town, which is placed upstream of the confluence of the two streams. The fence raising of the Logistics METRO protects a rather large area from flooding and diverts a significant amount of flow into the stream at checkpoint S6, causing higher water depths there and downstream along Soures stream. Also, the flood progress is the same regarding the two branches. Small differences are observed comparing the occurrences of the maximum depths downstream S6 due to the diversion of the flow which is caused from the fence raising of the Logistics METRO.

A moderate total impact is verified from the comparison of the maximum water depths at the checkpoints, as shown in Figures 56 and 57. The RMSE and MAE (0.492 and 0.289) are low and the NSE (0.885) is fairly close to 1. Yet, taking into consideration that there is no impact along Agia Aikaterini stream and upstream of (6), the impact is crucial along Soures stream downstream of (6).

6.3.2. Maximum water depths of area

The fence surrounding the Logistics METRO causes very slight difference on the maximum water depths in the main residential area (see Figure 59) with an average wet maximum water depth percentage of 100.8% and an average maximum water depth of 103.0%.

However, the significant amount of water diverted to Soures stream moves along the stream causing higher water depths and reaches the technical work of the PEOATH (10). There, the flow is divided into two parts. One part flows to the south along the PEOATH, mostly restricted by the surrounding fences, producing high water depths, flooding the common lands and sequentially, underpassing Attica Road and flooding the Papakosta

settlement. The other part underpasses and surpasses the technical work of the PEOATH (10), moves along Soures stream overflowing in small water depths and finally underpasses Attica Road flooding a significant area with small water depths. Despite the higher water depths along the PEOATH and in the common lands, the protection of the previously severely flooded properties leads to a low impact considering the average wet water depth percentage (91.6%) and a clear impact considering the average water depth percentage (41.9%) in the industrial area. This ascertainment in conjunction with the small water depths downstream Attica Road leads to a moderate impact regarding the corresponding percentages (78.7%, 75.0%) in the hydraulic simulation area.

6.3.3. Flood extent and flooding

There is a negligible impact in the main residential area, as it is verified in Figure 59, where the flood extents percentage and the floodings percentage are 100.8% and 102.2%, respectively. Considering the main industrial area, there is a clear impact on the flood extent and flooding with a corresponding flood extents percentage of 51.5% and a floodings percentage of 45.7% despite the overflow of Soures stream. This is due to the raising of fences which protect the previously severely flooded properties. The reduction of the flood extent in the main industrial area is balanced by the increase in the flooded area south of Attica Road resulting in very small differences of the flood extents percentage (98.2%) and the floodings percentage (95.3%) and therefore a very low impact on the hydraulic simulation area.

6.4. Impact of Scenario “Spatially extended rainfall”

6.4.1. Checkpoints – Maximum water depths and flood progression

The excess rainfall results in the increase of the maximum water depth at all checkpoints. Regarding flood progression the effect of the rainfall extension is obvious, particularly along Soures stream as it is observed a much earlier rising of the upward branch because the rain starts half an hour earlier than the Soures hydrograph. The earlier rising of the upward branch is not followed by an earlier lowering of the downward branch. This is alleviated due to the preceding higher water depths.

A moderate impact is verified from the comparison of the maximum water depths at the checkpoints, as shown in Figures 65 and 66. The RMSE and MAE (0.403 and 0.271) are low and the NSE (0.923) is fairly close to 1.

6.4.2. Maximum water depths of area

The water covers the whole area except for some specific parts with a high altitude, mainly in the northern part of the hydraulic simulation area out of the main residential area and the main industrial area.

The huge increase of the flooded area lowers the average wet maximum depth for all the particular areas. More precisely, the average wet maximum depth percentages are 56.7%, 72.8% and 62.4% for the hydraulic simulation area, the main residential area and the main industrial area, respectively. Yet, the averaging considering both the wet and dry parts demonstrates the impact of the Scenario “Spatially extended rainfall” on the average maximum depths, where, on the contrary, the excess runoff leads to higher average maximum depth percentages of 146.1% for the hydraulic simulation area, a large impact due to the contribution of the extended rainfall in the whole area where the average maximum depth is relatively low and of 124.6% and 132.2% for the main residential area and the main industrial area, respectively.

6.4.3. Flood extent and flooding

The impact of the Scenario “Spatially extended rainfall” is huge on flood extent and flooding for all the particular areas. More precisely, the flood extents percentages are 355.2%, 214.9% and 273.0% and the floodings percentages are 257.5%, 171.1% and 211.7% for the hydraulic simulation area, the main residential area and the main industrial area, respectively.

6.5. Impact of Scenario “Diversion and retention pond”

6.5.1. Checkpoints – Maximum water depths and flood progression

The impact of the diversion is clear.

It results in much lower to zero maximum water depths at every checkpoint of Agia Aikaterini stream and to higher maximum water depths at every checkpoint of Soures stream downstream the location of the diversion at Soures stream.

Also, the flood progression at every checkpoint of Agia Aikaterini stream follows the overflow of the technical work of separation after the discharge exceeds the capacity of the diversion conduit, which is designed for T=50 years. The earlier rising of the upward branch downstream S3 is due to the contribution of the diversion from Agia Aikaterini stream, where the storm starts half an hour earlier. Also, the earlier rising of the upward

branch is not followed by an earlier lowering of the downward branch, which is alleviated due to the higher water depths.

A strong impact is verified from the comparison of the maximum water depths at the checkpoints, as shown in Figures 76 and 77. The RMSE and MAE (1.131 and 0.912) are large and the NSE (0.393) is much lower than 1.

6.5.2. Maximum water depths of area

The diversion conduit diverts the majority of the flow to Soures stream. The main residential area has significantly lower depths reflecting the very strong impact on the average maximum depth percentage which is 24.7%. On the other hand, the flooded area is restricted very much. Yet, this results in a smaller but strong impact on the average wet maximum depth percentage of 52.3% in the main residential area. Also, there are lower water depths in the part of the main industrial area that is in the south of the PEOATH bridge and even in the south of Attica Road, where the flood is mainly due to the Agia Aikaterini stream. On the contrary, the higher water depths of Soures stream downstream the diversion cause overflow and the flood initially hits severely the Logistics METRO area and then it is divided in two branches. One branch spreads out to the east, inundates a significant part of the hydraulic simulation area, underpasses Attica Road and meets the flood that is caused from the overflow of Soures stream. The other branch moves to the south and mainly contributes to the flood along Soures stream. Soures stream overflows from both sides and inundates a relatively large area after underpassing Attica Road. In the main industrial area the impact on the average maximum depth percentage of 88.7% is low because the great impact on the southern of the PEOATH area is relatively balanced by the flooding due to Soures and particularly to the east. The increase of the flooded area due to Soures overflow leads to a moderate impact of 72.3% on the average wet maximum depth percentage. The extensive flooding southeast of Attica Road contributes to a low impact of 83.2% on the average maximum depth percentage and a moderate impact of 69.9% on the average wet maximum depth percentage, respectively.

6.5.3. Flood extent and flooding

There is a large difference in the main residential area, as it is verified in Figures 80 and 81. This is due to the diversion of Agia Aikaterini stream to Soures stream. On the other hand, the inundation due to the serious overflow of Soures stream causes the larger flood extent in both the hydraulic simulation area and the main industrial area. Thus, there is a strong impact of 57.8% on the flood extents percentage and of 47.1% on the

floodings percentage in the main residential area. However, there is a low to moderate impact of 120.2% on the flood extents percentage and of 122.7% on the floodings percentage in the main residential area and 119.0, 122.5% in the hydraulic simulation area, respectively.

6.6. Influence of the return period – Scenario “Real flood”

6.6.1. Checkpoints – Maximum water depths

The comparison of the simulated maximum water depths of the Scenario “Real flood” at the checkpoints with those for return period of T=20, 50, 100 and 1000 years shows that almost at all the checkpoints the simulated maximum water depths of the Scenario “Real flood” are higher than the maximum water depths for return period of T=20, 50 and 100 years and lower than those for T=1000 years.

The values of RMSE, NSE, and MAE confirm that the real flood is better fitted by the flood of T=1000 years (NSE=0,903 is the biggest and very close to 1, smallest RMSE and MAE).

6.6.2. Maximum water depths of area

A very brief reference not only relative to the maximum water depths but also to the flood extent is considered useful in order to have a better understanding of the severity of the real flood and the influence of the return period.

Figures 93 and 94 reveal that for T=20 and 50 years Soures stream overflows only at the clogged technical works and the inundation takes place from the technical work (10) to southeast and south, mainly along the PEOATH, where a rather small amount of basements, on either side of the PEOATH in the main industrial area, is flooded.

Figure 95 shows that for T=100 years Soures stream overflows also at the technical work (6) and therefore floods the Logistics METRO property and the flood then moves along the PEOATH joining the stream just downstream the confluence at the technical work (10). A rather large amount of basements, on either side of the PEOATH in the main industrial area, is flooded. Also, the flood is more obvious after underpassing Attica Road to the south, even with water depths lower than 50 cm.

Figure 96 shows that for T=1000 years the flood moves to the east. Soures stream overflows along most of its length, even after underpassing Attica Road, where the flood from Soures stream joins the flood that comes from the PEOATH in the south part of the hydraulic simulation area.

Figures 97 and 100 show a gradual increase of the average wet maximum water depth and the average maximum water depth for every particular area as the return period increases.

The increase is smooth only for the main residential area which is not affected from phenomena like stream banks overflows and basements flooding. Therefore, the main residential area is the most representative area for the evaluation of the return period of the real flood. It seems that the return period of the real flood is much larger than 100 years but smaller than 1000 years.

The comparison of the average wet maximum water depth percentage between floods with return period $T=20, 50, 100$ and 1000 years and real flood for the particular areas reveals that the return period of the real flood in the main residential area, as a representative one, is 235 years (see Figure 99).

The comparison of average maximum water depths for the particular areas between floods with return period $T=20, 50, 100$ and 1000 years and real flood reveals that all the particular areas are representative for comparison reasons because both the wet and dry parts are incorporated. There is a consistency in the gradual increase of the average maximum water depth, as the return period increases, for all the particular areas. However, it is obvious for the main industrial area that the relative depth increase accelerates for $T=100$ years and more, like the return period of the real flood, and then it slows for $T=1000$ years. This is due mainly to the increase of the number of the flooded basements and at the same time of the water depth inside them, which are observed in the cases of $T=100$ and 1000 years. The return period of the real flood in the main residential area, as a more representative area even in this case, is 243 years, as it is shown in Figure 102 which considers the evolution of the average maximum water depth percentage as a function of time.

6.6.3. Flood extent and flooding

Figure 103 shows illustratively the increase of the flood extent as the return period increases from $T=20$ to $T=1000$ years.

It is obvious from Figure 104 and 105 that the real flood extent is larger than the flood extent for $T=100$ years and smaller than $T=1000$ years for all the particular areas.

Figure 106 considers the evolution of the flood extent as a function of time and shows illustratively that the return period of the real flood in the main residential area, as a more representative area even in this case, is 391 years.

Figure 107 shows illustratively the increase of the flooding as the return period increases from T=20 to T=1000 years.

It is obvious from Figure 107 that flooding of the Scenario “Real flood” is larger than the flooding for T=100 years and smaller than T=1000 years for all the particular areas.

Figure 108 considers the evolution of flooding as a function of time and shows illustratively that the return period of the real flood in the main residential area, as a more representative area even in this case, is 255 years.

6.7. Evaluation of Scenario “Diversion and retention pond” and the alternative Scenarios for T=50 years

6.7.1. Maximum water depths of area

Figure 65 shows the maximum water depths of the Scenario “Diversion and retention pond” in the particular areas for a return period of T=50 years. It reveals that there is no overflow at the units of the retention pond and the flow separator therefore the designed diversion works operate properly. Yet, the flood compared to the flood of the Scenario “Real flood” in the particular areas for a return period of T=50 years (see Figure 77) shows new flooded areas as the area downstream of the location of the diversion into Soures, the Logistics METRO area, the area to the east and a significant part of the main industrial area. The above findings are verified considering the average water depth percentage, as a representative index, which is only 17.9% in the main residential area and 88.9% in the hydraulic simulation area but 173.5% in the main industrial area (see Figure 79).

Figure 76 shows the maximum water depths of the alternative Scenario “Diversion, retention pond and METRO fence” in the particular areas for a return period of T=50 years. The flood compared to the flood of the Scenario “Diversion and retention pond” in the particular areas for a return period of T=50 years (see Figure 65) eliminates the flood at the Logistics METRO area and to the east but strengthens the flood in the main residential area due to the METRO fence and therefore the diversion of the overflow to the south. The above findings are verified considering the average maximum water depth percentage, as a representative index, which is only 27.9% in the main residential area and 90.2% in the hydraulic simulation area but 169.0% in the main industrial area (see Figure 79).

Figure 77 shows the maximum water depths of the alternative Scenario “New diversion and retention pond” in the particular areas for a return period of T=50 years. The flood compared to the flood of the Scenario “Diversion and retention pond” in the particular

areas for a return period of $T=50$ years (see Figure 65) eliminates the flood upstream (6), at the Logistics METRO area and to the east thus alleviating the flood in the main industrial area and in the hydraulic simulation area but strengthens the flood in the main residential area due to the contribution of the new diversion. The above findings are verified considering the average water depth percentage, as a representative index, which is only 26.3% in the main residential area, and 76.5% in the hydraulic simulation area but 135.7% in the main industrial area (see Figure 79).

Conclusively, concerning the maximum water depth, the Scenario “New diversion and retention pond” has the highest overall (on the hydraulic simulation area) impact with a moderate mitigation of 23.5%. Also, the Scenario “New diversion and retention pond” has the smallest negative impact on the average maximum water depth in the main industrial area with a moderate increase of 35.7%, while the Scenario “Diversion and retention pond” is the best for achieving the goal of reducing the maximum water depth in the main residential area with a great reduction of 82.1%.

6.7.2. Flood extent and flooding

The conclusions, concerning flood extent and flooding, differ to a certain degree. More precisely, the Scenario “New diversion and retention pond” has the highest overall (on the hydraulic simulation area) impact with moderate mitigations of 34.3% and 25.8%, respectively. The Scenario “Diversion and retention pond” is the best for achieving the goal of mitigating flood extent and flooding in the main residential area with great mitigations of 81.4% and 85.0%, respectively and has the lower negative impact on the main industrial area with increases of 15.4% and 26.2%, respectively.

The results of the three scenarios verify the overall positive impact and especially on the main residential area but also demonstrate a negative impact concerning the main industrial area. This means that the corresponding technical works of the diversion, which are included in the study (ETME – Peppas et al. 2014), as well as the examined alternatives, contribute partially but are not adequate to solve completely the flood problem. The results of the model are reliable as they demonstrate the necessity of the canalisation works along Soures stream in conjunction with the technical works of the diversion and retention pond as it is stated in the above approved study.

Although the assessment of uncertainty is beyond the scope of this thesis, it is obvious that except for the other sources of uncertainty (rainfall data, few and unequally distributed observations, mesh resolution, flow resistance, sewer system etc.) the topographic and structural changes provide a great deal of uncertainty as well.

7. Conclusion

Rapid urbanization and climate change increase flood risk and establish urban flood modelling as an indispensable tool to support risk assessment and management. 1D/2D coupled hydrodynamic models, which combine a 1D sewer system model with a 2D hydrodynamic model to simulate overland flow and allow interaction between the systems model are reliable choices in urban flood modelling. The present thesis uses a 1D/2D coupled model (1D SWMM/ 2D P-DWave) to simulate the flash flood of 2017 at the town of Mandra, Greece. The coupled 1D/2D approach is also used to apply flood mitigation and protection strategies in areas of weakness and to assess the impact of the proper maintenance of the closed conduits, the implementation of private protection measures, the extension of the rainfall zone over the flooded area and the incorporation of a stream diversion and a retention pond. Additionally, the model is applied to four rainfall scenarios in order to investigate the influence of the return period. Finally, alternative cases without canalisation are examined.

The 1D/2D coupled model is validated through the basic Scenario "Real flood". The model satisfactory represents the maximum water depths almost at all checkpoints of Agia Aikaterini and Soures streams. Small deviations are due to limitations of the 5 m mesh resolution of the DEM (narrower riverbed than 5 meters at S1, composite cross section with different Manning's n over the height of 3 m at S11, S12). The lack of observations (only one observation in the majority of the checkpoints) and their position (only along the water paths of the streams) do not permit safe conclusions regarding flood progress. Generally, there is a good representation and the delay in the downward branch of the water depth's time change is mostly due to the shape of the inflow storm hydrograph of Agia Aikaterini stream. The hydrological simulation is a subject of another thesis (Mavrogeorgos 2019). Yet, there is an inherent uncertainty in the rainfall data as well as the rainfall-runoff process and therefore in the inflow storm hydrographs of the two streams (Agia Aikaterini stream and Soures stream) involved in the hydraulic simulation, where the 1D/2D coupled model (1D SWMM/ 2D P-DWave) is used. The good statistical evaluation (RMSE=0.494, NSE=0.871, MAE=0.362) of the maximum water depths at the checkpoints in conjunction with the very high percentage of 96.0% of the real flood extent compared to the recorded flood extent, taking into consideration that the relative surplus and deficit are only 12.4% and 16.4%, respectively, validate the coupled 1D/2D model and its set-up. The refined DEM (building-block method (BB), elevation reduction at streets and flooded buildings, additional topographic maps and data), is validated as well. It is obvious that the model's mesh resolution of 5 m, as a

compromise between detail (or precision), accuracy and computational time, is unable to represent small features but the study proves that a mesh resolution of 5 m, even for narrow streams and streets, is adequate to accurately model a flash flood. Also, it is shown that P-DWave is suitable for flash flood simulations as it presents satisfactory results and is fairly easy to set up.

The statistics (RMSE, NSE, MAE) of the comparison between the simulated maximum water depths of each scenario with the simulated water depths of the scenario “Real flood” at the 19 checkpoints present a variety of impacts on the maximum water depths of the two streams. More precisely, proper maintenance has a low impact (small reduction), extension of rainfall zone over the flooded area has a moderate impact (moderate increase), private protection measures (raising fences) have a moderate impact (increase of the depths of Soures stream) and the diversion and retention pond has a high impact (large reduction of the depths of Agia Aikaterini stream and increase of the depths of Soures stream).

Proper maintenance has a low but not negligible impact on the average wet maximum water depths, the average maximum water depths as well as on the flood extent and the flooding. It reduces the average wet maximum water depth by 13.1% (88.3 to 76.7 cm), it reduces the average maximum water depth by 7.8% (16 to 14.8 cm) but increases the flood extent by 9.4% (2.535 to 2.774 km²) and flooding by 6.0% (flooding percentage 18.1 to 19.2%).

Private protection measures have a moderate overall impact on the average maximum water depth with a moderate reduction of 25% (16 to 12 cm), with a negligible increase of 3% (20.1 to 20.7 cm) in the main residential area but a high reduction due to fences raising of 58.1% (33.5 to 14 cm) in the main industrial area. Also, the impact remains high regarding the main industrial area as it reduces the flood extent by 48.5% (1.097 to 0.565 km²) and the flooding by 54.3% (28.7 to 13.1%).

Extension of rainfall zone over the flooded area has a moderate impact on the average maximum water depths and a huge impact on the flood extent and the flooding for all the particular areas. More precisely, the average maximum water depths increase by 46.1%, 24.6% and 32.2%, the flood extents increase by 255.2%, 114.9% and 173.0% and the floodings increase by 157.5%, 71.1% and 111.7% for the hydraulic simulation area, the main residential area and the main industrial area respectively. Also, the flood progress presents an expected earlier rising of the water depths.

The diversion and the retention pond technical works combined with proper maintenance have a high impact on the flood extent and on the flooding in the main residential area

as the diversion conduit diverts the majority of the flow of Agia Aikaterini stream to Soures stream. This reduces the flood extent by 42.2% (0.711 to 0.411 km²) and the flooding by 52.9% (25.7 to 12.1%). However, the diversion causes a severe overflow in Soures stream contributing to the increase of the flood extent by 20.2% (1.097 to 1.318 km²) and of the flooding by 22.7% (28.7 to 35.3%) in the main industrial area as well as in the increase of the flood extent by 22.5% (2.535 to 3.105 km²) and of the flooding by 19% (18.1 to 21.6%) in the hydraulic simulation area, flooding a significant part to the east and southeast. Moreover, there is a very high impact on the average maximum water depth in the main residential area as it is reduced by 75.3% (20.1 to 5 cm) and due to the mentioned increase of the flood extent a low impact in both the hydraulic simulation area and the main industrial area where the average maximum water depths are reduced by 16.8% (16 to 13.3 cm) and 11.3% (33.5 to 30 cm), respectively. Also, there is a high impact on the flood progression along Agia Aikaterini stream as it follows the overflow of the technical work of separation. The earlier rising of the upward branch downstream S3 is due to the contribution of the diversion from Agia Aikaterini stream, where the storm starts half an hour earlier.

All the parameters (average wet maximum water depth, average maximum water depth, flood extent and flooding) increase as the return period increases. The increase is smooth only for the main residential area which is not affected from phenomena like stream banks overflows and basements flooding. The statistical evaluation of the maximum water depths at the 19 checkpoints shows that the flood is better fitted by the flood of T=1000 years (NSE=0.903 is the biggest and very close to 1, smallest RMSE and MAE). The evaluation of the time change of water depths at the checkpoints, the average wet maximum water depth, the average maximum water depth, the flood extent and the flooding show that the return period of the flood is over T=100 years and more precisely between T=235 and T=391 years.

The comparison of 3 different scenarios regarding public protection measures (Scenarios “Diversion and retention pond”, “Diversion, retention pond and METRO fence” and “New diversion and retention pond”) with the Scenario “Real flood” for T=50 years, proves an overall positive impact and especially on the main residential area but also demonstrates a negative impact concerning the main industrial area. More precisely, there is a consistency in reductions for all the parameters ranging from values of 9.8 to 34.3% in the hydraulic simulation area to high values of 72.1 to 85% in the main residential area and in increases ranging from 15.4 to 73.5% in the main industrial area. This means that the corresponding technical works of the diversion, which are included in the approved study (ETME – Peppas et al. 2014), as well as the examined alternatives, contribute

partially but are not adequate to solve completely the flood problem. The results of the model are reliable as they demonstrate the necessity of the canalisation works along Soures stream in conjunction with the technical works of the diversion and retention pond as it is stated in the above approved study.

Although the assessment of uncertainty is beyond the scope of this thesis, it is obvious that except for the other sources of uncertainty (rainfall data, few and unequally distributed observations, mesh resolution, flow resistance, sewer system etc.) the topographic and structural changes provide a great deal of uncertainty as well.

On the basis of the findings of the present thesis, future research may address certain issues which are suggested as following.

The assessment of the corresponding impacts that will arise with the integration of the Soures stream regulation projects (canalisation), according to the relevant approved study, is an unquestionable challenge. The implementation of a fully integrated sewer system will certainly add to the complexity and the high degree of uncertainty of the model but it will provide fruitful ground for further research on the 2017 Mandra flash flood. Finally, a very fine mesh resolution (2 m or less) to represent the small scale features (e.g. the narrow streets and riverbed) with a further refinement to represent the peculiarities of the town of Mandra (e.g. fences) is suggested to investigate the influence on maximum water depth, flood progress and flood extent.

Appendix

Table 36 Summary of input, output and application files for P-DWave, SWMM and the coupling (P-DWave/SWMM)

	Type	Model	Format
Input Data	DEM	P-DWave	.ASC
	Manning roughness	P-DWave	.ASC
	Boundary Conditions	P-DWave	.ASC
	Initial Conditions	P-DWave	.ASC
	Grid Location Code	P-DWave	.ASC
	Precipitation Data	P-DWave	.txt
	Checkpoint Input	P-DWave	.txt
	Linking Points	P-DWave/SWMM	.txt
	SWMM5 input file	SWMM	.inp
	SWMM5 initialization file	SWMM	.ini
Output Data	Mass Overview	P-DWave	.OUT
	Time Overview	P-DWave	.OUT
	Max Depth and SL	P-DWave	.FLT
	Depths, SL, Velocity Raster	P-DWave	.ASC
	Checkpoint Output	P-DWave	.OUT
	Linking Points Outputs	P-DWave/SWMM	.OUT
	SWMM5 report file	SWMM	.rpt
	SWMM5 output file	SWMM	.out
Application Files	P-DWave application	P-DWave	.exe
	P-DWave Master File	P-DWave	.DAT
	Dlllogin	P-DWave	.dll
	libifcoremd	P-DWave	.dll
	libifportMD	P-DWave	.dll
	libmmd	P-DWave	.dll
	VC2005-DLL	P-DWave/SWMM	.dll
	VC2005-DLL	P-DWave/SWMM	.lib




```




* BASIC parameters
*****
* IND X Y LLX LLY CELLSIZE
BO 2 1114 943 453773.032801 4211318.966605 5
*****
* PDWS parameters
*****
* KKK MS tr BoxC perc mpi tupdate(s) DFwave alfa (0-1) VelInvIntensity (1-20) teta
PD 1 20 0.001 20000 1 500 0.0001 3 1 80 10 0.99 0.7
*****
* TIME related parameters
*****
* S E MM DT SEC RATIO ADAPTIVE_TIME
T0 0 32401 2 2 1.0 1
F0 ELEVATION dem_housel.txt
F0 ROUGHNESS mann_tel_66.txt
F0 STAGE_P Rain_real.txt
F0 LINKPOINT lkpointf2_1.txt
F0 INFPOINT BCTYPE_str.txt
F0 BPOINT BType_5.txt
F0 DEPTH INIDepth11_5m_nohead.txt
F0 CHECKPOINT CK_2.txt
F0 STAGE4 Sim_SG_P_BC_real.txt
F1 GLOBAL INTERVAL_S 900
F1 LKPOINT INTERVAL_S 30
F1 ASCII INTERVAL_S 7200
F2 SECOND
P1 OPENBOUNDARY TRUE
P0 MINDI 0.06




```




Figure 115 Exemplary P-DWave master file (Scenario "Real flood")




Table 37 Flood progress with a time step of 30 min (Scenario “Real flood”)




Total time (h)	Actual time (h)	Image
0.5	06:15	
1	06:45	
1.5	07:15	

<p>2</p>	<p>07:45</p>	
<p>2.5</p>	<p>08:15</p>	
<p>3</p>	<p>08:45</p>	

<p>3.5</p>	<p>09:15</p>	
<p>4</p>	<p>09:45</p>	
<p>4.5</p>	<p>10:15</p>	

<p>5</p>	<p>10:45</p>	
<p>5.5</p>	<p>11:15</p>	
<p>6</p>	<p>11:45</p>	

<p>6.5</p>	<p>12:15</p>	
<p>7</p>	<p>12:45</p>	
<p>7.5</p>	<p>13:15</p>	

<p style="text-align: center;">8</p>	<p style="text-align: center;">13:45</p>	
<p style="text-align: center;">8.5</p>	<p style="text-align: center;">14:15</p>	
<p style="text-align: center;">9</p>	<p style="text-align: center;">14:45</p>	

Bibliography

- Allitt, Richard; Blanksby, John; Djordjević, Slobodan; Maksimović, Čedo; Stewart, Dave (2009): Investigations into 1D-1D and 1D-2D Urban Flood Modelling. WaPUG Autumn Conference.
- Apostolidis, E.; Perleros, B.; Tsatiris, B.; Vasilopoulos G. (2017): *Report for the 15th of November 2017 flood in Mandra and in Nea Peramos Attica*, 46 pages, Geotechnical Chamber of Greece-Branch of Eastern Continental Greece, Athens.
- Bates, Paul D.; Pappenberger, Florian; Romanowicz, Renata J. (2014): Uncertainty in Flood Inundation Modelling. In Keith Beven, Jim Hall (Eds.): *Applied Uncertainty Analysis for Flood Risk Management*. London: Imperial College Press, pp. 232–269.
- Bazin, Pierre-Henri; Nakagawa, Hajime; Kawaike, Kenji; Paquier, André; Mignot, Emmanuel (2014): Modeling Flow Exchanges between a Street and an Underground Drainage Pipe during Urban Floods. In *J. Hydraul. Eng.* 140 (10), p. 04014051. DOI: 10.1061/(ASCE)HY.1943-7900.0000917.
- Beg, Md Nazmul Azim; Carvalho, Rita F.; Leandro, Jorge (2017): Comparison of Flow Hydraulics in Different Manhole Types. Proceedings of the 37th IAHR World Congress 2017. DOI: 10.5281/ZENODO.3246831.
- BEYOND Center of EO Research and Satellite Remote Sensing of the National Observatory of Greece. Available online at <http://beyond-eocenter.eu/index.php/floods>, checked on 9/18/2019.
- Bradbrook, K.F.; Lane, S.N.; Waller S.G.; Bates, P.D. (2004): Two dimensional diffusion wave modelling of flood inundation using a simplified channel representation. In *International Journal of River Basin Management* 2 (3), pp. 211–223. DOI: 10.1080/15715124.2004.9635233.
- Chen, A. S.; Hsu, M. H.; Chen, T. S.; Chang, T. J. (2005): An integrated inundation model for highly developed urban areas. In *Water science and technology: a journal of the International Association on Water Pollution Research* 51 (2), pp. 221–229. DOI: 10.2166/wst.2005.0051.
- Chen, Albert; Djordjević, Slobodan; Leandro, J.; Savic, Dragan (2007): The urban inundation model with bidirectional flow interaction between 2D overland surface and 1D sewer networks. NOVATECH 2007, Lyon, France.
- Chen, Albert; Leandro, J.; Djordjević, Slobodan (2015): Modelling sewer discharge via displacement of manhole covers during flood events using 1D/2D SIPSON/P-DWave dual drainage simulations. In *Urban Water Journal* 13 (8), pp. 830–840 DOI: 10.1080/1573062X.2015.1041991.
- Chen, Albert S.; Leandro, Jorge; Djordjević, Slobodan (2016): Modelling sewer discharge via displacement of manhole covers during flood events using 1D/2D SIPSON/P-DWave dual drainage simulations. In *Urban Water Journal* 13 (8), pp. 830–840. DOI: 10.1080/1573062X.2015.1041991.
- CHI (Ed.) (2020a): About CHI. Computational Hydraulics International. Available online at <https://www.chiwater.com/Home/About>, checked on 1/14/2020.
- Chow, V.; Maidment, T. D. R.; Mays, L. W. (1988): *Applied Hydrology*, 572 pages, McGraw-Hill International Editions, Civil Engineering Series.

- Coles D.; Yu D.; Wilby RL.; Green D.; Herring Z. (2017): Beyond ‘flood hotspots’: modelling emergency service accessibility during flooding in York, UK. *J Hydrol* 546:419–436. DOI: 10.1016/j.jhydrol.2016.12.013.
- Crispino, Gaetano; Gisonni, Corrado; Iervolino, Michele (2015): Flood hazard assessment: comparison of 1D and 2D hydraulic models. In *International Journal of River Basin Management* 13 (2), pp. 153–166. DOI: 10.1080/15715124.2014.928304.
- Dawson, R.J.; Peppe R.; Wang M. (2011): An agent-based model for risk-based flood incident management. In *Natural Hazards* 59 (1), pp. 167–189. DOI : 10.1007/s11069-011-9745-4.
- Delleur, J.W. (2003): The Evolution of Urban Hydrology: Past, Present and Future. In *Journal of Hydraulic Engineering* 129 (8), pp. 563–573. DOI: 10.1061/(ASCE)0733-9429(2003)129:8(563).
- DHI (Ed.) (2020): MIKE Powered by DHI. Available online at <https://www.mikepoweredbydhi.com/>, checked on 1/24/2020.
- Disse, Markus; Kaiser, Maria (Eds.) (2018): Starkregen und Sturzfluten – Erfassen, Erforschen, Evaluieren. Beiträge zum Seminar am 6. Juni 2018 an der Technischen Universität München. Seminar Starkregen und Sturzfluten (Forum für Hydrologie und Wasserbewirtschaftung, Heft 40.18). Available online at https://www.fghw.de/download/forumsbeitraege/40.18_Gesamt.pdf, checked on 3/10/2020.
- Djordjević, Slobodan.; Prodanović, Dusan.; Godfrey, A. Walters (2004): Simulation of Transcritical Flow in Pipe/Channel Networks. In *Journal of Hydraulic Engineering* 130 (12), pp. 1167–1178. DOI: 10.1061/(ASCE)0733-9429(2004)130:12(1167).
- Djordjević, S.; Prodanović, D.; Maksimović, Č.; Ivetić, M.; Savić, D. (2005): SIPSON – Simulation of Interaction between Pipe flow and Surface Overland flow in Networks. In *Water Science and Technology* 52 (5), pp. 275–283. DOI: 10.2166/wst.2005.0143.
- Djordjević, Slobodan; Prodanovic, Dusan; Maksimovic, Čedo (1999): An approach to simulation of dual drainage. In *Water Science and Technology* 39, pp. 95–103. DOI: 10.1016/S0273-1223(99)00221-8.
- Dottori, F.; Di Baldassarre, G.; Todini, E. (2013): Detailed data is welcome, but with a pinch of salt: Accuracy, precision, and uncertainty in flood inundation modeling. In *Water Resour. Res.* 49 (9), pp. 6079–6085. DOI: 10.1002/wrcr.20406.
- Efstratiadis, A.; Koukouvinos, Kousis, A.; Mamassis, N.; Galiouna, E.; Tzouka, K.; Michailidi, E. and Koutsoyiannis, D. (2014): Technical report describing regional relations for the assessment of characteristic hydrological parameters, DEUCALION research program – Estimation of flood flows in Greece under conditions of hydroclimatic variability: Development of naturally established conceptual-probabilistic framework and computational tools, Contractors: ETME: Peppas & Collaborators L.P., Mahera Office, Department of Water Resources and Environment Engineering – National Technical University of Athens, National Observatory of Athens. Available online at <https://www.itia.ntua.gr/en/getfile/1469/1/documents/DeukalionClosureDK.pdf>, checked on 9/25/2019.
- Ellis, J. H.; McBean E. A.; Mulamootil G. (1982): Design of dual drainage systems using SWMM. In *ASCE Journal of Hydraulics Division* (108(10)), pp. 1222–1227.
- Ernst J.; Dewals B.J.; Detrembleur S.; Archambeau P.; Epicum S.; Piroton M. (2010): Micro-scale flood risk analysis based on detailed 2D hydraulic modelling and high

- resolution geographic data. In *Natural Hazards* 55 (2), pp. 181–209. DOI: 10.1007/s11069-010-9520-y.
- ETME: Peppas & Collaborators L.P.; Kontos, E.; Roikos Consultant Engineers SA; Kaimaki, P.; Mastathis, E. (2014): STUDY OF AG. AIKATERINI DIVERSION TO SOURES STREAM AND CANALISATION OF SOURES STREAM IN THE RARYO-THRACE FIELD.
- Flood risk management plan, YPEKA 2017.
- Fewtrell, Timothy J.; Duncan, Alastair; Sampson, Christopher C.; Neal, Jeffrey C.; Bates, Paul D. (2011): Benchmarking urban flood models of varying complexity and scale using high resolution terrestrial LiDAR data. In *Physics and Chemistry of the Earth, Parts A/B/C* 36 (7-8), pp. 281–291. DOI: 10.1016/j.pce.2010.12.011.
- Gallegos, Humberto A.; Schubert, Jochen E.; Sanders, Brett F. (2009): Two-dimensional, high-resolution modeling of urban dam-break flooding: A case study of Baldwin Hills, California. In *Advances in Water Resources* 32 (8), pp. 1323–1335. DOI: 10.1016/j.advwatres.2009.05.008.
- Hsu, Ming-Hsi; Chen, Shiuan-Hung; Chang, Tsang-Jung (2002): Dynamic inundation simulation of storm water interaction between sewer system and overland flows. In *Journal of the Chinese Institute of Engineers* 25 (2), pp. 171–177. DOI: 10.1080/02533839.2002.9670691.
- Hunter, N. M.; Bates, P. D.; Neelz, S.; Pender, G.; Villanueva, I.; Wright, N. G. et al. (2008): Benchmarking 2D hydraulic models for urban flooding. In *Proceedings of the Institution of Civil Engineers - Water Management* 161 (1), pp. 13–30. DOI: 10.1680/wama.2008.161.1.13.
- IPCC (2014): *Climate change 2014: impacts, adaptation, and vulnerability*. Cambridge University Press, Cambridge.
- Kalogiros, I.; Retalis, A.; Katsanos, D.; Anagnostou, M.; Nikolopoulos, E. (2017): Press release of the National Observatory of Athens. Available online at http://www.noa.gr/index.php?option=com_content&view=article&id=1074&catid=86&Itemid=547&lang=el, checked on 11/12/2019.
- Kontoes, C.; Antoniadis, S.; Ieronimidi, E.; Karagiannopoulou, K.; Tsouni, A.; (2018): *Flood analysis in western Attica on 15/11/2017 with the use of satellite remote sensing*, National Observatory of Athens, Athens.
- Koutsoyiannis, D.; Xanthopoulos, T. (2016): *Technical Hydrology*, Edition 4, 418 pages, National Technical University of Athens, Athens.
- Koutsoyiannis, D.; Kozonis, D.; Manetas, A. (1998): A mathematical framework for studying rainfall intensity-duration-frequency relationships. In *Journal of Hydrology* 206 (1-2), pp. 118–135. DOI: 10.1016/S0022-1694(98)00097-3.
- Leandro, J.; Chen, A. S.; Schumann, A. (2014): A 2D parallel diffusive wave model for floodplain inundation with variable time step (P-DWave). In *Journal of Hydrology* 517, pp. 250–259. DOI: 10.1016/j.jhydrol.2014.05.020.
- Leandro, J.; Djordjević, S.; Chen, A. S.; Savić, D. A.; Stanić, M. (2011): Calibration of a 1D/1D urban flood model using 1D/2D model results in the absence of field data. In *Water Science and Technology* 64 (5), pp. 1016–1024. DOI: 10.2166/wst.2011.467.
- Leandro, J.; Schumann, A.; Pfister, A. (2016): A step towards considering the spatial heterogeneity of urban key features in urban hydrology flood modelling. In *Journal of Hydrology* 535, pp. 356–365. DOI: 10.1016/j.jhydrol.2016.01.060.

- Leandro, Jorge; Chen, Albert S.; Djordjević, Slobodan; Savić, Dragan A. (2009): Comparison of 1D/1D and 1D/2D Coupled (Sewer/Surface) Hydraulic Models for Urban Flood Simulation. In *J. Hydraul. Eng.* 135 (6), pp. 495–504. DOI: 10.1061/(ASCE)HY.1943-7900.0000037.
- Leandro, Jorge; Martins, Ricardo (2016): A methodology for linking 2D overland flow models with the sewer network model SWMM 5.1 based on dynamic link libraries. In *Water science and technology: a journal of the International Association on Water Pollution Research* 73 (12), pp. 3017–3026. DOI: 10.2166/wst.2016.171.
- LfU (Ed.) (2018): Starkregen und Sturzfluten. Bayerisches Landesamt für Umwelt. Available online at https://www.lfu.bayern.de/wasser/hw_risiko_umgang/starkregen_und_sturzfluten/index.htm, checked on 3/20/2020.
- Lopes, Pedro; Leandro, J.; Carvalho, Rita; Martins, Ricardo (2012): Numerical and experimental investigation of a gully under surcharge conditions. In *Urban Water Journal* 12 (6), pp 468–476. DOI: 10.1080/1573062X.2013.831916.
- Mark, Ole; Weesakul, Sutat; Apirumanekul, Chusit; Aroonnet, Surajate Boonya; Djordjević, Slobodan (2004): Potential and limitations of 1D modelling of urban flooding. In *Journal of Hydrology* 299 (3-4), pp. 284–299. DOI: 10.1016/j.jhydrol.2004.08.014.
- Martins, Ricardo; Leandro, Jorge; Chen, Albert S.; Djordjević, Slobodan (2017): A comparison of three dual drainage models: shallow water vs local inertial vs diffusive wave. In *J Hydroinform* 19 (3), pp. 331–348. DOI: 10.2166/hydro.2017.075.
- Mavrogeorgos, K. (2019): Examination of the impact of the inlet storm hydrograph on the floods hydraulic behavior using the Telemac model in the case of Mandra, Attica, Diploma thesis, Department of Water Resources and Environmental Engineering–National Technical University of Athens.
- Michailidi, E. M.; Antoniadis, S.; Koukouvinos, A.; Bacchi, B.; Efstratiadis, A. (2018): Timing the time of concentration: shedding light in a paradox. In *Hydrological Sciences Journal* 63 (5), pp. 721–740. DOI: 10.1080/02626667.2018.1450985.
- Mignot, E.; Li, X.; Dewals, B. (2019): Experimental modelling of urban flooding: A review. In *Journal of Hydrology* 568, pp. 334–342. DOI: 10.1016/j.jhydrol.2018.11.001
- Mimikou, M. A.; Baltas, E. A. (2012): *Technical Hydrology*, Edition 5, 395 pages, Papasotiriou Editions, Athens.
- Nash, J. E.; Sutcliffe, J. V. (1970): River flow forecasting through conceptual models part I — A discussion of principles. In *Journal of Hydrology* 10 (3), pp. 282–290. DOI: 10.1016/0022-1694(70)90255-6.
- Peppas, I.; Karavokyris, I. (2004): Raryo-Thrace field flood protection, Conference «Attica Flood Protection», TBT, Athens. Available online at http://library.tee.gr/digital/m2022/m2022_peppas.pdf, checked on 04/02/2020.
- Risva, K. (2018): *Development of a distributed hydrological software application employing novel velocity-based techniques*, MSc Thesis, 157 pages, Department of Water Resources and Environmental Engineering - National Technical University of Athens, Athens.
- Rossmann, L. A. (2015): Storm Water Management Model User's Manual Version 5.1 - EPA- 600/R-14/413b, checked on 2/5/2020.

- Rossmann, L. A. (2017): Storm Water Management Model Reference Manual Volume II – Hydraulics, EPA/600/R-17/111.
- Salvadore, Elga; Bronders, Jan; Batelaan, Okke (2015): Hydrological modelling of urbanized catchments: A review and future directions. In *Journal of Hydrology* 529, pp. 62–81. DOI: 10.1016/j.jhydrol.2015.06.028.
- Schubert, Jochen E.; Sanders, Brett F. (2012): Building treatments for urban flood inundation models and implications for predictive skill and modeling efficiency. In *Advances in Water Resources* 41, pp. 49–64. DOI: 10.1016/j.advwatres.2012.02.012.
- Schubert, J.E.; Sanders, B.F.; Smith, M.J.; Wright, N.G. (2008): Unstructured mesh generation and landcover-based resistance for hydrodynamic modeling of urban flooding. In *Advances in Water Resources* 31, pp. 1603–1621. DOI: 10.1016/j.advwatres.2008.07.012.
- Seyoum, Solomon Dagnachew; Vojinovic, Zoran; Price, Roland K.; Weesakul, Sutat (2012): Coupled 1D and Noninertia 2D Flood Inundation Model for Simulation of Urban Flooding. In *J. Hydraul. Eng.* 138 (1), pp. 23–34. DOI: 10.1061/(ASCE)HY.1943-7900.0000485.
- Snyder, F. F. (1938): Synthetic unit-graphs. In *EOS Transactions, American Geophysical Union* 19 (1), pp. 447–454. DOI: 10.1029/TR019i001p00447.
- Stamou, A.I. (2018): The Disastrous Flash Flood of Mandra in Attica-Greece and now What? In *Civil Engineering Research Journal* 6 (1), p. 555677. DOI: 10.19080/CERJ.2018.06.555677
- Sutcliffe, J.V. (1978): *Methods of Flood Estimation, A Guide to Flood Studies Report, Report No 49*, Institute of Hydrology, UK.
- U.S. Department of the Interior, Bureau of Reclamation (1977): *Design of Arch Dams*, U.S. Government Printing Office, Denver, CO.
- USDA Soil Conservation Service (1972): National engineering handbook, Section 4, hydrology, Washington DC, USA.

Declaration of Authorship

I hereby declare that this Master's Thesis has been authored solely by myself and that all external sources used have been acknowledged and fully cited.

Munich, 08.06.2020, Nikolaos Zafeirakos